NATIONAL ACADEMY OF SCIENCES OF UKRAINE
V. LASHKARYOV INSTITUTE OF SEMICONDUCTOR PHYSICS
BULGARIAN ACADEMY OF SCIENCES
INSTITUTE OF SOLID STATE PHYSICS

E.D. Atanassova, A.E. Belyaev, R.V. Konakova,
P.M. Lytvyn, V.V. Milenin, V.F. Mitin, V.V. Shynkarenko

EFFECT OF ACTIVE ACTIONS ON THE PROPERTIES OF SEMICONDUCTOR MATERIALS AND STRUCTURES

NTC “Institute for Single Crystals”
Kharkiv 2007

Effect of Active Actions on the Properties of Semiconductor Materials and Structures / E.D. Atanassova, A.E. Belyaev, R.V. Konakova, P.M. Lytvyn, V.V. Milenin, V.F. Mitin, V.V. Shynkarenko – Kharkiv: NTC "Institute for Single Crystals", 2007.– page. --

ISBN 966-02-2555-5 ; ISBN 978-966-02-4268-5

The monograph deals with the physico-technological aspects of interaction of microwave radiation with semiconductor materials and device structures made on their basis. The effect of active actions (microwave treatment, ^{60}Co γ-irradiation and rapid thermal annealing) on the processes of structural relaxation in the TiB_2–GaAs (InP, GaP, SiC) contacts is considered. An analysis is made of the features of the effect of microwave and ^{60}Co γ-radiation on the electrical characteristics of resonant tunneling diodes made on the basis of AlGaAs–GaAs heterojunctions, as well as gallium arsenide tunnel diodes with a δ-layer in the space-charge region. The experimental data on the effect of microwave radiation on defect modification in the SiO_2-GaAs (SiC) structures are presented. The effects in the nanocrystalline silicon–silicon systems induced by microwave radiation are considered. Much space is given to the effects produced by microwave and ^{60}Co γ-irradiation in the Ta_2O_5–Si structures, depending on the conditions of Ta_2O_5 formation.

The monograph is intended for researchers and those engaged in development of microwave devices. It may be of use also to post-graduates and undergraduates specializing in the corresponding areas.

Рецензент: академік НАН України
доктор фіз.-мат. наук професор В.М. Яковенко

Головний редактор серії
академік НАН України Б.В. Гриньов

Відповідальний секретар
канд. фіз.-мат. наук Е.В. Щербина

ISBN 966-02-2555-5;
ISBN 978-966-02-4268-5

© Атанасова О.Д., Беляєв О.Є.,
Конакова Р.В., Литвин П.М.,
Міленін В.В., Мітін В.Ф.,
Шинкаренко В.В. 2007
© НТК "Інститут монокристаллів", 2007

Вплив активних дій на властівості напівпровідникових матеріалів і структур / О.Д. Атанасова, О.Є. Беляєв, Р.В. Конакова, П.М. Литвин, В.В. Міленін, В.Ф. Мітін, В.В. Шинкаренко – Харьков: НТК "Институт монокристалів", 2007.– стр. --

ISBN 966-02-2555-5 (серія); ISBN 978-966-02-4268-5

В монографії розглянуті фізико-технологічні аспекти взаємодії НВЧ ви-промінювання з напівпровідниковими матеріалами та приладовими структу-рами на їх основі. Показано вплив активних обробок (НВЧ обробка, γ-опромінювання ^{60}Co і швидкий термічний відпал) на процеси структурної релаксації в контактах TiB_2–GaAs (InP, GaP, SiC). Проаналізовані особливо-сті впливу НВЧ і γ-випромінювання ^{60}Co на електричні характеристики ре-зонансно-тунельних діодів на основі гетеропереходів AlGaAs–GaAs і арсе-нідгалієвих тунельних діодів з δ-шаром в області просторового заряду. На-ведені експериментальні дані з впливу НВЧ випромінювання на модифіка-цію дефектів в структурах SiO_2–GaAs (SiC). Розглянуті стимульовані НВЧ випромінюванням ефекти в системах нанокристалічний кремній–кремній. Значне місце відведено ефектам, викликаним НВЧ і γ-опромінюванням ^{60}Co в структурах Ta_2O_5–Si, в залежності від умов формування Ta_2O_5.

Монографія призначена для наукових працівників і розробників НВЧ приладів. Вона може бути корисною також аспірантам і студентам вузів, які навчаються за відповідними спеціальностями.

Рецензент: академік НАН України
доктор фіз.-мат. наук професор В.М. Яковенко

Головний редактор серії
академік НАН України Б.В. Гриньов

Відповідальний секретар
канд. фіз.-мат. наук Е.В. Щербина

ISBN 966-02-2555-5 (серія);
ISBN 978-966-02-4268-5

© Атанасова О.Д., Беляєв О.Є.,
Конакова Р.В., Литвин П.М.,
Міленін В.В., Мітін В.Ф.,
Шинкаренко В.В. 2007
© НТК "Інститут монокристаллів", 2007

PRINCIPAL ACRONYMS AND SYMBOLS

AES	- Auger electron spectroscopy
AFM	- atomic force microscopy
CTO	- conventional thermal oxidation
CW	- continuous wave
2(3)D	-two-(three-)dimensional
DBRTD	- double-barrier resonant tunneling diode
DLTS	- deep level transient spectroscopy
DRAM	- dynamic random access memory
ER	- electroreflectance
IC	- integrated circuit
IS	- intrinsic stress
MBE	- molecular-beam epitaxy
MIS	- metal–insulator–semiconductor
MOCVD	- metal-organic chemical vapor deposition
MOS	- metal–oxide–semiconductor
MOSFET	- metal-oxide-semiconductor field-effect transistor
nc	- nanocrystalline
NC	- nanocrystals
NDC	- negative differential conductivity
OA	- oxygen annealing
OD	- optical density
PF	- Poole–Frenkel
PL	- photoluminescence
PLD	- pulsed laser deposition
rf	- radio frequency
RMS	- root-mean square
RTA	- rapid thermal annealing
RTD	- resonant tunneling diode
RTS	- resonant tunneling structure
SBD	- Schottky barrier diode
SCR	- space-charge region
TD	- tunnel diode
TEM	- transmission electron microscopy

ULSI	- ultra large-scale integration
XPS	- x-ray photoelectron spectroscopy
XRD	- x-ray diffraction
a	- thermal diffusivity
B	- modulus of elasticity
c	- molar thermal capacity
C	- capacitance
d	- spacing between δ-layers
D	- diffusion coefficient
E	- energy; electric field
E_0	- electric field in p-n junction
E_{bd}	- breakdown electric field
E_{eff}	- effective field strength
E_F	- Fermi energy
E_g	- bandgap
f	- frequency
h (= $2\pi\hbar$)	- Planck's constant
$h\nu_m$	- PL peak position
I	- current
I_{ex}	- excess current
I_p	- peak tunnel current
I_r	- excess current
J	- current density
k	- absorption coefficient; dielectric constant (throughout Chapter 5)
k_B	- Boltzmann constant
k_r	- dynamic dielectric constant (throughout Chapter 5)
l	- sample thickness
m^*	- electron effective mass
m_0	- electron mass
n_{eff}	- effective refractive index
n_r	- refractive index
n	- impurity concentration

N	- number of defects in a cluster
N_0	- silicon impurity concentration
N_D	- donor concentration
P	- radiating power
P_{max}	- maximum output power
P_T	- heat power density
q	- electron charge
Q	- *total charge in the* δ_1*-layer*
Q_f	- oxide charge
R	- radius of curvature; inclusion radius
S	- sample area
t	- time
t_i	- irradiation time
T	- temperature
T_0	- temperature at the semiconductor–"inclusion" interface
T_{max}	- maximal heating temperature
T_{ox}	- oxidation temperature
T_s	- *substrate temperature*
U	- diffusion activation energy
V	- voltage
V_{fb}	- flat-band voltage
V_g	- gate voltage
Γ	- LO-phonon peak half-width; broadening parameter
ε	- local deformation
ε_0	- electron energy at a temperature of 300 K
ε_{el}	- electron energy
λ	- wavelength
μ	- charge carrier mobility
ν_m	- PL peak position
ρ	- density
ρ_Λ	- linear density

σ	- intrinsic stress
τ	- electron energy relaxation time
τ_ε	- energy relaxation time
τ_p	- momentum relaxation time
τ_T	- total duration of microwave treatment
χ	- thermal conductivity
φ_b	- Schottky barrier height
ω	- angular frequency (of the electromagnetic field)

PREFACE

The present-day microelectronics is characterized by the tendency for drastic decrease of the geometric sizes of the active device elements. The technological procedures required for manufacturing of such objects may be provided by developing novel technologies, in particular, those using purposeful dosed action on the device structure components [1–16]. The attained level of understanding of the physico-chemical processes occurring at interaction of electrons and ions with solids ensured the leading role in manufacturing of microelectronic devices for the technologies using ion beams and particle radiation [5, 8–10, 17–35].

Along with the noted technological processes, a significant place among the semiconductor technologies is occupied by those which apply microwave radiation. The best known of them are different modifications of the magnetron sputtering technique. They are applied when forming the multilayer metallizations, as well as ohmic and barrier contacts to microelectronic semiconductor devices and integrated circuits [36–38].

An analysis of the engineering and technological possibilities to apply microwave radiation in the production of semiconductor devices shows that the main aspects of the problem concern annealing of semiconductor materials and device structures aimed at provision of control over the structural properties and impurity-defect composition. Following are some of these aspects:

- annealing of radiation defects in semiconductors that were produced by ion doping [39–41];
- low-temperature annealing with a narrow beam of microwave energy of local regions produced by ion doping [42, 43];

- surface microwave annealing of semiconductor materials (involving crystallization of amorphous layers, solid phase recrystallization and melting) [44];
- growth of silicon single crystals in microwave fields [45];
- formation of ohmic and barrier contacts using microwave irradiation [46, 47];
- cutting of polycrystalline silicon ingots into pieces [48];
- gettering of impurities and defects in silicon in the course of treatment in microwave fields [49].

It should be noted also that, along with the above possibilities of technological application of microwave radiation, a big cycle of researches of the problem of interaction of microwave radiation with semiconductors have been performed in recent years. These investigations served to development of the physical foundations of microwave treatments in semiconductor electronics. Some of these works are generalized in the theses made at the N.G. Chernyshevsky Saratov State University [50–52] and V. Lashkaryov Institute of Semiconductor Physics of the National Academy of Sciences of Ukraine [53–58], as well as in [59]. In most of these studies low-power cm-wave radiation was used.

Despite the apparent simplicity of the technologies applying electromagnetic beams (as compared to those using particle radiation), a number of important problems still remain unsolved, thus restricting application of the microwave technologies. These are, e.g., the problem of micrometallurgical processes induced by electromagnetic radiation, defect formation in the semiconductor near-surface layers, appearance and relaxation of thermomechanical stresses at the interfaces between phases, structural phase transitions at the nano- and subnanosecond scale, overheating, etc. Electromagnetic radiation from the 10–100 GHz frequency range practically has not been applied to solve such problems.

The previous investigations of the interaction of high-power electromagnetic beams with semiconductor structures dealt mainly the aspects of their destructive effect [60–64]. At the same time one should note that microwave treatments are promising for develop-

ment of novel semiconductor technologies. The factors favoring such conclusion are as follows:

- a wide range (0.1–10^9 W/cm^2) of radiating power at variation of polarization and strength of the electric field of the electromagnetic wave;
- a possibility to realize both short-time (nano- and microsecond) pulse actions, as well as continuous thermal treatment;
- high controllability and reproducibility of the parameters of microwave radiation (and, as a result, possibility of precise dosing when supplying energy to the active areas of the irradiated object);
- a possibility to ensure uniform treatment of large-area objects;
- a possibility of selective uniform effect on the components of semiconductor device structures;
- non-contact treatment of materials in a vacuum or special media.

The above factors served as foundation for performance of investigations of the effect of microwave irradiation on the structural-chemical and electrophysical characteristics of III–V semiconductor materials and devices made on their basis.

Chapter 1 of this book deals with elucidation of the role of thermal and non-thermal factors in variation of the structural parameters of III–V semiconductor compounds. This is illustrated by the example of GaAs, GaP and InP exposed to high-power microwave irradiation. The data on variation of the point and extended defect concentration, as well as on relaxation of intrinsic stresses in GaAs, GaP and InP bulk and epitaxial structures are obtained. The results on the effect of microwave radiation on the energy spectrum of defect states in CdS single crystals are presented.

Chapter 2 presents the comparative data on the effect of microwave and ^{60}Co γ-radiation on the electrical characteristics of resonant tunneling diodes and tunnel diodes made on the basis of AlGaAs/GaAs heterojunctions and GaAs. The models and mechanisms that are responsible for variation of the device structure parameters are considered.

Chapter 3 deals with the effects in the SiO_2–GaAs structures that are induced by ^{60}Co γ-irradiation or microwave treatment. An analysis

of the mechanisms of modification of the SiO_2–GaAs defect structure under short-term microwave treatment is given. The experimental data on the effect of microwave irradiation on the structural and morphological properties of SiO_2–SiC structures are presented.

Chapter 4 deals with the effect of microwave irradiation on the morphological and structural properties of semiconductor systems "nanocrystalline silicon–silicon".

In Chapter 5 the results of experimental investigations of the effect of microwave and ^{60}Co γ-irradiation on the structural and electrical characteristics of Ta_2O_5–Si heterostructures and MIS structures made on their basis are analyzed and generalized.

Preface, Chapters 1–4 and Conclusion are written by A.E. Belyaev, R.V. Konakova, V.V. Milenin and P.M. Lytvyn. Chapter 5 is written by E.D. Atanassova, in co-authorship with R.V. Konakova, V.F. Mitin and V.V. Shynkarenko.

This book, as the previous one [65], is intended, first of all, for those engaged in development of semiconductor microwave devices, as well as for technologists. So it presents the material that is necessary for understanding of the physical processes occurring at the semiconductor surfaces and interfaces, as well as in the bulk, under action of high-power electromagnetic radiation. The authors will be grateful to the readers for their critical comments and propositions.

* * *

When writing this book, the authors used numerous materials by other researchers published in literature, as well as the results of their joint investigations with the researchers from the Institute of Technical Physics of the Hungarian Academy of Sciences (Budapest), Institute of the Physics of Solids of the Bulgarian Academy of Sciences (Sofia), State Enterprise Research Institute "Orion" (Kiev), Taganrog State Radio Engineering University (Taganrog, Russia) and Institute of Physics of the National Academy of Sciences of Ukraine (Kiev). The authors are sincerely grateful to all of them.

The authors are grateful also to Dr. Phys.-Math. Sci. L.A. Matveeva, Dr. Phys.-Math. Sci. E.B. Kaganovich and Dr. Phys.-Math. Sci.

V.E. Primachenko for cooperation and fruitful discussion of the results obtained, to Cand. Phys.-Math. Sci. O.S. Lytvyn, Cand. Phys.-Math. Sci. O.B. Okhrimenko, Cand. Phys.-Math. Sci. A.B. Kamalov and Cand. Tech. Sci. Ya.Ya. Kudryk who took part in the studies of the effect of microwave irradiation on the device structure parameters, and to the referee Academician of the National Academy of Sciences of Ukraine Prof. Dr. Phys.-Math. Sci. V.M. Yakovenko for his valuable comments and advices.

The authors deem it their duty to especially note the valuable contribution that late Prof. Dr. Phys.-Math. Sci. Irina B. Ermolovich and late Prof. Dr. Phys.-Math. Sci. Dmitry I. Sheka made to understanding of the physical processes occurring at interaction of microwave radiation with semiconductor materials and resonant tunneling device structures. Close cooperation and fruitful discussions with them have afforded great pleasure to the authors of this book, as well as to all those who had luck to communicate with these highly gifted researchers and outstanding persons.

Chapter I

INVESTIGATION OF THE ROLE OF THERMAL AND NON-THERMAL FACTORS IN TRANSFORMATION OF STRUCTURAL PARAMETERS OF III–V SEMICONDUCTOR COMPOUNDS, SiC AND CdS EXPOSED TO HIGH-POWER MICROWAVE IRRADIATION

Thermal and non-thermal actions on semiconductors still remain a wide area of physical and technological investigations and developments. Suffice is to mention rapid thermal annealing (RTA) of semiconductor materials using high-power sources of light pulses. Such RTA is applied, in particular, for annealing of ion-implanted semiconductor layers. Various types of lasers and electron guns are also used for this purpose [1–6]. Non-thermal actions due to irradiation of semiconductor wafers with Cs and Co γ-quanta, high-energy (E = 1−4 MeV) electrons or those electrons whose energy is below the threshold are also used in manufacturing technology of different semiconductor devices [7–9].

Considerable recent attention has been focused on the possible applications of microwave treatments in both manufacturing technology and diagnostics of semiconductor materials and devices [10–13]. The physics of interaction of various radiations with solids makes a serious problem. Of this wide area, we consider here RTA and microwave treatment only (to be more precise, such their modes that are sufficient for production of some structural transformations at the interfaces between phases or in semiconductor bulk but do not lead to material disintegration).

1.1. PROCESSES OF STRUCTURAL ORDERING INDUCED BY MICROWAVE TREATMENT AT THE SURFACES OF GaAs SINGLE CRYSTALS AND CONTACT SYSTEMS ON THEIR BASIS

Considerable interest to study of the mechanisms of microwave radiation effect on semiconductor materials and structures is generated mainly by the following two factors. One of them is the possibility to improve degradation resistance of semiconductor devices and circuits and ensure their high fault-tolerance. Another factor is the possibility to use microwave treatments in the manufacturing technologies for semiconductor materials and structures. During the last few years it was demonstrated that microwave radiation is promising for application at all stages of semiconductor manufacturing, from synthesis of single crystals [10] and deposition of thin films [11] to different techniques used for processing of materials and structures (surface cleaning, complementary thermal and microwave annealings, microwave treatments for controlled variation of electrophysical parameters, etc.) [12–14].

Whereas the effect of thermal annealing on the processes of structural ordering in semiconductor materials and structures has been studied rather well, elucidation of the mechanisms of relaxation enhanced by microwave radiation still needs comprehensive investigations. In this case the energy of electromagnetic wave is insufficient for ionization of atoms or production of various structural defects. It is sufficient, however, to excite the electron subsystem of semiconductor and affect the processes of point defects ordering. A microwave wave that penetrates into semiconductor heats local defect areas in the crystal due to ohmic and dielectric losses. In this case the total increase of object temperature is not big (less than 100 °C).

At the same time, the interaction of microwave field with semiconductor single crystals and structures made on their basis goes beyond the thermal processes. An electromagnetic wave of considerable radiating power (about 100 W/cm^2) excites all the thermodynamic subsystems of an object, and one has to take into account object interaction with electric and magnetic fields, stress fields, etc. when analyzing the ob-

ject behavior. Earlier we have shown [15] that, due to such complex action, one can obtain (at appropriate modes of microwave treatment) structural relaxation in the treated semiconductor single crystals and device structures. Such relaxation is accompanied with improvement of the electrophysical parameters of the treated objects. In this case the duration of microwave treatment (several minutes) is much shorter than that of the traditional thermal annealing. This factor makes microwave treatment a fast and energy-saving technology.

It is known [16] that motion of point defects in a crystal is determined by thermally activated diffusion, with diffusion coefficient

$$D = D_0 e^{-U/k_B T}. \quad (1.1)$$

Here U is the diffusion activation energy, k_B is the Boltzmann constant, T is temperature, and a constant D_0 is practically independent of temperature. The U value depends essentially on the external parameters a (stresses, electric field and other external factors) that determine the state of the system. This dependence enables one to exert control over the rates of thermally activated processes by varying not only temperature but the external parameters as well.

The probability of the elementary acts (whose sequence realizes the corresponding process) is related to the activation energy by the following expression:

$$W(T,a) = W_0 e^{-U(a)/k_B T}. \quad (1.2)$$

So one may expect rather intense processes of structural ordering (induced by microwave field) through diffusion of point defects and their interaction with two- and three-dimensional (2D and 3D) crystal lattice defects, even at moderate heating of single-crystalline objects.

Most of the techniques used in studies of structural ordering in single crystals (x-ray diffraction (XRD), photoluminescence (PL), etc.) are integral (i.e., they give information that is averaged over some volume) or require special preparation of the objects studied, thus complicating investigation of structural ordering on the nanoscale. Combination of integral and local techniques enables one to obtain some quantitatively new information on the processes of structural ordering. For instance, application of XRD and scanning atomic force microscopy (AFM) made it possible to characterize the effect of microwave field on the processes of structural ordering in the near-surface layers of semiconductor single crystals and structures made on their basis.

1.1.1. Structural ordering at the surface of GaAs single crystals

We studied the commercial substrate wafers of Czochralski-grown GaAs (100) и (111) doped with tin and tellurium ($10^{16} \div 10^{18}$ cm^{-3}). The substrate sides were exposed to similar mechanical and chemo-dynamic treatments. We studied also the effect of microwave irradiation on the barrier structures made on the basis of TiB_2–GaAs using magnetron sputtering in the vacuum.

The TiB_2 film thickness varied from 10 up to 100 nm for different test structures. Microwave irradiation was made in the magnetron chamber (radiation frequency of 2.45 GHz, radiating power of 100 W/cm^2) and lasted from several seconds up to several minutes. To compare the effects produced by microwave and thermal treatments, some TiB_2–GaAs samples were exposed to RTA. Halogen lamps were used for this.

The surface morphology of GaAs single crystals and TiB_2–GaAs contact systems was studied with an atomic force microscope NanoScope IIIa (Digital Instruments). The measurements were performed in the contact and tapping modes. The rated radii of probe points were 5–20 nm. The level of residual macroscopic strains in the structures studied, as well as the degree of structural perfection of the GaAs near-surface layers and structural parameters of the metal films that formed contacts, were determined from the XRD results. The x-ray and optical measuring instruments were made on the basis of diffractometers ДРОН-3М. $Cu_{K\alpha}$-radiation was used in all our x-ray measurements.

The AFM patterns of surface areas of GaAs single-crystalline substrates that are shown in Figs. 1.1–1.4 illustrate the dynamics of surface morphology variation under microwave irradiation. To determine

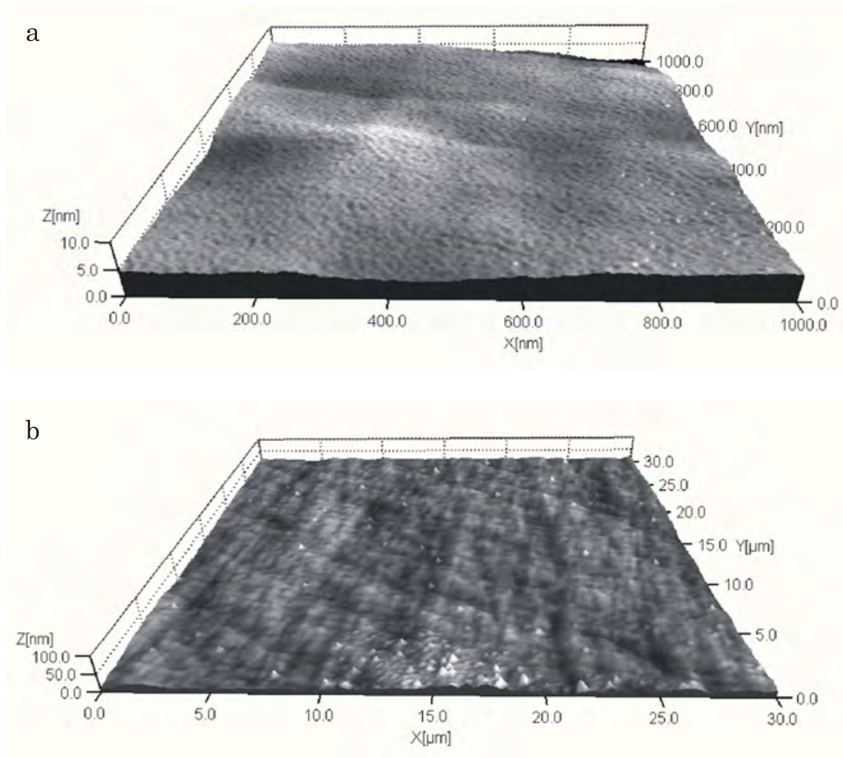

Fig. 1.1. AFM images of the surface fragments of the initial single-crystalline GaAs (111) substrate doped with Te up to a concentration of $3{\cdot}10^{16}$ cm^{-3}. Scan size: a — 1×1 µm (X:Y:Z = 1:1:10); b — 30×30 µm (X:Y:Z = 1:1:20).

how the processes of structural ordering in the near-surface regions of single-crystalline substrates depend on their surface orientation and doping, we studied two batches of GaAs samples, namely: batch 1 – the Te-doped (up to $3{\times}10^{16}$ cm^{-3}) samples with surface orientation (111); batch 2 – the Sn-doped (up to $2{\times}10^{16}$ cm^{-3}) samples with surface orientation (100).

One can see from Figs. 1.1 and 1.3 that there are slight differences between the initial surfaces which can be observed in the imaging region 1×1 µm only (areas a). The surface of the samples from the batch 2 is

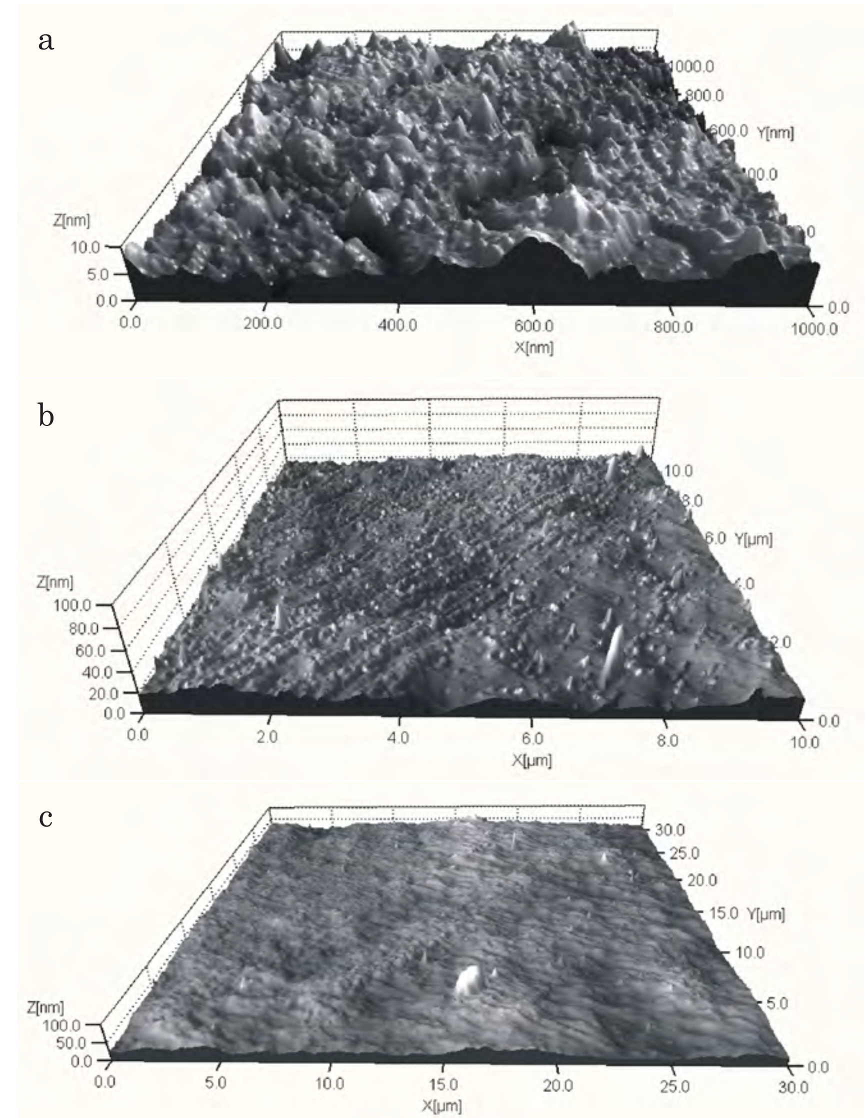

Fig. 1.2.(a,b,c) As in Fig. 1.1 but after microwave irradiation for 20 s. Scan size: a - 1×1 µm (X:Y:Z = 1:1:10); b - 10×10 µm (X:Y:Z = 1:1:20); c - 30×30 µm (X:Y:Z = 1:1:20).

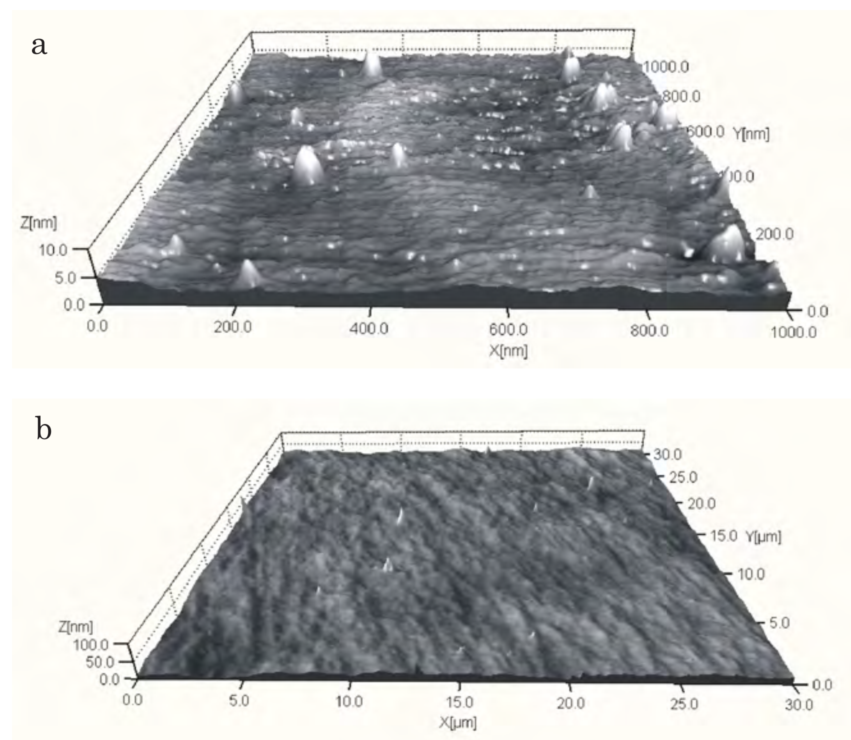

Fig. 1.3. AFM images of the surface fragments of the initial single-crystalline GaAs (100) substrate doped with Sn up to a concentration of $2 \cdot 10^{16}$ cm^{-3}. Scan size: a – 1×1 μm (X:Y:Z = 1:1:10); b – 30×30 μm (X:Y:Z = 1:1:20).

covered with a thicker film of natural oxides that makes the surface nanorelief smoother; there are isolated oxide islands in some places (Fig. 1.3a). However, even in the imaging region 5×5 μm, these surfaces are practically the same; their relief is typical for the commercial wafers that were exposed to chemo-dynamic polishing (Fig. 1.1b, c and 1.3b).

After microwave irradiation during 20 s, the nanosized islands appear at the surface of GaAs single-crystalline wafers. Both density and character of these islands distribution over the surface are substantially different for the samples from the batches 1 and 2 (see Fig. 1.2a

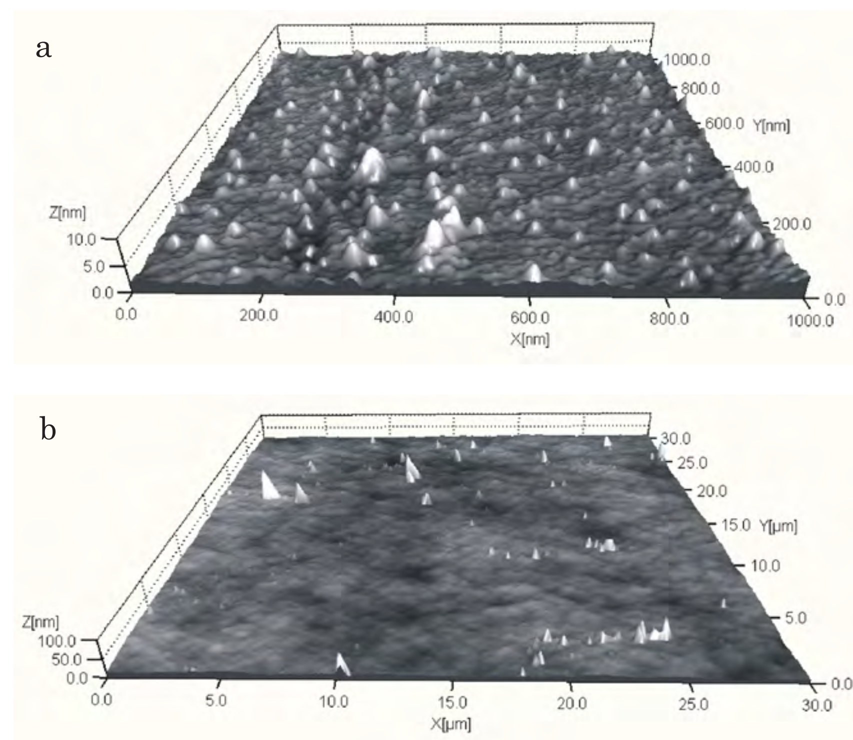

Fig. 1.4. As in Fig. 1.3 but after microwave irradiation for 20 s.

and 1.4a). Taking into account that microwave irradiation is performed in the magnetron chamber at standard conditions (in the air), one can conclude that these islands are most likely the products of reaction between the free gallium and arsenic atoms and atmospheric oxygen. These free atoms appear at the surface because microwave irradiation enhances diffusion of the atomic components of the substrate. Taking into account the data given in [17], one can suppose that the β-Ga_2O_3 and As_2O_3 phases are formed at the surface.

The oxide phases are formed more intensely at the surface of substrates from the batch 1 (Fig. 1.2a). This fact should be related to the surface orientation and slight distinctions in the doping character

for single-crystalline substrates belonging to different batches. At the surface of these substrates one can observe the oxide islands whose thickness is about 5 nm. The surface (111) of GaAs single crystal is polar (i.e., it involves the atoms of one type only – either Ga or As). This fact imposes certain extra conditions on the character of diffusion and oxidation. In addition, the direction <110> is more favorable for diffusion of interstitial atoms. On the single crystal surface one can clearly see the oxide island chains that are ordered along this direction (see the 10×10 and 30×30 μm surface areas - Fig. 1.2b, c).

At the surfaces of single-crystalline GaAs (100) substrates (batch 2) there are separate nanoislands only (with diameter of 5–20 nm and height up to 2 nm). They are distributed uniformly over the surface (Fig. 1.4a). No ordered formations are observed in the imaging region of 30×30 μm. Occasional islands of big size (diameter up to 500 nm and height up to 60 nm) appear.

To obtain confirmation of the assumption concerning the island nature, we studied the concentration depth profiles of the substrate components both before and after microwave irradiation. The initial (before irradiation) substrates demonstrated a thin (several nanometers) near-surface layer that was enriched with oxygen. The interrelation between the Ga and As contents practically does not change up to a depth of 500 nm (Fig. 1.5a). After microwave irradiation for 20 s, the concentration depth profiles demonstrate a considerable near-surface region (enriched with oxygen) where essential changes of arsenic and gallium concentrations occurred (Fig. 1.5b). The depth at which the composition stoichiometry changes is about 250 nm. Along with redistribution of the amounts of the main single crystal components, the dopant concentration in the near-surface layer increased.

Our previous works [8, 14, 15] demonstrated the effect of microwave irradiation on the structural parameters of single-crystalline GaAs and device structures made on its basis. It was shown that almost complete relaxation of stresses in these structures can be obtained in the optimal modes of microwave treatment. In this case transformation occurs at the level of point defects.

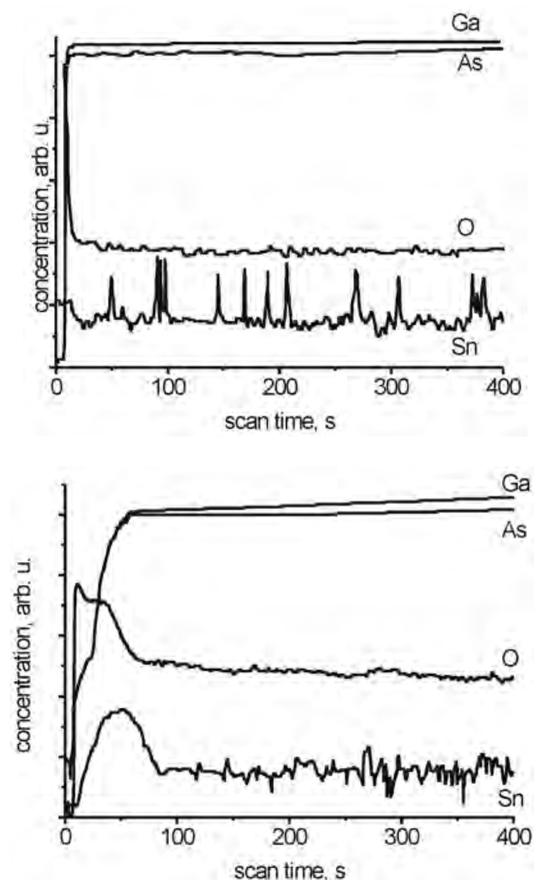

Fig. 1.5. SIMS depth profiles of the GaAs single crystal components before (a) and after (b) microwave irradiation. The crater depth (i.e., thickness of the layer studied) is 500 nm.

Sometimes, when the regions with big gradients of stresses are present, the dislocation structure may change (Fig. 1.6). In this case, according to the results of x-ray topographic studies (that are based on the effect of irregular transmission of x-rays), the dislocation density distribution in the n-n^+-GaAs structure is of weakly pronounced W-shaped type that is not changed by microwave treatments in the

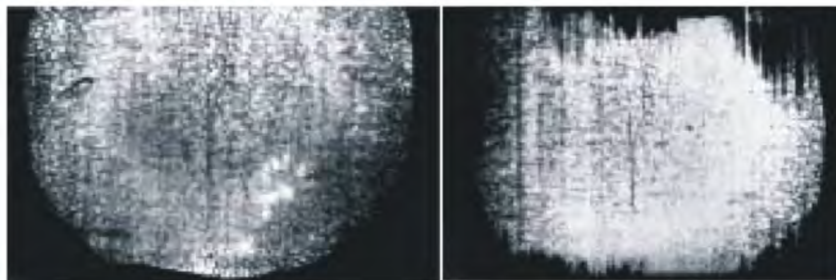

Fig. 1.6. X-ray topogram of GaAs wafer: a – initial, b – after microwave treatment.

above modes. Single dislocations appear and propagate from the substrate boundary into the bulk via the slip planes. The contrast from microinclusions disappears – the inclusions decompose. The changes in the dislocation structure of such samples are accompanied with intense redistribution of structural defects over the sample, which correlate (for device structures with the diode, as well as transistor, layouts) with increase of yield of devices having identical parameters. The experimental data obtained correlate with variation of the radius of curvature in the homo- and heterosystems after microwave irradiation.

The abovementioned results of AFM measurements dealing with surface reconstruction due to microwave irradiation are confirmed also by the results of independent experiments made by other authors. For instance, the amount of free Ga and As atoms at the surface changes considerably due to microwave irradiation (75 GHz, 15 mW, up to 300 s) [18]. The photometric measurements show (see Fig. 1.7) that, even at the first stages of microwave treatment, the mass of free gallium and arsenic decreases by 75% relative to its initial value. As the duration of microwave treatment grows, the mass of free Ga and As atoms at the surface may become half its initial value.

Thus, at first stages, microwave treatment induces formation of bonds between Ga and As atoms, while further (up to 5 min.) treatment leads to progressive damage of the surface and appearance of free atoms of semiconductor components [18].

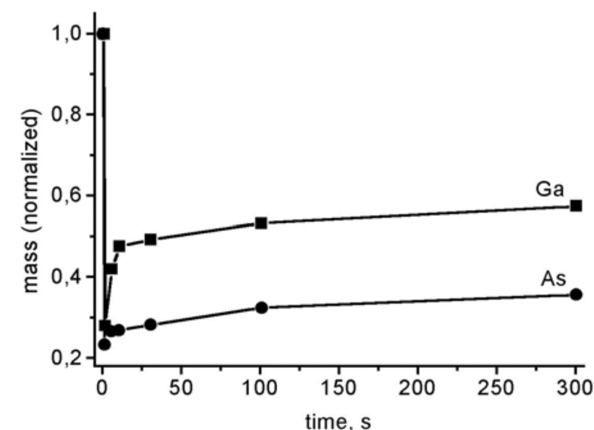

Fig. 1.7. The amount of free Ga and As on the surface as function of the duration of microwave treatment [18].

The free Ga and As atoms may appear at the surface due to the following reasons:

- chemical reactions, say, oxidation [19, 20]. It should be noted that, when oxide film is growing, an electric charge builds up on the GaAs surface. This charge favors penetration of oxygen ions into the oxide film and enhances diffusion of charged point defects from the bulk to the surface [21];
- special surface treatments or epitaxy with excess of gallium or arsenic using in the course of growth [22];
- thermal treatments at which interstitial Ga and As atoms can appear in the bulk and diffuse to the surface [23];
- complex processes of surface oxide layer decomposition or interaction with thin metal contact films [24];
- gradients of residual stresses. In the deformation fields, the interstitial atoms (vacancies) diffuse into the regions of tensile (compressive) stresses [25]. The forces acting on the interstitial atoms and vacancies are proportional to the deformation gradient. The processes of stress relaxation via redistribution of point defects proceed at presence of constant deformation or at heating. The diffuse motion of point

defects can begin and stop not only at free crystal surface but at grain boundaries, stacking faults and dislocations as well, transforming considerably the impurity atmospheres of these structural defects.

Atoms diffuse along the grain boundaries or dislocations and at the surface quicker than in the bulk. Atomic diffusion along dislocations (the so-called tubular diffusion) manifests itself at low temperatures only (when the contribution from diffusion in the bulk into the total diffusion flow is insignificant). This diffusion, realized by the pairs "vacancy–interstitial atom", occurs mainly along the line of vacancies in the extra plane. At excess concentration of vacancies, the drift diffusion flows of vacancies on dislocations take place in the bulk. In the dislocation core, the vacancies adhere to the edge of the extra plane, thus leading to dislocation creep. This seems to be one of the reasons for intense dislocation motion along the slip planes at microwave irradiation (Fig. 1.6).

1.1.2. Structural ordering in the TiB_2–GaAs barrier contacts

The barrier structures on the basis of TiB_2–GaAs were prepared using magnetron sputtering. They were exposed to microwave irradiation in the same modes as the substrate materials.

An analysis of XRD patterns (obtained at grazing incidence) of the TiB_2–GaAs structures showed that all the films studied contained two phases, namely, quasi-amorphous and polycrystalline titanium diboride of hexagonal crystal structure. The preferred crystallite orientation is <0001>. The degree of block ordering in this direction depends on the film thick-ness. The films of smaller thickness demonstrate clearly pronounced texture in the above direction. Formation of quasi-amorphous phase in the polycrystalline films is due to rather low substrate temperature at magnetron sputtering.

The initial surface of metal TiB_2 film is a granular aggregation whose grains, practically are of the same size (about 30 nm), have well-defined boundaries (Figs. 1.8a, b). In some areas, there are circular hollows (up to 4 nm) whose diameterdoes not exceed 1 μm. Some regions of the TiB_2 film may have subnanometer films of foreign phases

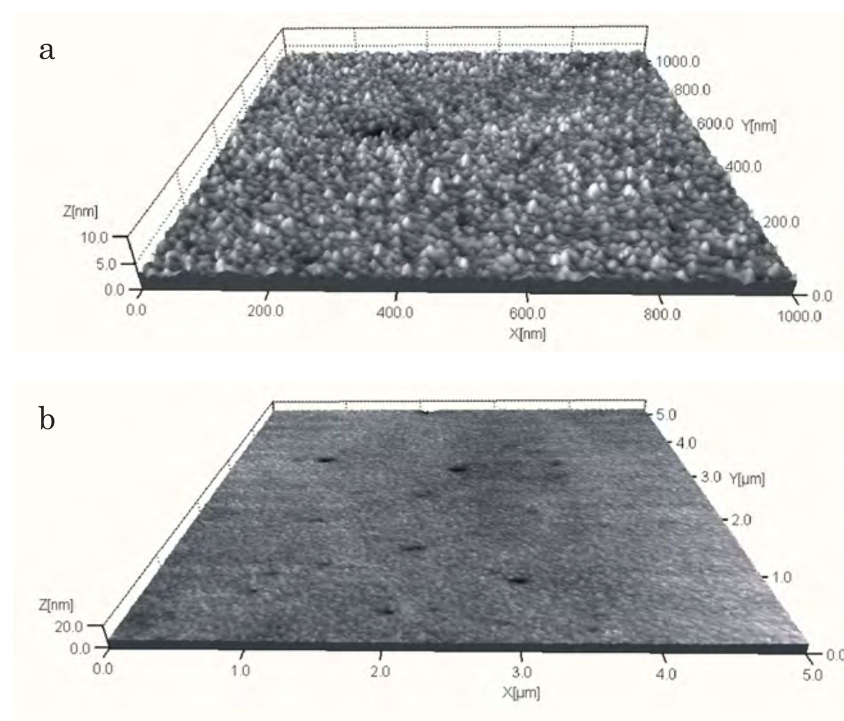

Fig. 1.8. AFM images of the surface fragments of the initial 50 nm TiB_2 film deposited onto the GaAs substrate. Scan size: a – 1×1 μm; b – 5×5 μm. X:Y:Z = 1:1:10.

that somewhat mask small relief details (Fig. 1.9a). In addition, there are protrusions of the surface, with base diameter up to 500 nm and height up to 40 nm.

No considerable changes in surface morphology were found after microwave treatment during 1 s. A weak trend to removal of thin adsorbed layer of foreign phases from the surface can be observed (Fig. 1.10). As treatment duration is increased up to 10 and 60 s, the number of nanoislands at the film surface grows. Their sizes and density are proportional to the duration of microwave treatment (Figs. 1.11 and 1.12). One can clearly see from Fig. 1.12a a trend to organization

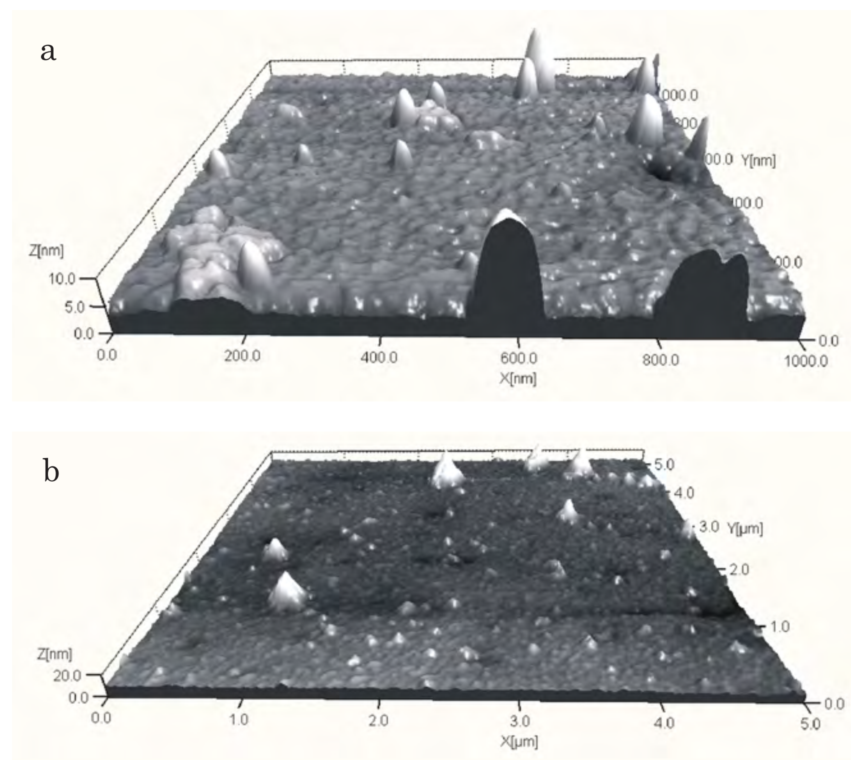

Fig. 1.9. As in Fig. 1.8 but with films of foreign phases.

of these nanoislands in chains along the crystallographic direction <110> of the GaAs substrate. There are strong grounds to believe that the nanoislands on the surface of 50 nm TiB_2 film brought on by microwave irradiation are the oxide phases of substrate components, just identical to those that have been considered by us for single-crystalline substrates.

Even though considerable portion of microwave power is reflected from the metal film and high-conductance region of heteroboundary, still sufficient amount of it is scattered by the single-crystalline substrate in the form of heat. It seems that this heat is the reason for certain heating of the metal film in the alternating microwave magnetic

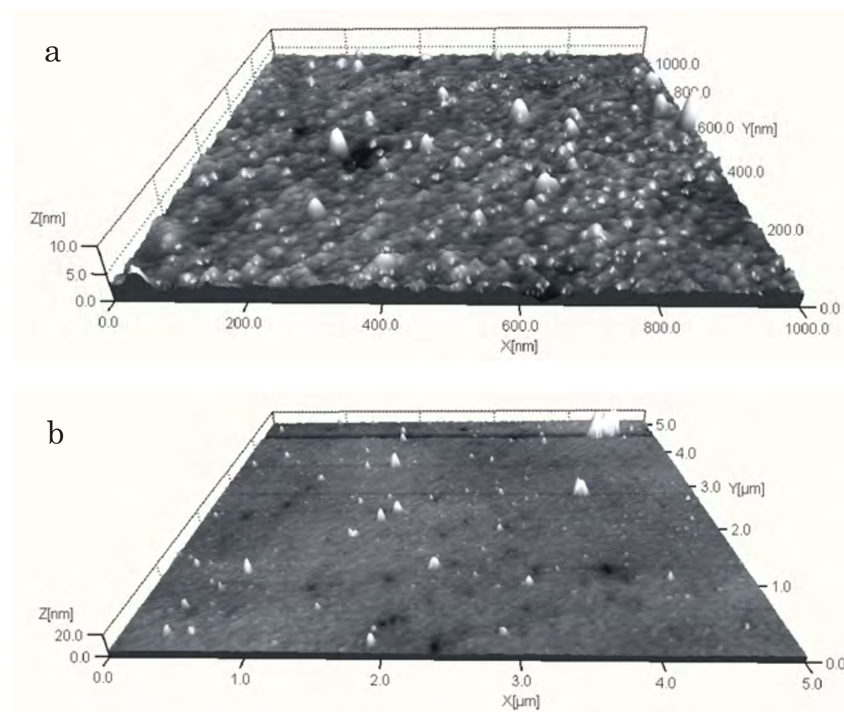

Fig. 1.10. As in Fig. 1.9 but after microwave irradiation for 1 s.

field due to induced eddy currents. Structural defects of various types are collected at the metal–semiconductor interface and grain boundaries in the metal film, and chemical segregation occurs. This serves to increasing atom mobility as compared to the semiconductor substrate bulk. One should expect activation of the diffusion of free atoms of semiconductor near the heteroboundary and over the boundaries of titanium diboride grains whose sizes and structure are suitable for intense grain-boundary diffusion.

Since heating is one of the mechanisms of the effect of microwave field on semiconductor structures, we carried out model experiments on the effect of RTA (for 60 s) on the TiB_2–GaAs device structures. Owing to high resolving power of the AFM technique, we managed

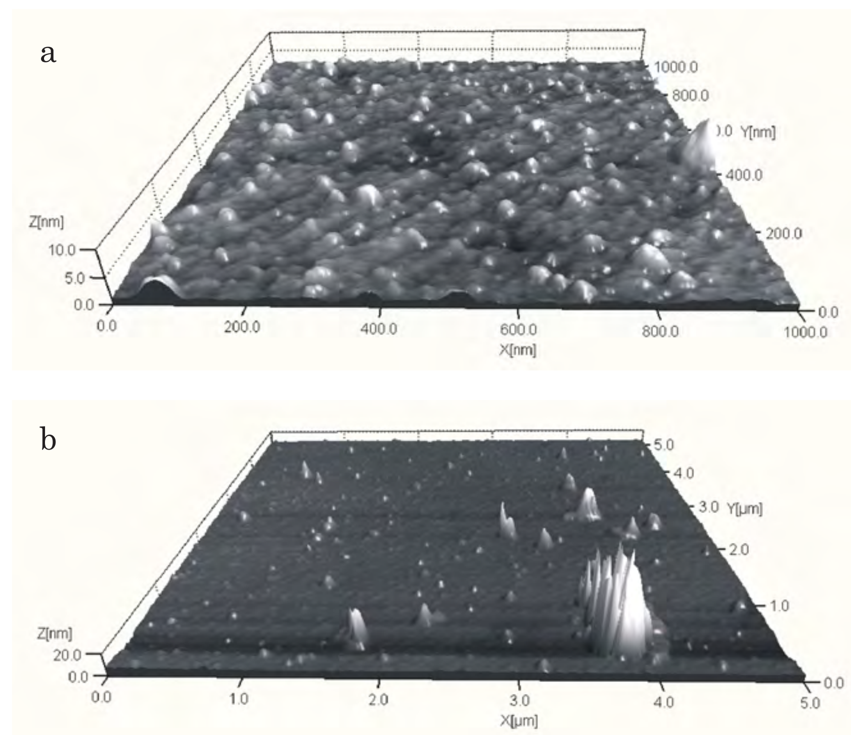

Fig. 1.11. As in Fig. 1.9 but after microwave irradiation for 10 s.

to observe indirectly variation of the point defect density distribution over the cross-section of the TiB_2–GaAs contact system when studying the actual surface of the (110) chips kept in the air atmosphere for 300 h (Fig. 1.13a). It is known that a layer of natural gallium and arsenic oxides is formed on as-cleaved surface of gallium arsenide in the air. Therefore the density of oxide islands may indicate indirectly the distribution of concentration of free Ga and As atoms.

The distribution and density of oxide islands at chips before annealing shows that the unbounded atoms of substrate components are distributed uniformly with the structure thickness, except for the

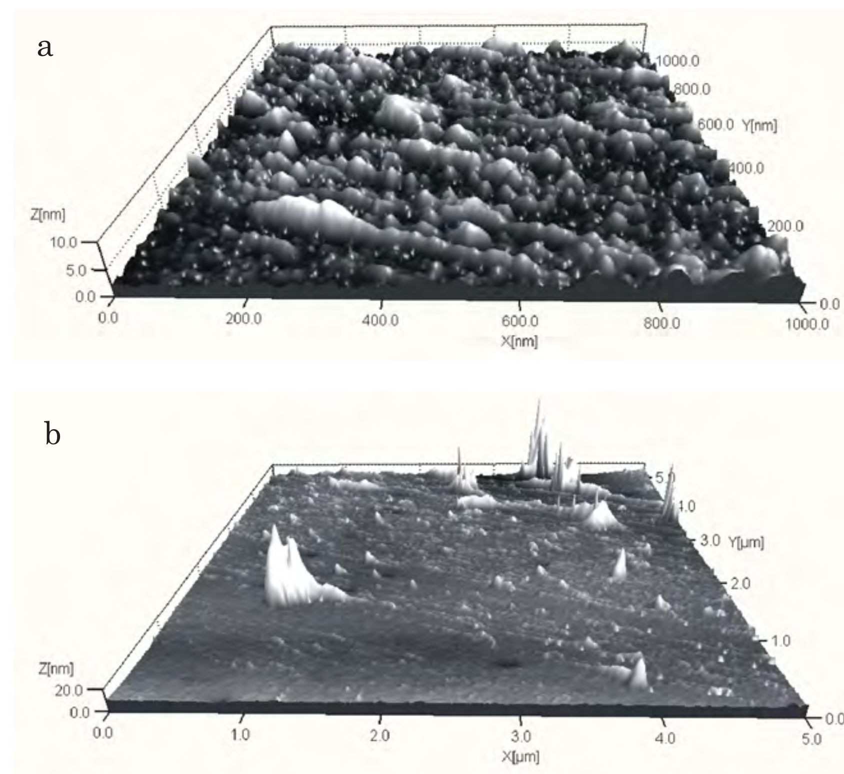

Fig. 1.12. As in Fig. 1.9 but after microwave irradiation for 60 s.

heteroboundary region where the island density and sizes are somewhat smaller (Fig. 1.13a).

The distribution of nanoislands over the chip changes considerably after RTA at 800 °C (see Fig. 1.13b): the area (about 2 µm thick) near the heteroboundary is completely free of the oxide islands. This indicates intense RTA-induced diffusion processes of point defects migration in the deformation fields. These processes are so intense that the interstitial Ga and As atoms are capable of diffusing to the surface of TiB_2 metal film (Fig. 1.14). One can see that the oxide nanoislands line up along the crystallographic direction <110> of the GaAs substrate. It should be noted,

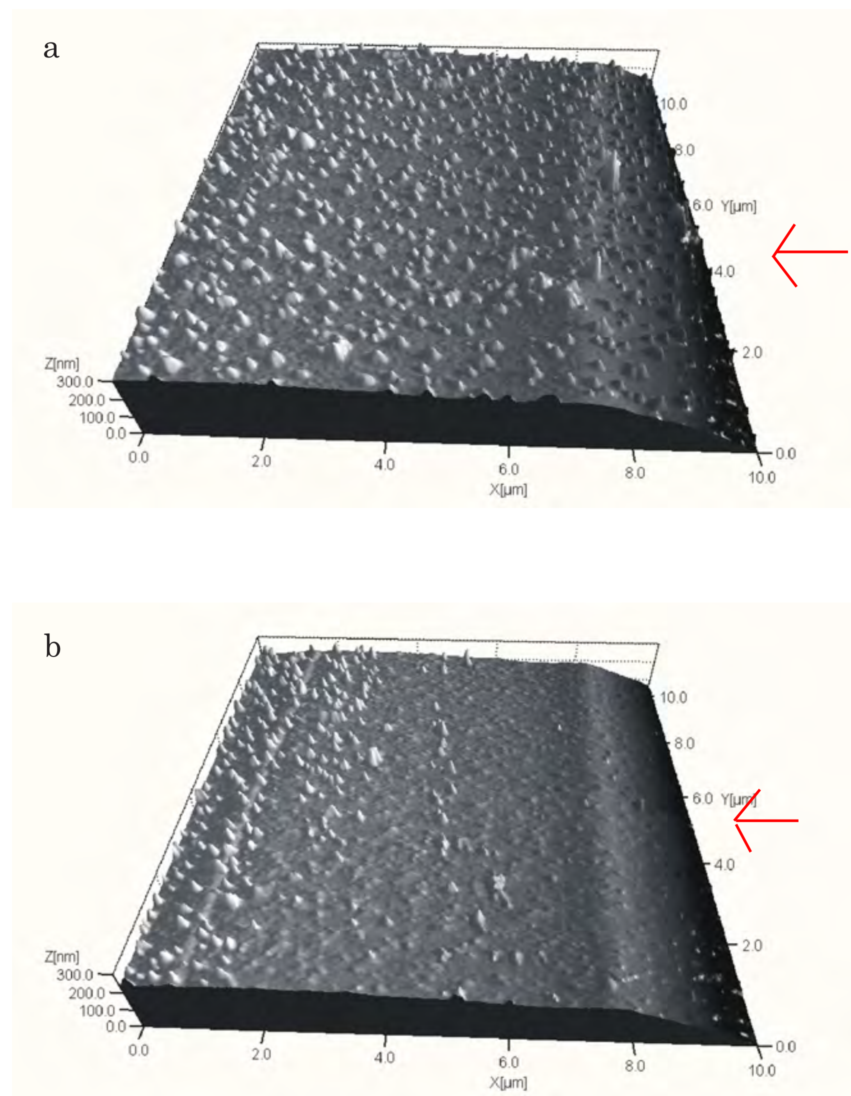

Fig. 1.13. AFM images of the cross section of 10 nm TiB_2 structures sputtered onto the GaAs substrate: a – initial; b – after RTA at 800 °C.

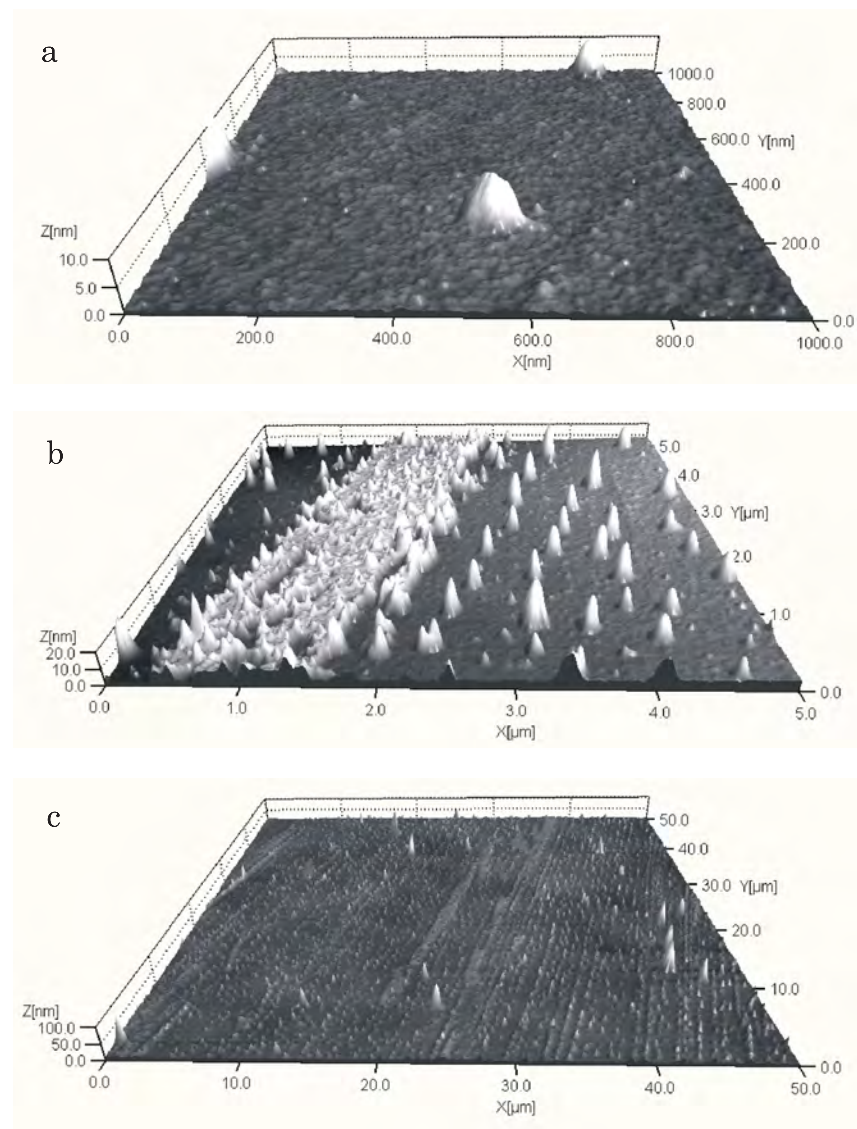

Fig. 1.14. AFM images of the surface fragments of TiB_2 film on GaAs after RTA at 400 °C. Scan sizes are 1 (a), 5 (b) and 50 μm (c).

however, that such situation is not typical for the whole surface. The density and character of such nanoislands distribution are determined by the local deformation fields in the near-surface layers of GaAs substrate.

1.2. DEFORMATION EFFECTS IN THE TiB_2–GaAs (InP, GaP) STRUCTURES INDUCED BY EXTERNAL ACTIONS (RAPID THERMAL ANNEALING, MICROWAVE AND ^{60}Co γ-IRRADIATION)

Our investigations of structural-impurity ordering in GaAs induced by microwave treatments demonstrated that, along with changes of GaAs and TiB_2 surface morphology, there are structural changes in the TiB_2–GaAs (InP, GaP) systems after RTA, microwave and ^{60}Co γ-irradiation. In this case redistribution of the deformation fields and deformation levels occur in the heterosystems studied [30–36].

Redistribution of the deformation fields leads to surface profile variation in the TiB_2 (50 nm)/GaAs structures (Fig. 1.15). Curve 1 shows that the profile of the initial surface is nonuniform and has many bends. Microwave irradiation for 10 s results in appearance of cylindrical bending (curve 2). This fact indicates establishment of a uniform deformation field in the structure studied due to transformation of structural defects and more uniform distribution of them in the substrate and at the heteroboundary. Microwave treatment for longer period (600 s) results in decrease of the radius of surface curvature (curve 3). At the same time, the profile fluctuations are observed which evidence violation of uniformity of the residual deformation fields.

In this case the AFM studies of the TiB_2–GaAs film surface demonstrated essential variations of surface topography after microwave irradiation for 600 s only. Irradiation of the granular surface (that was characteristic of the initial samples (Fig. 1.16a)) results in appearance of a thin (maximal thickness of several nanometers) uniform film on it (Fig. 1.16b). This may be due to oxidation of the substrate components (and, maybe, the metal film) or to other physico-chemical reactions at the metal contact surface. The higher stability of the TiB_2 film is due

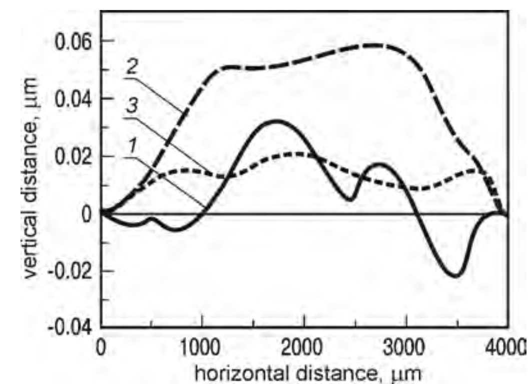

Fig. 1.15. Surface profile of the TiB_2–GaAs structure: 1 – initial, 2 (3) – after microwave irradiation for 10 (600) s.

to the features of its crystal structure. According to the data of XRD analysis, the most part of the film is quasi-amorphous.

RTA promotes more intense processes of structural ordering than microwave irradiation. This fact seems to be related to substantial heat ing of metal contact at RTA resulting in appearance of considerable thermal gradients and intense interdiffusion.

Although the intensity of ordering processes is higher than in the case of microwave treatment, the trend to transformation of deformation fields retains. Shown in Fig. 1.17 is variation of the degree of GaAs substrate deformation with RTA temperature in the TiB_2–GaAs system. One can see that intense stress relaxation takes place at the first stage of thermal annealing (up to 400 °C); however, as the annealing temperature is increased up to 800 °C, structure degradation occurs.

Surface morphology also demonstrates considerable variations. Even at the first stages of thermal annealing, 3D islands are formed at the surface. They are not related to the recrystallization processes in the metal film (XRD studies indicate slight transformations of the quasi-amorphous phase only). As temperature grows, the island sizes increase (Fig. 1.18).

It should be noticed that after microwave irradiation, as well as RTA, oriented chains of other phase may be released in some areas

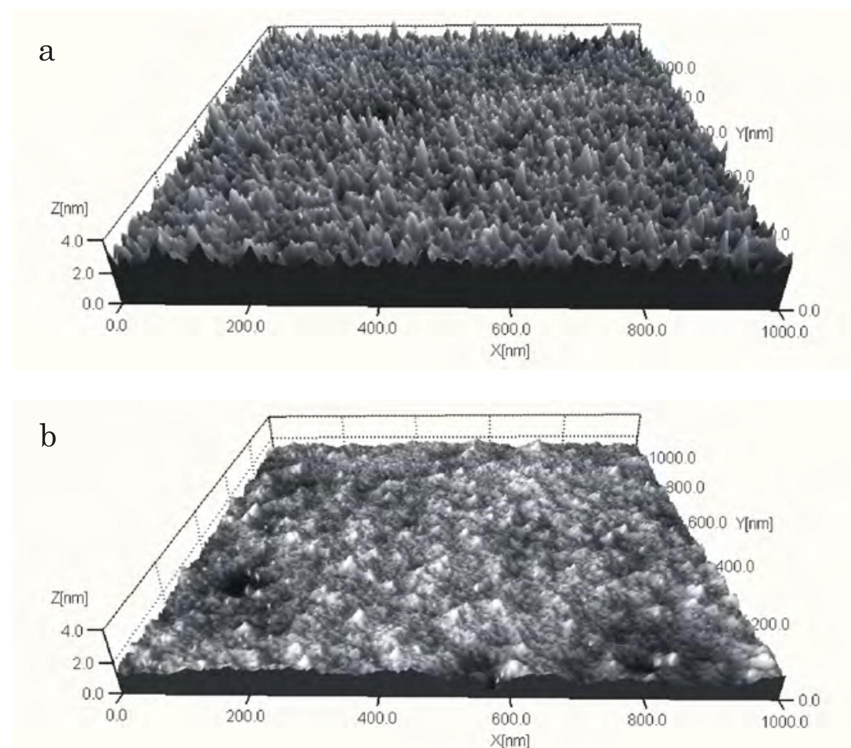

Fig. 1.16. AFM images of TiB_2 film surface: a – initial, b – after microwave irradiation for 600 s. X:Y:Z = 1:1:30.

of the metal film (Fig. 1.19). Most likely this is due to outcropping of substrate atoms in the local regions with high level of stresses. Chemical reactions with atmospheric oxygen can lead to formation of islands of gallium and arsenic oxides.

Table I presents the typical deformation levels in the TiB_2–GaAs (InP, GaP) heterosystems before and after RTA (for 60 s), microwave (frequency $f = 2.5$ GHz, radiating power $P = 1.5$ W/cm^2) and ^{60}Co γ-irradiation.

One can see from the above data that, after short-term thermal and microwave treatments, as well as ^{60}Co γ-irradiation, the deformation level decreases in all the heterosystems studied. In this case, as

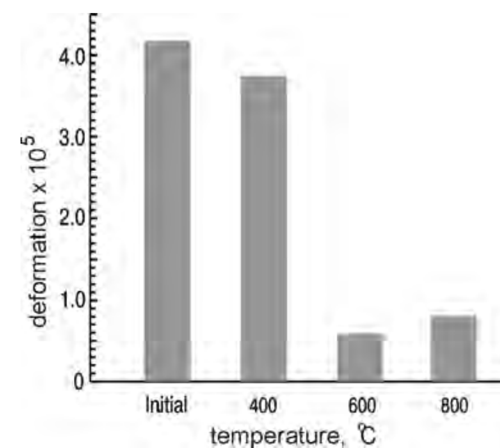

Fig. 1.17. Variation of the deformation level in TiB_2/GaAs structures as function of the 60 s RTA temperature.

was shown by us in [37], decrease of the deformation level after RTA is due to relaxation of intrinsic stresses (ISs) through generation of dislocations in the semiconductor bulk. At ^{60}Co γ-irradiation, relaxation of deformations in the heterosystems occurs due to excitation of the electron subsystem. And the effect of microwave irradiation on the deformation effects in the above heterosystems occurs through several mechanisms [13], in particular, thermal, electrostatic, and electrodynamic ones. Determination of the role of each of the mechanisms makes a separate complicated problem. At the present stage of investigations, we can only establish the fact that the dislocation level in the heterosystems decreases under microwave irradiation, and the predominant mechanism of this effect is non-thermal.

Thus, microwave irradiation of the substrate GaAs single crystals and device structures made on this basis gives rise to intense processes of structural ordering through redistribution of point defects. A major portion of the free atoms of semiconductor components diffuse toward the surface along certain crystallographic directions in the fields of residual stresses, as well as under action of the temperature and electric fields induced by the microwave field. In the case of microwave treatment in the air atmosphere, the islands of natural oxides are formed

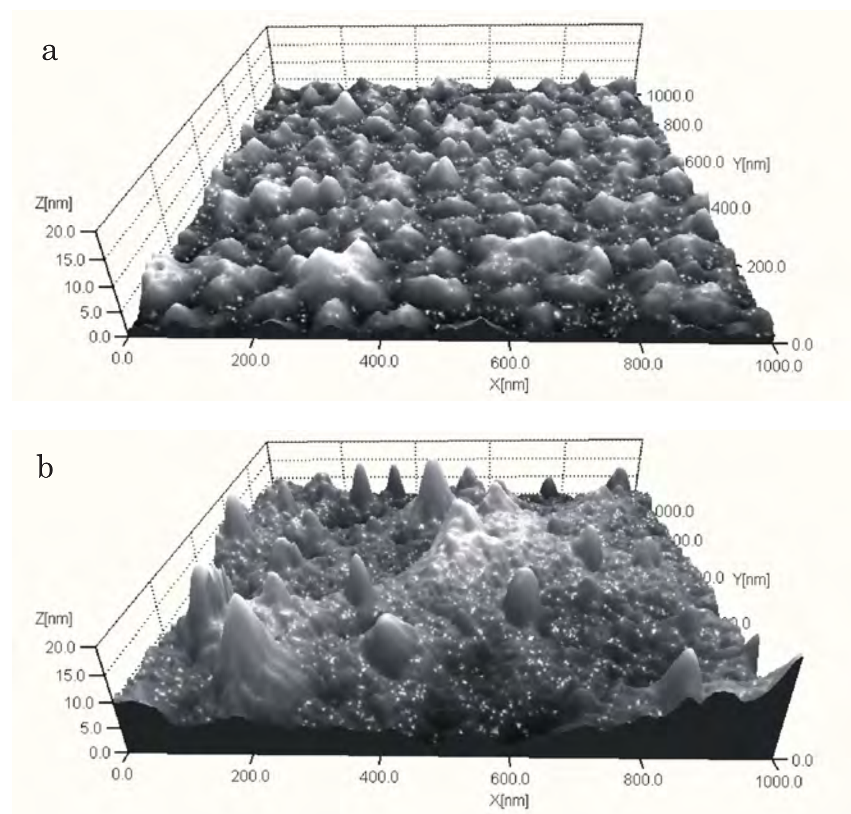

Fig. 1.18.(a) AFM image of TiB_2 film surface after RTA at 600 °C (a) and 800 °C (b). X:Y:Z = 1:1:10.

on the surface of single crystals and contact structures. The density and sizes of these islands are determined by the initial structural parameters of the irradiated material and the modes of microwave irradiation. The effects found are to be taken into account when choosing the microwave treatments intended for improvement of the structural and electrophysical parameters of semiconductor structures. These treatments can be used applied also as technological procedures used to obtain self-organizing nanostructures.

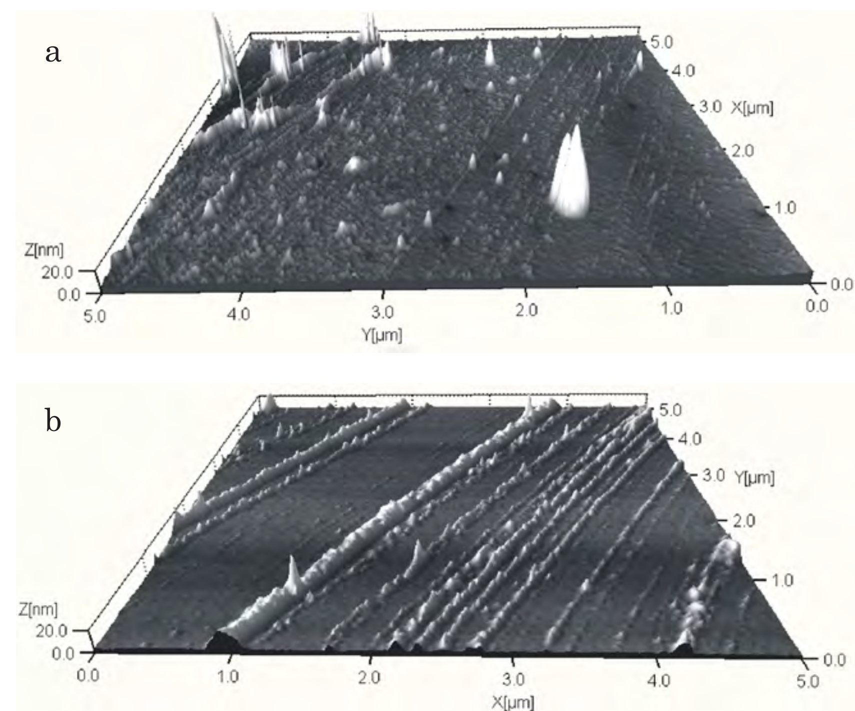

Fig. 1.19. AFM image of the TiB_2 film surface fragment after microwave irradiation for 60 s (a) and RTA at 500 °C (b). X:Y:Z = 1:1:10.

Table 1.1. Deformation levels (×10^5) in the TiB_2–GaAs (I), TiB_2–InP (II) and TiB_2–GaP (III) heterosystems before and after RTA, microwave and ^{60}Co γ-irradiation.

Hetero-system	RTA				Microwave irradiation		^{60}Co γ-irradiation			
	initial	400°C	600°C	800°C	for 1 s	for 2 s	initial	10^3 Gy	10^4 Gy	10^5 Gy
I	4	3.8	0.6	0.8	2	0.7	3.5	3.5	1	0.5
II	2	1.5	0.7	0.2	1	0.7				
III	80	70	50		80	70	70	70	60	60

1.3. STRUCTURAL RELAXATION IN THE n-GaAs AND n-SiC 6H INDUCED BY MICROWAVE IRRADIATION

Microwave treatment may lead to fluctuations of the dopant distribution, as well as to redistribution of the fields of residual stresses and generation of various defects [13]. In some cases, these physical effects may result in variation of the electrical and functional characteristics of semiconductor devices and integrated circuits (ICs).

The effect of microwave irradiation on variation of the electrical characteristics of semiconductor materials and device structures were reported in [1–19, 30–36, 38–46]. It was shown that short-term action of cm-wave radiation leads (at optimal treatment modes) to structural-impurity ordering in the near-contact layer of semiconductor. This results in increase of the diffusion length of the minority charge carriers and thus improves the parameters of the Schottky-barrier diode structures. In this case relaxation of ISs (enhanced by microwave treatment) was also observed [12, 30–36, 43, 45, 48, 49], as well as transformation of the PL spectra; the latter was investigated by Ermolovich et al. [12, 18, 48–51].

In [31, 52–54], to estimate the degree of the effect of similar microwave treatment on the structural parameters of GaAs and SiC single crystals, the samples with different doping levels and initial residual stress levels were chosen. The gallium arsenide single crystals were cut from the 300 μm thick wafers oriented in the (100) plane. The wafers were doped with tin. The electron concentration n in the samples studied was $(1.5\div2.5)\times10^{18}$ cm^{-3} (sample GaAs–1) and $(3\div5)\times10^{16}$ cm^{-3} (sample GaAs–2). The n-SiC samples were obtained using the Lely technique. They belonged to the 6H polytype and were doped with nitrogen. The samples were 490 μm thick wafers with $n = (3\div6)\times10^{18}$ cm^{-3} (sample SiC–1) and 460 μm thick wafers with $n = (1\div3)\times10^{18}$ cm^{-3} (sample SiC–2).

The microwave treatment (frequency of 2.45 GHz, radiating power of 1.5 W/cm^2, duration of 20 s) was performed at room temperature. We measured (both before and after such treatment) (i) the radius of curvature R of the near-surface crystallographic planes of the samples with XRD technique (from the variation of the angular position of diffraction peak at sample translation) [55] and (ii) the surface curvature with a profilometer DekTak 3030 Veeco Instruments. For some GaAs wafers, the character of the structural defects distribution over the surface was studied with the Borrman x-ray projection topography.

The results of our studies of x-ray topography showed that the GaAs single crystal had a nonuniform cellular structure formed by dislocation walls (see Fig .1.20a). The aggregations of dislocations going from the wafer center to its periphery along the <100> direction were observed against the background of the cellular structure. The dislocation density varied along the GaAs wafer diameter from 2×10^4 up to 2×10^5 cm^{-2}. Such nonuniform distribution of dislocation density (Fig. 1.20b) indicates considerable level of elastic deformations in the GaAs samples.

The Si samples studied by us were characterized by low dislocation density (Fig. 1.21). Typical of them are individual growth dislocations radiating outward from the defect regions of the crystal.

As was noted earlier, the degree of a semiconductor single crystal susceptibility to microwave treatment is determined mostly by its initial state. This statement is supported by the results of x-ray studies of topography in the silicon carbide single crystals with low dislocation density and small residual stresses: practically no structural changes under microwave treatment were detected.

The situation in GaAs single crystals is quite different (see Fig. 1.22). At the optimal parameters of microwave action, the processes of defect-impurity ordering are promoted in a uniform single crystal.

These processes are of oscillating type and last for a long (up to several weeks) time [13]. The most drastic structural changes occur during the first day after treatment. These changes do not affect the cellular structure of the crystals studied (see, e.g., a light “loop” at the center of the topogram). However, after microwave treatment the light and dark contrast areas in the topogram (which correspond to the local deformation fields around the structural nonuniformities) become less smeared. This fact indicates relaxation of the residual ISs

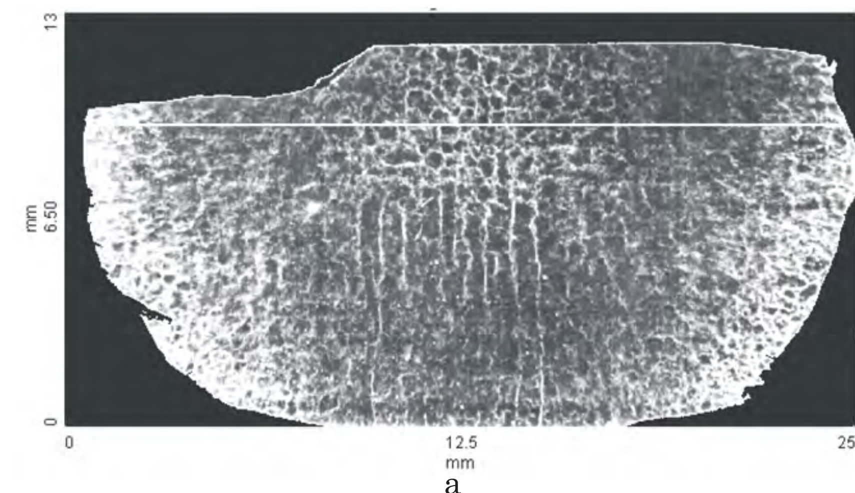

a

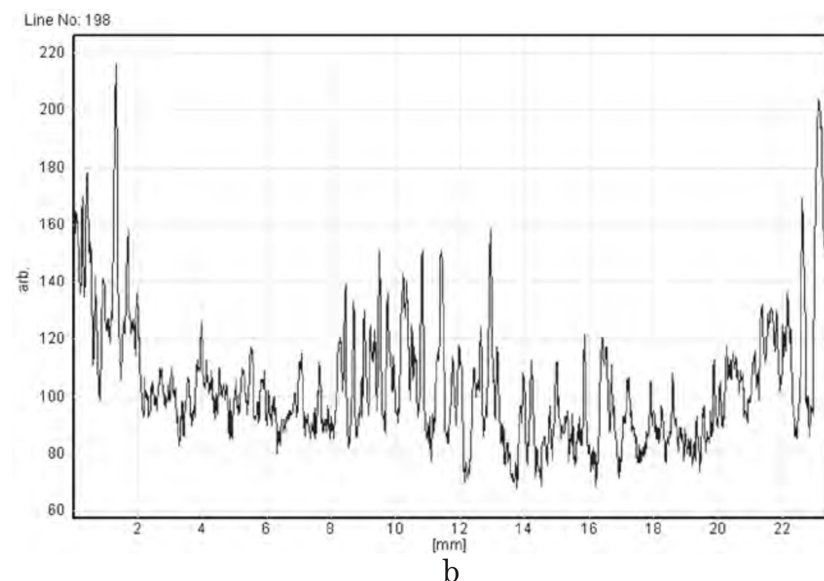

b

Fig. 1.20. a – x-ray topogram of a GaAs single crystal obtained with the Borrman method (irregular x-ray transmission). ($Cu_{K\alpha}$-radiation, reflection 220, the diffraction vector is aligned with the x-axis.) b – transmitted x-ray intensity section clearly demonstrates W-like dislocation density distribution along the wafer diameter.

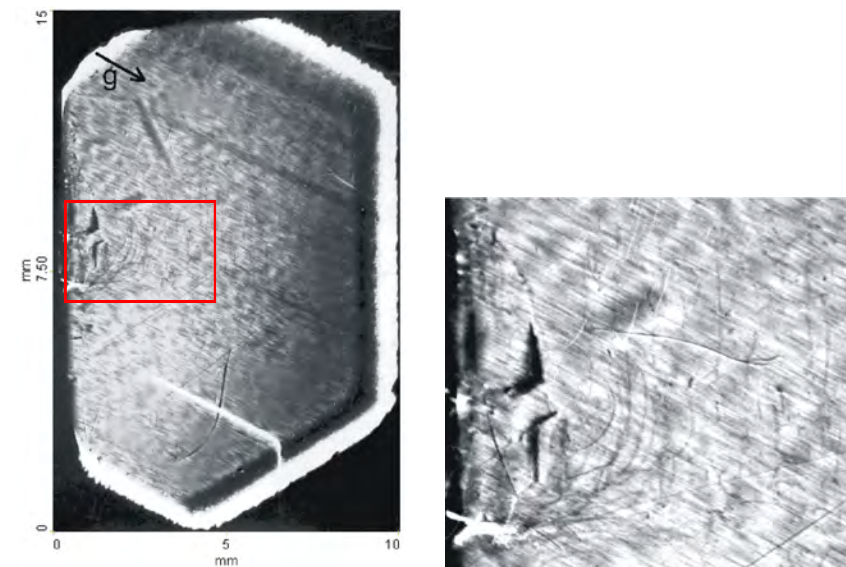

Fig. 1.21. a – x-ray topogram of a SiC single crystal ($Mo_{K\alpha}$-radiation, reflection $11\bar{2}0$, the diffraction vector orientation is shown with an arrow). Inset: a crystal region with dislocations (b –its blowup).

in the crystal. At the same time, additional small (several hundreds of microns) defects appear in some crystal; areas. This fact confirms a possibility of buildup of small dislocations.

Susceptibility to microwave treatment in strongly nonuniform GaAs single crystals is much higher. In this case, the processes of dislocation generation and gliding play a leading part Fig. 1.23). The dislocations generated in the crystal defect area can propagate over the whole crystal in the <110> directions. Their motion is restricted by the initial dislocation structure of the crystal. The dislocations induced by microwave treatment slip over long distances in the areas with low density of growth dislocations.

Obviously, new fields of macroscopic deformations are formed by the above processes of structural transformation induced by microwave treatment. These fields were registered with the x-ray and mechanical

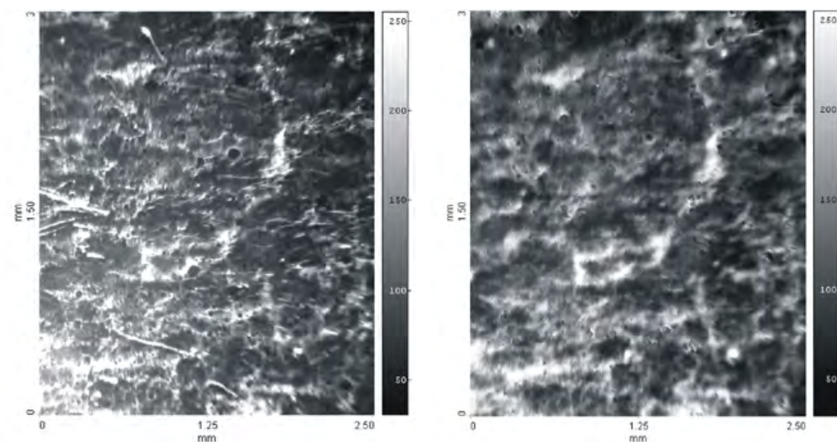

Fig. 1.22. X-ray topograms of a GaAs single crystal obtained with the Borrman method before (a) and after (b) microwave treatment (frequency of 2.45 GHz, radiating power of 1.5 W/cm^2, duration of 20 s). (Cu$_{K\alpha}$-radiation, reflection 220, the diffraction vector is aligned with the x-axis.)

curvimeters from the changes in bending of the near-surface crystallographic planes, as well as the surface profile itself.

The general result of the action of microwave fields on the samples studied was homogenization of the elastic stress fields (establishment of cylindrical of spherical distribution of stresses). It should be noted that the results of our profile measurements correlate with those of the x-ray studies given above. Structural-impurity ordering occurs, at which redistribution of elastic deformations may be accompanied with not only their decrease (as was observed in [13]) but also some increase and more uniform distribution. To illustrate, the sample GaAs–1, according to the results of XRD and profilometric studies, became more uniform and reversed the sign of curvature. And the sample GaAs–2 demonstrated small decrease of the radius of curvature only (see Table 1.2).

The SiC 6H samples also demonstrated changes in the fields of macroscopic deformations after microwave treatments (see Table 1.2). To illustrate, for the sample SiC–1 the radius of curvature (whose initial

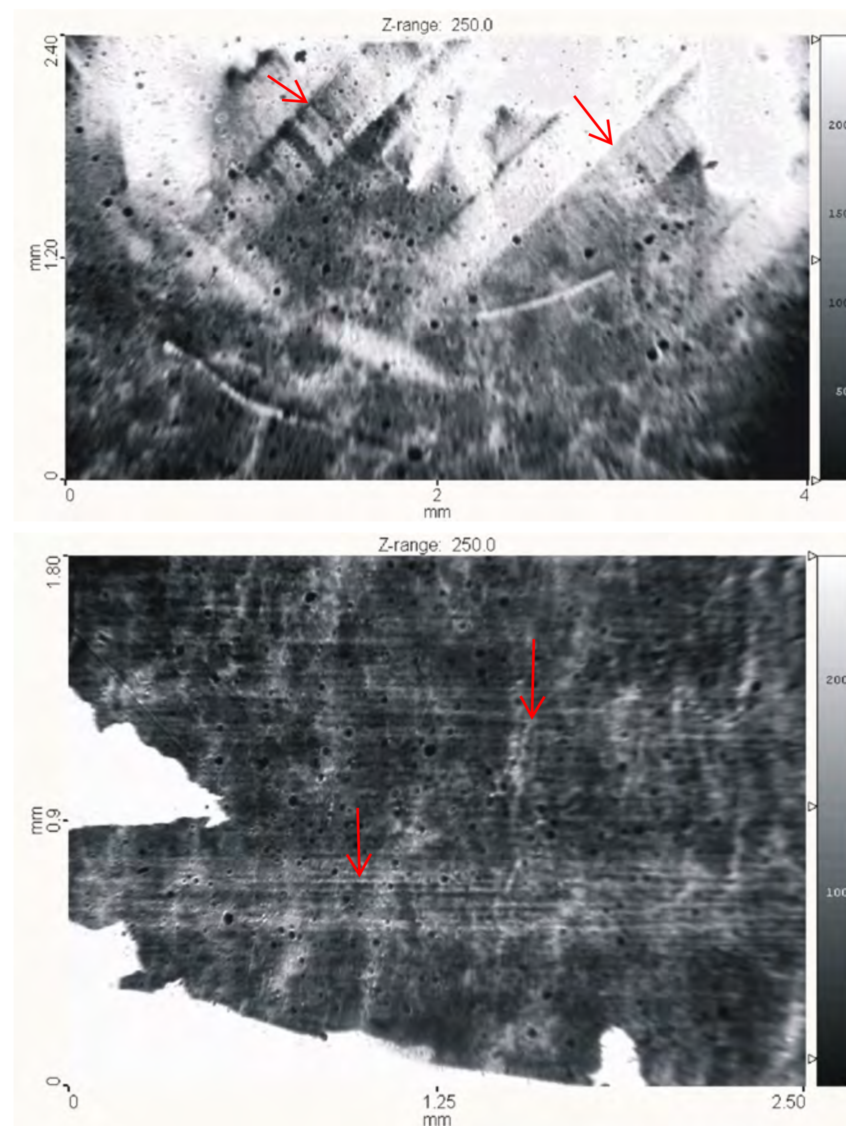

Fig. 1.23. Dislocation slipbands in a GaAs single crystal after microwave treatment (frequency of 2.45 GHz, radiating power of 1.5 W/cm^2, duration of 20 s): regions with higher (a) and lower (b) defect concentration.

Table 1.2. Radius of curvature R and deformation ε in n-GaAs and n-SiC 6H single crystals measured before and after microwave treatment for 20 s.

Sample	State of the sample	Mechanical curvimeter		X-ray curvimeter	
		R, m	$10^6\ \varepsilon$	R, m	$10^6\ \varepsilon$
GaAs-1	initial	−34.15	−4.39	−53.81	−2.79
	irradiated	14.59	10.31	22.92	6.54
GaAs-2	initial	42.06	3.57	17.19	8.73
	irradiated	36.34	4.16	14.73	10.18
SiC-1	initial			> 2000	< 0.12
	irradiated			171.9	1.4
SiC-2	initial			3.8	61
	irradiated			5.5	42

value was big – over 2000 m) decreased down to 171.9. This indicates a rather low level of stresses and absence of considerable structural transformations in this sample. At the same time, for the sample SiC–2 the radius of curvature (whose initial value was small) increased by a factor of about 1.5 after microwave treatment.

It should be noted also that the structural-impurity transformation in the GaAs and SiC single crystals induced by microwave treatment correlates with the experimental data obtained (using the acousto-electric transient spectroscopy) from variations of the activation energy and capture cross-section of deep levels in the same GaAs and SiC samples [31, 52–54].

1.4. EFFECT OF MICROWAVE TREATMENT ON THE IMPURITY-DEFECT STATE OF CdS CRYSTALS

Despite much success achieved in micro- and optoelectronics on the basis of Si and GaAs active elements, the interest in wide-gap II–VI semiconductor compounds and optoelectronic devices made on their basis still persists [56–61]. As a result, the problem of investigation of interaction of electromagnetic radiation with CdS remains actual

nowadays. Of wide-gap II–VI semiconductors, cadmium sulfide is the best known material. A major contribution in growth of this material and investigation of its properties was made by the researchers from the Institute of Semiconductors (at present Institute of Semiconductor Physics) of the Academy of Sciences of the Ukrainian SSR (AS UkrSSR). In this connection, one should note, first of all, the works made by Academician of AS UkrSSR Prof. V.E. Lashkaryov (the first Director of the Institute) [62, 63] and outstanding expert in materials science Prof. I.B. Mizetskaya [64, 65].

The features of the effect of microwave radiation on the electrical and photoelectric properties of compensated nonuniform CdS single crystals and CdS radiation detectors were studied in [66, 67]. The source of microwave radiation was a pulsed magnetron (operating frequency of 50 GHz). The microwave field heated the CdS single crystals up to a temperature of 60 °C. For the sake of comparison, the authors of [66, 67] also investigated (along with the irradiated CdS samples) relaxation of photoconductivity in (i) the similar reference samples (not exposed to any treatment) and (ii) those exposed to the standard gradient heating up to 60 °C. It was found that microwave irradiation induces defect migration in nonuniform crystals more intensely than the standard thermal treatment and electrostatic field applied to the sample. The increase of time of transition from the state with residual conductivity to the state of equilibrium (that was observed after microwave treatment) was related by the authors of [66] to formation of local regions with different conductivities in irradiated CdS single crystals.

A negative photocapacitance effect was observed in CdS radiation detectors exposed to the above microwave treatment [67]. The authors of [67] related this effect to variation of charge state of the electrically-active centers due to microwave treatment.

More close examination of the effect of microwave action on CdS crystals was made by Ermolovich and Red'ko using the luminescence technique [68]. (Unfortunately, this was the last research paper by Prof. I.B. Ermolovich whose research activity dealt with investigation and determination of the nature of the impurity-defect composition of

wide-gap II–VI semiconductors, in particular, CdS crystals obtained using various technological procedures [69–74].) Following are the results of the work [68].

In [68] the effect of high-power microwave radiation on the impurity-defect composition of CdS (a typical wide-gap binary semiconductor) was investigated. The radiation source was a magnetron generator (operating frequency of 2.45 GHz, radiating power of 90 W/cm^2). The exposure was 5 and 15 s. The samples were irradiated in the magnetron work chamber in the air atmosphere.

The impurity-defect composition of the crystals studied was monitored from the spectra of radiation recombination (luminescence) over a wide (0.45–2.5 μm) spectral range at a temperature of 77 K. In addition, the dark resistance and photoresistance were measured at 77 K. The light source was an incandescent lamp (illumination of 100 lx); the filters СЗС-21 and ЖС-17 were used. The above characteristics were measured for both initial crystals and those exposed to microwave irradiation (after several hours).

The mechanism of interaction of microwave radiation with semiconductor CdS crystals is still not understood and makes one of the problems to be studied. The samples for investigation were chosen from (i) the crystals synthesized from. the gas phase (about 100 ∝m thick, with natural smooth surfaces, they had different dark resistance and photosensitivity values) and (ii) the crystals obtained from the gas phase using the vapor-phase free growth technology (bulky boules, of which the samples 0.5–5 mm thick were cut; the surfaces were exposed to chemo-mechanical treatment). The crystals of both types were not specially doped. Those crystals were chosen which differed to the biggest degree in the initial impurity-defect composition: with different dark resistances (high- and low-resistance ones), different bands in the PL spectra, etc. In all, over 20 samples were studied.

It was found, on the whole, that after microwave irradiation the intensity of luminescence increases, the luminescence bands become narrower and their intensities are redistributed. For some samples, new bands appear that were not observed in the initial state of those

samples. Thick crystals demonstrate difference between the radiation recombination spectra measured on the irradiated and opposite sides. It should be noted that such crystals were predominantly low-resistance. So one can draw a conclusion concerning the role of skin layer in absorption of microwave radiation that leads to transformation of the defect states of crystal lattice.

Of many results obtained, the following should be mentioned:

- microwave irradiation for even 5 s results in essential changes in the PL spectra (this is observed more clearly in low-resistance and thick samples);
- in many cases (different luminescence bands) the effect of microwave irradiation is not a monotone function of time; for example, the band intensity decreases after microwave irradiation for 5 s but increases considerably at exposure of 15 s;
- the structure of the excitonic luminescence spectrum very often changes essentially, i.e., the intensities of the bands of free excitons and those bound at the acceptors or donors are redistributed; this indicates variation of the impurity-defect state of the crystal studied under short-term microwave irradiation;
- in all cases (for all the crystals studied) the intensities of the edge green (G, λ_{max} = 0.514 μm), orange (O, 0.56–0.64 μm), red (R, 0.72–0.78 μm), IR–1 (1.03–1.06 μm) and IR–2 (1.52–1.78 μm) impurity-defect PL bands are redistributed; this indicates directly variation of the defect state of the crystals studied under microwave irradiation;
- the most pronounced changes occur for the low-resistance and thick crystals: for some of them, the intensity of the IR–2 band increases by a factor of 10^2 after microwave irradiation for 15 s;
- as a rule, the intensities of the G, O, and R bands decrease for all the crystals studied; in this case the dark resistance drops from 10^7 down to 10^2 Ω·cm. Since the centers of all the above bands are related to the corresponding complexes – donor-acceptor pairs ($[S_i^- + D^+]^0$, $[V_{Cd}^- + Cd_i^+]^0$) [69–71], $[V_{Cd}^- + V_S^+]^0$ and $[Cu_{Cd}^- + V_S^+]^0$ [69, 72–74], one can state that microwave irradiation breaks these complexes, and the appeared donors serve to increase the dark conductivity of the crystals;
- in most cases, the R and IR–1 bands vary in opposite way: when intensity of one band increases, that of another band decreases, and

vice versa. This fact also confirms decay of the complex to which the R band center is related and formation of a separate IR-1 band whose center is related to the V_{Cd} (Cu_{Cd}) complexes [69, 73]. It should be noted that sometimes the intensities of the R, IR–1 and IR-2 bands increase concurrently;

- as to the dark conductivity, some crystals demonstrated its increase, while in other it decreased. We did not manage to determine any general rule for its variation.

The observed changes in the impurity-defect state of CdS crystals of both types are irreversible and persist for 5 years.

Thus, a comparison between the results obtained and previous data concerning the nature of the centers of all PL bands observed in CdS made it possible to elucidate the role of free electrons in the effect of microwave irradiation on the transformation of complex defects (R- and O-centers), as well as increase of concentration of the single vacancy-type defects.

Chapter 2.

EFFECT OF γ-RADIATION AND MICROWAVE RADIATION ON THE ELECTRICAL CHARACTERISTICS OF RESONANT TUNNELING AND TUNNEL DIODES MADE ON THE BASIS OF GaAlAs–GaAs HETEROJUNCTIONS AND GaAs

In recent years the resonant tunneling structures (RTSs) have demonstrated their advantages when being used in various systems for recording and storage of information (SRAM - static random access memory), digital and analog converters, and low-power microwave oscillators. The specific character of RTS enables one to design super-high-speed facilities (up to hundreds of GHz) with extremely low energy consumption.

It should be noted that the electronic (in particular, semiconductor) industry is the principal constituent of the modern economy. The electronic production makes the foundation for development of such sectors as aerospace and automobile industry, telecommunication, consumer electronics, etc. [1–6]. The microelectronic production has made a major contribution to national economic development and improvement of material welfare in many countries. So the necessity of supporting further advance of microelectronics is obvious.

Nowadays there is a trend to provide switch over from micro- to nanoelectronics, because the conventional technologies can no longer meet the growing demands of industry. And the role of RTS as the elemental base for novel generation of the nanoelectronic devices and facilities is unquestionable. The amount of financing of the programs on RTS by the European Commission may serve as evidence of the above statement. At

a period of 1994–1998 the European commission appropriated almost €100 million for researches in nanotechnology. The following specialized programs involving researches of RTS were financed in 1997–1998: Esprit (information technologies) — €6 million; Brite (materials) — €4 million; SMT (surface mounted technology) — €2 million; Biomed (medical applications) — €2 million; Biotech (biological and genetic applications) — €4 million (see, e.g., "Technology Roadmap for Nanoelectronics", ed. by R. Compañó, EC, Luxembourg, 2001).

Great interest in the above problems has been expressed at the same period (1996–1998) by the United States. This interest was supported by vigorous activity of the special US Government Commission and World Technology Evaluation Center [7]. However, long before the nanotechnology boom of the late nineties, a considerable contribution to the development of nanotechnologies has been made by the Soviet researchers A.V Rzhanov, Zh.I. Alferov, S.I. Stenin et al. [8–10]. Further evolution of these works in Russia resulted in development and practical realization of a number of National Programs on nanophysics and nanoelectronics which led to progress in the submicron semiconductor electronics (in particular, due to application of RTS).

It should be noted that progress in semiconductor nanotechnologies and nanophysics of semiconductors owes in many respects to the earlier investigations of real and atomically clean surfaces and contact phenomena in spatially-nonuniform metal (dielectric)–semiconducto r systems that were performed in the seventies by V.B. Aleskovsky, V.F. Kiselev, S.F. Timashev, K.K. Svitashev, O.V. Snitko, B.A. Nesterenko, V.I. Strikha et al. in Leningrad, Moscow, Novosibirsk and Kiev (USSR) [11-16].

RTS have a number of advantages over the traditional microwave devices and facilities, in particular, (i) high operation speed due to very small characteristic times of tunneling processes, (ii) presence of a negative differential conductivity (NDC) which makes it possible to use RTS in analog circuits as filters and oscillators, (iii) presence of at least two working points with positive differential conductivity that are separated by the current peak on the $I–V$ curve (this fact makes RTS an

ideal element of ICs intended for two-valued (and even many-valued) logic [9, 17-29]. There are two well-studied solutions for realization of charge carrier tunneling with the above-mentioned properties, namely, (i) tunnel diodes (TD) - interband tunneling in a p-i-n junction, and (ii) resonant tunneling diodes (RTD) – intraband tunneling in multilayer heterostructures with thin layers of a wide-gap semiconductor that are separated with layers of a narrow-gap semiconductor.

The concept of transistors with lateral tunneling has been developed too. However, a vertical architecture is usually applied in RTS. This enables one to reliably monitor layer growth with molecular-beam epitaxy (MBE) or metal-organic chemical vapor deposition (MOCVD) and form lateral layout with lithography. In this case the structure size along the tunneling direction may be about several monolayers, while the lateral sizes are determined by the capabilities of the lithography technique used.

TDs are diodes with heavily doped contact layers. The NDC mode in such diodes was observed for the first time by Esaki in 1958. Interband tunneling occurs at coincidence of the energy bands filled with electrons (holes) in the conduction (valence) band in the extremely doped contacts. The tunnel barrier thickness (and hence the current density) are determined by the undoped layer thickness, impurity concentration in the contacts, bandgap values in the semiconductors used, and applied voltage. When the bias is close to zero, then $I–V$ curve is of ohmic character. As the forward bias increases, a mode comes at which the above energy bands fall into the bandgap of the opposite contact. This leads to current decrease with bias voltage, i.e., to the NDC mode.

RTDs also are a facility whose concept is based on intrinsic multistability and (extremely small) characteristic times of tunneling. This makes it possible to use RTDs in very compact circuits of the GHz range. The NDC mode in RTD is realized after the electrons injected from emitter finished their resonance passing via a quasi-stationary state in a quantum well. At appropriate choice of structure parameters, one can obtain several NDC portions of $I–V$ curve. This opens good

Table 2.1. Comparison of tunneling devices parameters.

Parameter	High-speed RTD logic	Low-power RTD memory	Scaled RTDs
	Demo/Forecast	Demo/Forecast	Demo
Peak-to-valley current ratio	4/3	2/3	3
Peak current density (kA/cm^2)	40/10	0.0002/0.0001	10
Minimum feature size (μm)	2/0.2	0.5/0.2	0.05
Peak voltage (V)	0.35/0.16	0.2/0.2	0.2
Maximum clocking frequency (GHz)	12.5/6.25	592/56.8	6.25
RTD time constant (ns)	0.02/0.04	422/4.4	0.04

prospects for RTD application in the systems with many-valued logic. Now the manufacturing technology for RTDs made on the basis of III–V compounds is well developed and makes it possible to ensure rather wide realization of the potentialities of these quantum devices.

The RTD structure depends in many respects on what are the diode functions in an IC. For instance, if RTD is used in the high-speed logic units, one has to ensure the peak current level over 10 kA/cm^2 at a locking frequency of about 10 MHz. But if RTD is used in the low-power storage systems, then it is necessary to ensure the peak current level below 0.2 A/cm^2 and a locking frequency of about 0.5–1 MHz.

The progress in RTS application, as well as the problems to be solved, are illustrated by the data given in Table 2.1 (see "Technology Roadmap for Nanoelectronics", ed. by R.R. Compañó, EC, Luxembourg, 2001). Here the main parameters of RTDs (made on the basis of III–V compounds) are given, both achieved at present and predicted for the nearest future.

The tasks in TD application that exist at the moment refer to solution of the problems dealing with optimization of the TD parameters. The aim is to obtain the best characteristics, namely, (i) high (> 10 kA/cm^2) current densities, (ii) high ($(I_p/I_v > 3)$ peak-to-valley current ratios, and (iii) improvement of the capacitive characteristics. The solution of these problems, as well as investigation of the degradation processes and the effect of external factors (in particular, radiation action) on the operating parameters of the above devices, make one of the stages of the studies considered in this book.

2.1. RADIATION EFFECTS IN RESONANT TUNNELING DIODES EXPOSED TO ^{60}Co γ-RADIATION AND MICROWAVE RADIATION

In recent years intense investigations of the effect of ionizing radiation on the properties of various semiconductor materials (in particular, GaAs and AlGaAs that are the basic materials of the modern microelectronics) have been performed. Each of the effects resulting from different types of radiation action has its own peculiarities. However, most of the studies in this area use γ-irradiation. The reasons for such choice are as follows. First, in this case it is possible to form the radiation defect pattern which is rather complete and common for all the types of irradiation. Second, such technique demonstrates wide experimental possibilities, namely, performance of experiments in situ, wide temperature range, possibility to carry out the measurements immediately after irradiation, etc.

The radiation effects in semiconductors have been investigated for a long time, and a great body of date has been gathered. To illustrate, it has been determined surely with the DLTS (deep level transient spectroscopy) technique [30–32] that, when *n*-GaAs is bombarded at 300 K with 1 MeV electrons, the donor centers are produced whose energy levels are 0.08 (E_1), 0.19 (E_2), 0.45 (E_3), 0.76 (E_4) and 0.96 eV (E_5). Increase of irradiation dose results in appearance of deep traps whose energy lies 0.13 eV below the conduction band bottom. In this case the rate of charge carrier removal depends practically linearly on the total irradiation dose. The results obtained for AlGaAs are rather scarce. It was stated (practically by all the authors) that, along with

production of deep traps with activation energy of about 0.76 eV, the DX-centers were present.

Change of concentration of interfacial states in the GaAs–AlGaAs heterojunctions exposed to -irradiation is the dominant reason for variation of the parameters of 2D channel (charge carrier concentration and mobility). An analysis of the radiation effects in semiconductor devices is a rather complicated problem because one should take into account the layers of different semiconductor materials, interfaces metallizations, etc. One should note that variation of the device parameters depends not only on the device functional tasks but on its design and principle of operation as well. For instance, the dose rate value affects essentially generation of photocurrents. These photocurrents may lead to a shift of switching voltage in the logic devices, thus resulting in degradation of logic circuits. At the same time, the MOS designs and bipolar devices are rather insensitive to the dose rate but response strongly to the total dose of irradiation. As a result, the doses of about 10^5–10^6 Gy are critical for the lateral transport devices. As to the vertical transport devices (e.g., RTD), there were practically no data on the effect of radiation on their efficiency. Nevertheless, one may assume that the effects related to the total dose are predominant.

Our investigations supported the above assumption and also demonstrated high radiation tolerance of RTDs [33, 34]. The samples were irradiated with Co^{60} γ-quanta at room temperature. The RTD *I–V* curves taken at 77 K, both before and after γ-irradiation, are presented in Fig. 2.1. No noticeable changes of *I–V* curves occurred at low (up to 10^6 Gy) doses. (It should be noted that conversion of conductivity in bulky samples of gallium arsenide was observed at equivalent irradiation doses.) Variations of operating parameters in our RTDs were observed only when the irradiation doses exceeded 10^6 Gy. Moreover, an improvement of such parameters as peak current and the peak-to-valley current ratio was observed at γ-irradiation doses up to 5×10^6 Gy (Fig. 2.2). Further increase of dose led to progressive degradation of the RTD parameters. However, our RTDs retained their serviceability even after irradiation with a dose of 2×10^7 Gy (Fig. 2.3).

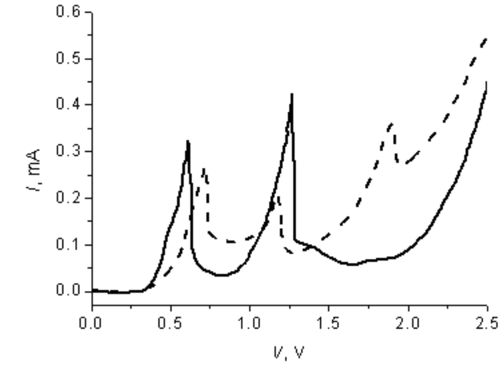

Fig. 2.1. Forward branches of *I–V* curve of RTD structure at 77 K (dotted curve – after γ-irradiation up to a dose of 2×10^7 Gy).

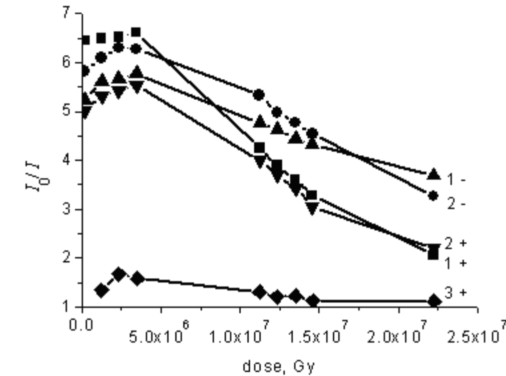

Fig. 2.2. Peak-to-valley current ratio at different irradiation doses (+ - forward branch, – - reverse branch) at 77 K.

Our investigations enabled us to determine the main factors of radiation action on RTDs. It was noted earlier that RTD is a sequence of thin layers of different semiconductor materials with different doping levels. The principal effect of the irradiation action is removal of the majority charge carriers. Therefore, taking into account that the measured removal rate is about 10^6 cm^{-1}, one can conclude that heavily doped ($N_d = 10^{17}$ cm^{-3}) layers do not change considerably the electri-

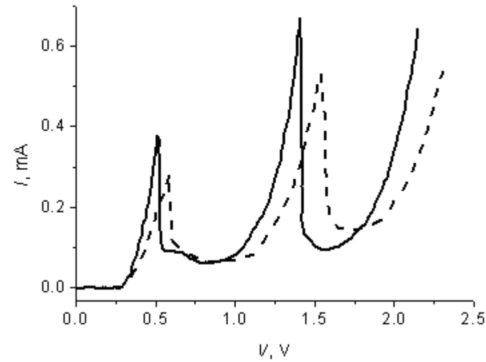

Fig. 2.3. Reverse branches of *I–V* curve of a RTD structure at 77 K (dotted curve – after γ-irradiation up to a dose of 2×10^7 Gy.)

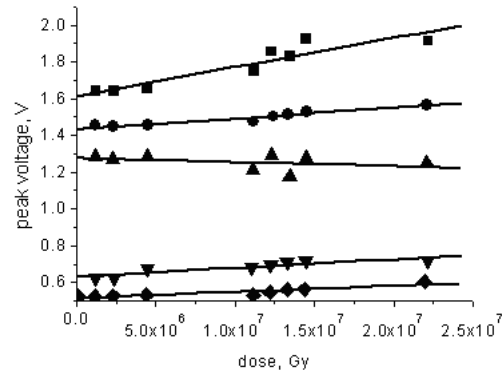

Fig. 2.4. Position of voltage peaks 1, 2 and 3 at 77 K: square (1), circle 2) and triangle (3) (filled marks – forward branch of *I–V* curve).

cal parameters up to irradiation doses of 10^7 Gy. In this case most of the irradiation effect is produced on the undoped (active) part of the structure. This leads to an increase of its resistance and change of the potential profile. As a result, the peak voltage shifts towards bigger values, and the resonance current decreases (Fig. 2.4).

One should note one more aspect related to action of radiation. We found that γ-irradiation leads to considerable decrease of Au–AuGe

contact resistance. This effect is due to intense diffusion of Ge into GaAs and solution of Ga in the Au film. As a result of radiation-enhanced diffusion of the heteropair components, the concentration depth profiles in the contact regions change. This, in its turn, leads to redistribution of voltage (depending on the structure) which leads to variation of the *I–V* curves. The above effect becomes noticeable at irradiation doses over 10^7 Gy.

Thus our investigations proved that radiation tolerance of RTDs is better than that of the devices which use lateral transport. This result opens good prospects for RTD application in those devices which operate under rather high radiation.

Another aspect related to investigation of the effect of external actions is determination of the effect of microwave irradiation on the RTD operating parameters. The problem is of importance for the following reasons. First, RTD is considered as the elemental base of the microwave devices. Therefore one should know how electromagnetic irradiation (either internal or external) affects the main RTD characteristics. Second, microwave treatment is used as technological technique for purposeful variation of the parameters of an initial semiconductor material, as well as finished product. At present there exists practically no such information dealing with RTDs.

To study the effect of microwave treatment on the RTD operating parameters, high-quality GaAlAs/GaAs/GaAlAs double-barrier resonant tunneling diodes (DBRTDs) were used [35]. The structures were grown by molecular beam epitaxy (MBE) on the GaAs (100) substrates. The layer structure was as follows. The active part of the devices consisted of two 1.7 nm $Al_{0.3}Ga_{0.7}As$ layers and a 5.6 nm GaAs layer in-between. In order to achieve flat-band conditions in the resonance, p^--GaAs (5×10^{14} cm^{-3}) spacer layers were also incorporated into the structure on both sides. The emitter part was grown with the following layer sequence (beginning from the substrate): 50 nm n^+-GaAs layer (3×10^{18} cm^{-3}), 70 nm graded-doped GaAs layer (from 3×10^{18} cm^{-3} down to 10^{17} cm^{-3}), and 14 nm p^--GaAs spacer layer. After having grown the active part of the structure, the growth was followed with a 1.5 nm

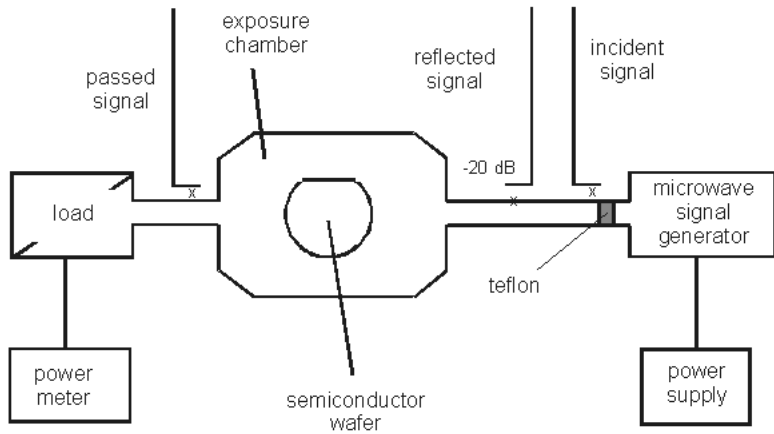

Fig. 2.5. The setup for microwave treatment.

p^--GaAs layer, then with a 50 nm graded-doped GaAs layer, and at last the growth was completed with a 50 nm n^+-GaAs layer. The doping levels of this collector part were the same as in the emitter part of the structure. Then 80 to 100 μm diameter mesas were prepared with evaporated GeAuNi contacts.

The microwave heat treatment was performed in a set-up shown in Fig. 2.5 (cf. [36, 37]). The sample to be irradiated is placed into a waveguide resonator with cross section of 45×90 mm^2. 3 kW power (approximately (40–80) W/cm^2 on the samples) at 2.45 GHz is provided with a continuous wave (CW) magnetron. The incident, reflected and transmitted signals were monitored with the help of –30 dB directional couplers. The transmitted microwave energy is dissipated in a water-cooled matched load connected to a calorimetric power meter. The exposure chamber and the waveguides were separated by Teflon windows. The microwave treatments were carried out for various periods (up to 20 min.). During the treatment the exposure chamber was flushed with a mixture of nitrogen and 5% hydrogen.

The DBRTDI–V curves were taken (before and after the microwave treatment) using the conventional DC technique and also with the transient pulse technique [38, 39]. This latter method is especially useful to overcome the difficulties posed by oscillations, hysteresis and jumps in the I–V curves in the NDC region.

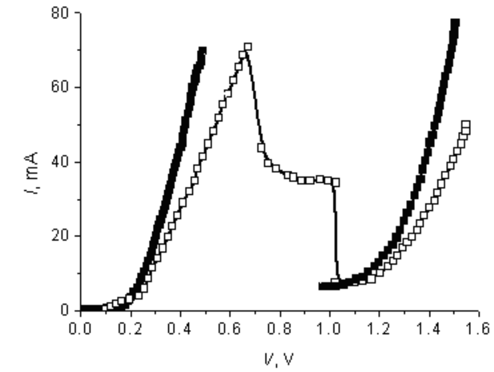

Fig. 2.6. Static I–V curves of RTD taken before (open marks) and after (filled marks) microwave irradiation for 14 min. (frequency of 2.45 GHz, magnetron power of 50 W).

Shown in Fig. 2.6 are typical DBRTD I–V curves measured at 77 K temperature before and after microwave treatment for 14 min. A resonant peak is observed for both bias polarities, with peak current densities of the order of 10^4 A/cm^2 and peak-to-valley current ratio of about 9 at 77 K. One can see from Fig. 2.6 that, after microwave treatment, the device current in the range of the fundamental resonance peak and beyond it increases by about 15% (except for a small region of the valley current where it decreases slightly). The maximum output power estimated from the I–V curves ($P_{max} = (3/16)\Delta I \Delta V$ [39] where ΔV is voltage range of the negative conductivity and ΔI is the current swing between the peak and valley currents) also increases after microwave treatment. In the initial state, the calculated value of DBRTD P_{max} was about 6 ∝W; after microwave treatment it increased by about 25%.

Figure 2.7 shows similar characteristics measured by the transient pulse technique at 84 K. It should be noted that the peak current increased by 10% after microwave treatment. In the range of NDC a shoulder can be seen on the I–V curves whose strength decreased after

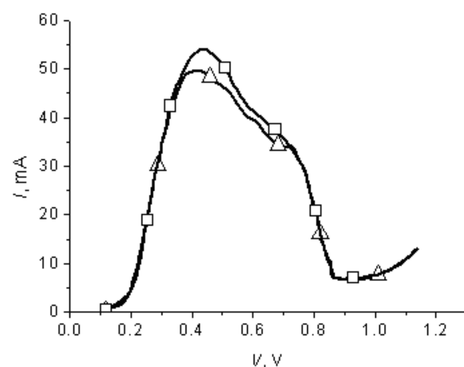

Fig. 2.7. I–V curves of RTD at an operating frequency taken before (triangles) and after (squares) microwave irradiation for 14 min. (frequency of 2.45 GHz, magnetron power of 50 W).

microwave treatment. The form of the *I–V* curves remained the same (except for the above-mentioned regions) within the errors of measurements, as was obtained by the standard DC method.

Another interesting experimental observation is the fact that, 3 months after the microwave treatment, relaxation was observed, and the form of the *I–V* curves returned to the initial one.

The DBRTDs studied contain several semiconductor–semiconduc tor and metal–semiconductor interfaces. The MBE growth technique is known to result in a nearly perfect structure of the individual semiconductor layers, without deep centers, defects and dislocations. The ohmic contacts were also annealed at an optimum temperature from the point of view of the contact quality. For this reason it is not expected that microwave treatment, even if it might result in an additional forming of the contact, could affect appreciably the current flow processes in the device structure. Therefore the observed increase of the peak current (as well as a small but detectable decrease of the valley current) after the microwave treatment can only be ascribed to a presumable decrease of the number of structural imperfections in the device active area, first of all in the GaAs well layer near the heteroboundaries with the barrier layers. This is also supported by

the observation that the strength of the shoulder in the NDC region also decreases. According to the literature [40], the appearance of a shoulder (and its strength) depends on the size and concentration of defects at the interfaces between the barrier and well layers.

The observation that 3 to 4 months after the microwave irradiation the DBRTD *I–V* curves return close to their initial form indicates that internal stress fields might exist near the heteroboundaries, thus leading to the observed relaxation process.

In conclusion it may be said that we presented experimental observations concerning the effect of 2.45 GHz microwave heat treatment on DBTRD *I–V* curves. A certain (about 10%) improvement in the relevant parameters of the diodes was observed. In this way a new technological method for possible improvement of the DBRTD characteristics was demonstrated. On the basis of the analysis of *I–V* curves of the devices taken before and after the microwave treatment, a certain rearrangement of the defect structure near the heteroboundaries was suggested as the mechanism leading to improvements of the conditions for tunneling transport of the charge carriers in DBRTD.

2.2. ENHANCED RADIATION TOLERANCE OF TUNNEL DIODES WITH δ-DOPING

The effect of penetrating radiation on TDs has been studied quite well. It reveals some common, as well as specific, features depending on semiconductor material. Basic changes in *I–V* curves of GaAs TD under irradiation are related to the increase of excess current (I_{ex}) that flows through radiation defects levels arising in both sides of *p-n* junction as well as inside it [41–44].

The dependence of I_{ex} at certain voltage bias on total radiation dose can be divided into three regions. At low doses, a linear growth of I_{ex} occurs due to increase of the radiation defect concentration. At moderate doses, the rate of I_{ex} growth decreases due to reduction of tunneling probability. In some cases an additional peak appears in the valley region of *I–V* curves at 77 K. This happens due to preferred introduction of defects with a certain energy level. The peak tunnel

current I_p decreases concurrently under these radiation doses. At high total doses, a sharp increase of I_{ex} is observed. It is stimulated by appearance of an additional conductivity. The I_p drops abruptly at these doses. Further increase of radiation dose leads to deterioration of *p-n* junction. The fluence at which this occurs (the so-called permissible dose) is approximately the same for all the diodes studied.

However, as the experimental data show, the radiation tolerance of GaAs TDs is higher than that of Ge or Si TDs. The permissible radiation dose is a function of current density which is determined by the ratio I_p/C_0 where C_0 is the TD capacitance. Thus, the higher the operating frequency of TD, the higher its permissible dose.

At first sight, the use of heavily doped *p*- and *n*-type semiconductors when TD is fabricated allows to enhance the TD radiation tolerance. However, a number of negative effects which make the TD operating parameters considerably worse appear in this case. First, the density of peak tunnel current decreases. Second, the NDC region becomes narrower. Basically it happens because the tails of the density of states appear in the gap of heavily doped semiconductors, as well as due to reduction of barrier height in heavily doped *p-n* junctions.

In recent years, such technological technique as δ-doping attracts considerable attention of researchers. A quasi-2D electron system is realized by introducing a very thin (from one to several monolayers) layer with high ($N_D \geq 10^{12}$ cm^{-2}) impurity concentration. On the one hand, high impurity concentration leads to high electron density in the system. In such a system several subbands can be populated. On the other hand, it is easy to manage the electron concentration in the layer if to make a gate electrode, for instance, a *p-n* junction, not far from a δ-layer. One can expect that this may lead to improvement of the TD characteristics.

Following are the results of our study of *I–V* curves of a GaAs-based TD with double-coupled δ-layers near the *n-p* junction. A device (10 μm in diameter) was fabricated from a structure grown on a semi-insulating GaAs substrate. The layer structure is as follows: i) p^+-GaAs (1.5 μm); ii) n^+-GaAs (5 ∝m); iii) Si-doped δ-layer; iv) n^+-GaAs (5 nm); v) Si-doped δ-layer; vi) n^+-GaAs (300 nm). The dopant concentrations in the *p*- and *n*-layers and the δ-layer were 10^{20} cm^{-3} and 10^{13} cm^{-2}, respectively.

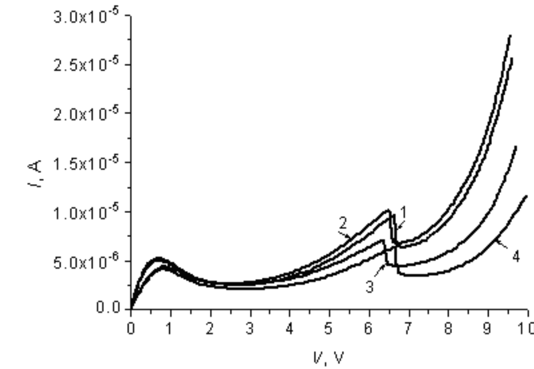

Fig. 2.8. I–V curves of GaAs TD with δ-layers taken at 300 K before (1) and after (2-4) γ-irradiation.

The structures studied were exposed to ^{60}Co γ-irradiation at a temperature of 300 K. The total dose at which noticeable changes of the TD main parameters were not observed was 3×10^7 Gy. The typical *I–V* curves for one of the diodes studied are shown in Fig. 2.8. An additional peak in the valley current region is clearly seen even at room temperature. This peak appeared due to tunneling of electrons localized in the lowest energy level of the δ-layer into the valence band of the *p*-region under the appropriate bias voltage. As long as the distance between the δ-layers is small, the discrete levels in each layer spread out forming subbands. The system becomes a single doped layer with impurity concentration $2N_D$. A schematic potential profile of the structure studied is shown in Fig. 2.9. A theoretical description of a single non-compensated δ-layer with an additional gate electrode has been presented in [45]. By using the formalism developed in [45] for description of our structure, we found a good agreement between the calculated and experimental data.

Let us consider some unusual data related to radiation tolerance of the above structures. One can see from Fig. 2.8 that the *I–V* curves

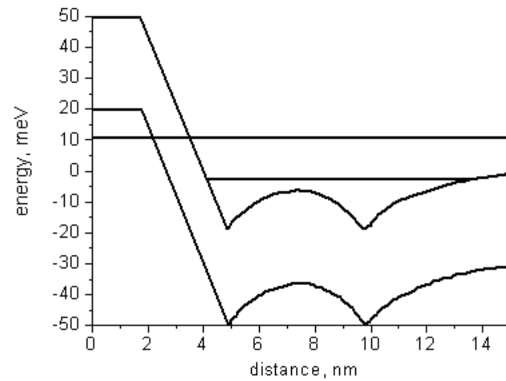

Fig. 2.9. A schematic profile of the structure studied (not scaled).

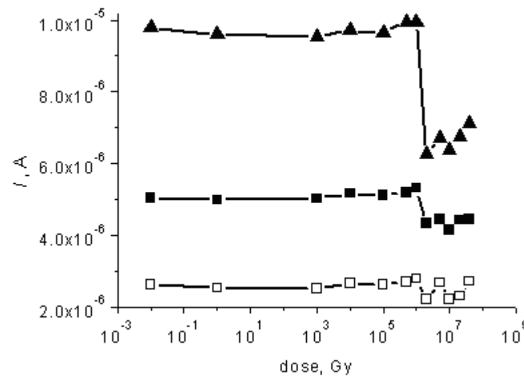

Fig. 2.10. The additional peak current (triangles), tunnel peak current (crosses) and excess current (squares) as function of total dose of γ-irradiation.

of a TD with δ-layers do not demonstrate noticeable changes until the total dose reaches 3×10^7 Gy. It is considerably higher than the permissible doses known for the standard GaAs-based TDs. The dose dependencies of the tunnel peak current, excess current and additional peak current also indicate high radiation tolerance. A comparison of these dependencies (presented in Fig. 2.10) with the experimental data obtained on TD without δ-layers under similar conditions [46] enables

us to draw the following conclusion: use of δ-doping in fabrication of TDs makes it possible to raise considerably their radiation tolerance. In our opinion, the main reason for this effect is enhancement of the tunnel component contribution when a δ-layer is inserted close to the *p-n* junction. Opening of this active current channel decreases the probability of jumping via the levels of radiation defects which determines the excess current amplitude. It should be noted that TDs with a δ-layer have certain advantages over the other types of tunneling devices. They result from a possibility to manage the electron concentration and conductivity in the layer, as well as from improvement of the device operating parameters (for instance, obtaining of several NDC regions in *I–V* curves).

2.3. EFFECT OF MICROWAVE IRRADIATION ON *I–V* CURVES OF GaAs TUNNEL DIODES WITH δ-LAYERS

Considerable recent attention has been focused on the development and investigation of combined structures of microwave electronics on the basis of traditional semiconductor elements (diodes and transistors) with a RTD placed in their active area [9, 17-21, 47-52]. One of such elements is a GaAs TD with a *p-n* junction and one or several δ-layers built in the space-charge region (SCR). It should be noted that presence of electric fields built in SCR increases considerably the effect of external factors on the geometric and electrophysical parameters of such RTSs.

We investigated the TDs with two δ-layers in the immediate vicinity of the SCR boundary [51, 52]. The structures were MBE-grown on a semi-insulating GaAs (100) substrate. The *p-n* junction thickness was $l' \approx 10$ nm, the spacing between the δ-layers was $d = 5$ nm. The concentration of silicon impurities in the δ-layers was $N_0 \approx 10^{13}$ cm^{-2}, the charge carrier concentrations in the p^+- and n^+-GaAs layers were about 10^{20} and 10^{19} cm^{-3}, and, correspondingly, the Fermi energy E_F in the n^+-GaAs layer was about 0.023 eV.

The *p-n* junction diameter was 10 μm. The diodes were mounted in the packages of the microwave oscillating diodes. The microwave

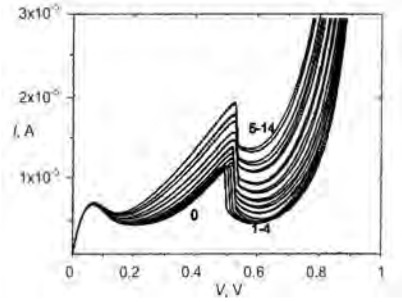

Fig. 2.11. I–V curves of GaAs TD with δ-layers: initial (0) and after microwave treatment with radiating power of 3 W/cm^2 and duration of 20 s (1-4 – low level) and 30 s (5-14 – high level).

power generated by the diodes at a frequency of 10 GHz was about 50 μW. The electric field in the *p-n* junction was $E_0 = 2\times10^6$ V/cm. The quantum well formed by the δ-layers determined a resonance level via which the resonant-tunneling current flowed.

The TDs with δ-layers were exposed to microwave irradiation (frequency of 2.5 GHz, radiating power of (3÷30) W/cm^2) in a wave-guide of a magnetron, as well as to thermal annealing at a temperature of 300 °C. A pronounced anisotropy of the microwave field action was observed: the electromagnetic irradiation dose required for variation of the *I–V* curves at the normal incidence of microwave wave on the sample was 2–3 orders less than that at the grazing incidence. The small irradiation doses ("low level" in Fig. 2.11) led to shifting of the resonant-tunneling peak in the *I–V* curve towards higher voltages, as well as to some reduction of the TD excess current.

As the irradiation dose increases, the position of the resonant-tunneling peak becomes fixed, and the excess current I_r increases according to the following expression:

$$I_\mathrm{r} = i_1 \exp(a_1 V) + i_2 \exp(a_2 V). \tag{2.1}$$

Here V is the applied voltage, i_1 and i_2 vary linearly with the microwave irradiation dose (starting from a certain threshold value), and the constants a_1 and a_2 are independent of the dose.

2.3.1. Total heating model

To estimate the temperature T at which noticeable diffusion occurs, we used the following considerations. The impurity concentration in a layer Δx located at a distance of $-x_0$ from $x = l$ has to be comparable (of the same order of magnitude) to the charge carrier concentration n in the n^+-region. Since $\Delta x \cong E_\mathrm{F}/eE_0$, then

$$n(\Delta x) \cong \frac{Q^{2/3}}{\Delta x}\left\{\mathrm{erfc}\left(\frac{x - \dfrac{DeEt}{kT}}{2\sqrt{Dt}}\right) - \mathrm{erfc}\left(\frac{x + \Delta x - \dfrac{DeEt}{kT}}{2\sqrt{Dt}}\right)\right\}. \tag{2.2}$$

Here Q is the total charge in the δ_1-layer, $D = D_0 e^{-U/kT}$, and E is the strength of microwave electromagnetic field. For D_0 and U the known values for Si diffusion in GaAs are taken: $D_0 = 4\times10^{-4}$ cm^2/s and $U = 2.45$ eV [53]. The estimation showed that the temperature of the heated sample has to exceed 550 °C to ensure noticeable diffusion, but such was not the case in our experiment.

2.3.2. Local heating model

Let us consider the following model: a sample (in the form of an infinite plate of thickness l) is placed in the area of microwave field action. There is a conducting layer (2D) in the middle of the sample; the layer is parallel to the plate faces (Fig. 2.12). Let us assume that the microwave field power is absorbed in the above layer only, and the absorbed power is $W = kP$, where P is the microwave power and k is the absorption coefficient.

The spatial distribution of temperature is given by the heat equation

$$\frac{\partial T}{\partial t} = a\frac{\partial^2 T}{\partial x^2} + \frac{kP}{\rho_\Lambda c}\delta\left(x - \frac{l}{2}\right), \tag{2.3}$$

$$\begin{aligned} &0 \le x \le l \\ &t \ge 0 \end{aligned} \tag{2.4}$$

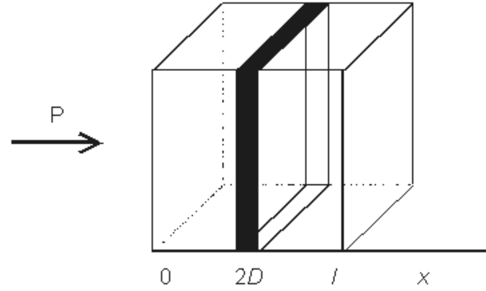

Fig. 2.12. The TD geometry used when calculating the local heating model.

(the power is switched on at the instant $t = 0$). Here $a = \chi/\rho c$ is the thermal diffusivity, χ is the thermal conductivity, $\rho_\Lambda = \rho S$ is the linear density (ρ and S are the sample density and area, respectively), c is the molar thermal capacity. For GaAs $\rho = 5.317$ g/cm^3, $c = 5.48$ cal/mole·deg, $\chi = 0.37$ cal/cm·s·deg [54-57].

Let the initial and boundary conditions be

$$T\big|_{t=0} = 0 \tag{2.5}$$

(the initial temperature T_0 is to be added to the solution) and

$$\left(\frac{\partial T}{\partial x} - hT\right)\bigg|_{x=l} = 0$$
$$\left(\frac{\partial T}{\partial x} + hT\right)\bigg|_{x=0} = 0 \tag{2.6}$$

These conditions correspond to convective heat exchange with the medium of zero temperature (i.e., the same temperature T_0 as that of the plate). The parameter h characterizes the intensity of heat exchange of the sample with the external medium: at $h = 0$, the plate walls are heat-insulated, at $h \to \infty$, a constant temperature is maintained at the plate walls.

The general solution of Eq. (2.3), with the conditions given by Eqs. (2.4)–(2.6), is

$$T(x,t) = \frac{P}{\rho_\Lambda ca}\sum_{n=1}^{\infty}\frac{1}{\lambda_n^2}C_n^2\sin\left(\frac{1}{2}\lambda_n l - v_n\right)\sin(\lambda_n x - v_n)\left(1 - e^{-a\lambda_n^2 t}\right). \tag{2.7}$$

Here
$$C_n = \sqrt{2}\cdot\left(l - \frac{2h}{\lambda_n^2 + h^2}\right)^{-1/2}, \tag{2.8}$$

λ_n is determined from the following equation:

$$\tan\lambda_n l = \frac{2h\lambda_n}{h^2 - \lambda_n^2}, \tag{2.9}$$

and

$$v_n = \tan^{-1}(\lambda_n/h). \tag{2.10}$$

Let us consider the limiting cases.

a) $h = 0$. In this case $T(x,t) = \frac{2P}{\rho_\Lambda cl}t$. This corresponds to a very quick linear heating.

b) $h \to \infty$. In this case the curve $T(1/2, t)$ flattens out as $t \to \infty$ approaching the value $T_{\max} \cong \frac{2Pl}{c\rho_\Lambda a\pi^2}\sum_{n=1}^{\infty}\left(\sin^2\frac{n\pi}{2}\Big/n^2\right)$.

We believe that the above dependencies are due to electric stimulation (by the external electric field and that of SCR) of impurity thermal diffusion from the nearest to SCR δ-layer. In this case the form of the potential well (where the local level responsible for the resonant-tunneling current is generated) changes: that wall of the well which is the nearest to the *p-n* junction becomes flatter, and the level in the well (measured from the bottom of the well) becomes shallower. According to this, this level moves farther from the bottom of the conduction band in the n^+-layer, and the peak of the resonant-tunneling current somewhat shifts towards higher voltages.

At further microwave irradiation, the position of this peak does not vary, thus indicating that the form of the potential well remains the same. The reason for this may be that all the impurities have traveled from the first δ-layer to SCR. Still further microwave irradiation leads to appearance of two impurity levels in SCR via which interband tunneling may occur. Their energies do not vary with the exposure time, while their concentration varies. In this case a_1 and a_2 (see Eq. (2.1)) are determined by the nature of the levels and configuration of the electric fields (i.e.,

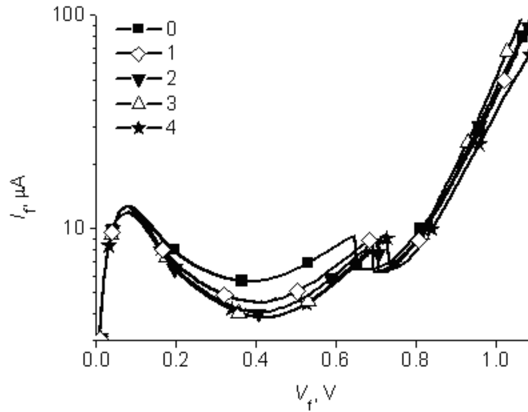

Fig. 2.13. I–V curves of TD with δ-layers taken before (0) and after (1-4, at interval of 5 min) RTA at $T = 300$ °C.

the structure geometry) only, while i_1 and i_2 are proportional to the concentration of the centers responsible for interband tunneling.

When analyzing the experimental results obtained at high-power microwave irradiation of the TDs with built-in δ-layers (Fig. 2.11) and at RTA at a temperature $T = 300$ °C (Fig. 2.13), one can assume that two degradation processes occur in TRD. At first the quantum-confined well becomes wider because the interface between the δ-layer and SCR is smeared due to electric stimulation of mass transfer. Then the generation-recombination centers are accumulated, thus leading to increase of the excess diffusion current.

Thus, it is shown that RTDs on the basis of AlGaAs/GaAs heterojunctions and gallium arsenide TDs with a δ-layer in SCR retain their serviceability after being irradiated with ^{60}Co γ-quanta up to doses of 10^7 and 3×10^7 Gy, respectively. Rather low γ-irradiation doses result in improvement of the electrical parameters of RTDs and TDs. A short-term microwave treatment of TDs and RTDs also leads to some improvement of their parameters. An analysis of the degradation effects under action of microwave radiation on TDs with a δ-layer in SCR showed that impairment of the TD parameters may result from diffusion smearing of the δ-layer stimulated by electromagnetic radiation.

Chapter 3.

EFFECT OF ^{60}Co γ-RADIATION AND MICROWAVE RADIATION ON THE PROPERTIES OF SiO_2–GaAs (SiC) STRUCTURES

The advanced modern technologies make it possible to produce the materials and device structures with preset parameters (composition, thickness, residual impurity concentration, etc.). But in the course of their further application in the semiconductor device technology it is impossible to exclude some negative consequences (e.g., structural changes related to plastic deformation during high-temperature technological processes). So one should not only take into account the structural relaxation and phase transitions in semiconductor heterosystems but search for novel ways of improvement of semiconductor device characteristics as well. With that end in view, we tried to apply dosed electromagnetic irradiation. Some examples of the effect of microwave and γ-irradiation on a number of semiconductor objects of technical importance are considered below.

3.1. RADIATION-INDUCED EFFECTS AT THE SiO_2–GaAs INTERFACE

The dielectric layers on the basis of SiO_2 are widely used for passivation, masking and isolation when producing GaAs-based microelectronic devices [1, 2]. The manufacturing technology and properties of SiO_2 have been much investigated [3–21]. However, intense formation and transformation of point and extended defects in the semiconductor near-surface layers occurs in the course of dielectric film deposition. This is due to low thermal stability of GaAs, as well as appearance of

considerable stresses at the boundaries between phases in the course of silicon oxide deposition onto GaAs. The above factors strongly restrict application of SiO_2 layers for solving the above problems and make impossible use of these layers as gate dielectric.

Thus the necessity of improvement of the technological processes which use SiO_2 films poses the problem of searching the ways of purposeful action on the properties of the SiO_2–GaAs interface that could remove (or at least decrease) the action of the above negative factors.

In our experiments, several techniques were applied to deposit the dielectric SiO_2 layers onto the GaAs:Te substrates with surface orientation (100). The substrate thickness was 300 μm; the tellurium concentration was 2×10^{17} cm^{-3}. The data on the techniques of SiO_2 deposition are given in Table 3.1.

The samples were exposed to ^{60}Co γ-irradiation in the 10^3–10^5 Gy range. The dose rate was 3 Gy/s. The data on the chemical composition and structure of the grown SiO_2 layers were obtained with Auger spectroscopy.

Table 3.1. The data on the techniques used for SiO_2 deposition onto GaAs and parameters of the SiO_2–GaAs structures.

Sample #	SiO_2 deposition technique	SiO_2 layer thickness, μm
1	High-frequency plasma: tetraethoxysilane + Ar + O_2, T = 250 °C, t = 60 min.	0.25–0.3
2	Monosilane pyrolysis, T = 350 °C, t = 15 min.	0.35–0.4
3	Tetraethoxysilane decomposition, T = 650 °C, t = 2.5 h	0.25–0.3
4	Tetraethoxysilane decomposition, T = 650 °C, t = 3 h	0.35–0.4
5	High-frequency low-temperature plasma: tetramethoxysilane + (Ar + O_2), T = 20 °C, t = 15 min.	0.36

An analysis of the structural disordering in the contacts of GaAs with SiO_2 was made using the results of Raman scattering of light and optical reflection. The Raman spectra were taken at a temperature T = 300 K with a plant assembled on the basis of spectrometer ДФС-52. The Raman scattering signals were registered in the photon-counting mode with a cooled photomultiplier tube ФЭУ-136. The Ar^+ laser line (wavelength λ = 488 nm) was used for excitation. The experiment was performed in the reflection geometry; the angle of incidence was close to the Brewster one. The spectral resolution at Raman scattering measurements was 1.5 cm^{-1}. The accuracy of determination of the Raman scattering band peaks (0.1 cm^{-1}) was ensured by concurrent recording of the gas discharge Ne spectral lines. The Raman spectra were measured without removal of the dielectric layer [22].

Two peaks (at 267 and 290.5 cm^{-1}) were observed in the Raman spectra. These peaks corresponded to scattering on the TO- and LO-phonons. It should be noted that the term “near-surface layer” means the layer where the Raman scattering signal is formed. Its thickness d is determined by the GaAs absorption coefficient α ($d = 1/2\alpha$). To illustrate, d = 80 nm at λ = 488 nm.

It is known that the position and half-width (Γ) of the LO-phonon peak are determined by presence of deformation and defects of crystal lattice. Practically all types of crystal lattice defects that lead to additional damping of optical phonons result in broadening of the LO-phonon peak (increase of Γ). So primary attention will be concentrated on this parameter of the LO-phonon peak.

The plant for measurement of the optical reflection spectra enabled us to detect the areas of 5% local concentration nonuniformity; the charge carrier mobility was determined accurate to ±200 cm^2/V·s. The main informative parameters in this technique, as well as in electroreflectance (ER), are the half-widths of the optical reflection peaks (which correlate with charge carrier mobility and peak heights) that depend on charge carrier concentration. The advantage of the optical reflection technique (as compared to ER) is the possibility to study the near-surface semiconductor layers and interfaces without sample

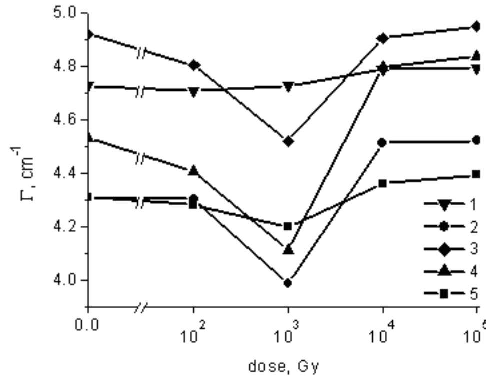

Fig. 3.1. LO-phonon peak half-width at Raman scattering as function of γ-irradiation dose for the samples 1-5 (for sample parameters see Table 3.1).

destruction. We investigated the SiO_2–GaAs structures near the fundamental absorption edge of GaAs (1.45 eV) using for modulation the He–Ne laser radiation (λ = 0.6328 μm, P = 1 mW) whose penetration depth was 250 nm. To remove distortions due to light interference in oxide, the reflection spectra were measured using the immersion technique, with sample immersed into ethanol. In this case, due to the fact that the refractive indices of SiO_2 and ethanol are close, oxide becomes antireflecting and optical interference does not occur.

Figure 3.1 presents the dose dependencies of the half-widths of LO-phonon peaks of Raman scattering. They were taken for the SiO_2–GaAs samples which were obtained using different techniques (see Table 3.1). After SiO_2 deposition using the technique 1, 3 or 4, the LO-phonon peak of GaAs becomes broader. This effect is most pronounced for the samples with dielectric obtained with tetraethoxysilane decomposition at T = 650 °C. Taking into account that practically all the crystal lattice defects that lead to additional damping of optical phonons cause broadening of the LO-phonon peak, one can assume that plasma anodization of GaAs in tetramethoxysilane and SiO_2 deposition using monosilane pyrolysis make it possible to obtain SiO_2–GaAs interface with minimal structural imperfections (see Table 3.1).

Small-dose ^{60}Co γ-irradiation of GaAs samples with SiO_2 layers results in narrowing of the phonon peaks not accompanied with their shifting and considerable change of their form. The features observed can be explained by radiation-induced gettering of defects followed with their annihilation at the interface [23]. When the irradiation dose is increased, the parameter Γ begins to grow. This results from intensification of destructive action at high irradiation doses.

The above features of the effect of γ-irradiation on the structure of SiO_2–GaAs junctions got support when studying optical reflection from these objects. The increase of reflection peak height at low doses of irradiation indicates reduction of defect concentration in the GaAs near-surface region and increase of the crystal perfection degree in the near-surface layers. These effects are accompanied with a decrease of Γ and growth of charge carrier mobility $\propto$ in the near-surface region (see Table 3.2). The data obtained are in a good agreement with the results of investigation of Raman scattering (variation of the half-widths of LO-phonon peaks).

Table 3.2. The dose dependencies of the parameters Γ and α of the GaAs near-surface layer calculated from the optical reflection spectra.

Sample # from Table 3.1	The measured parameters	Irradiation dose, Gy				
		0 (initial)	10^2	10^3	10^4	10^5
1	Γ, meV	25	22	20	21	23
	α, cm^2/V·s	3600	3800	4000	3800	3700
3	Γ, meV	28	25	23	24	26
	α, cm^2/V·s	3400	3600	3700	3600	3400
	Γ, meV	30	26	24	25	27
	α, cm^2/V·s	3200	3400	3600	3600	3400
5	Γ, meV	32	25	20	23	25
	α, cm^2/V·s	3100	3600	400	3700	3600
	Γ, meV	25	20	27	27	27
	α, cm^2/V·s	3600	4000	3400	3400	3400
	Γ, meV	22	20	23	23	24
	α, cm^2/V·s	3800	400	3700	3700	3600

An analysis of the Auger spectra and concentration depth profiles of the SiO_2–GaAs structure components measured before and after γ-irradiation (with doses of 10^3 and 10^5 Gy) showed that there was a transition region in the initial structures. This indicates interaction of the substrate with the deposited layer which affects the structure of both the oxide layer and semiconductor near-surface region.

^{60}Co γ-irradiation changes the distribution of components in the transition region. Concurrently the thickness of this region decreases at low irradiation doses, while increasing at high doses (Fig. 3.2.). Similar results were obtained in [23] with ellipsometry measurements of the junction layer parameters in the initial (before irradiation) and irradiated SiO_2–GaAs structures that were similar to ours. The observed non-monotone variations of the junction layer thickness in the irradiated SiO_2–GaAs structure may result from two counteractive factors, namely, increase of diffusion mass transfer at the interface enhanced with γ-irradiation (this factor favors spreading of the transition region [23–29]) and irradiation-induced clusterization of the building blocks of oxide layer into continuous spatial networks of SiO_2 tetrahedrons connected to each other [30].

Enhancement of crystallization under x-ray irradiation was observed earlier in silicate glasses of different compositions [31]. This factor is responsible for slight penetration of semiconductor components into oxide layer at low doses of γ-irradiation. The character of clusterization depends on presence of impurities in the oxide [32]. Penetration of Ga deep into oxide at high doses of γ-irradiation leads to deformation of the spatial network of the oxide phase, thus preventing its condensation. Bounding of the silicon–oxygen complexes is realized with the participation of these components. The main role in building of such layers belongs to the oxygen polyhedrons of cations rather than silicon–oxygen radicals. The above polyhedrons favor formation of microscopic nonuniformities of oxide layer structure in the region contacting with GaAs and hence deterioration of electrophySiCal parameters of the dielectric–semiconductor interface.

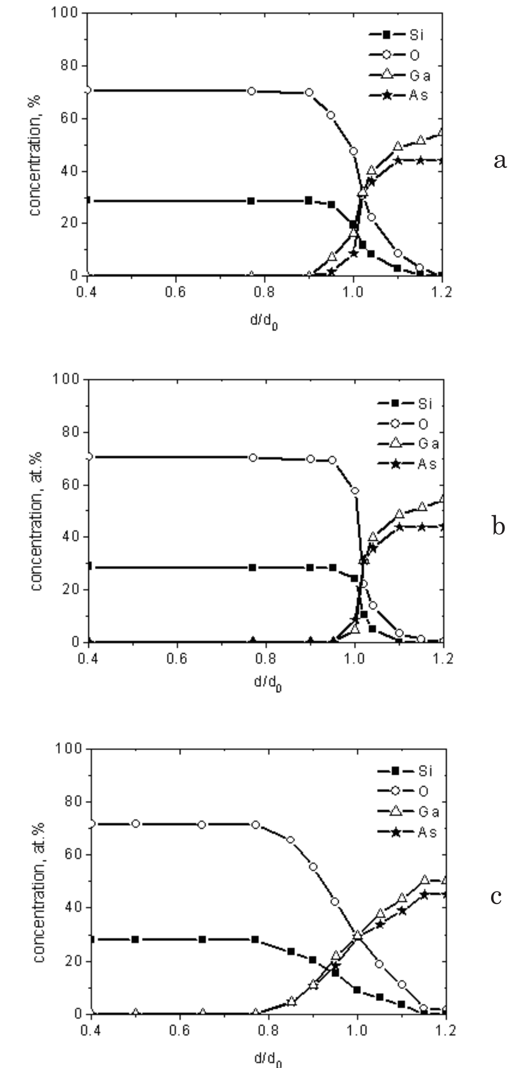

Fig. 3.2. Component concentration depth profiles in the SiO_2–GaAs structure (sample # 2, Table 3.1): a – initial sample; b (c) - after ^{60}Co γ-irradiation up to a dose of 10^3 (10^5) Gy.

Thus the results of investigations of SiO_2–GaAs interface modification under low-dose ^{60}Co γ-irradiation [22–29] can serve as the starting point when solving the problem of obtaining the dielectric–GaAs interfaces with improved electrophySiCal characteristics.

3.2. EFFECTS INDUCED BY MICROWAVE IRRADIATION IN THE SiO_2-GaAs STRUCTURE

The progress of the modern solid-state electronics is determined to a large extent by the possibilities to apply purposeful dosing non-contact actions on the electrophySiCal parameters of semiconductor materials and structures at the stage of their manufacturing and production on their bases of various discrete devices and ICs [33–42]. Obviously the techniques using interaction of microwave electromagnetic fields with semiconductor structures belong to such technological procedures. The higher are the density of defects (point, cluster, extended) and degree of structural-impurity disordering in the samples, the more sensitive to microwave irradiation are the samples. This effect occurs also in spatially-nonuniform dielectric–semiconductor structures.

We considered the effect of microwave treatment on the properties of GaAs near-surface layer in the SiO_2–GaAs structure. The samples were prepared using electron-beam evaporation of quartz in a chamber at a pressure of 6×10^{-4} Pa [43]. The substrate was *n*-GaAs (100) with free charge carrier concentration of ~ $(2\div5)\times10^{16}$ cm^{-3}. The substrate thickness was 350 μm, that of SiO_2 layer was (0.4÷0.5) μm. Before dielectric deposition, the GaAs wafers were treated in sulfuric etchant and washed in deionized water and isopropyl alcohol.

The defect structure of the samples was studied with the PL at a temperature of 77 K in the spectral range $\Delta h\nu = (0.5\div2.04)$ eV, on the side of both the SiO_2 film and GaAs substrate. The excitation source was a high-power incandescent lamp ПЖ-100. The energy range with photon energy ≥ 2.0 eV (in that region the GaAs absorption coefficient is ~ 10^5 cm^{-1}) was separated from the lamp radiation spectrum using the corresponding filters. Thus, the spectrum of defect states was studied in the near-surface layers whose thickness was ~ 10^{-5} cm. A PbS photoresistor served as luminescence radiation detector.

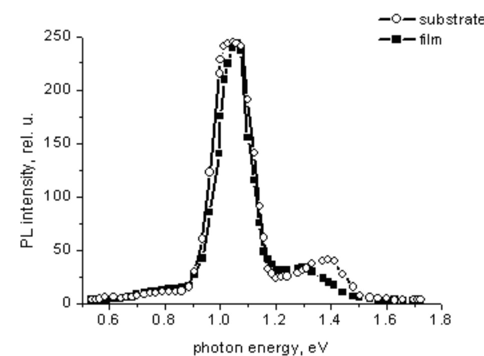

Fig. 3.3. PL spectrum of the SiO_2–GaAs structure (initial sample) on the side of the substrate (-○-) and SiO_2 film (-■-).

The samples were exposed to microwave irradiation in the work chamber of magnetron loaded with a quasi-stationary microwave resonator at a frequency of 2.45 GHz. The radiating power was 1.5 W/cm^2. The sequential times of irradiation of the same sample were 1; 1; 1; 5 and 5 min. (the total times of irradiation were 1, 2, 3, 8 and 13 min., respectively).

Two bands in the PL spectra of the structure studied are observed, no matter on what side (SiO_2 film or substrate) the PL spectra were measured. The band peaks are at 1.04 and 1.3 eV (the peak positions are indicated for the initial sample) (Fig. 3.3). So one can believe that the main features of the PL spectrum in the SiO_2–GaAs structure come from luminescence at the GaAs surface and SiO_2–GaAs interface. The band 1.04 eV is usually related to radiative capture of a free electron in gallium arsenide by a separate acceptor center Cu_{Ga} [35–43]. The band 1.3 eV also is related to presence of copper impurity in gallium arsenide: the emitting centers responsible for this band are the (Cu_{Ga}–D) complexes, where donor D is either intrinSiC (V_{As}) or foreign [44–55]. The parameters of PL bands are presented in Tables 3.3 and 3.4.

The distinguishing feature of the PL spectra in the SiO_2–GaAs structures (at total time of microwave treatment ≤ 8 min.) is that the PL spectra obtained on the side of GaAs substrate and SiO_2 film are essentially

Table 3.3. The parameters of PL bands measured on the substrate side.

Structure	Total time of microwave irradiation, min.	$h\nu_m$, eV		PL band intensity, rel. units		PL band half-width Γ, rel. units	
		1 Cu_{Ga}–D	2 Cu_{Ga}	1	2	1	2
SiO_2–GaAs	initial	1.39	1.04	132	805	0.14	0.19
	1	1.29	1.055	21	187	0.16	0.12
	2	1.20	1.01	214	462	0.185	0.21
	3	1.26	1.01	165	281	0.12	0.21
	8	1.24	1.025	416	479	0.18	0.24
	13	1.22	1.01	390	759	0.22	0.18

Table 3.4. The parameters of PL bands measured on the SiO_2 film side.

Structure	Total time of microwave irradiation, min.	$h\nu_m$, eV		PL band intensity, rel. units		PL band half-width Γ, rel. units	
		1 Cu_{Ga}–D	2 Cu_{Ga}	1	2	1	2
SiO_2–GaAs	initial	1.295	1.04	102	799	0.23	0.14
	1	1.31	1.04	42	233	0.20	0.141
	2	1.20	1.01	152	442	0.19	0.21
	3	1.22	1.01	122	320	0.18	0.21
	8	1.26	1.025	383	406	0.14	0.26
	13	1.28	1.02	1500	350	0.15	0.21

similar (Fig. 3.3). However, when the total time of microwave treatment of the sample amounts to 13 min., such behavior changes: the intensity of the PL spectrum taken on the side of the GaAs substrate is about three times that taken on the side of the SiO_2 film (Figs.3.4 and 3.5). Besides, in the spectra taken on the side of the film, the band peaking at 1.04 eV is of higher intensity than that with a peak at 1.3 eV, and the same band intensity relation is at smaller times of microwave treatment (Fig. 3.3). But in the spectra taken on the side of the substrate, the intensity of the band 1.04 eV becomes lower than that of the band 1.3 eV (Figs.3.4 and 3.5).

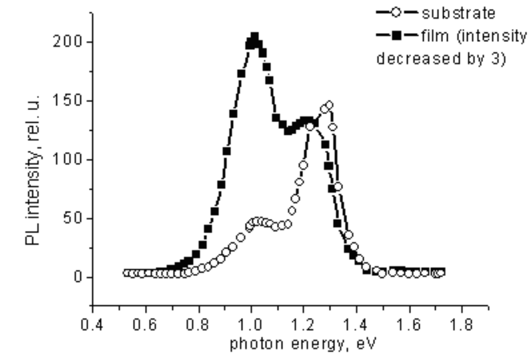

Fig. 3.4. PL spectrum of the SiO_2–GaAs structure after microwave treatment (the total time of 13 min.) on the side of the substrate (1) and SiO_2 film (2) (in the latter case the spectrum intensity is reduced by a factor of three).

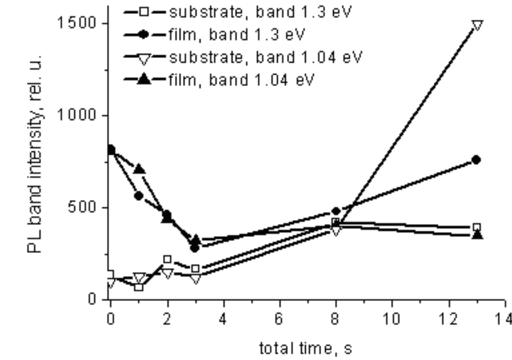

Fig. 3.5. The PL band intensity as function of the total time of microwave treatment.

As the total time of microwave treatment increases, the positions of PL band peaks change slightly (Fig. 3.6). At first (the time of microwave treatment being 1 min.) they somewhat shift towards higher frequencies, then (when the total time of microwave treatment is 2 min.) they shift towards lower frequencies, as compared with the band peak positions in the initial (before microwave treatment) sample. At further increase of the time of microwave treatment the positions of the PL band peaks vary but slightly.

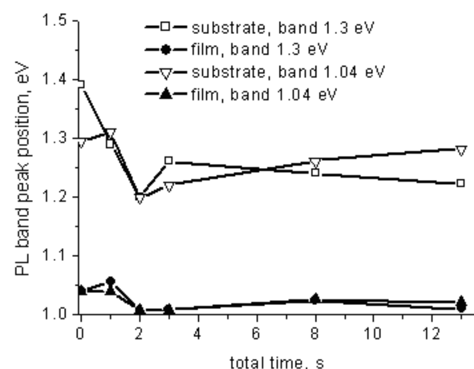

Fig. 3.6. The position of the PL band peaks as function of the total time of microwave treatment.

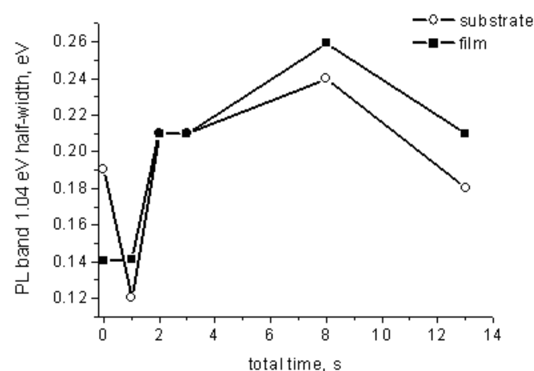

Fig. 3.7. The half-width of the PL band 1.04 eV as function of the total time of microwave treatment.

Under microwave irradiation the half-width of the band 1.04 eV (Fig. 3.7) first decreases considerably (the time of microwave treatment being 1 min.), then (when this time increases up to 8 min.) increases, and, as the total time of microwave treatment is equal to 13 min., the PL band half-width begins to decrease again. Such behavior of the PL band half-width is common to the spectra taken on the side of the GaAs substrate and the SiO_2 film as well.

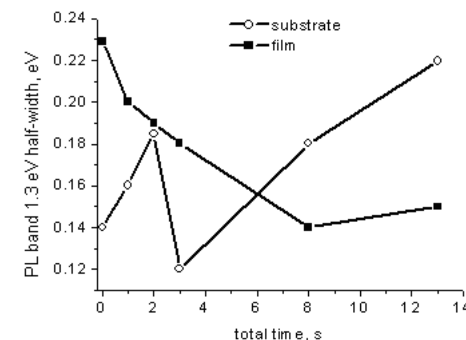

Fig. 3.8. As in Fig. 3.7 but for the PL band 1.3 eV.

The dependence of the half-width of the PL band with peak at 1.3 eV on the time of microwave treatment is different (Fig. 3.8). To illustrate, for the above band these dependencies for the spectra taken on the side of the GaAs substrate and SiO_2 film differ considerably, while for the band 1.04 eV they are similar. In the case of the band 1.3 eV, the band half-width of the spectrum taken on the side of the SiO_2 film decreases smoothly as the total time of microwave treatment increases, while for the spectrum taken on the side of the GaAs substrate the PL band half-width increases with the total time of microwave treatment.

Generally PL band narrowing (decrease of the band half-width) may be considered as evidence of structural-impurity ordering, while band broadening (increase of half-width) indicates intensification of degradation processes [56, 57]. Taking into account that the SiO_2 film is practically transparent in the spectral range studied, one should suppose that the PL spectra taken on the film side carry information on a junction layer formed at the SiO_2–GaAs interface. The fact that in the SiO_2–GaAs structure the PL bands taken on the side of the SiO_2 film become narrower when the total time of microwave treatment is 13 min. enables one to assume that structural-impurity ordering occurs in the junction layer under microwave irradiation.

3.3. MECHANISMS OF MODIFICATION OF SiO_2–GaAs DEFECT STRUCTURE BY MICROWAVE IRRADIATION

Along with PL investigation of the defect structure of microwave-irradiated SiO_2–GaAs samples, we studied also the effect of microwave treatment on the atomic composition of the semiconductor near-contact regions. The phase composition of the GaAs sample surfaces was determined with x-ray photoelectron spectroscopy (XPS). The composition of an interlayer in the SiO_2–GaAs structure was determined using Auger electron spectroscopy (AES) after SiO_2 film was etched off in hydrofluoric acid solution [58]. To characterize structural perfection of the substrates, we applied metallography [59] and studied distribution of the breakdown voltage threshold values in the Schottky barrier diodes (SBDs) made on the above-mentioned substrates [60].

Figure 3.9 presents the results of our investigations of phase composition of the gallium arsenide surface that was prepared for deposition of a dielectric layer. It follows from these results that an oxide film which appears spontaneously at the surface after chemical treatment involves three phases: two oxides (Ga_2O_3 and As_2O_3) and chemically unbound As atoms. Their distribution with the oxide film depth is nonuniform and

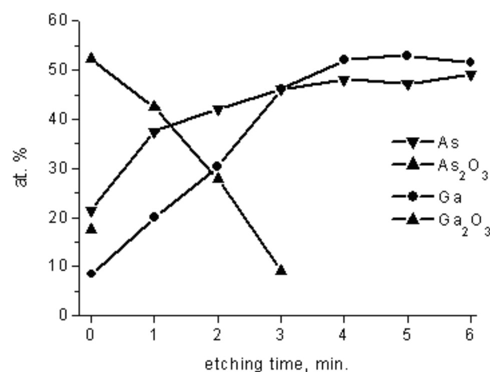

Fig. 3.9. Phase composition depth profiles of the GaAs near-surface layer before SiO_2 deposition.

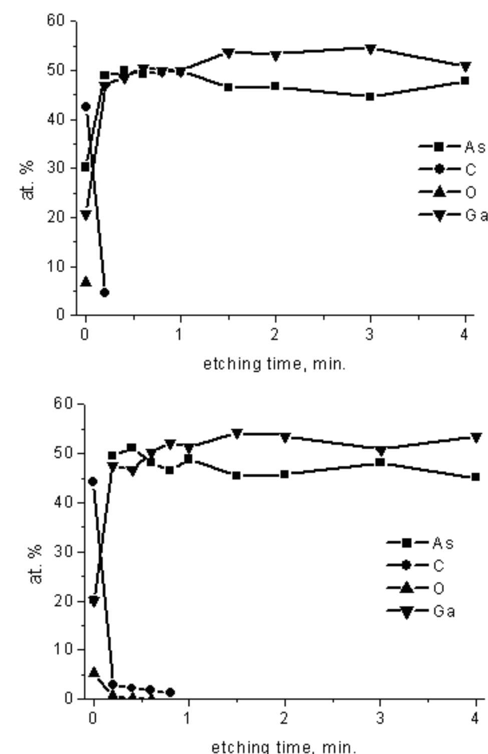

Fig. 3.10. Concentration depth profiles of the GaAs near-surface region under the SiO_2 layer before (a) and after microwave treatment for 13 min. (b).

most likely corresponds to the condition of oxide appearance, when the concentration ratio As/Ga ≈ 1 [61]. This conclusion is supported also by the results of [62]. According to them, treatment of GaAs in sulfuric etchants leads to the ratio between the Ga and As concentrations at the surface that is close to the stoichiometric one. The thickness of the formed intrinSiC oxide (estimated from the time of its sputtering with argon ions) is 2.5–3.5 nm. Thus, it prevents efficiently from variation of the atomic composition of semiconductor surface.

Deposition of SiO_2 film leads to a change in the chemical composition of GaAs surface (it becomes enriched with As atoms - see Fig. 3.10a).

This result is in agreement with those previously obtained in [27] where it was found that, at SiO_2 deposition onto GaAs, gallium is efficiently captured by the growing dielectric layer.

The solid-state interactions between the sputtered SiO_2 layer and GaAs may be considered as process of predominant removal of Ga. This results in increase of the concentration of gallium vacancies V_{Ga} in the semiconductor near-surface region. Due to their increased concentration, the gallium vacancies will either diffuse into the crystal bulk (with further transformation into point defects of another nature) or promote impurity segregation in the semiconductor near-surface region [63].

After microwave irradiation (maximal dose) of the SiO_2-GaAs structure, the concentrations of Ga and As under the oxide layer became equal and changed non-monotonously when going deep into the semiconductor (Fig. 3.10b). These variations were accompanied with increase of the oxygen and carbon contents in the GaAs near-surface layer, i.e., the microwave treatment affected "oxidability" of the surface and its contamination with carbon impurities. The authors of [64, 65] also observed that the content of carbon and oxygen solved in the semiconductor increased after microwave treatment. It should be noted that carbon atoms form in GaAs acceptor levels lying above the top of the valence band by 0.02 eV, while oxygen atoms form the defects of the O_{As}-type with energy level lying below the bottom of the conduction band by 0.825 eV [61].

The PL studies showed that the samples studied can be separated into two groups differing in their impurity-defect composition (Fig. 3.11a, b). The intensity of PL bands in the samples of the first group is several times bigger than that in the samples belonging to the second group, and the band with $h\nu_m' = 1.04$ eV dominates in the PL spectra. The bands with $h\nu_m' = 1.04$ eV and $h\nu_m' = 1.30$ eV are related to diffusion of uncontrolled copper impurity into the semiconductor [44]. Such drastic distinctions in the PL spectra of two groups of the samples may result from the structural-impurity microscopic nonuniformities of the GaAs material used in our investigations. This statement is supported by the results of (i) studies of breakdown voltage distribution

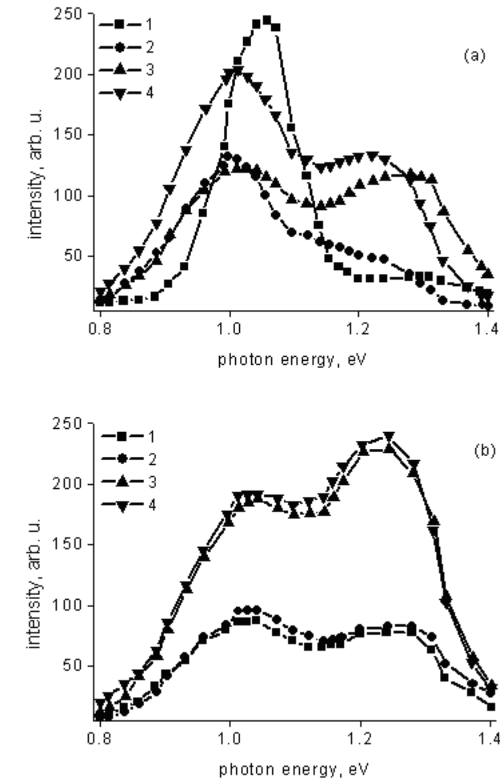

Fig. 3.11. PL spectra of the SiO_2–GaAs structure samples from the first (a) and second (b) group: 1 - initial samples, 2–4 – after microwave treatment for 2, 8 and 13 min., respectively.

in the SBDs made from the same material and (ii) metallographic investigations (Fig. 3.12) that indicate presence of structural-impurity microscopic nonuniformities in the material.

Microwave treatment of the samples belonging to the second group leads to increase of intensity for both PL bands as some threshold values of exposure are attained (Fig. 3.11b). One can assume that such action of microwave irradiation results from relaxation of the nonradiative recombination channel due to structural disordering of

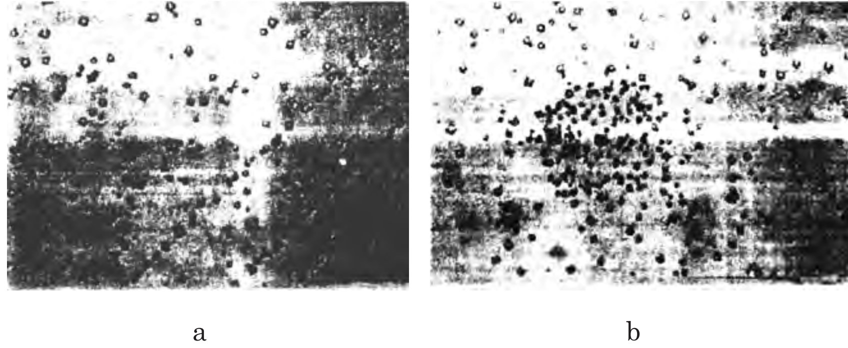

a b

Fig. 3.12. Microphotographs of different GaAs wafer areas with increased defect concentration: a – defects localized predominantly on the glide lines, b – defect cluster.

the semiconductor near-surface layer. This relaxation occurs when an oxide layer appears. The data generalized in [40] also indicate modification of the semiconductor structural-impurity subsystem under the action of strong microwave field and gettering effects related to the structural-impurity transformation. It was found that microwave treatment results in variation of the parameters of impurity aggregations, charge carrier lifetime and dislocation density. The character of structural transformations in semiconductors under action of microwave field shows that the nature of phySiCal processes proceeding in this case differs from that of the processes resulting from RTA or traditional thermal annealing in the vacuum.

After microwave treatment of the samples belonging to the first group, we observed PL peak shifting towards lower energies and antiphase variation of peak intensities as function of exposure dose (Fig. 3.11a). The intensity of the band with $h\nu' \approx 1.04$ eV first decreased with time, while that of the band with $hv'' = 1.30$ eV increased. At exposure $t_{\mathrm{exp}} \approx 8$ min. The intensities of the above two PL bands became practically equal. At bigger exposures the intensity of the first band decreased, while that of the second band decreased. Such behavior of transformation of PL spectra indicates change of both the type and

concentration of the radiating centers. The antiphase variation of the PL band intensities indicates that the defect centers are transformed into each other.

The phySiCo-chemical nature of the centers of PL with $h\nu' = 1.04$ eV and $hv'' = 1.30$ eV still is not conclusively understood. That is why it is difficult to explain the features of structural transformation of the centers of radiative recombination under action of microwave irradiation. Taking the above into account, it is of interest to analyze possible energy sources related to microwave treatment which could lead to the observed structural changes.

In our experiments the SiO_2 layer practically did not absorbed microwave radiation, and the semiconductor conductivity was rather low. So one can assume that the centers responsible for dissipation of microwave energy might be the regions with elevated content of defects and impurities. Such regions were observed in the material studied (Fig. 3.12). Let us estimate possible increase of local temperature taking into account that, at a fixed radiation wavelength, the largest inclusions have a dominant role, because the absorption cross section $\tau \sim R^3/\lambda$ (R is the inclusion radius). For a spherical inclusion, the maximal heating temperature $T_{\max}$ can be calculated from the following expression [66]:

$$T_{\max} = T_0 + \frac{P_{\mathrm{T}} R^2}{3k_0}. \tag{3.1}$$

Here T_0 is the temperature at the semiconductor–"inclusion" interface, P_{T} is the heat power density in the inclusion region (where microwave energy is absorbed), and k_0 is the heat conductivity.

From Eq. (1) it follows that $T_{\max} \approx T_0$, even if one takes the maximal inclusion size (that was about 100 $\propto$m) and assumes that P_{T} is equal to the maximal value of microwave radiating power. So there are no heating of local nonuniformity regions in semiconductor and temperature gradients related to them that could affect both diffusion redistribution of impurities and defects and the character of distribution of elastic stresses in the samples (which also could lead to redistribution of structural defects).

Let us consider one more possible mechanism of variation of the defect-impurity composition of semiconductor that is related to the non-thermal factors of action of microwave radiation. It is known that free charge carriers of a semiconductors placed in a strong electromagnetic field acquire kinetic energy that is sufficient for interband or impurity ionization: a low-temperature avalanche breakdown occurs which is accompanied with drastic increase of charge carrier concentration. As a result, the charge state of lattice atoms in local crystal regions changes. Further electrostatic interaction of these atoms with each other or with impurities leads to formation of point defects (vacancies and interstitial atoms), as well as complexes "point defect–impurity atom".

Let us estimate if the strength E of the microwave electric field used in our experiments is sufficient to form an ionized avalanche in GaAs at the maximum density of radiation energy flow incident on the sample studied. In our estimation we use the expression for loss power of electromagnetic wave in free space [67]. (For our microwave treatment, the calculated electric field strength E was about 75 V/cm.)

We may consider the acting electromagnetic field to be quasi-stationary, i.e., $\omega\tau_e < 1$ (this inequality is a fortiori valid at a frequency of 2.45 GHz). Then the electron energy ε_{el} can be written down as [67]

$$\varepsilon_{el} = \varepsilon_0 \left(1 + \beta E^2\right). \qquad (3.2)$$

Here ε_0 is the electron energy at a temperature T_0 = 300 K, $\beta = \frac{2}{3}\frac{q^2}{m^* \varepsilon_0}\tau_p\tau_e$ depends on the degree of heating, q is the electron charge, m^* = 0.067 m_0 is the electron effective mass (m_0 is the electron mass), τ_p (τ_μ) is the momentum (energy) relaxation time.

Taking $\tau_p \approx 10^{-13}$ s, $\tau_e \approx 10^{-12}$ s and $E \sim 75$ V/cm, one obtains $\varepsilon_{el} \approx \varepsilon_0$, i.e., the electron energy practically does not change under microwave irradiation. So the strength of the electric field of electromagnetic wave is explicitly insufficient to produce interband impact ionization, as well as impurity breakdown in GaAs which requires considerably lower electron energies [68].

Thus it seems that solution of the problem related to GaAs structure modification under microwave treatment should be searched beyond the scope of traditional approaches to the reasons of structural defects generation and annihilation. One of such mechanisms may result from presence in a crystal of unstable Frenkel pairs [69]. Annihilation of such pair in a microwave electromagnetic field can lead to over-the-barrier motion of a dopant or dislocation. In [64] the effect of non-activation variation of residual deformation in GaAs exposed to microwave irradiation was found. This indicates occurrence in crystals of some processes whose nature is different from that of the "traditional" mechanism of dislocation motion at thermal annealing in the vacuum.

The existence of non-thermal action of microwave radiation on atomic diffusion in InGaAs solid solutions was proved in [70]. One of the reasons for such action of microwave radiation on annealing kinetics and transformation of both extended and point defects may be related to the fields of static stresses in semiconductors (if these stresses and their gradients that appear due to semiconductor structural disordering are sufficiently big). In actual practice, however, the effect of stresses on defect migration is insignificant as a rule. This effect may increase drastically if the transformation process is of collective character. The following conditions are required for this: (i) small-size defect aggregations should be present in a semiconductor, and (ii) the time needed to involve the whole cluster in the transformation process should be small as compared with the time of material deformation response to the structural variations. In this case (as was shown in [71]) the decrease of the barrier to defect transformation or annihilation is $\Delta E = 8\times10^{-23}\, B\varepsilon N$ where B is the modulus of elasticity, ε is the local deformation in the neighborhood of defect, N is the number of defects in the cluster. One can see easily that this decrease may be several tenths of electronvolt for sufficiently big clusters.

In different semiconductor regions, the inclusion concentrations are different. Therefore the local fields of elastic stresses vary over the wafer, and their effect on the local defect transformation also varies. Taking into account that the types and activation energies of the defects in a cluster are different, one should expect different structural modifications in the such defect regions samples made from the same wafer.

One should note one more factor that may affect the character of PL spectrum variation under microwave treatment. Nonuniform distribution of charged defects over the wafer leads to nonuniform distribution of quickly diffusing impurities (say, copper) gettered by such defect regions. A change of static elastic stresses or charge state of clusters induces diffusion redistribution of impurities. In this case composite defects involving the impurities may be formed, or the impurities may become inactive.

In conclusion it should be noted that a deeper insight into the nature of the effects occurring in the dielectric–semiconductor structures exposed to microwave treatment requires further investigations, in particular, those aimed at elucidation of the nature of PL centers and their relation to the semiconductor structural nonuniformity and deformation effects (appearing due to the above nonuniformity, as well as deposition of dielectric layers).

3.4. EFFECT OF MICROWAVE RADIATION ON THE SiO_2–SiC STRUCTURES

Silicon carbide is known as a promising material for development on its basis of various microelectronic devices. Such its features as heat and radiation tolerance serve to improvement of reliability of diode and transistor operation, even under extreme service conditions [72-86].

SiO_2 films find application in the manufacturing technology for silicon carbide devices [87–92]. However, in this case (as for the silicon electronic devices) formation of high-quality dielectric layers poses a grave phySiCo-technological problem [74, 93–95]. Some authors believe that this problem can be solved by application of photostimulated processes for SiO_2 layer deposition [96, 97]. The effect of electromagnetic radiation on the properties of such dielectric layers still is not clearly understood.

In [98-101] an attempt was made to perform comparative investigation of the effect of microwave irradiation (frequency of 2.45 GHz, radiating power of 1.5 W/cm^2) on the properties of SiO_2–SiC structures. They were prepared by Svetlichnyi, Agueev, Polyakov and Kocherov (Taganrog State Radio Engineering University) using the conventional

thermal oxidation (CTO) in water vapor at a temperature $T = 1273$ K and RTA at $T = 1373$ K with quartz halogen lamps [102, 103].

The initial Lely-grown 6H-SiC samples were doped with nitrogen (concentration of (2–3)×10^{17} cm^{-3}). Before SiO_2 film growing, the samples were exposed to the standard chemical cleaning. Oxidation was made concurrently at the (0001) and $(000\bar{1})$ faces.

The transmission and PL spectra were measured (both before and after microwave treatment) in the 400–800 nm wavelength region at room temperature using a spectrometer СДЛ-2. A PbS photoresistor was used as detector of secondary radiation when studying the PL spectra in near IR. A spectral lamp СІРШ-200 served as source of radiation in continuous spectrum. A nitrogen-vapor laser (radiation wavelength of 337 nm) and a high-power incandescent lamp ПЖ-100 were used as radiation sources to excite PL.

The AFM studies of surface morphology were performed with a commercial microscope NanoScope IIIa in the tapping mode of scanning. The radius of curvature was measured for all the samples studied with a profilometer П201 (both before and after microwave treatment).

Table 3.5 presents the results of measurements of radius of curvature (on the sample face (0001) side) as function of the total time of microwave treatment τ_T. One can see that the radius of curvature of the samples exposed to RTA in the dry oxygen atmosphere at a temperature of 1273 K practically does not depend on the total time of microwave treatment. The structures exposed to long-term CTO in water vapor at a temperature of 1373 K were more sensitive to microwave treatment: the degree of variation of the sample radius of curvature as function of τ_T was proportional to the time of oxidation of the initial sample.

Additional information on the interaction of microwave radiation with the SiO_2–SiC structures was obtained when studying their optical spectra. A typical dependence of the optical density (OD) of the SiO_2–SiC structure on the wavelength of light for different τ_T (at a temperature $T = 300$ K) is shown in Fig. 3.13.

It should be noted that the absorption spectrum of the SiO_2–SiC in the 400–800 nm wavelength region is an integral characteristic, i.e., the resulting spectrum is determined by the following three factors: (i) absorption in the SiC bulk, (ii) absorption in the oxide film, and (iii) absorption at the SiO_2–SiC interface. The main contribution to the total absorption spectrum comes from the factor which is the strongest in the above spectral region. In our case, this is absorption in the SiC bulk.

A distinguishing feature of the presented spectrum is a broad band in the region about 630 nm (Fig. 3.13) which is related in the literature to the ground state of the donor centers stemming from nitrogen impurities in the silicon carbide crystals [82, 104-107]. It should be noted that this band is observed against a general broad background. The authors of [107] give the following explanation for this background absorption. The broad band with a peak near 630 nm partially overlaps with two absorption bands (the more intense broader near-edge band and the

Table 3.5. Radii of curvature R of the samples as function of the total time of microwave treatment τ_T.

Sample # (the data refer to the face (0001))	τ_T, s	R, m
A (RTA, 60 s)	0	0.5
	10	0.6
	30	0.5
	40	0.5
B (RTA, 180 s)	0	0.6
	10	0.7
	30	0.75
	40	0.8
1 (CTO, 30 min.)	0	9
	10	9
	30	8
	40	8.6
2 (CTO, 30 min.)	0	1.4
	10	1.2
	30	3.35
	40	1.3
3 (CTO, 120 min.)	0	4.1
	10	1.4
	30	1.5
	40	1.9
4 (CTO, 180 min.)	0	16.8
	10	14.7
	30	31
	40	8

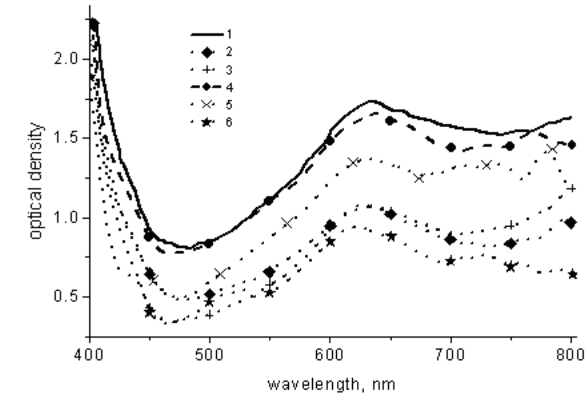

Fig. 3.13. Typical OD spectral dependencies of a SiO_2–SiC structure (temperature T = 300 K) at different total times of microwave treatment: 1 - 0 (initial sample), 2–6 – after 10÷50 s microwave treatment (at interval of 10 s).

high-energy tail of the IR absorption band) that are related to photoionization of nitrogen impurity, with transition of electron to different minima of the conduction band.

Figure 3.14 shows OD of the SiO_2–SiC samples as function of the total time τ_T of microwave treatment. The character of these curves depends on the way of SiC oxidation.

To illustrate, for the sample # 1 (Fig. 3.14, curve 1), OD decreases at τ_T = 10 s. Then, after repeated 10 s microwave treatment, OD remains the same, and increases practically up to its initial value when τ_T becomes equal to 30 s. At further increase of τ_T, first an increase of OD is observed (at 40 s microwave treatment), and then it becomes to decrease.

The sample # 2 (Fig. 3.14, curve 2) also demonstrates a decrease of OD at 10 and 20 s microwave treatment (the OD values are the same for these two durations). At the total time of microwave treatment τ_T = 30 s, the OD value increases (as in the sample # 1). In this case, however, the OD value after 30 s microwave treatment remains below that of the initial sample. At further increase of τ_T, first an increase

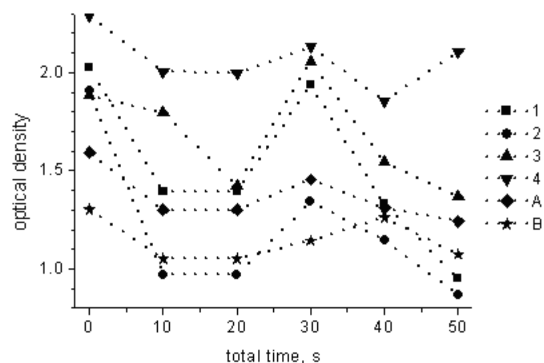

Fig. 3.14. Sample OD as function of the total time of microwave treatment. Curves 1–4 correspond to the structures obtained using CTO in water vapor at a temperature of 1373 K (time of oxidation, min.: 1 - 30, 2 - 60, 3 - 120, 4 - 180). Curves A and B correspond to the structures obtained using RTA in the dry oxygen atmosphere at a temperature of 1273 K (time of oxidation, min.: A - 60, B - 180).

of OD is observed at 40 s microwave treatment (as for the sample # 1), and then it becomes to decrease.

A somewhat different dependence of OD on τ_T was observed for the sample # 3 (Fig. 3.14, curve 3). Its absorption spectrum remains practically unchanged after microwave treatment for 10 s. But when $\tau_T =$ 20 s, the OD value decreases, while at the 30 s microwave treatment it increases. In this case the OD value after microwave treatment is over that for the initial sample. At further increase of τ_T, OD of the sample # 3 varies in the same way as for the samples # 1 and 2.

The 630 nm band in the OD spectrum of the sample # 4 is pronounced most clearly. At the same time, as one can see from Fig. 3.14 (curve 4), the sensitivity of this sample to microwave irradiation is the lowest of the four samples that were prepared using CTO in water vapor at a temperature of 1373 K. If τ_T is 10 or 20 s, then OD of the sample somewhat decreases as compared to that for the initial sample. But when τ_T is 30 s, then OD somewhat increases. Contrary to the samples # 1–3, further increase of τ_T first leads to decrease of OD of the sample (at 40 s microwave treatment), and then its OD increases slightly.

For the sample A (Fig. 3.14, curve A), the OD dependence on τ_T at the starting values of total time is the same as for the sample # 4: insignificant OD decrease at τ_T = 10 and 20 s and slight increase of OD at τ_T = 30 s. However, as τ_T increases up to 40 s, OD of the sample A first increases and then (at further growth of τ_T) decreases, as for the samples # 1–3.

For the sample B, OD decreases after microwave treatment for 10 s and then remains unchanged as τ_T increases up to 30 s. Further increase of τ_T first leads (as for the sample A) to increase of OD as τ_T grows up to 40 s, and then OD decreases.

One can see from Fig. 3.14 that those samples are most tolerant to microwave irradiation that were obtained using RTA in the dry oxygen atmosphere at a temperature of 1273 K (curves A and B). It is of interest that (judging from the optical transmission spectra) those of the samples obtained using CTO in water vapor at a temperature of 1373 K are most tolerant to microwave irradiation whose time of oxidation is the biggest (Fig. 3.14, curve 4). Although one would expect, on the basis of the results of measurements of the samples radii of curvature (see Table 3.5) that just the above samples would demonstrate the strongest dependence of OD on the total time τ_T of microwave treatment.

The half-width of the band 630 nm vs τ_T curve is shown in Fig. 3.15. Here (as in Fig. 3.14) curves 1–4 refer to the structures obtained using CTO in water vapor at a temperature of 1373 K, the time of oxidation being 30 (1), 60 (2), 120 (3) and 180 min. (4), respectively; curves A and B refer to the structures obtained using RTA in the dry oxygen atmosphere at a temperature of 1273 K, the time of oxidation being 60 (A) and 180 s (B). Contrary to the case of OD, one cannot detect a general trend in the dependence of the half-width of absorption band with a peak at 630 nm on the total time of microwave treatment. The above dependence is nonmonotone.

The following assumption may be proposed for explanation of variation of the band half-width resulting from microwave treatment. According to [107], the band 630 nm results from photoionization of three nonequivalent nitrogen donors (with hexagonal and cubic

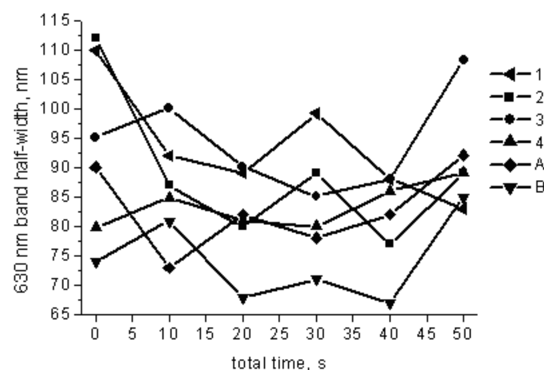

Fig. 3.15. Half-width of the band 630 nm as function of the total time of microwave treatment (same marks as in Fig. 3.14).

coordination of the nearest surroundings). It factually involves three close lines that merge in a broad band. The symmetry of the nearest surroundings of some nitrogen impurities possibly changes under the action of micro-wave radiation, and this may lead to redistribution of the intensities of single lines that form the band 630 nm. As a result, this may lead to change half-width of this band.

Our investigations of the surface morphology showed that growth of oxide film at the SiC surface starts in the defect areas (scratches) (Fig. 3.16). Further oxidation stage - growth of the so-called crystalline whiskers with diameter up to 10 µm – occurs predominantly at the (0001) surface (Fig. 3.18).

Beside this, we observed a microrelief against the macroscopic relief background at the (0001) surface of the samples B, 2 and 3. It was formed by nanoislands (most likely, also SiO_2) of different sizes and density, depending on the way of oxidation (Fig. 3.18a). Microwave treatment for 10 and 20 s did not lead to changes of surface morphology. However, microwave irradiation for 30 s resulted in disappearance of the nanoislands for all the samples where they have been detected earlier, although macroscopic relief of the (0001) surface did not change in this case (Fig. 3.16b). 30 s microwave irradiation led to appearance of the above-mentioned

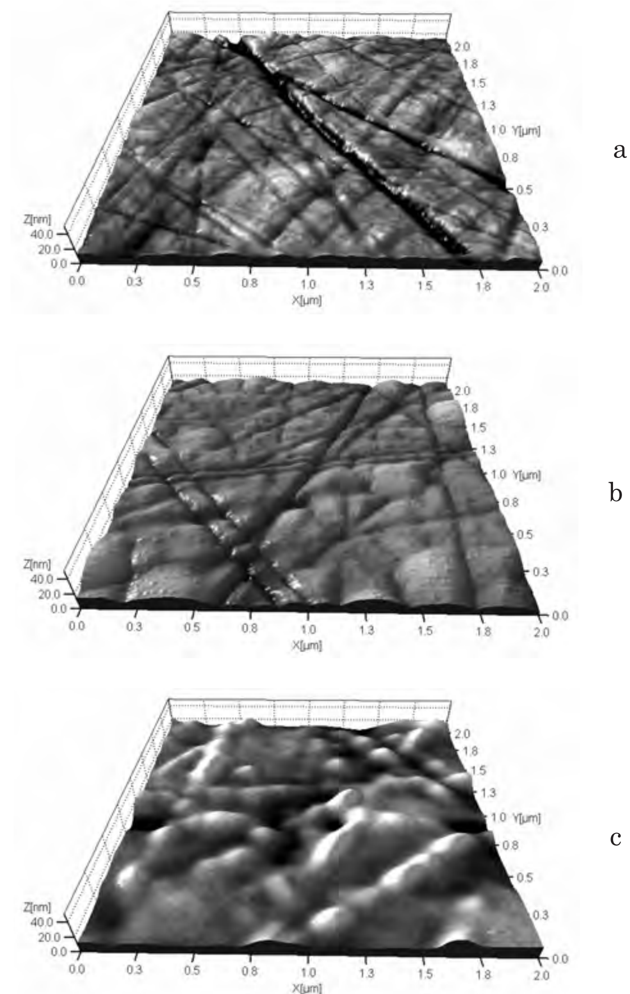

Fig. 3.16.(a,b) Morphology of SiC (0001) surface: a - initial, b (c) – after oxidation for 1 (30) min. X:Y:Z = 1:1:5.

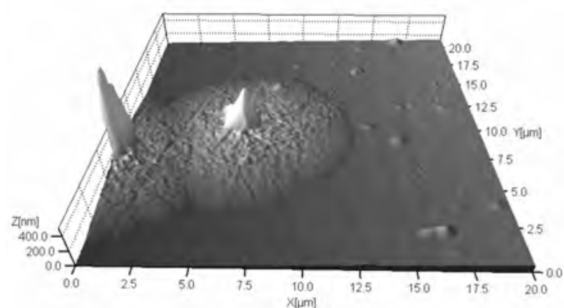

Fig. 3.17. Growth of big oxide clusters at the SiC (0001) surface after oxidation for 120 min. X:Y:Z = 1:1:5.

crystalline whiskers at the $\left(000\bar{1}\right)$ surface. Further increase of the total time of microwave treatment did not lead to variation of the macroscopic relief and microrelief. One may assume that a phase or structural change of oxide film occurred at the surface of the samples B, 2 and 3 at 30 s microwave irradiation. This change manifested itself as nanoscale smoothing of the surface, with the final roughness size of about 0.3 nm.

Our experimental results enable one to conclude that the structures obtained using RTA in the dry oxygen atmosphere are the most tolerant to microwave irradiation. In addition, it was found that microwave treatment with total time of 30 s and more leads to decrease (and even disappearance) of nanoislands in the oxide films at silicon carbide surface, as well as make the irradiated surface smoother.

The experimental results on the effect of electromagnetic radiation on the electrophySiCal properties of the SiO_2–GaAs (SiC) structures presented in this Chapter indicate the following. Despite high reproducibility of the effects observed which lead to changes in the properties of near-surface semiconductor regions and dielectric–semiconductor interfaces, a mechanism of such action is very complicated, and some additional theoretical and experimental investigations are required for its determination. It is obvious, however, that the effects induced by microwave irradiation must be taken into account by the developers of novel technologies of microwave devices.

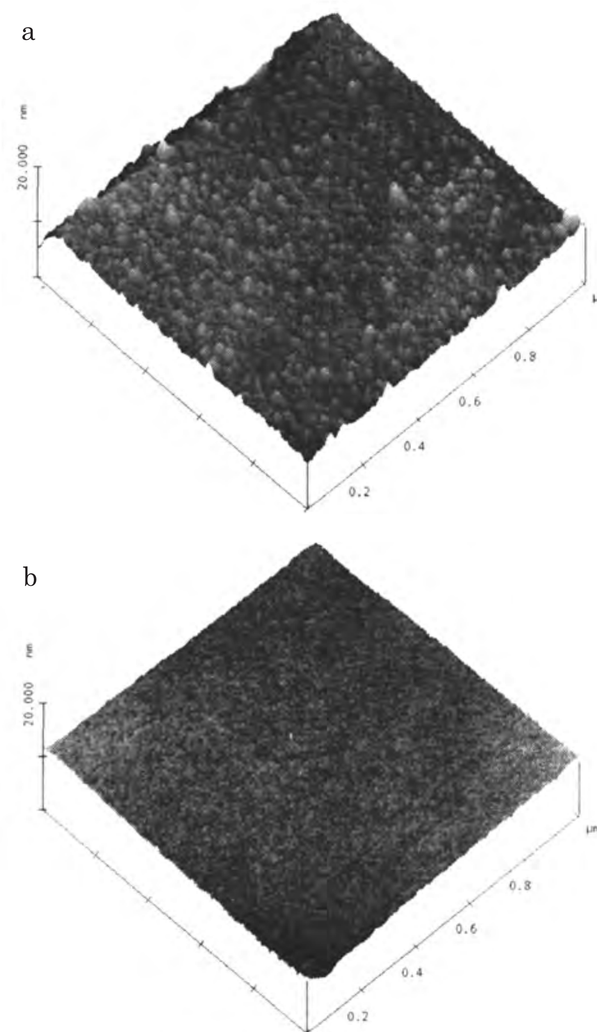

Fig. 3.18.(a) Surface morphology of the sample # 3 before (a) and after 30 s microwave treatment (b).

Chapter 4.

EFFECT OF MICROWAVE IRRADIATION ON THE MORPHOLOGICAL AND STRUCTURAL PROPERTIES OF NANOCRYSTALLINE SILICON–SILICON SYSTEMS

Photoluminescence of silicon nanocrystals (NCs) in the visible spectral region at room temperature is intensely investigated because it can elucidate the processes in quantum-confined nanostructures which could be applied in the quantum optoelectronics. Silicon NCs are in a dielectric medium, most often, in silicon oxide SiO_x ($0 < x \leq 2$). Porous silicon (por-Si) that is formed using (electro)chemical etching of single-crystalline silicon (c-Si), as well as the films of nanocrystalline silicon (nc-Si) obtained using various techniques (sputtering, chemical deposition, ion implantation, laser ablation, etc.), belong to the above nanocomposite systems.

It is known that electromagnetic radiation from various frequency bands is widely used in semiconductor materials science and instrument-making industry [1–43]. It can play a great role in the manufacturing technology when forming the required properties of nc systems. There are some data on the effect of high-power laser radiation (see, e.g., [44]) and various doses of γ-radiation (see, e.g., [45]). However, except for the works [46–48], there exist practically no investigations of the effect of microwave treatment on the structural and PL properties of nc-Si.

Compared to por-Si films, those of nc-Si have higher mechanical strength. Their structure can be controlled easier, and it is possible to form nc-Si films on any substrates. Of different methods used to obtain nc-Si films, the pulsed laser deposition (PLD) technique

(which belongs to the well-developed methods) has advantages in what refers to composite formation (congruence of film composition). This technique was applied by Kaganovich, Svechnikov, Manoilov et al. [49–51] for determination of the conditions of nc-Si film formation using PL in the visible spectral range. However, clear interrelations between PL and the features of nc-Si film formation (which could help in determination of the nature of PL in the Si 0D NCs) still have not been found.

In [52] the features of surface morphology and structure of nc-Si films depending on the PLD modes were investigated, as well as interrelation between the film structure and PL properties was determined. A possibility of control over the structural and photoelectric properties of such objects was demonstrated in [46–48]. Some results of these investigations are considered below.

4.1. EXPERIMENTAL PROCEDURES

The films were deposited in the vacuum (see Fig. 4.1) from a particles flow in an erosion spray. The erosion spray was formed at scanning of a c-Si target (5) with a YAG:Nd^{3+} laser beam (1) (λ = 1.06 μm). The laser was operating in the *Q*-spoiled mode, with pulse energy of 0.2 J, pulse length of 10 ns and pulse-repetition rate of 25 Hz. The substrates (6, 7) were commercial wafers made of *p*-silicon (100) (brand mark КДБ-10) with resistivity of 10 Ω·cm.

We prepared films of two types. They were obtained in different ways. The films of the first type (films I) were formed in the oxygen atmosphere (the pressure varied from 1.5×10^{-2} up to 20 Pa) from a direct particle flow in a spray onto the substrate (7) that was located on the spray axis at a distance from the target (technique I). The films of the second type (films II) were formed in the argon atmosphere (the pressure of about 13 Pa) from a reverse particle flow onto the substrate (6) located in the target plane (technique II). The feature of technique II was that the particles scattered by the argon atoms came back to the target plane. Such film had a wedge-shaped profile whose width

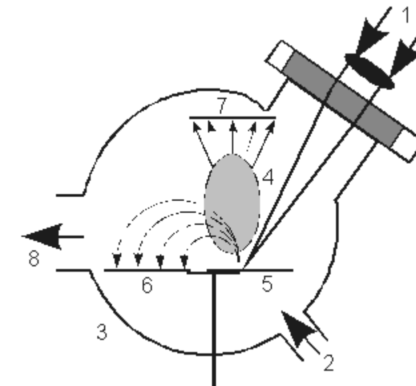

Fig. 4.1. Schematic of the setup for PLD film formation: 1 – YAG:Nd^{3+} laser beam, 2 – letting-to-air, 3 – vacuum chamber, 4 – erosion spray, 5 – target, 6 and 7 – substrates, 8 – to the vacuum pump.

(at a section of 12 mm) varied from 500 down to 50 nm in the course of sputtering that lasted about 30 min.

The film surface morphology was studied with scanning AFM in the tapping mode using a microscope NanoScope IIIa (produced by Digital Instruments) [53]. We used silicon needles with rated point radius of 5 nm. The needle points were checked (both before and after surface measurements) using a test grid TGT 1(produced by NT-MDT) [54]. This was made from the patterns of single grid elements [55], as well as from the algorithm for needle form determination from the results of measurement of a surface about which we had no prior knowledge (the so-called blind reconstruction) [56].

When performing AFM studies of surfaces with reliefs whose small part sizes are comparable to that of the needle point, one should not ignore the effects of superposition of the point form on the actual small parts of surface relief in the AFM patterns. To take the above effects into account, we performed reconstruction of the measured surface patterns from the known form of the needle point. The reconstruction procedure is based on the algorithms described in [56, 57]. The general result of such reconstruction is decrease of the lateral sizes of projections and increase of the pore diameters.

We determined the level of deformations in the c-Si substrate near the nc-Si/c-Si heteroboundary from the results of XRD measurements of radius of curvature R of the near-surface crystallographic planes of the substrate [58]. The deformation level was estimated using the approximate expression $\varepsilon \approx t/2R$ where t is the substrate thickness. The informative layer thickness (i.e., the depth of x-ray penetration) was 42 μm for the reflection 400.

The crystalline structure of the films was studied with x-ray phase analysis using the $Cu_{K\alpha}$-radiation and a focusing LiF monochromator before the detector. This ensured high sensitivity of the technique.

4.2. EFFECT OF THE CONDITIONS OF FORMATION OF NANOCRYSTALLINE SILICON FILMS ON THEIR STRUCTURE

The data of x-ray phase analysis show that the nc-Si films II obtained using the reverse particle flow in the erosion spray are x-ray-amorphous. The films II deposited near the erosion spray axis demonstrate (along with an intense halo in the small angle region which is characteristic of an x-ray-amorphous material) weak broad diffraction maxima that belong to polycrystalline silicon. The sizes of the coherent scattering regions of nc-Si film II are several nanometers; they are increasing when approaching the spray axis. There are also weak peaks on the XRD patterns. These peaks seem to be related to presence of another phase – silicon oxide. Thus the films II are two-phase systems (Fig. 4.2).

For the films I obtained using the direct particle flow in the erosion spray at a pressure of oxygen of 6.5 Pa, the diffraction peaks related to polycrystalline silicon are more intense than those in the films II. This fact indicates somewhat bigger content of polycrystalline phase of silicon in the films I (these films are two-phase too). Polycrystalline silicon is the predominant phase in the films I deposited without introduction of oxygen, while silicon oxide is the predominant phase in the films I obtained at a pressure of oxygen of 16 Pa.

Our AFM studies revealed (see Figs.4.3 and 4.4) that surface morphology in the two-phase nc-Si films depends essentially on the

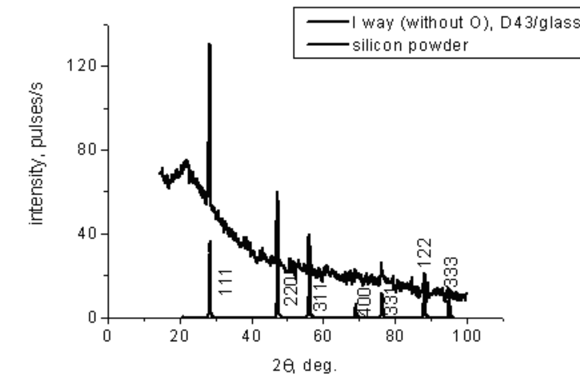

Fig. 4.2. XRD pattern of nc-Si in SiO_x film deposited in the way I at a big distance from spray. (A simulated XRD pattern of Si powder is also shown.)

conditions of film formation. One can see that the surface of the films I obtained at a pressure of oxygen of 6.5 Pa (see Fig. 4.3a) consists of clusters whose lateral sizes are 100–300 nm and height values are spread considerably (from 1.5 up to 13 nm), although the average surface roughness is 1.8 nm. The above clusters and flat surface areas are covered with grains (mean diameter of 10–15 nm). The films have good adhesion and contain practically no pores.

The films II (see Fig. 4.3b) are characterized by higher degree of surface uniformity. They have no clusters, there are pores in them, and the mean grain diameter values are smaller than those in the films I. Figure 4.5 shows the histograms of the relief heights and grain diameters for fragments of surfaces of films II deposited at a distance from the erosion spray axis and in the immediate vicinity of it. One can see that, when going from the spray axis, the mean size of the grains on the film surface decreases from 15.2 down to 7.0 nm, while the average roughness reduces from 1.5 down to 0.6 nm. Besides, the thinner films are characterized by more uniform grain size distribution than the thicker ones. Characteristic of the latter films is presence of (i) another peak on the histogram which is due to the grains with diameters from 20 up to 25 nm, and (ii) bigger (about 10 nm) pores (see Fig. 4.5b, curves 1 and 2).

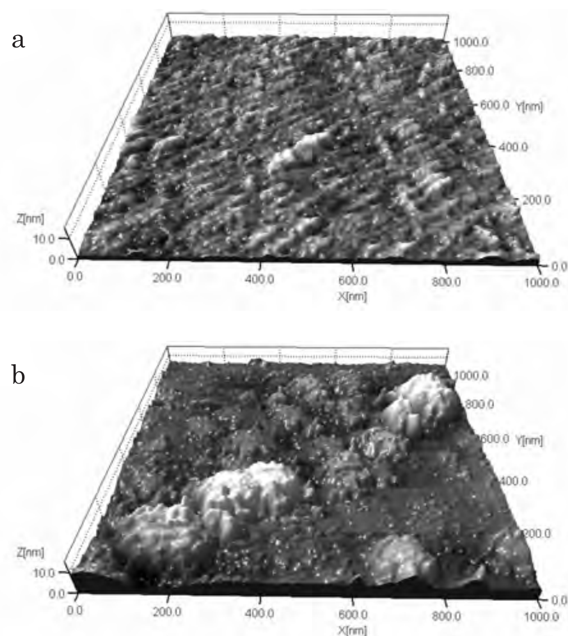

Fig. 4.3. AFM 3D images of the surfaces of films: a - deposited in the way I (at a pressure of oxygen of 6.5 Pa), b - deposited in the way II.

When the thin film regions lying far from the erosion spray axis are doped with gold, this results not only in shifting the peak of distribution towards bigger grain sizes but also in increase of the half-width of the grain size distribution curve (Fig. 4.5b, curve 3). And doping with gold of the thick areas (that are obtained in the immediate vicinity of the spray axis) results in disappearance of the bimodal grain size distribution. Beside this, some grains appear whose diameters are several times that corresponding to the distribution peak (Fig. 4.5b, curve 4). In this case, however, both surface roughness and height distribution for thick films do not change considerably after film doping with gold (see Fig. 4.5a, curves 2 and 4).

Before coming to an analysis of the results of AFM studies, one should note that, even after performing reconstruction of the surfaces,

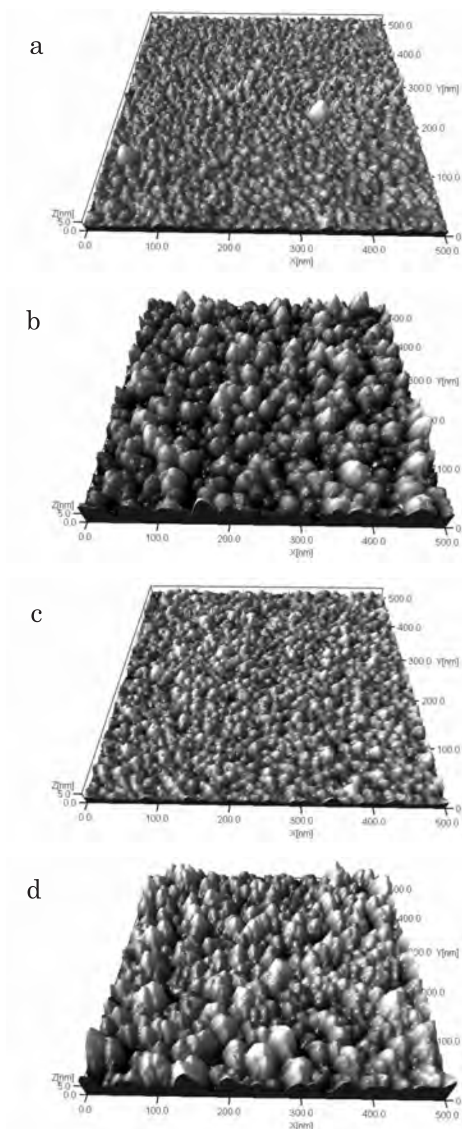

Fig. 4.4.(a,b) Surface morphology of undoped (a and b) and Au-doped (c and d) nc-Si films: a, c – thin, with smaller Si NC; b, d – thick, with larger Si NC. X:Y:Z = 1:1:5.

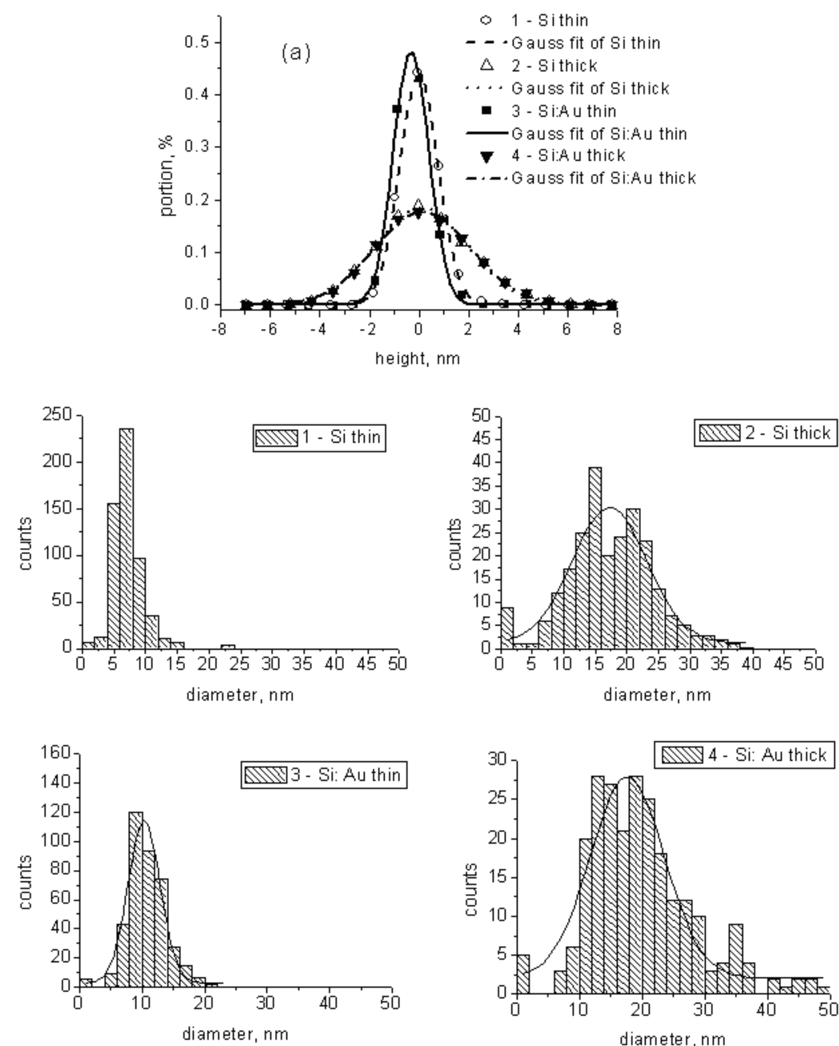

Fig. 4.5. a – surface height histograms for films deposited in the way I: near spray (1, 3); at a distance of 12 mm (2, 4). (Films 3 and 4 were doped with Au.) Point count of histogram bins was normalized to the total number of surface points. b – grain diameter histograms for films deposited in the way I: near spray (1, 3); at a distance of 12 mm (2, 4). (Films 3 and 4 were doped with Au.) The normal distribution curves are shown over the histograms.

the obtained magnitudes of the geometric sizes of their details may be somewhat overestimated. In addition, the crystallites that form the surface are in special conditions (as compared to those for the crystallites in the bulk) because the growth of surface crystallites is less constrained. It should be also noted that the surface grains consist of silicon NCs and their oxide coatings, so the factual sizes of Si NCs are below the size values obtained for the surface grains.

The above distinctions in the surface morphology of the films I and II result, above all, from the different character of particle flows that are forming the films. In the technique I, when deposition occurs from an intense direct particle flow in the erosion spray at an oxygen pressure of 6.5 Pa, film growth involves the high-energy particles whose sizes are spread widely. The film growth rate is high, and soon large clusters become coated with small-size particles. The same factors ensure high film adhesion and absence of pores.

In the technique II, the films are formed from a reverse particle flow in the erosion spray at a high pressure of inert gas (argon). Therefore the silicon atoms and clusters from the target are scattered by the argon atoms, slow down and return to the target plane with energy much lower than in the technique I. The larger particles are accumulated on the substrate near the spray axis, while the smaller ones are accumulated at a bigger distance. The diffusion processes practically do not occur in this case, so the films obtained are porous, and their adhesion is much weaker.

Probably increase of the size of grains at the film surface at doping with gold is related to the following two factors. One of them is the activation properties of gold in the course of crystallization. This assumption is supported by the fact that a nucleation layer of an undoped film is formed with the grains whose boundaries are not well-defined, while doping with gold leads to formation of well-defined grain boundaries in the layer. Another factor is that gold is an electropositive metal, and so it serves as catalyst for oxidation of Si NCs due to trapping of valence electrons from weak Si–Si surface bonds. The volume of silicon dioxide is almost three times that of Si from which SiO_2 has been formed. So doping

Table 4.1. The deformation levels in different nc-Si/c-Si structures.

Parameters	c-Si substrate	Types of nc-Si films		
		I	II	II doped with Au
Radius of curvature R, m	30.00	24.27	51.57	–74.35
Deformation ε ($\times 10^6$)	5.00	6.18	2.91	–2.07

with gold results in a considerable increase of the surface grains (which, as was stated before, are Si crystallites with an oxide coating).

Table 4.1 presents typical values of stresses in the near-surface layers of the c-Si substrates in the nc-Si/c-Si structures. Before deposition of nc-Si film, a typical radius of curvature of c-Si was $R \approx 30$ m, and the level of macroscopic deformation was $\varepsilon \approx 5\times10^{-6}$. The structure studied was convex on the side onto which a film was to be deposited. Such a considerable value of residual deformation was due to different treatments of both sides: after mechanical polishing of the c-Si wafer, further chemo-dynamic polishing was made only on the side intended for film deposition. It was found that the stresses in the nc-Si/c-Si structures vary depending on the technique of film deposition, as well as on film thickness and doping.

One can see from Table 4.1 that, if the films were formed using the technique I, the macroscopic deformations increased by 23%, while deposition of films II decreased deformations by 42%. When the films II were doped with gold, not only the deformation demonstrated further decrease (by 59%) but the sign of system curvature reversed (the system became concave on the side with nc-Si film).

To explain such behavior of the system studied, some additional experiments are required. The following assumptions, however, can be made now. Different deformation values for the films obtained using different deposition techniques (without doping with gold) may be due to the fact that high- and low-energy Si particles interact with the substrate surface (and modify it) in different ways. When doping with gold is made at concurrent laser ablation of silicon and gold, a surface phase Si–Au is formed near the substrate–film heteroboundary, thus causing negative deformation.

In [52] it was shown that the structural and morphological properties of the nc-Si films correlate with the PL spectra of these films.

4.3. EFFECT OF MICROWAVE TREATMENT ON THE STRUCTURAL PROPERTIES OF NANOCRYSTALLINE SILICON–SILICON SYSTEMS

Both doped and undoped nc-Si films deposited onto a *p*-Si substrate are in a nonequilibrium state. Processes of structural ordering are to occur in them under various external actions, in particular, microwave irradiation. AFM studies of the films exposed to microwave radiation (even of the maximal – 7.5 W/cm^2 – irradiance) did not reveal noticeable changes in their surface morphology. The results of high information ability have been obtained, however, when measuring radius of curvature for the *p*-Si, *p*-Si/nc-Si and *p*-Si/nc-Si<Au> samples with the XRD technique (Fig. 4.6). For the samples consisting of the *p*-Si substrate only, the radius of curvature R was about 30 m; the samples were convex toward the side at which the nc-Si films were later deposited (curvature sign “plus”). The calculation gave for the strain $\Delta d/d$ the value of about 5×10^{-6}. Stressed state of the initial substrate was due to different treatments of its sides. That used for nc-Si films deposi-

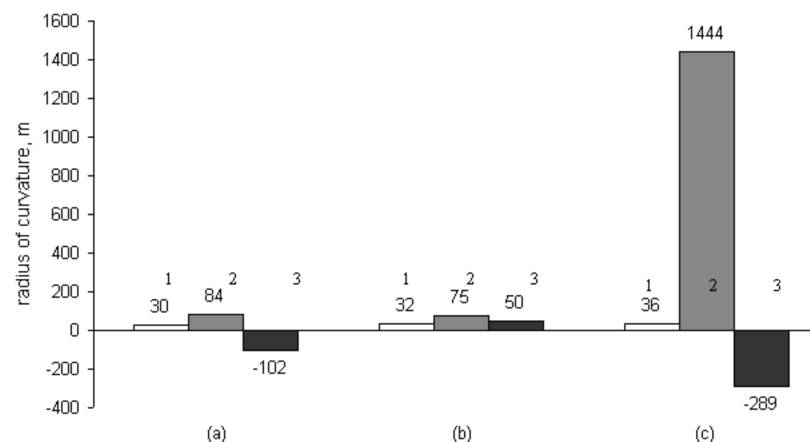

Fig. 4.6. Variation dynamics for radii of curvature of structures: 1 – substrate; 2 – substrate with undoped film; 3 – substrate with Au-doped film. a – initial; b – after microwave irradiation for 5 s; c – after further keeping out of doors for 120 h.

tion was at first chemo-dynamically treated, then treated in HF and washed in water. As a result, it had a hydride coating that, being exposed to air, gradually gave place to a thin oxide film. Another side of the substrate experienced only mechanical lapping before the HF treatment. One can see from Fig. 4.6 that the radius of curvature of the *p*-Si substrate practically did not change after microwave irradiation followed by keeping out of doors.

After deposition of an undoped nc-Si film onto the *p*-Si substrate, the strain in the system studied dropped (R = 84 m). Microwave irradiation somewhat increased strain (R = 75 m), but then, after keeping the sample out of doors for 120 h, strains strongly relaxed (the radius of curvature grew up to 1444 m). Very interesting results were obtained after deposition of an nc-Si<Au> film onto the substrate. In this case the radius of curvature changed its sign, i.e., the nc-Si<Au>/*p*-Si system became concave toward the film, and its strain considerably decreased (R = –102 m). This fact can be related to both the above mechanism for a gold–silicon phase formation at the film/substrate interface and thermal strains caused by the difference of the film and substrate thermal expansion coefficients.

Changes of sign and value of the radius of curvature immediately after microwave irradiation (R = 50 m) seem to result from both disordering of the above surface phase and structural defects redistribution under microwave field action. However, during keeping samples out of doors that phase restores and metastable defect clusters dissociate. As a result, the radius of curvature becomes negative again, and its magnitude substantially increases (R = –289 m). Thus in both cases (undoped and Au-doped films on the *p*-Si substrate) microwave irradiation induces processes of structure relaxation proceeding after it. As a result, the residual strains in the nc-Si/*p*-Si and nc-Si<Au>/*p*-Si systems drop abruptly.

Summing up the results obtained, one should note that the change of the properties of the nc-Si/*p*-Si structures exposed to microwave treatment depends on (i) the microwave radiating power and exposure time and (ii) the initial (before microwave irradiation) properties of the

structure. High radiating powers of the microwave field result in degradation of the structure parameters. This was illustrated in [47, 48] by the example of PL decrease in the undoped structure and complete PL disappearance in the Au-doped structure exposed to microwave irradiation with radiating power of 7.5 W/cm^2. At the same time, action of microwave field with moderate (1.5 W/cm^2) radiating power may impair, as well as improve, the structure parameters [47].

Chapter 5.

MICROWAVE AND γ-RADIATION IMPACT ON Ta_2O_5–Si STACK CAPACITORS

The steady trend towards smaller dimensions of ICs has placed high priority on finding *new materials* to replace the long-standing SiO_2 dielectric. Continued scaling below 100 nm node refers to top-down microelectronics, and respectively determines the research in process technology [1]. Although great successes have been achieved, the further miniaturization of Dynamic Random Access Memories (DRAMs) cannot be realized with conventional SiO_2-based insulators, because they have reached their physical limit of thinning defined by direct tunneling current through the dielectric. (In fact the exact thickness limits are currently the source of significant research and debate.) The inevitable reduction in capacitor area of DRAMs has made it difficult to maintain the stored charge in nanoscale memory capacitors needed to prevent soft errors caused by α-rays incidence. So the scaling down of Si ICs has pushed conventional SiO_2 and SiO_xN_y insulators to their physical limits in terms of reduction of thickness and dielectric strength. New storage capacitors using active dielectric films with an equivalent SiO_2 film thickness, d_{eq}, of less than 1 nm and having low enough leakage current for favorable memory operation are required to realize the fabrication of low-power and high-density DRAMs. (The equivalent oxide thickness refers to the thickness of any dielectric scaled by the ratio of its permittivity to that of SiO_2.) One solution of the problem is the replacement of SiO_2-based insulators by an alternative insulator(s) with a high dielectric constant (high-k). Worldwide research efforts to find valuable candidate materials have so far shown very promising results. New alternative ma-

terials with higher dielectric constant instead of SiO_2 providing the same capacitance but at considerably larger physical thickness are proposed in order to minimize the impact of miniaturization and to overcome the leakage current limitations of extremely thin conventional dielectrics. High-*k* metal oxides are currently under consideration as novel active dielectrics for both types of Si devices, DRAMs and metal-oxide-semiconductor field-effect transistors (MOSFETs). Determination of the best materials, the best processing techniques for obtaining these materials and integrating them into the mainstream technological process are all extremely challenging tasks. Among the single metal oxides, *tantalum pentoxide* appears to be *one of the best candidates* to replace SiO_2 and SiO_xN_y in high-density (Gigabits) DRAMs, due to its compatibility with Ultra Large Scale Integration (ULSI) processing, high dielectric constant (up to 20–30), relatively low leakage current, high breakdown fields and chemical stability. Respectively, Ta_2O_5 capacitor technologies are widely studied in order to meet the critical requirement of nanoscale manufacturing [1–11]. A number of important film-related parameters must be carefully and simultaneously optimized and controlled in order to gain a success in the minimization of the leakage current to the required tolerable levels in accordance with the requirements of International Technology Roadmap for Semiconductors. To overcome these issues, persistent efforts in both the fundamental understanding of stack dielectrics material and materials engineering including optimization of technology steps are required. The major focus on Ta_2O_5 films research is to optimize the *leakage current* and the *dielectric constant* - the two most important parameters for the material to be used as memory dielectric in highly integrated dynamic memories. In order to improve the electrical characteristics of the Ta_2O_5–Si system, *high-temperature post-fabrication treatments are absolutely necessary*. As a rule, however, these annealing processes result usually in two undesirable effects:

(i) Unavoidable increase of the interfacial layer thickness which can compromise the benefits of Ta_2O_5 as high-*k* material. The interfacial layer at Si (1–4 nm thick depending on the technological conditions) consists of silicon oxides, i.e., it is a lower-*k* layer. The phenomenon of

formation of interfacial layer is related to thermodynamic instability of most of high-*k* insulators (Ta_2O_5 is no exception), in direct contact with Si against formation of SiO_2 [1, 3, 7]. This layer reduces the global dielectric constant of the stack capacitor but at the same time ensures better interfacial properties. The lower-*k* layer in series with the Ta_2O_5 can, in some cases, even nullify the benefits of Ta_2O_5 as a high-*k* dielectric with a capacitance corresponding to the desirable value of d_{eq}.

(ii) Partial crystallization of the films which is unacceptable for ULSI applications. Usually as-fabricated films are amorphous due to the low temperature of formation. As typical high-*k* insulator, however, Ta_2O_5 crystallizes if subjected to temperatures over about 873 K [3–6, 9, 12–21]. This is accompanied usually with a reduction of breakdown strength [3, 13]. Generally, the exact value of crystallization temperature depends on both the film thickness and amorphous status of the initial film [13, 19]; the crystallized films show orthorhombic (β-Ta_2O_5), hexagonal (δ-Ta_2O_5) or monoclinic phase (usually detected above 973 K) [3, 13, 14, 18, 21, 22]. Although crystalline Ta_2O_5 has a higher dielectric constant than amorphous one [7, 17, 18, 20], its leakage current can be higher because the grain boundaries serve as an additional leakage current path. On the other hand, it is generally recognized that annealing repairs the oxygen vacancies and various structural imperfections in the films [3, 5, 7, 19, 20, 23–25]. Thus the leakage current could be effectively reduced [19, 20]. Although post-fabrication annealing at high temperatures can in some cases effectively reduce the leakage current (stimulating net annealing) [7, 19, 23, 24], one has to consider all other effects which might influence the physical and electrical properties of the layers.

So, one solution of the problem with high-temperature treatment of Ta_2O_5 (and generally of high-*k* dielectrics) is to find *alternative annealing method(s) to replace high-temperature heating* and thus to avoid both the crystallization effects in the films and the additional growth of the interfacial layer.

We have shown in a number of investigations [5, 8, 11, 13, 14, 18, 19, 23, 25–27] that amorphous and stoichiometric Ta_2O_5 can be

successfully obtained by two methods: (i) radio frequency (rf) sputtering of Ta in $Ar + O_2$ gas mixture, and (ii) thermal oxidation (at temperatures of 823–873 K) of thin Ta layer deposited on Si. It has been established that the initial films are amorphous whereas crystalline Ta_2O_5 (orthorhombic β-Ta_2O_5 phase) has been obtained after treatment in O_2 or N_2 at 1123 K. The high-temperature treatment is beneficial for: dielectric constant (it reaches values of 35–37 after 30 min. annealing); a reduction of oxide charge to ~10^{10} cm^{-2}; an increase of breakdown strength and a reduction of the leakage current, i.e., the crystalline Ta_2O_5 shows better leakage current properties than the amorphous one. A current density as low as 10^{-8}–10^{-9} A/cm^{-2} at 1 MV/cm applied field for 15–25 nm annealed layers has been obtained. Improvement of leakage current at oxygen annealing (OA) could be associated with the specific phenomena of heating in O_2 ambient: smaller amount of imperfections in the arrangement and less deficiency of oxygen atoms bonded to tantalum one as well as higher quality of the interfacial SiO_2. Probably these effects (at annealing conditions used) dominate over those of the crystallization-induced grain boundaries and, as a result, the leakage current reduces. It was established that N_2 annealing improves the stoichiometry and microstructure of both the bulk Ta_2O_5 and the interfacial transition region at Si, which manifests as a reduced amount of suboxides. The anneal process reduces the excess Si and decreases the width of the interface region (a trend to more abrupt interface is observed) resulting generally in improvement of dielectric and interface parameters of the stack capacitor. Despite the beneficial influence on the leakage current, however, the crystallization is unacceptable for high-density devices because it leads to poor point-to-point uniformity and variation of the parameters from one device to another.

Recently we have shown [28–30] that microwave irradiation (2.45 GHz) for several seconds at room temperature *could be successfully used as a method for improving electrical and structural parameters* of the Ta_2O_5–Si system (a significant reduction of leakage current and an increase of the dielectric constant), and in this sense *it could*

be alternative to high-temperature annealing steps. The big advantage of microwave irradiation annealing is the *strongly reduced thermal budget*: room temperature and extremely short (seconds) annealing times. The results imply that most likely the effect is universal and will be valid for other high-*k* dielectrics.

Here we will demonstrate the microwave irradiation-induced improvement of the structures of very thin Ta_2O_5 (obtained by two methods: rf sputtering and thermal oxidation) on Si. Comparing the electrical, structural and optical properties of the films before and after irradiation we aim to clarify the effects of the microwave treatment. The relationship between the electrical and physical characteristics will also be discussed.

The second part of this chapter is dedicated to the influence of γ-radiation on thin Ta_2O_5–Si structures [31]. As is known, an important factor on which the electrical parameters of thin layers depend and which in many cases causes electrical conduction in the microstructures is their *radiation hardness*. Since the tantalum pentoxide could be potentially used in radiation-rich conditions, it is of importance to have knowledge of the radiation effects in Ta_2O_5-based metal–oxide–semiconductor (MOS) devices. These effects in MOS capacitors with Ta_2O_5 are very poorly studied. It is found [3] that, in general, the trapped positive oxide charge, the interface states concentration and the leakage current density increase after irradiation. The conditions, however, under which the change in the leakage currents and in both the electrical and dielectric properties occurs in dependence on the parameters of the irradiation have not yet been clarified. The purpose here is to show the effect of γ-irradiation on the properties of thin Ta_2O_5 layers (rf sputtered and thermally grown) on Si depending on the technological conditions of films preparation.

5.1. EFFECT OF MICROWAVE RADIATION ON Ta_2O_5–Si MICROSTRUCTURES: RF SPUTTERED Ta_2O_5

5.1.1. Experimental procedure

Chemically cleaned *p*-type (15 Ω·cm) Si (100) wafers were used as substrates. Tantalum pentoxide was deposited by reactive sputtering of Ta target in a mixture of Ar and O_2 to a thickness *d* of 30–33 nm. (Only for optical and AFM measurements, in order to verify some thickness-related effects, films with thickness in the 20–65 nm range were used.) Presputtering of the target was carried out in Ar. The details concerning the sample preparation can be found elsewhere [8, 18]. Briefly, the total pressure of the mixture during the deposition was 0.33 Pa and the gas composition was 10% O_2 + 90% Ar. The rf power density was 3.6 W/cm^2; the distance between the target and the samples was 3.5 cm; the substrate temperature during deposition was 493 K. The electrical characterization of the films was carried out using metal–insulator–semiconductor (MIS) capacitors with rf sputtered W top electrode, deposited through a shadow mask, with areas in the range of $1{\times}10^{-4} \div 2.5{\times}10^{-3}$ cm^2. Tungsten was chosen as a metal electrode due to its chemical and thermal stability (it does not react with Ta_2O_5 below 1100 K [17].) The oxide charge was evaluated from high-frequency (1 MHz) capacitance–voltage (*C–V*) curves. The dielectric constant ε_{eff} was determined from the capacitance at accumulation using the ellipsometrically measured (λ = 632.8 nm) film thickness. Ramped current–voltage *(I–V)* characteristics were used to investigate the leakage current at low and high voltages (HP4145B Semiconductor Parameter Analyzer). The breakdown field E_{bd} was defined as the average applied field at which the current density through the dielectric exceeds $2{\times}10^{-3}$ A/cm^2. The breakdown voltage of approximately 25 capacitors was measured on each sample (a quarter of 3 in. Si wafer).

The Ta_2O_5–Si structures with and without metallization (MIS and Ta_2O_5–Si structures, respectively) were exposed to microwave irradiation in a magnetron (*f* = 2.45 GHz, radiating power of 1.5 W/cm^2). The irradiation times t_i were 1, 5 and 10 s. During the exposure the temperature of the samples was close to room temperature. The elemental composition and chemical bonding of the films were analyzed with AES. The distribution of the microscopic nonuniformity in the films before and after irradiation was studied with AFM. For optical properties, the film transmittance in the visible wavelength range (from 400 to 800 nm) was measured for samples deposited onto glass substrate.

5.1.2. Results and discussion

Dielectric parameters and C–V curves

The values of the refractive index for both as-deposited and irradiated layers are in the range of 1.92–2.15, with a very slight (less than 4%) tendency of increasing after irradiation. The *C–V* data were taken at room temperature for the devices before and after irradiation (Fig. 5.1). The curves were obtained by sweeping the gate voltage from

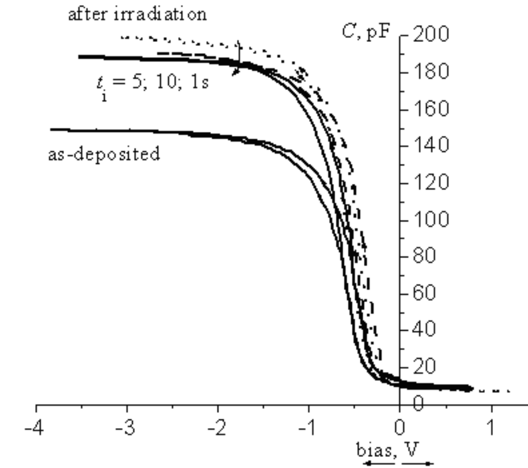

Fig. 5.1. C-V curves at 1 MHz of W–Ta_2O_5–Si capacitors before (as-deposited Ta_2O_5) and after microwave irradiation (exposure time t_i = 1; 5; 10 s), *d* = 33 nm.

inversion to accumulation at a ramp rate of 50 mV/s. By correlating the accumulation capacitance C_0 measured at about –3 V and physical thickness of the film, the dielectric constant of 9–10 was obtained for as-deposited films. Recently [5, 8, 26] we have reported that the effective dielectric constant ε_{eff} of the rf sputtered tantalum pentoxide shows a thickness dependence (ε_{eff} rises with increasing d) which corresponds to a two-layer model assuming in-series connected capacitors with the dielectrics Ta_2O_5 and ultrathin SiO_2, respectively. The results agree with the XPS [8, 27] and transmission electron microscopy (TEM) [13] data both demonstrating that a layer of mixed silicon oxides is inevitably formed at the interface with Si during sputtering. The thickness d_s of this interfacial layer as determined by TEM is 2.5 nm, and the values of ε_{eff} are affected by its presence. The intrinsic dielectric constant ε_t of the bulk Ta_2O_5 assuming a double-layer (Ta_2O_5–SiO_2) model for the system is determined to be 27 for the as-deposited films [5, 8, 26]. For the film thickness investigated here we will focus our attention on the effect of microwave irradiation on the electrical and microstructural properties only. High-frequency C–V measurements were performed using 6.25×10^{-4} cm^2 square capacitor patterns. The measurements on smaller (2.25×10^{-4} and 1×10^{-4} cm^2) and bigger (2.5×10^{-3} cm^2) areas showed similar and consistent results. The as-deposited films show negative values (–0.54 to –0.56 V) of the flat-band voltage V_{fb} (the work function difference φ_{ms} between W and Si is –0.42 eV, the work function of the W gate is 4.55 eV [32]), and, respectively, the values of oxide charge are $Q_f = (1.8–2.1)\times10^{11}$ cm^{-2}. Q_f for Ta_2O_5 is attributed mainly to the trapped charges in bulk neutral traps. One can see that the irradiation increases C_0 of the capacitors as compared to as-deposited Ta_2O_5. This increase is not due to the reduced film thickness (we did not detect a change in the physical layer thickness after irradiation), but it is related to the higher value of ε_{eff}. The smallest value of ε_{eff} is obtained for the initial films; after irradiation ε_{eff} increases up to 11 and 12 for t_i = 1 and 5 s, respectively. There is a slight tendency of ε_{eff} decreasing with increasing t_i to 10 s, $\varepsilon_{eff} \sim 11.5$. The measurements of the effective dielectric constant for samples with the rest electrode

areas produced similar results. The deviation of the measured dielectric constant from ε_t is due to the presence of the ultrathin SiO_2-like layer at the interface. Over the irradiation time range, V_{fb} first decreases (t_i = 1; 5 s) and than increases slightly remaining smaller than V_{fb} for the non-irradiated samples. (V_{fb} decreases to –0.37 and to –0.3 V as a result of 1 and 5 s exposure time, respectively; further, for t_i = 10 s, V_{fb} shifts to more negative values (–0.46 V) indicating generation of positive charge, but still remains below that in the initial non-irradiated samples.) In this way, the oxide charge density decreases after irradiation for the three irradiation times. Generally, Q_f is of $(8–9)\times10^{10}$ cm^{-2} after irradiation but changes its sign (negative for t_i = 1 and 5 s and positive for the as-deposited and 10 s irradiated samples, respectively) depending on the value of (φ_{ms}–V_{fb}). The negative charge density for t_i = 1 and 5 s may be due to the OH groups (for example, $[Si–OH]^-$ and/or $[Ta–OH]^-$) in the film formed during irradiation. A shift in flat-band voltage can be attributed generally to oxide charge, mobile charge or interface trapped charge. Since C–V curves after high-temperature (~473 K) measurements indicate that there is no measurable change with respect to the room temperature results, the effect of the mobile charge can be neglected. There is no visible change in the sharpness of the C–V curves in the depletion region after irradiation suggesting that the concentration of fast interface states, to a first approximation, is not significantly affected by microwave treatment. This leaves oxide charge term to be accounted for. The presence of an extremely thin SiO_2 layer between Ta_2O_5 and Si may be responsible for the formation of high-quality interface at Si. There are two possibilities for the observed decrease of Q_f: a net annealing (real reduction of Q_f as a result of improvement of the oxide parameters) or a partial compensation of the positive charge by a negative one incorporation during the irradiation. Having in mind that usually the electrically active defects in Ta_2O_5 are oxygen vacancies and the expected annealing effect of microwave irradiation, we are inclined to assume that the process of true annealing is more likely. We speculate that irradiation improves the stoichiometry of the oxide and reduces oxygen vacancies in the

initial film observed as oxide charge. The change of sign of Q_f after 1 and 5 s exposure implies that the eventual irradiation-induced negative charge in tantalum oxide cannot be ruled out completely. The AES results (presented in the next section) indicate, however, improvement of film stoichiometry, in this way implying that the process of real annealing occurs.

When sweeping the voltage from inversion to accumulation and then back to inversion mode, small hysteresis effects of 100 mV were observed in the depletion region suggesting small concentration of slow states. The arrows in the curves (Fig. 5.1) indicate the direction of the hysteresis. Hysteresis in C–V curves is normally attributed to charge trapping in the states located very close to the interface with Si (border or slow states). All samples exhibit a hysteresis behavior; ΔV_{fb} is negative before and after irradiation. The slow state concentration Q_{sl} is estimated to be ~2×10^{11} cm^{-2} which is not dependent on irradiation at all (usually these traps are interrelated by the presence of oxygen vacancies in the oxide close to the interface with Si [33]). As is evident from Fig. 5.1, there is no change in the C–V hysteresis suggesting any measurable effect of irradiation on the concentration of carrier-trapping defect sites that contribute to the hysteresis.

Auger analysis

A sputter Auger depth profile analysis was used to study the elemental composition of the films studied here. The ion sputter profiling was performed with a 1.5 keV Ar^+ ion beam raster over a 6×6 mm^2 area at an angle of 78° to the normal of the surface. We used ion energy of 1.5 keV, low enough to give shallow-damaged surface layer [8]. Additional support of this choice is the known fact [34] that 1.5 keV Ar^+ ions sputter conventional SiO_2 keeping its stoichiometric ratio (ions remove Si and O at a rate very close to 1:2). Our recent results [8, 27] from XPS and Auger depth profiles of thick enough Ta_2O_5 have shown that the ion-induced damage is not severe for 1.5 keV Ar^+. All this supports the assumption that 1.5 keV Ar^+ sputtering does not perturb the stoichiometry of the films and the eventual unfavorable effects of

the ion beam sputtering should not influence considerably the results obtained, and the data are reliable enough. Figure 5.2 shows Auger profiles of 33 nm Ta_2O_5 before and after irradiation. The elemental Ta (27 eV), main Ta_{NNN} (176 eV), O and Si peaks were measured as a function of the depth d_0 into the film. The Si line was monitored in order to define the Ta_2O_5–Si interface which was arbitrarily taken to correspond to the point at which the Ta and Si signals crossed (the sputtering rate is ~1 nm/min). The thickness of the steady-state region (nearly constant intensities of Auger peak-to-peak heights) corresponding to the bulk oxide is approximately 25 nm for the as-deposited films. The composition of the initial oxide is uniform up to the interface transition region: oxygen concentration ~63 at.% and tantalum concentration ~37 at.%. The existence of non-oxidized elemental Ta (peak at 27 eV) is not detected indicating relatively effective oxidation process. The bulk composition (O/Ta ratio is 1.7) suggests, however, a deviation from the stoichiometric Ta_2O_5 and presence of suboxides of Ta, although the layers are homogeneous without remarkable change of the chemical composition through the depth (Fig. 5.2a). The formation of a transition region at the Si consisting generally of Si, Ta and O atoms is observed: oxygen atoms bonding in tantalum oxide (176 eV peak position) and silicon oxide (peak at 76 eV) are detected. The interface width W_i is defined as a region over which the oxygen profile changes from 0.9 to 0.1 of its steady-state value by analogy with the common practice for the Si–SiO_2 system. The definition of W_i should be considered only as a qualitative characteristic of the layer, because the correct extraction of the layer parameters from Auger profiles needs the knowledge of the exact influence of the matrix elements and the different artefacts. At present there is no common standard for determination of the interface width from the Auger depth profiles of two-component materials and in particular of high-k dielectrics. Having this consideration in mind, W_i is found to be 12 nm, and about 8 nm from W_i is situated in Si substrate (Fig. 5.2a). Here we will not discuss all effects which impact the W_i and especially the argon bombardment. We will focus only on the influence of the irradiation on the depth profiles and the

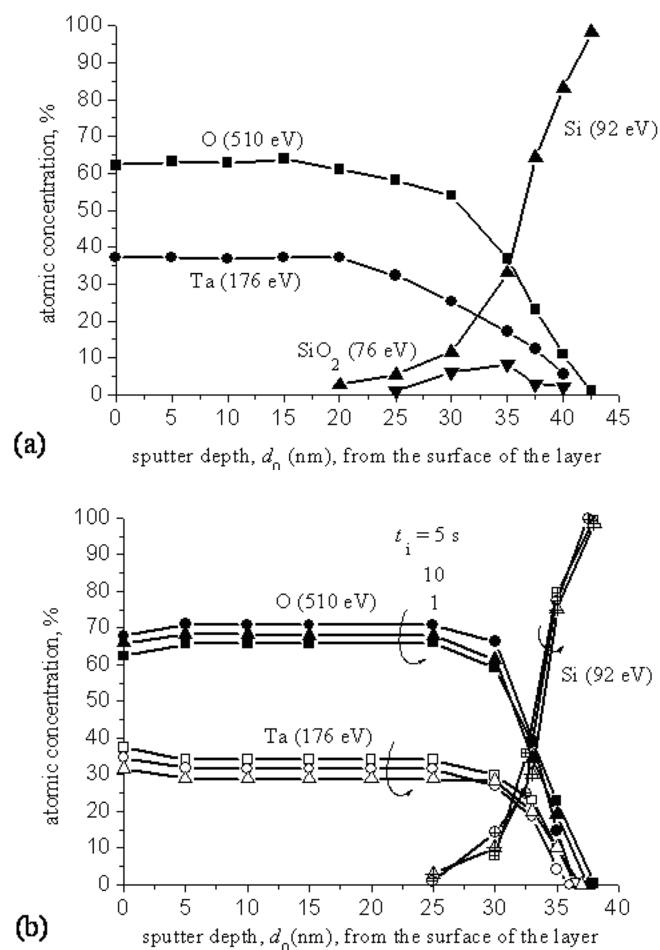

Fig. 5.2. AES depth profiles of 33 nm Ta_2O_5 before (a) and after (b) microwave irradiation.

relative changes of W_i, respectively. The interface is relatively broad for the as-deposited films. The depth profile shows presence of a thin SiO_2 layer in the interfacial region. The signal (of negligible intensity) corresponding to Si bonded in silicon oxide appears at 25 nm from the surface. Further it increases slightly and reaches its maximum value

(~7 at.%) at d_0 = ~35 nm, then rapidly loses its intensity to ~2 at.% at d_0 = 35–40 nm, i.e., the interface transition region penetrates in the substrate itself. This is associated with some unavoidable effects of ion sputtering despite relatively low energy of Ar^+ ions. A part of the oxide species in the transition region consists probably of knock-on implants [35] driven into the relatively conductive silicon matrix during the sputtering. This effect may result in the fact that some of the observed Ta–O and Si–O bonds in the interfacial region are not present before sputtering but are produced by the sputtering itself. Thus, part of the substrate appears to mimic oxides (tantalum and silicon) which manifests in an artificial broadening of the transition region. Having this in mind we assume that the real interface region, all the same, extends from d_0 ~ 27 nm to d_0 = 33 nm, where we define the interface, i.e., the estimated W_i is about 6 nm. The thickness of SiO_2 as determined by XPS and TEM [8, 13, 27] is 2.5–3 nm for the layer thickness studied here. The disagreement with the value of W_i is related to the definition of W_i itself: W_i involves not only a net thickness of SiO_2 detected by TEM but also parts of both interfaces Ta_2O_5–SiO_2 and SiO_2–Si which are not abrupt. After 1 and 5 s irradiation, the stoichiometry of the bulk oxide is improved and the interface becomes somewhat more abrupt. The atomic concentration ratio of the oxygen and tantalum (in the steady-state regime which defines bulk oxide and is characterized by constant intensities) is 1.9 and 2.45 for t_i = 1 and 5 s, respectively (Fig. 5.2b). The signal associated with silicon oxide(s) is missing, i.e., the irradiation changes near-interfacial composition and W_i is about 5.5 nm. The concentrations of Ta and O reduce gradually down to a minimum at d_0 ~37 nm for t_i = 1 s and at d_0 ~33 nm for t_i = 5 s. The results clearly imply more perfect microstructure of both the bulk oxide and the interfacial layer after irradiation. The structural modifications are related to chemical changes: the stoichiometry of the bulk oxide is better and the amount of suboxides of Ta and Si in the interface region decreases; the measurable signal due to SiO_2 is not detected and the width of interface transition region slightly decreases. With increasing t_i up to 10 s, broadening of the interface

region is observed. However, the value of W_i typical of the as-deposited film is not reached. The stoichiometry of the bulk oxide changes for the worse (O/Ta ratio concentration is 2). A relatively small deterioration of the quality of the bulk oxide as well as interfacial region emerges. In this way, we have evidence *of optimal irradiation time in the terms of annealing, namely, about 5 s*. We speculate that longer irradiation time stimulates undesirable degradation processes resulting in various structural imperfections (broken and/or strained Ta–O and Si–O bonds). The shape of O, Ta and Si concentration profiles does not significantly change during the exposure. The quality of the bulk and the interfacial region, however, tends to become poorer with increasing t_i above 5 s. It seems that the increase of exposure time above ~5 s degrades slightly stoichiometry of the Ta_2O_5 films in the terms of AES analysis. That is why we interpret the data for t_i = 10 s as an indication of an initial stage of degradation of the films.

I–V curves and conduction mechanisms

The typical room temperature *I–V* curves taken before and after microwave treatment are shown in Fig. 5.3 for the samples with an electrode area of 6.25×10^{-4} cm^2 and with the gate positively and negatively biased, respectively. (There is no contribution due to ramp voltage-induced displacement current in the Figure.) The leakage current characteristics did not show a difference from capacitor to capacitor on the same wafer. The effect of irradiation on the curves for samples with the rest capacitor areas is similar. The results presented (here and further) are reproducible from sample to sample and reflect the specific effects of irradiation. One can see that there are only slight differences between the current of positive and negative polarities of as-deposited films. The films show a low leakage current density, $J \le 10^{-6}$ A/cm^2, up to about ±1 V applied voltage, and above this voltage, the current increases monotonically. The current might originate from non-perfect stoichiometry (presence of suboxides, as indicated by the Auger depth profile). After irradiation, the leakage current decreases and becomes strongly dependent on gate-bias polarity. The current lowers about

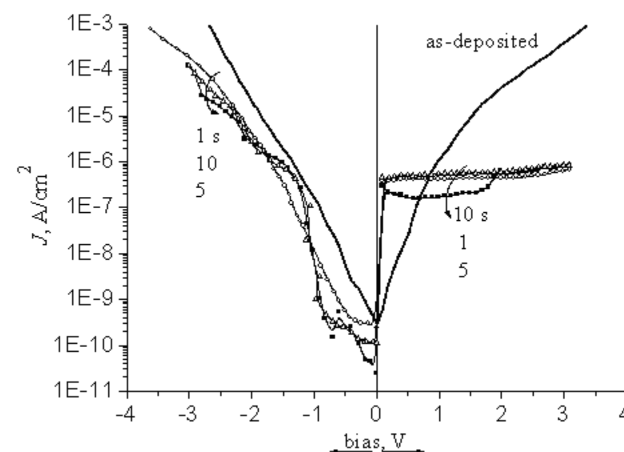

Fig. 5.3. *I-V* curves of capacitors with Ta_2O_5 before and after microwave irradiation.

one order after 1–5 s irradiation (Fig. 5.3) when the electrode is biased negatively (i.e., a forward bias is applied to form an accumulation layer on Si). The increase of t_i up to 10 s has no further significant effect on the curves. The current density vs the electric field E across the dielectric film is shown in Fig. 5.4a (the gate electrode is negatively biased; *p*-Si surface is in accumulation and the entire applied electric field appears across the oxide; exposure time is a parameter). As is seen, 1 s irradiation reduces J by an order of magnitude in the whole applied field range studied (up to ~1.1 MV/cm). For longer exposure times the irradiation is beneficial in the terms of leakage current only for low electric fields (≤ 0.35 MV/cm). J reduces with increasing t_i from 1 to 5 s and further $J(E)$ dependence does not change any more with increasing t_i up to 10 s. The lowest leakage current density is measured for the 5 s irradiated samples, resulting in a value of ~10^{-10} A/cm^2 at E of 0.1–0.3 MV/cm. The *I–V* curves for t_i = 10 s are almost the same as those of 5 s irradiated films. Obviously irradiation times of about 5 s are effective for reduction of leakage current, i.e., the data confirm the Auger spectra results for the existence of optimal exposure time in the

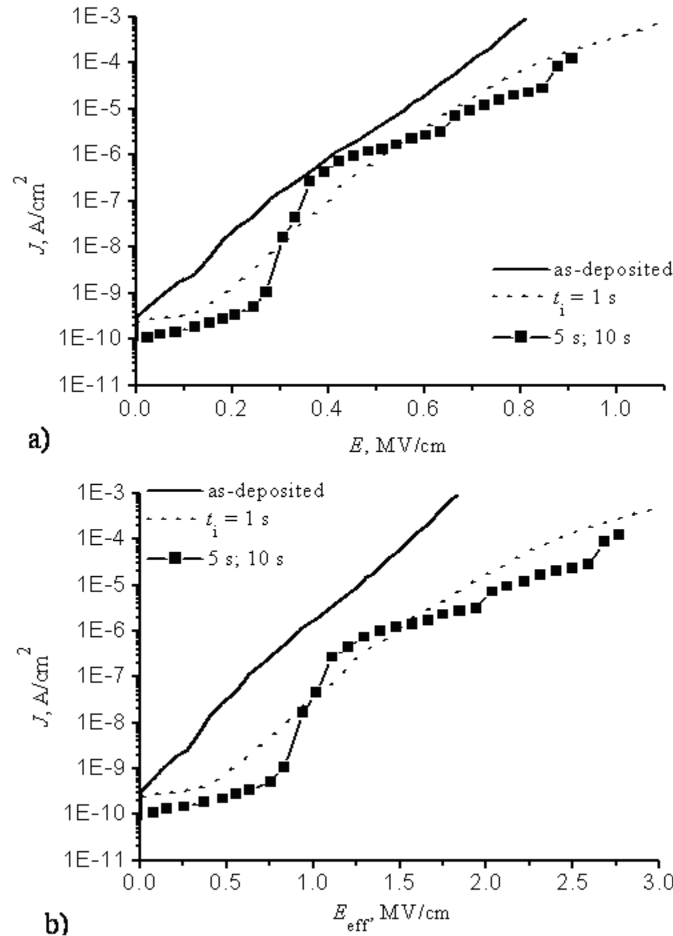

Fig. 5.4. Capacitor leakage current density vs applied electric field (a) and E_{eff} (b) curves before and after microwave irradiation, $d = 33$ nm (negative applied voltage at the gate).

terms of annealing. Current jumps for irradiated films are observed at low applied fields without clear dependence on t_i. They do not change the general tendency of I–V curves. At present we have no reasonable explanation for the nature of these jumps although it is likely that they are related to some kind of soft breakdown in Ta_2O_5.

The 20–65 nm Ta_2O_5 films were examined with XRD technique for evidence of crystallinity. Both types of the films (as-deposited and irradiated ones) were x-ray amorphous. This means that there is no indication of irradiation-induced crystallization effect in Ta_2O_5 and all the characteristics studied here correspond to amorphous layers. Having in mind the Auger data, the improvement of I–V characteristics after irradiation could be attributed to decrease of the contribution of suboxides and increase of the stoichiometric ratio up to 2.45, which is very close to that typical of Ta_2O_5. The detected improved parameters of the interfacial transition region also cause the decrease of the leakage current. The irradiation provides also lower leakage current for reversely biased electrode at relatively high (> 0.7 V) bias (Fig. 5.3, positive applied voltage at the gate) when electrons are injected from the substrate. The current is virtually independent of t_i , having saturated value of 5×10^{-7} A/cm^2 for applied voltages from about 70 mV up to 4 V. For the as-deposited films, the electrons injected from the Si tunnel through the SiO_2 to the bulk traps in Ta_2O_5, i.e., the conduction is combined by the tunneling mechanisms (Fowler–Nordheim or direct tunneling) in the SiO_2 and the Poole–Frenkel (PF) effect in the Ta_2O_5. This can explain the existence of higher leakage current compared to the irradiated ones and the absence of abrupt current increase as well. This is also an electrical manifestation of the weakness of the interfacial region at Si. The weakness is related to the classical interfacial defects such as dangling bonds as well as to a strained and imperfect SiO_2. The interfacial layer detected by AES analysis is in fact not "ideal" stoichiometric SiO_2 because Si is not perfectly oxidized due to the spontaneous oxidation during sputtering in active oxygen ambient. The incompletely oxidized Si contributes also to the increase of the overall conductivity of the dielectric. The lower leakage current at higher voltages for the irradiated films is associated generally with improvement of the quality of this stack dielectric in a good accordance with the Auger data. The current increase at small applied voltages, after irradiation, could be a result of redistribution of the field in Ta_2O_5 and interfacial transition region. An additional study, however, of the

current due to electron injection from Si through interfacial layer into Ta_2O_5 (reverse gate bias), is needed. As a tendency there is no difference in the *J–V* curves with varying t_i, in the positive voltage range studied. This means that there are some kinds of electrically active defects in the initial films acting as a leakage current enhancement factor, which are annealed even after 1 s irradiation; further their behavior does not depend on the irradiation duration.

In order to compare the characteristics of Ta_2O_5 with those of SiO_2, the effective field strength E_{eff} is calculated as $E_{eff} = V/d_{eq}$. Here d_{eq} is the equivalent oxide thickness, therefore E_{eff} is determined assuming that the film consists of a single layer having a dielectric constant of SiO_2. Figure 4.b shows J vs. E_{eff} for the as-deposited and irradiated films (the capacitor is in the accumulation mode). The equivalent film thicknesses are d_{eq}^0 (before) and d_{eq}^i (after irradiation). The effective field strength was calculated using the measured parameters ε_{eff} and V, $E_{eff} = \varepsilon_{eff}V/\varepsilon_s d$; d represents the total, physical thickness of the film, and ε_s is the dielectric constant of SiO_2. The layers show improved $J(E_{eff})$ characteristics after irradiation ($J \sim 10^{-8}$ A/cm^2 for E_{eff} up to 1 MV/cm, and below 10^{-6} A/cm^2 for E_{eff} = 1–1.5 MV/cm), i.e., the irradiated films have potential for deep submicron application in the terms of leakage current: the lowest leakage current density, $J \sim 10^{-10}$ A/cm^2 ($E_{eff} \sim$ 0.5 MV/cm) corresponds to 5 or 10 s irradiated layer (d^i_{eq} = 10.8 nm) and in this sense t_i = 5 s might be a beneficial annealing time for DRAM applications. Generally, our results suggest that the poor-oxidation-related defects are the dominant factor in the leakage current for as-deposited films and the irradiation stimulates better oxidation, resulting in improvement of the dielectric properties and *I–V* characteristics. The SiO_2 equivalent thickness for the as-deposited films is about 14.5 nm. The irradiation gives the benefit of reducing the d_{eq}, namely, d^i_{eq} = 11.5 and 10.8 nm for t_i = 1 and 5–10 s, respectively, indicating improved quality of the Ta_2O_5–Si system as a whole. The lowest d_{eq} in this comparison is for 5–10 s irradiated samples, i.e., d_{eq} values decrease with t_i keeping all the same high values. The total thickness of the films is not changed and the signal

corresponding to SiO_2 in Auger spectra after irradiation is missing completely, for all t_i. That is why we may rule out an additional oxidation of Si during irradiation with subsequent influence of SiO_2 thickness on the voltage distribution and the leakage current value. Then, the improvement of the leakage characteristics for irradiated layers can be explained with repairing of the stoichiometry of the initial oxide, as well as enhancement of the interface properties mainly due to the improved interface at Si. The tendency of "stopping" of leakage current improvement after 10 s irradiation can be due to the change of the mechanism of interaction of radiation with the Ta_2O_5–Si system, namely, from annealing to degradation, according to the AES data, for longer irradiation times. This change probably depends in a complex manner on the thickness and microstructural status (chemical bonds, imperfect bonds, suboxides) of the initial layer.

Now we will discuss the conduction mechanisms of Ta_2O_5 layers before and after irradiation. The possible conduction mechanisms of the leakage current may be due to several mechanisms including Schottky emission and the PF effect. If PF mechanism is assumed, the current through the dielectric is

$$J = C_t E \exp\left\{-q\left[\Phi - \left(qE/\pi\varepsilon_0 k_r\right)^{1/2}\right]/k_B T\right\} \quad (5.1)$$

Here C_t is a trap concentration related constant, E is the electric field, Φ is the barrier height of bulk traps, ε_0 is the vacuum permittivity, k_r is the dynamic dielectric constant, k_B is the Boltzmann constant and T is the absolute temperature. The current governed by the Schottky emission is described by the Richardson–Dushman equation:

$$J = AT^2 \exp\left[1/k_B T\left(q^3 E/4\pi\varepsilon_0 k_r\right)^{1/2}\right], \quad (5.2)$$

$$A = C_{RD} \exp\left(-\varphi_b/k_B T\right) \quad (5.3)$$

is the Richardson constant, φ_b is the Schottky barrier height). In order to distinguish these two mechanisms, the *I–V* curves (forward gate bias) are expressed in the scale J/E vs. $E^{1/2}$ (Fig. 5.5) and J vs. $E^{1/2}$ (Fig. 5.6), respectively. The linearity of the plots in the certain field regions of Fig. 5.5 is consistent with a PF transport limitation,

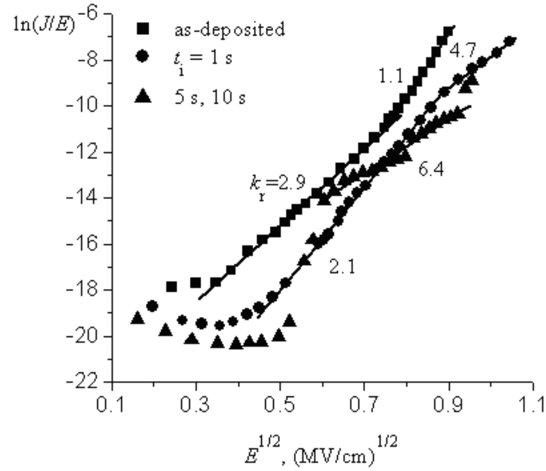

Fig. 5.5. The Poole–Frenkel plot of the Ta_2O_5 film (33 nm) before and after microwave irradiation.

and from the slope of the straight lines we have determined the values of k_r: 2.9 and 1.1 for the as-deposited films in the fields range 0.1–0.6 and 0.6–0.8 MV/cm, respectively. Therefore, we suggest that the PF effect is operating in the field region 0.1–0.8 MV/cm. After irradiation, when t_i = 1 s, k_r = 2.1 and 4.7 for fields of 0.2–0.8 MV/cm and 0.8–1.1 MV/cm, respectively. The same mechanism is observed for $E \sim 0.4$–0.9 MV/cm (k_r = 6.4), for 5 and 10 s irradiated samples. As is well known, however, only a self-consistent dynamic dielectric constant can ensure that current conduction is due to the PF effect. Taking this into account it is clear that the obtained low k_r values deviate from the optical dielectric constant ε_{opt} (typically < 5 [36]) and are not consistent with the "net" PF process, regardless the fact that at a first glance the symmetry of the I–V curves for as-deposited films (Fig. 5.3) implies for domination of a bulk-limited conduction process. This indicates that other mechanisms exist for the layers with low k_r. Therefore, only for the layers with k_r = 4.7 and 6.4 (in fact irradiated samples), i.e., $\varepsilon_{opt} \le k_r < \varepsilon$ (1 MHz), the PF effect dominates the current at applied fields of about 0.4–1.1 MV/cm, and the relation with the

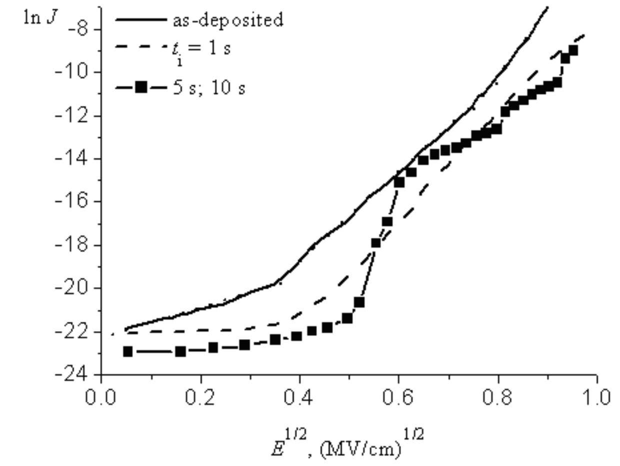

Fig. 5.6. The Schottky plot of the Ta_2O_5 film (33 nm) before and after microwave irradiation.

refractive index ($n_r = \sqrt{k_r}$ is about 2.2) is also accurate. In all other cases the values of k_r are not consistent with the value of n_r, which rules out the PF effect at the fields mentioned above. ε (1 MHz) is the static dielectric constant of the samples.

Figure 5.6 is the Schottky plot of the films before and after irradiation. As can be seen, when the top electrode is negatively biased ($-V_g$), i.e., the electrons are injected from the gate, the current of the as-deposited films can be well fitted by ln J vs. $\sqrt{E}$ (three straight sections of the curve), indicating that the conduction is Schottky emission in low and medium field regime (0.05–0.9 MV/cm). Combining the data from Figs. 5.5 and 5.6, we can conclude that for the initial films, the leakage current is dominated by Schottky emission at both low and medium electric fields. After microwave process the mechanisms of the leakage current have some variations: (i) the current is controlled by the Schottky effect at low electric fields and by the PF emission at medium fields (0.4–1.1 MV/cm); (ii) at very low electric fields, up to 0.15 MV/cm, the current is constant for 1 s irradiated samples, Figs. 5.4a and 5.6. The

rapid change of the conduction mechanism for 5–10 s treated films is observed at E ~ 0.3 MV/cm. This change of the conduction mechanism for the irradiated samples when varying the electric field and the data after irradiation can be best interpreted in the terms of transition from an electrode-limited to bulk-limited mechanism.

The data suggest that the conduction mechanism is highly dependent on the technological conditions. The fact that Schottky emission controls the current in the voltage region which is the working one for high-density DRAMs could have technological implementation, because the leakage current could be further decreased by using an electrode material with a higher work function than that of W. There are two dominant conduction mechanisms (in the field range of ~0.4–l MV/cm) for the films with different technological history, namely: Schottky emission limited current for as-deposited as well as 1 s irradiated films and the PF mechanism for 5 and 10 s irradiated films (Figs. 5.5 and 5.6), i.e., the conduction mechanism is related to the concentration of charged defects in the films. A transition from Schottky to PF conduction process occurs after longer t_i indicating irradiation-induced electrically active defects. (The next step for accurate conduction mechanism identification is to study the temperature dependence of the leakage current which is our future task.) Generally, the results here confirm the AES data where we observed clear evidence of worsening of the film microstructure after 10 s irradiation. Now, combining these two types of investigations we conclude that the critical exposure time is about 5 s when a change of the irradiation process from annealing (desirable) to degradation (undesirable) one takes place. The presence of interfacial SiO_2-containing layer leads to a reduction of ε_{eff} and to a modification of the conduction mechanism of the double structure; due to the presence of SiO_2, a high electric field exists (even at low applied voltages), across SiO_2 superior to the field in Ta_2O_5 [37]. Our data show that there are two mechanisms mainly governing the conductivity: (i) Schottky emission above the potential barrier for the initial films in the whole applied field range investigated as well as for irradiated films at low and medium fields, and (ii) PF mechanism,

i.e., bulk-traps-assisted transport from cathode (W electrode) to anode (Si substrate) for irradiated layers at higher fields; with increasing t_i the PF mechanism is detected at lower applied fields. The electrons released from the trap levels in Ta_2O_5 can also contribute to the current, i.e., the current component corresponding to tunneling of trapped electrons to the insulator conduction band. The nature of the traps, according to the Auger analysis, is structural imperfections and suboxides. In general, other mechanisms (direct and/or Fowler–Nordheim tunneling) can also contribute to the current. Their relative contributions depend on the applied field and the concentration of traps as well as on the SiO_2 to Ta_2O_5 thickness ratio. The irradiation anneals the electron traps such as oxygen vacancies and strained bonds, and we detect a reduction of leakage current for irradiated samples. This is accompanied with an increase of ε_{eff} due to the removal of structural defects present in Ta_2O_5. It should be emphasized, however, that the concentration of these bulk traps is low enough before as well as after irradiation. This can explain the domination of the Schottky-type mechanism observed for both as-deposited and 1 s irradiated samples - the microwave treatment anneals some kind of defects resulting in a leakage current reduction but this process is not related to changing of the mechanism of conductivity at fields close and below 1 MV/cm. Additionally, by combining AES and I–V data we can conclude that only a fraction of defects introduced during 10 s irradiation, according to the Auger analysis, are “active” or “effective” in causing an increase of current. Obviously their effect on the leakage current is negligible and therefore the I–V curves for t_i = 10 s are almost the same as those of 5 s exposed films. This might result from the different energy levels of the defects or from their different physical and/or chemical nature depending on t_i.

Breakdown fields

One can see from the I–V characteristics that after irradiation there is a general shift of the curves (at forward bias polarity) to higher voltages, indicating an increase of breakdown fields. Figure 5.7 illus-

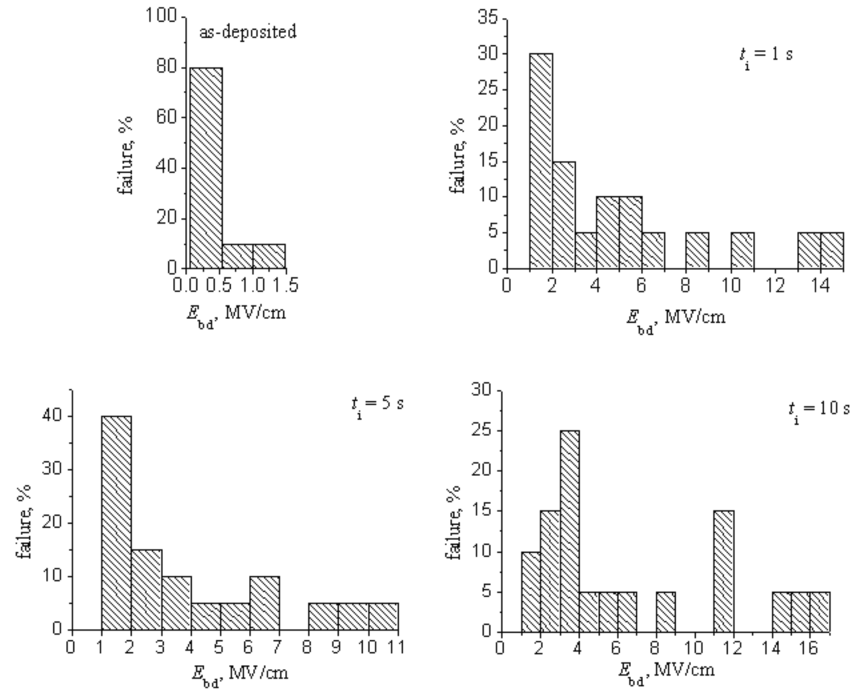

Fig. 5.7. Breakdown histograms of the Ta_2O_5 film (33 nm) before and after microwave irradiation.

trates the breakdown electric field E_{bd} characteristics of the capacitors (biased in the accumulation mode) before and after microwave treatment. The main fraction of capacitors for the initial films breaks down in the 0.1–0.5 MV/cm field range. The characteristics of the irradiated layers are better than those of the as-deposited ones. E_{bd} slightly increases with t_i implying that the longer irradiation time is beneficial in the terms of breakdown characteristics. We correlate the improvement of E_{bd} with an improvement of both the bulk oxide stoichiometry and interfacial parameters and with general densification of the layers too. The results are consistent with the leakage current reduction after irradiation. Additional information here, however, is that the longest t_i used is beneficial for breakdown fields regardless

the fact that an effect on leakage current at low and medium applied fields is missing. In spite of small (5%) intensity, the maximum E_{bd} after t_i = 10 s is surprisingly high (14–17 MV/cm). For all irradiated samples the breakdown frequencies are distributed randomly. The distribution of breakdowns for 1 s treated samples is characterized with a main peak (at 1 MV/cm) of 30% intensity and peaks of 10–15% intensities at higher (2–6 MV/cm) fields. There is a weak tendency for an increase of high-field breakdowns with increasing t_i. Their intensities, however, remain low for all treated samples, including the main peak at 11–12 MV/cm after 10 s irradiation. The physical understanding of breakdown in Ta_2O_5 is still under research, but generally it is related to the microscopic properties of Ta_2O_5 and interface with Si, and in this context it is associated with broken and/or strained bonds [1, 3, 21]. The breakdown data are consistent with the main results deduced from the *I–V* and *C–V* measurements – they indicate that microwave treatment efficiently lowers the defect concentration and leads to an improvement of E_{bd}.

At the end of this subsection it should be noted that the preliminary experiments indicate that after microwave annealing (for about 5–7 s), the characteristics of capacitors are stable enough after long (1 year) staying at air. The degradation of a number of important films-related parameters (dielectric constant, oxide charge, concentration of both slow and interface states, breakdown fields) is no more than 5% (to within the experimental errors) as compared with the initial values. So it emerges that the stack capacitor is thermodynamically more stable after microwave irradiation after which only negligible variations of its parameters with time are observed.

Surface roughness parameters and transmittance spectra

The AFM images of the films were analyzed and two roughness parameters were calculated: the root-mean square (RMS) surface roughness and maximum difference (Z_{range}) between the highest and the lowest points in the scan range. Our AFM analysis for a 1×1 μm^2

Table 5.1. RMS roughness of a 1×1 μm² area of the surface of Ta_2O_5 films on Si (before and after microwave irradiation).

Film thickness (nm)	RMS (nm)			
	As-deposited film	After irradiation, t_i (s)		
		1	5	10
20	0.092	0.107	0.113	0.121
25–30	0.127	0.143	0.091	0.147
50	0.128	0.150	0.102	0.154
55	0.140	0.156	0.101	0.146
60–65	0.157	0.197	0.155	0.211

area of the as-deposited films (thickness in the range of 20–65 nm) on Si shows that the surface is reasonably smooth, with rms values in the range of 0.092–0.157 nm. The representative micrographs of the surface morphology for the initial films are shown in Fig. 5.8. The quantitative data of rms variation with irradiation time and thickness are summarized in Table 5.1.

One can see that the roughness of the as-deposited films increases slightly with their thickness. The rms surface roughness increases (very weakly) as a result of 1 s irradiation. The effect of 5 s irradiation may be different depending on the surface characteristics before irradiation, which are actually related to the film thickness. If the surface of the initial film is smooth enough (the thinnest Ta_2O_5), it becomes more rough: its rms increases slightly as compared with the value before microwave treatment; 5 s irradiation has beneficial effect on the surface with some level of roughness (i.e., the surface which is not smooth enough, typical of thicker Ta_2O_5), namely, the rms roughness decreases and the surface becomes smoother. The 10 s irradiation increases the rms roughness in comparison with the values of the initial layers for all the thicknesses studied. The structure morphology is dominated by grains 10–20 nm in diameter, about 1 nm in height and which are randomly scattered every few micrometers over the wafer surface. Generally, the irradiation acts as micro-structuring process and changes the surface morphology: an improvement of surface quality occurs after

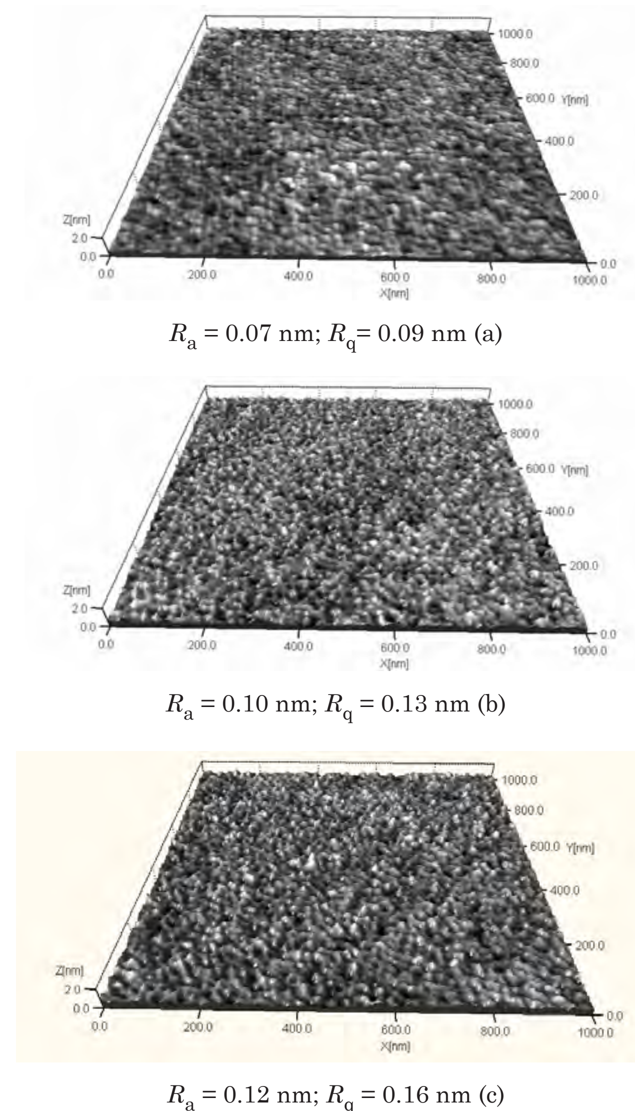

R_a = 0.07 nm; R_q= 0.09 nm (a)

R_a = 0.10 nm; R_q = 0.13 nm (b)

R_a = 0.12 nm; R_q = 0.16 nm (c)

Fig. 5.8.(a,b,c) AFM 3D topography of as-deposited Ta_2O_5 on Si, with different thicknesses d: 20 (a), 50 (b) and 65 nm (c). The average roughness R_a and the RMS roughness R_q are shown. X:Y:Z = 1:1:30.

t_i = 5 s and a degradation after t_i = 1 and 10 s, i.e., there is again evidence of annealing effect of 5 s irradiation, here in the terms of surface morphology. This can be attributed to relaxation of mismatch stresses between the Si substrate and the deposited film as well as improvement of the stoichiometry of the film (as demonstrated by the AES data). It should be noted that all radiation-induced changes of surface morphology (decrease or increase of rms roughness depending on t_i) are small and as a matter of fact both the as-deposited and irradiated films are smooth enough (the irradiated films have roughness similar to that of the initial ones). The irradiation does not affect also the thickness dependence of rms values detected for the as-deposited layers – the surfaces of thinner films are smoother than those of thicker ones before and after irradiation. The thickness-related morphology phenomena are probably an attribute of sputtering process itself and it needs additional special study. As far as the films are amorphous before and after treatment, the surface structure at 1 and 10 s irradiations (rms value increases) does not reflect crystallization process during irradiation. Additionally, for AFM evaluation the Ta_2O_5 films on Si are used, and respectively the irradiation acts directly on the surface of the Ta_2O_5 in contrast to irradiation of MIS structures (metal gate on Ta_2O_5) used for the electrical measurements. This peculiarity should be taken into account when comparing and combining the data of AFM with those of the electrical experiments.

Now we will focus on the films deposited onto glass which are the basis for optical measurements. The initial films with d = 20–50 nm have smooth surface with Z_{rangc} values of 1.101 and 1.906 nm, respectively; rms surface roughness is found to be nearly constant (0.235 nm) for this thickness range. The thicker films (55–65 nm) have rough surface with a Z_{range} value of 2.546 nm and rms roughness of 0.387 nm. The surface structure (not shown here) is dominated by mounds that are approximately 20–30 nm in diameter, and are randomly scattered. The irradiation, however, acts as microstructuring process only for the thinnest films (20–30 nm): a relatively sharp increase of rms value is observed (by a factor of 3 and 5 at t_i = 1 s and t_i = 5 or 10 s, respec-

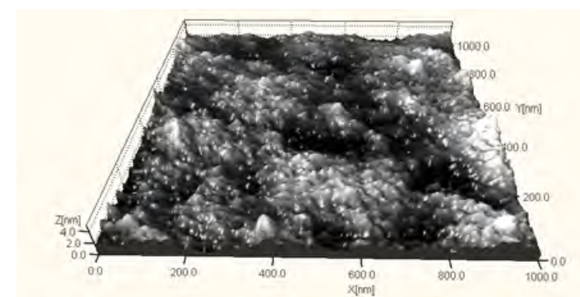

Fig. 5.9. AFM images of the surface of 20–25 nm Ta_2O_5 on glass after 1 s microwave irradiation. X:Y:Z = 1:1:20.

tively). The irradiated surface is covered with a quasi-ordered array of conical-like microstructures (Fig. 5.9) with randomly distributed areas ranging from 80 to 300 nm in diameter. The surface morphology of the films thicker than 30 nm is not changed by microwave treatment at all. Obviously, the microstructure and surface morphology of sputtered films on glass are different from those of deposited films on Si, and, respectively, the effect of irradiation is also different.

Figure 5.10 shows transmittance spectra of as-deposited films with various thicknesses (25–65 nm). All the transmittance values are above 50% in the 400–800 nm wavelength range, and their dependence on d reveals the expected higher density of thicker films. The microwave treatment changes only the spectrum of the thinnest film: at t_i = 1 s the transmittance decreases significantly over the whole wavelength range (the spectrum corresponding to t_i = 5 s is almost the same); after 10 s irradiation, the spectrum is indistinguishable from that typical of the initial, non-irradiated film. Roughly speaking (having in mind incompleteness of these kind of experiments), we have again evidence of a tendency toward parameters improvement of 20–30 nm thick layers, whose thicknesses are of practical interest, after short-time (1–5 s) microwave irradiation.

In summary, the results presented above allow to draw the following conclusions: microwave irradiation at room temperature can be used as an annealing post-deposition process of thin sputtered Ta_2O_5

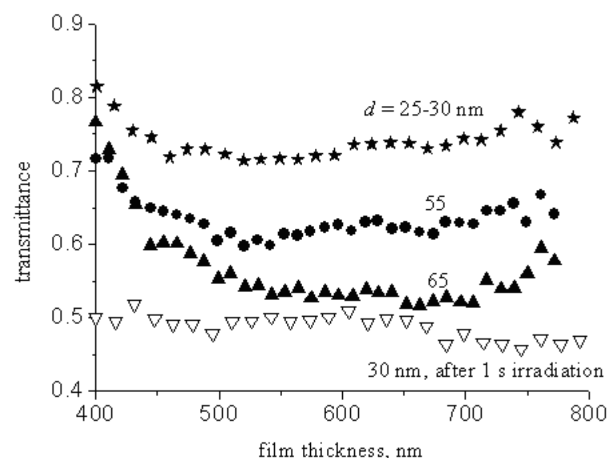

Fig. 5.10. Dependence of optical transmittance on thickness of as-deposited Ta_2O_5. A spectrum of 30 nm Ta_2O_5 after 1 s microwave irradiation is also shown.

films on Si, for achieving parameters required for storage capacitor application in DRAMs. The study indicates an annealing window of about 5 s exposure time which results in (i) improved stoichiometry of bulk oxide (O/Ta ratio reaches the values typical of ideal Ta_2O_5); (ii) better parameters of interfacial transition region at Si and more smooth film surface. Obviously the microwave treatment stimulates oxidation reactions in the as-deposited rf sputtered films and in this way is responsible for reduction of suboxides (in the interfacial transition region too) resulting in: lower oxide charge densities; higher dielectric constant; lower leakage current and better breakdown characteristics, i.e., the net effect of the irradiation is a real annealing of the parameters of Si-sputtered Ta_2O_5 system. The process is not accompanied either by an additional oxidation of Si substrate or by crystallization effects in Ta_2O_5 (almost insuperable problems in the course of high-temperature annealing processes of high-*k* materials). This effect of microwave irradiation is related in fact to its main advantage as an annealing process – a minimal thermal budget (extremely small exposure times at room temperature). In this sense, *the microwave irradiation appears to offer significant promise toward replacement of high-temperature processes as an annealing step for high-k insulators.*

As is known for most industrial applications, high-temperature processes should preferentially be avoided for these materials. In the same context, we plan an investigation of the electrical properties of the films irradiated before metallization, to check the suitability of the process as a post-deposition annealing. The observed irradiation-induced improvement of the films microstructure and their surface morphology motivate for such kind of experiments. A future work should be also aimed at optimization of irradiation times for annealing of thinner Ta_2O_5 films, in order to meet the demands of nanoscale technology.

5.2. EFFECT OF MICROWAVE RADIATION ON Ta_2O_5–Si MICROSTRUCTURES: THERMAL Ta_2O_5 ON Si

5.2.1. Experimental procedure

The *p*-Si (100) substrates (resistivity of 15–17 Ω·cm) were 2 in. in diameter. After a conventional chemical cleaning of the wafer, tantalum films were deposited onto Si by rf sputtering (13.56 MHz) of tantalum target (a plane magnetron cathode Leybold Heraus type system; 99.99% purity of the target) in the Ar atmosphere. Before deposition the chamber was evacuated to a pressure of 2×10^{-7} Pa. The working gas pressure was 3 Pa, the rf radiating power was 2.2 W/cm^2 and the deposition rate was 9 nm/min. The distance between the target and substrate was 3.5 cm. The substrates were not intentionally heated during Ta deposition and presumably remained at a temperature close to room one). Subsequently, the Ta films were oxidized at 823 K in dry O_2 at atmospheric pressure; O_2 flow rate was 5 l/min. The oxidation was performed in a standard oxidation furnace. It was suggested that the oxidation temperature was low enough, so oxidation of the silicon substrate was negligible and tantalum silicide formation seemed unlikely. The Ta_2O_5 layer thickness was determined using ellipsometry (λ = 632.8 nm).

The Ta_2O_5–*p*–Si structures (thickness of Ta_2O_5 layer being 16, 20 and 24 nm) and MIS structures were exposed to magnetron microwave radiation (frequency $f = 2.45$ GHz, radiating power of 1.5 W/cm^2, processing duration of 10 s).

The ER spectra have been measured before and after microwave irradiation of the Ta_2O_5–*p*–Si structures. From these spectra we calculated the values of the threshold energy E_g and collision line-broadening parameter Γ. The latter carried information on structural state of the Ta_2O_5–*p*–Si heteroboundary (the collision line-broadening parameter decreases when the interface becomes more perfect). For similar structures we measured, both before and after microwave irradiation, the curvature radius with a standard profilometer. Talyrond traces were registered on the Ta_2O_5 film side. The curvature radius R was determined with arm of curvature l on arc chord m from Talyrond trace:

$$R = m^2 / 8l. \quad (5.4)$$

The intrinsic stress value σ was estimated from the Stone formula:

$$\sigma = \frac{Yd^2}{6(1-\nu)Rd_{sub}}, \quad (5.5)$$

where d is the Ta_2O_5 film thickness; R is the curvature radius; Y (=1.3×10^{11} N/m^2 [38, 39]) is the Young's modulus of Si (100) substrate; d_{sub} is the substrate thickness; $\upsilon = 0.278$ is the Poisson ratio of Si substrate.

5.2.2. Results and discussion

The results of measurements of the curvature radii and intrinsic stresses before and after microwave irradiation for 10 s are given in Table 5.2. Our measurements of the radius of curvature R have shown that tensile ISs appeared in the Ta_2O_5 film on the Si substrate, while compressive stresses were present in the Si substrate at the interface. In this case one should expect that the Si gap E_g in the heterosystem is below that in the starting (without Ta_2O_5 film) substrate [40].

One can see from Table 5.2 that there are strains in all basic structures: the Ta_2O_5 film is expanded and the Si substrate is compressed.

Table 5.2. The changes of parameters R and σ in the Ta_2O_5–*p*–Si system and MIS capacitor after microwave treatment.

Layer thickness, nm	Duration, s	Flexure	l, nm	M, nm	R, m	σ, 10^9 N/m^2
16	0	Concave	70	1	38.3	5.7
	10	low profile	70	0	∞	0
20	0	Concave	68	1	36.1	5.9
	10	low profile	68	0	∞	0
24	0	Concave	67	1	35.1	6.1
	10	Concave	76	0	45.1	4.7
MIS	0	Concave	72	1	40.5	0
	10	low profile	74	0	∞	0

After microwave irradiation of the samples (Ta_2O_5 film thicknesses of 16 and 20 nm), intrinsic stress relaxation occurred and, as a result, the heterostructures became relaxed. In the sample with 24 nm Ta_2O_5 film, the curvature radius increased and σ value decreased after microwave treatment.

The results of ER spectra measurements for Ta_2O_5–*p*–Si structure with $d = 20$ nm in the 3.1–3.7 eV spectral range are shown in Fig. 5.11 and Table 5.3. After microwave irradiation the system became flat ($R = \infty$) and Si gap increased; the collision line-broadening parameter Γ decreased by a factor of 1.3 (see Table 5.3). The corresponding ER spectra of the Si substrate at the interface (transition at the center of the Brillouin zone) are given in Fig. 5.11.

The results obtained indicate IS relaxation and structural ordering of the Ta_2O_5–*p*–Si interface due to microwave processing. It also led to a decrease of the collision line-broadening parameter Γ and increase of electron energy relaxation time $\tau = \hbar / \Gamma$, as well as mobility of the photo-excited charge carriers.

According to the data obtained from the ER spectra, the above effect of structural ordering also took place in structures with Ta_2O_5 film thicknesses of 16 and 24 nm. In the last case the effect was essentially smaller than it was in the two other cases.

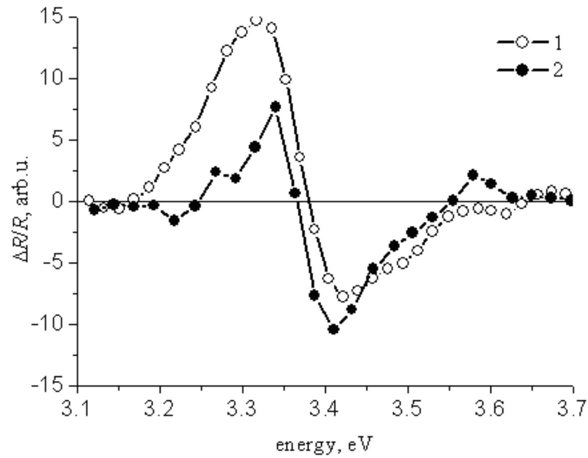

Fig. 5.11. Electroreflectance spectra from Si substrate in the Ta_2O_5–*p*–Si system (3.1–3.7 eV spectral range): 1 – initial sample (before microwave processing); 2 – after microwave processing.

It should be noted that in the initial samples the E_g value decreased when the Ta_2O_5 layer thickness increased. The effect was due to increase of intrinsic compression stresses in silicon substrate. This is confirmed by decrease of curvature radius (see Table 5.2). For all the samples, however, the microwave treatment led to E_g increase as compared to the initial value.

The results of ER spectra measurements for Ta_2O_5–*p*–Si structure (Ta_2O_5 film 20 nm thick) in the 3.7–5.0 eV spectral range are presented

Table 5.3. The changes of parameters E_g and Γ in the Ta_2O_5–*p*–Si structures after microwave treatment with different durations t_i.

t_i, s	$d_{Ta_2O_5}$, nm	Si gap E_g, eV	Γ, eV
0	16	3.333	0.096
10	16	3.334	0.091
0	20	3.346	0.102
10	20	3.384	0.076
0	24	3.364	0.109
10	24	3.367	0.082

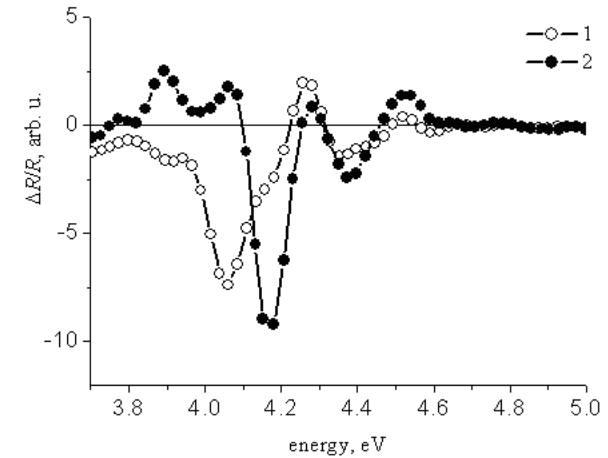

Fig. 5.12. Electroreflectance spectra from Si substrate in the Ta_2O_5–*p*–Si system (3.7–5.0 eV spectral range): 1 – initial sample (before microwave processing); 2 – after microwave processing.

in Fig. 5.12 and Table 5.4. The spectrum near 4.1 eV describes the energy transition for Si substrate at the Brillouin zone edge (point *X*). An increase of E_g after microwave irradiation (caused by IS relaxation) and considerable decrease of Γ are observed. These facts confirm the above conclusions about Si structural ordering at the Si interface due to microwave irradiation. There is also another transition near 4.3 eV in the ER spectrum (Fig. 5.12). We relate it to the presence of Ta_2O_5 film on Si surface. One can see from Table 5.4 that this transition energy also increases after microwave irradiation. This confirms IS decrease in the film. But Γ value has not changed after irradiation. So microwave

Table 5.4. The changes of parameters E_g and Γ for Si and Ta_2O_5 in the Ta_2O_5–*p*–Si structures after microwave treatment.

t_i, s	High-energy transition for Si		High-energy transition for Ta_2O_5	
	E_g, eV	Γ, eV	E_g, eV	Γ, eV
0	4.070	0.181	4.374	0.146
10	4.118	0.119	4.420	0.146

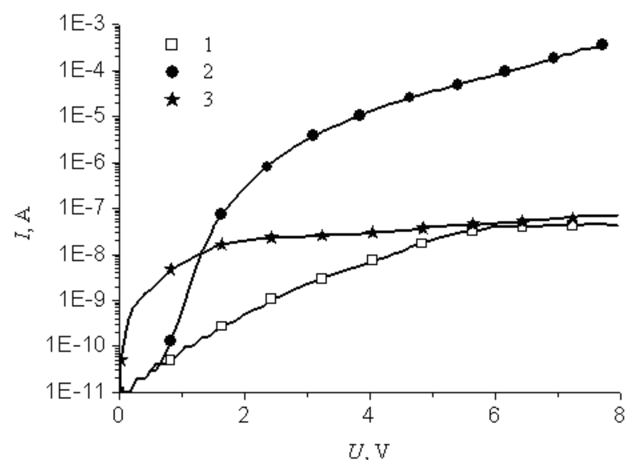

Fig. 5.13. *I-V* curve forward branches for Ta_2O_5–*p*–Si heterosystem: 1 – initial sample; 2 (3) – after microwave processing, duration of 5 (10) s.

irradiation during 10 s is not enough for structural ordering in Ta_2O_5 film, unlike the case of Si substrate where such ordering is observed after 10 s microwave treatment (according to the results of the ER spectra measurements at the points Γ and *X* of the Brillouin zone).

Similar effects took place in MIS structures too, e.g., the curvature of wafer with MIS topology increased after 5 and 10 s microwave treatment (Table 5.2). This serves as evidence of IS relaxation in the device structure induced by microwave irradiation.

The typical *I–V* curves of MIS structures before and after microwave irradiation during 5 and 10 s are given in Fig. 5.13.One can see that microwave treatment during 10 s led to essential change of *I–V* curve (as it was after irradiation of similar structures with ^{60}Co γ-quanta up to a dose of 5×10^5 Gy described in [31]). This correlated with the data on structural-impurity ordering of the Ta_2O_5–*p*–Si interface presented above in Table 5.3.

Shown in Fig. 5.14 are the topograms of current distribution over the wafer with fifty MIS structures. They were taken at forward and reverse biases (the voltage was fixed), both before and after microwave

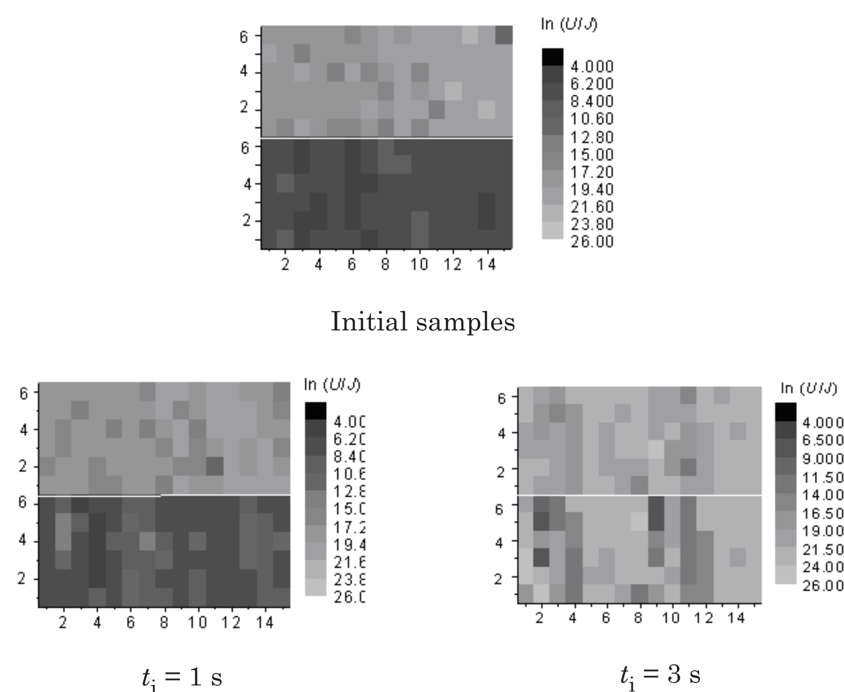

Fig. 5.14. The current density distribution over the wafer before (a) and after microwave irradiation for 1 (b) and 3 s (c); top (bottom) - back (forward) bias. (Arbitrary units are plotted along the axes; grades of gray color present the logarithm of current density at 10 V).

irradiation for 1 and 3 s. One can see that the current distribution in the initial samples was nonuniform. This was due to technological factors (such as stresses that appeared during MIS structure deformation) and nonuniformities of the initial material (silicon). Microwave irradiation of MIS structures during 1 s made current distribution over the wafer more uniform. This effect took place at forward and reverse biases on the MIS structures.

Considerable variations of current values were observed for different samples after 3 s irradiation of MIS structures. One can explain this fact if one assumes that it results from imperfections at the in-

Table 5.5. Effect of microwave irradiation on the curvature radius R and IS value σ for the Ta_2O_5–p–Si test structures and MIS capacitors.

Structure	t_i, s	R, m	σ, 10^9 N/m^2
Ta_2O_5–p–Si (16 nm)	0	30	6.8
	0.5	20	11
	1.0	26	8.4
	3.0	24	8.9
Ta_2O_5–p–Si (24 nm)	0	30	5.1
	0.5	40	3.7
	1.0	60	2.4
	3.0	50	2.6
MIS	0	40	-
	1.0	58	-

terface (metal–dielectric and dielectric–semiconductor) regions and modifications due to IS relaxation resulting from short-term microwave irradiation. Indeed, as it follows from the investigations (Table 5.5), bending existed in the initial state for both wafers -with test structures and with MIS structures. The changes of curvature radius value after irradiation (as a result of corresponding changes of ISs in the test structures with insulator thickness of 16 nm) are smaller than those in the MIS and test structures with Ta_2O_5 layer thickness of 24 nm. It should be also noted that IS relaxation is observed after microwave treatment. As a result, σ value drops.

The investigation of surface morphology for test structures before and after microwave irradiation (Fig. 5.15) showed that surface microrelief was different for structures with Ta_2O_5 layer thicknesses of 16 and 24 nm. The size of nonuniformities in the structures with “thin” (16 nm) dielectric is smaller than that in similar structures with layer thickness of 24 nm. The microrelief changes after microwave treatment for 1 and 3 s in “thin” structures are smaller than those in “thick” ones (Table 5.6).

Microwave treatment during 1 s improves uniformity of “thin” structures, while that during 3 s makes it worse (almost such as in the initial state). Contrary to this, for thicker films the surface uniformity monotonically grows with t_i indicating film ordering.

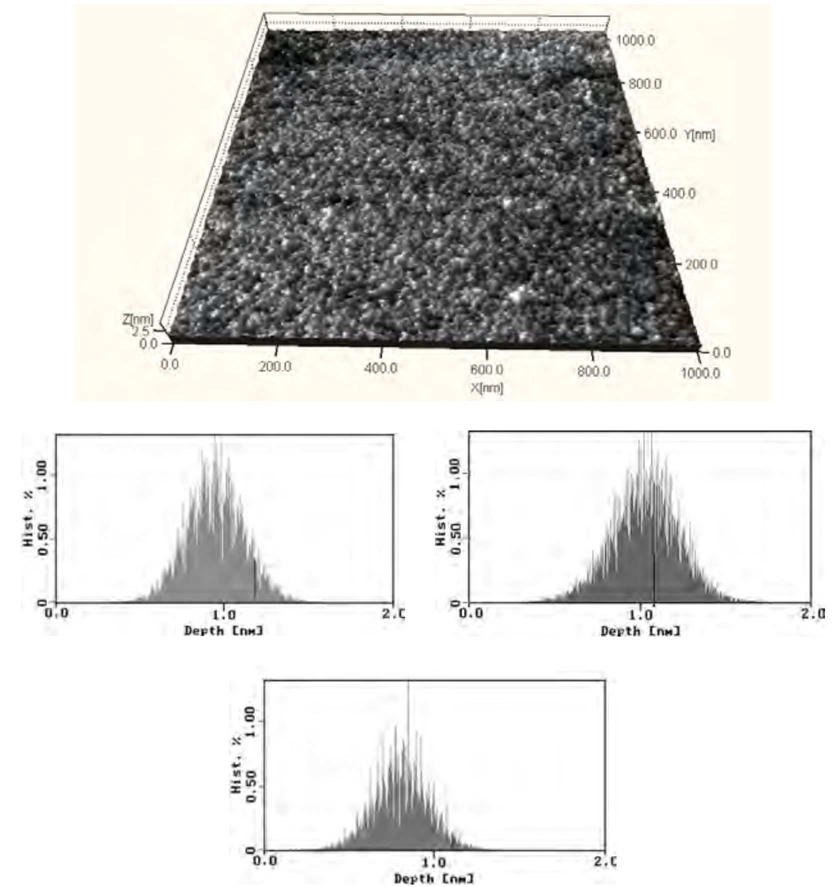

Fig. 5.15a. Surface morphology (a) and bearing analysis before (b) and after microwave irradiation for 1 s (c) and 3 s (d) for the Ta_2O_5–Si (16 nm) structure.

In structures of both types a trend for structural ordering is observed. We believe that this trend is related to the presence of tantalum suboxides (that is, not completely oxidized Ta) at the dielectric–silicon interface or in the transition layer. This can lead to nonuniform absorption of microwave radiation in the structures studied and, as a result, to microheating and disruption of Ta microclusters. Such factors could cause structural-impurity ordering in the Ta_2O_5–p–Si contact. This

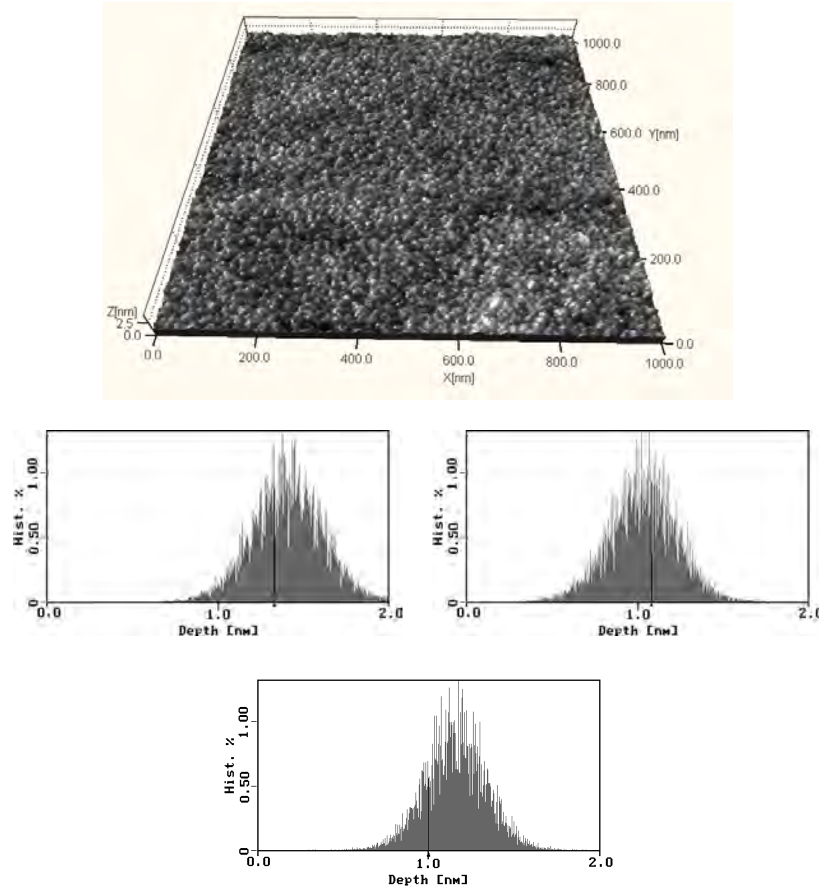

Fig. 5.15b. As in Fig. 5.15a but for the Ta_2O_5–Si (24 nm) structure.

conclusion is confirmed by the AFM results (Fig. 5.15) as well as by the experimental investigations of ER spectra of our systems performed before and after microwave irradiation. As it was also demonstrated in our work [41], the collision broadening parameter Γ is decreased by 20...30% in the samples of both types after microwave treatment (this parameter characterizes the imperfect state of interface and transition layer). The decrease of Γ value corresponds to structural-impurity

Table 5.6. Surface parameters of Ta_2O_5 films before and after microwave treatment.

Duration of oxidation, s	Ta_2O_5 (24 nm)–*p*–Si		Ta_2O_5 (16 nm)–*p*–Si	
	Z_{range}, nm	RMS, nm	Z_{range}, nm	RMS, nm
0 (initial)	2.648	0.164	2.333	0.138
1	2.153	0.158	1.336	0.118
3	1.983	0.140	2.205	0.130

ordering in the Ta_2O_5–*p*–Si contacts. This correlates with decrease of MIS parameter spread after microwave treatment during 1 s. However, MIS systems are more complicated structures than Ta_2O_5–*p*–Si test objects. So for more definite explanation of the effects stimulated by microwave irradiation one should perform additional investigations, including those of the component concentration depth profiles in MIS structures before and after microwave treatment. We suppose that, due to microwave irradiation of both the Ta_2O_5–*p*–Si heterostructures and MIS (as in the case of exposure to γ-quanta), excitation of the electron subsystem of semiconductor stimulated by microwave irradiation occurs. As a result, there is an IS relaxation in heterostructures leading to structural-impurity ordering. *This effect was obtained by us for similar heterostructures for the first time*. It seems to deserve further study, since it enables one to operate with electronic and structural properties of such objects as MIS structures.

The essential result here, however, is that microwave processing obviously enables one to obtain Ta_2O_5/Si systems with practically no stresses, and real increase of the degree of Ta_2O_5/Si interface ordering is observed.

5.3. EFFECT OF γ-RADIATION ON THIN Ta_2O_5–Si MICROSTRUCTURES

5.3.1. Experimental procedure

The p-Si (100) wafers with resistivity of 15 Ω·cm, cleaned with a standard for submicron technology process, were used as substrates in this study. The following two sets of samples were formed:

(i) After the chemical cleaning of the substrates, Ta film was deposited on Si by rf sputtering of a tantalum target in the Ar ambient. The process parameters were such: base pressure of 6×10^{-4} Pa; Ar pressure of 3 Pa; rf radiating power of 2.2 W/cm^2 and deposition rate of 9.3 nm/min. The substrates were not intentionally heated during the Ta deposition and presumably remained at a temperature close to the room one. Subsequently the Ta films were oxidized in dry oxygen at atmospheric pressure at two temperatures, 823 and 873 K; the O_2 flow rate was 5 l/min. The oxidation temperatures T_{ox} should be low enough to prevent formation of tantalum silicide. After oxidation, capacitors were defined by evaporation of Al (thickness of 500 nm) through a shadow mask; the capacitor areas were 10^{-4}, 2.25×10^{-4}, 6.25×10^{-4}, and 2.5×10^{-3} cm^{-2}. Postmetallization annealing was carried out in H_2 at 723 K for 1 h.

(ii) Tantalum pentoxide layers were deposited on Si by rf reactive sputtering of a tantalum target in an Ar + O_2 mixture: oxygen content of 10%, working gas pressure of 3.3 Pa, rf radiating power of 3.6 W/cm^2, deposition rate of 5 nm min^{-1}, substrate temperature T_s = 293 and 493 K. After deposition, the samples were annealed at 873 and 1123 K for 30 min. in dry oxygen.

All the samples were treated with ^{60}Co γ-radiation (1.25 MeV); the dose rate was 1.2 Gy/s. The temperature in the irradiation zone was under 313 K. Irradiation doses of 10^4, 10^5 and 5×10^6 Gy were used. The thickness d of Ta_2O_5 and the refractive index n_{eff} were determined by ellipsometry (λ = 632.8 nm). The samples with d in the range from 25 to 90 nm were studied. The dielectric and electrical characteristics

of the Ta_2O_5 structures were studied using measurements of high-frequency (1 MHz) C–V, I–V curves and oxide breakdown voltage V_{bd} histogram. The static dielectric constant ε_{eff} of the Ta_2O_5 layers was determined from the capacitance value C_0 at strong accumulation. The V_{bd} values for approximately 60 capacitors were measured on each wafer (2 in. in diameter). The gate electrode is negatively biased so that the p-type silicon surface is at accumulation and the applied electric field appears across the oxide. Ramp I–V characteristics were used to investigate the leakage current through Ta_2O_5 at low voltages. The data were acquired with a microcomputer through an IEEE interface bus. All electrical measurements were carried out in a screened dark chamber at room temperature.

5.3.2. Results and discussion

n_{eff} of the as-prepared Ta_2O_5 of both types (rf sputtered as well as thermally oxidized) was found to be in the range of 1.95–2.3 depending on the specific fabrication conditions of the layers [14, 26, 42]. The irradiation changed neither the layer thickness nor the n_{eff} values as indicated by ellipsometry. Here we examine the changes of the effective dielectric constant and the oxide charge as a result of irradiation.

Dielectric parameters

rf sputtered Ta_2O_5. The effective dielectric constant of the layers with thickness of 25 nm is 12–14 and 15–16 for the as-deposited and the annealed layers, respectively. After irradiation, ε_{eff} decreases to the values of 5–6 independently of the irradiation dose as well as of the initial values of ε_{eff}. The fixed oxide charge density Q_f has changed from 2×10^{11} cm^{-2} (as-deposited films) to 3×10^{12} cm^{-2} (after irradiation). The shift of the C–V curves has indicated positive charge build-up as a result of exposure to ionizing radiation for the as-deposited layers only. To illustrate, Fig. 5.16 presents HF C–V curves before and after exposure to a dose of 10^5 Gy for the samples obtained at T_s = 293 K. C_0 of the irradiated layer is lower as compared to the initial value; this is due to the radiation-induced decrease of ε_{eff}. The flat-band voltage shift

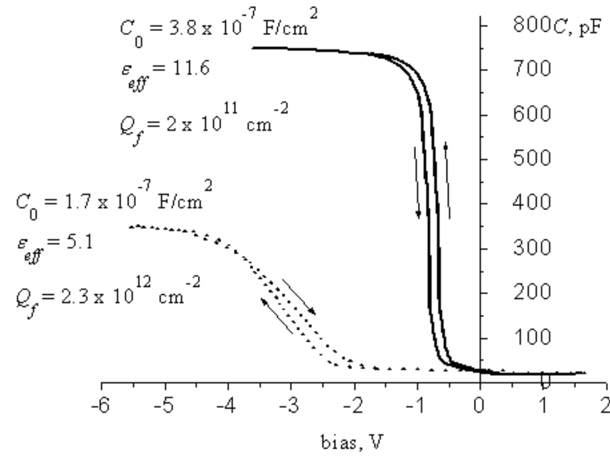

Fig. 5.16. Typical 1 MHz *C–V* curves with a ramp rate of 100 mV/s, for as-deposited 293 K sputtered 25 nm Ta_2O_5 MOS capacitor (4 nm thickness of SiO_2) before (-) and after (- -) 10^5 Gy γ-irradiation. (The dielectric constants are 11.6 and 5.1, respectively; the direction of voltage sweep is indicated by an arrow.)

ΔV_{fb} is negative in all cases indicating a net positive charge trapped in the films. The radiation-induced oxide charge (without gate bias during irradiation) ΔQ_f is about 5×10^{11}, 2×10^{12} and 3×10^{12} cm^{-2} for doses of 10^4, 10^5 and 5×10^5 Gy, respectively. After irradiation the curves are stretched outalong the voltage axis. This voltage stretch out can be caused by an increase of either charge nonuniformity or interface trap concentration. Even a dose of 5×10^5 Gy does not cause generation of oxide charge in the oxygen-annealed samples (873 or 1123 K), and the density of oxide charge in these layers remains about 10^{10} cm^{-2} before as well as after the irradiation.

Hysteresis effects are observed in the bidirectional scans of *C–V* curves in Fig. 5.16. The hysteresis of the curves for the as-deposited layers is positive and respectively the concentration of slow states is determined to be about 3×10^{10} cm^{-2}. After irradiation the hysteresis

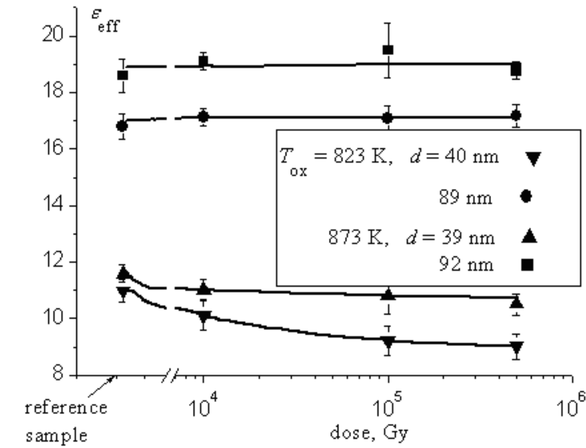

Fig. 5.17. Radiation dose dependence of the measured dielectric constant for thermal Ta_2O_5 obtained at two oxidation temperatures to thickness d ~ 40 and ~ 90 nm.

is negative indicating an additional ~2×10^{11} cm^{-2} positive charge build-up. No hysteresis was observed for annealed layers before as well as after irradiation. Since the slow states (which are also called border traps) are usually related to the presence of oxygen vacancies in the Ta_2O_5–Si system, the results provide evidence of a negligible amount of the oxygen vacancies in the annealed layers before as well as after γ-irradiation. The as-deposited non-annealed films, however, are not radiation-hard enough and the exposure generates oxygen vacancies in the form of slow states with significant concentration, which is practically independent of the dose.

Thermal Ta_2O_5. The values of ε_{eff} of thinner layers decrease slightly after exposure (Fig. 5.17) with a tendency to saturate at 10^5 Gy. The irradiation does not influence ε_{eff} for thicker (~90 nm) layers at all. (As it was reported earlier [9, 10], the dielectric constant of thicker layers as a rule is larger than that of thinner ones.) So, the results imply that the irradiation has not a significant effect on ε_{eff} values up to doses of 5×10^5 Gy. Very well-defined HF *C–V* curves together with a strong

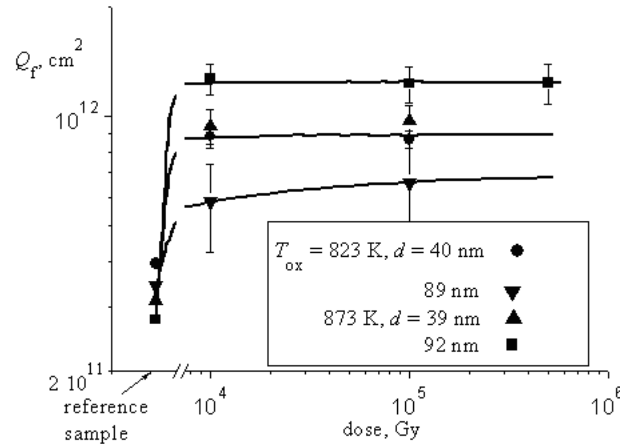

Fig. 5.18. Q_f vs radiation dose for the Ta_2O_5 layers presented in Fig. 5.2.

accumulation effect were obtained for the as-grown Ta_2O_5 [23, 43]. The variation of Q_f as a function of the dose is shown in Fig. 5.18 for the layers obtained at two temperatures of oxidation. For the reference samples,

Q_f is ~3×10^{11} cm^{-2} without a clear dependence on d and T_{ox}. After irradiation with 10^4 Gy, Q_f increases 2–4 times and after it does not change with dose. The temperature of oxidation does not influence Q_f values for thinner oxides. For thicker oxides, the radiation-induced fixed oxide charge is lower for the oxides obtained at lower oxidation temperature (823 K). In general, the irradiation does not degrade the radiation hardness of the layers significantly. As far as ΔQ_f is found to depend slightly on the oxidation temperature, it can be concluded that the oxides grown at different temperatures show no apparent difference in radiation hardness. However, it is hard to say if the oxidation temperature of 823 K is better than 873 K since ΔQ_f depends not only on T_{ox} but also on thickness. In general it seems that the increase of growth temperature above 823 K degrades the radiation hardness.

The hysteresis of the C–V curves of the samples before as well as after irradiation was negligible (the flat-band voltage shift arising from the hysteresis effects is about 0.1–0.2 V for all curves, after sweeping

from accumulation to inversion and back) and the curves were steep, indicating no generation of some kinds of traps (most likely slow states) located in the Ta_2O_5 very close to the interface with silicon. No change in the sharpness of the curves after irradiation was observed, i.e., to a first approximation, the irradiation did not affect the concentration of fast surface states. The presence of extremely thin SiO_2 layer between Ta_2O_5 and Si detected by us previously [5, 8] may be responsible for the formation of a high quality interface at Si.

Leakage current characteristics

Thermal Ta_2O_5. To clarify the effect of radiation on the conduction properties of Ta_2O_5 films, leakage current characteristics of the irradiated capacitors were examined. Figure 5.19 shows the leakage current density vs electric field characteristics for the MOS capacitors with Ta_2O_5 layers grown at 823 K. The as-grown Ta_2O_5 shows a low leakage current density, $J < 10^{-8}$ A/cm^2 up to 4 V applied voltage. Above 4 V, the leakage current increases monotonically. After irradiation J is higher than that of the as-grown layers, and the extent of the current increase depends on the layer thickness and the applied voltage. (The I–V characteristics of the initial samples as well as their change after irradiation for Ta_2O_5 obtained at 873 K are almost the same and they are not shown in the Figure.). The leakage current increase is bigger for thinner layers (Fig. 5.19a) and for low applied fields (≤0.7 MV/cm) the current it is 4–6 orders of magnitude higher than that in the as-grown samples. At higher fields, the current increases monotonically with the applied voltage. The leakage current increase for 40 nm layers is the same for irradiation doses in the range of 10^4–5×10^5 Gy, i.e., no obvious irradiation dose dependence in the behavior and values of the current was observed. No deterioration of the leakage current was found for the samples with thicker Ta_2O_5 (90 nm) irradiated with a dose of 10^4 Gy (Fig. 5.19b). The irradiation only reduced the catastrophic (hard) breakdown fields (from 3 MV/cm before to 1.6 MV/cm after irradiation). The catastrophic breakdown field is defined as a field at which a sudden and irreversible increase in leakage current occurs. The layers irradiated with doses of 10^5–5×10^5 Gy have inferior leakage

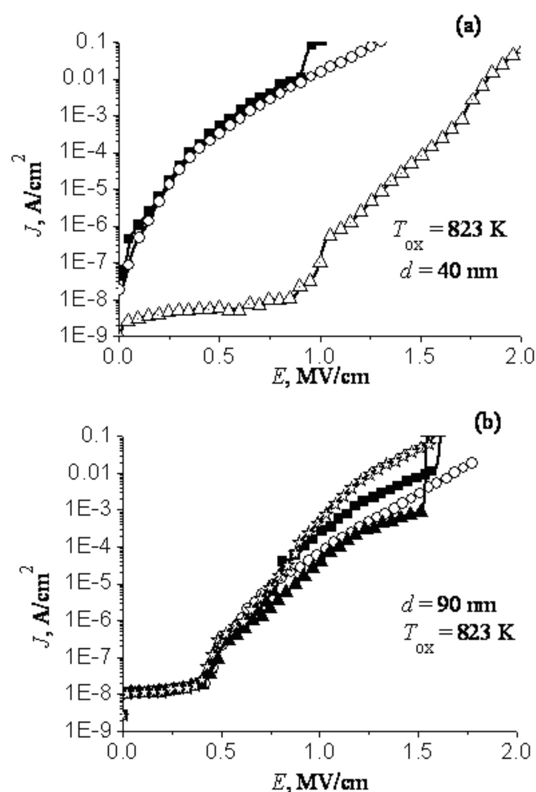

Fig. 5.19. Leakage cur-rent density depend-ence on the applied field, E, for the thermal Ta_2O_5 MOS capacitors, before -A- and after γ-irradiation: -■- 104; -O- 105, 5×105 Gy; (a) d = 40 nm; (b) d = 90 nm.

current characteristics for fields greater than 1 MV/cm as compared to the pre-irradiated ones – the leakage is increased by 1–2 orders of magnitude, leading quickly to an early breakdown (Fig. 5.19b).

Generally, the results show that γ-irradiation will be a problem for the Ta_2O_5–Si structures and the capacitors with irradiated films have deteriorated leakage characteristics compared to the initial ones. This effect is most probably due to the radiation-generated defects in the Ta_2O_5 and at the interface with Si, which leads to an increase of the leakage

current. On the other hand, at least two other factors could contribute to the increased leakage and they cannot be neglected. One of them is the radiation-induced change of the thickness of the interfacial SiO_2 (most likely increase of the thickness as indicated by the decrease of the global dielectric constant of thinner layers, Fig. 5.17), which is inevitably formed during the fabrication of Ta_2O_5. Our XPS investigations [42] clearly revealed the formation of interfacial SiO_2 layer (of about 2–3 nm) under all technological regimes used. The thickness and the quality of this layer depend on the oxidation temperature. As far as the total thickness of the layer (as measured with ellipsometry) is almost completely independent of the irradiation, the deterioration of the current may be due to the increase of SiO_2 thickness as a result of the reduced thickness of the outer Ta_2O_5. (The growth of SiO_2 layer at the interface leads to an increase of the equivalent oxide thickness of the layer. The change of the thickness of SiO_2 leads also to a redistribution of the electric field.) Another phenomenon can be correlated with an eventual radiation-induced crystallization effects in the initial layers, which have been found to be amorphous [5, 23, 42, 43] after the growth. A deterioration of the leakage current is usually observed when the layers are crystallized [44, 45]. The current increase is thought to be caused by the grain boundaries which serve as current paths resulting in poor leakage current characteristics. The relationship between the leakage current properties and the crystalline structure of the tantalum oxide has not yet been clarified. Eventual radiation-induced crystallization effects in Ta_2O_5 are not understood at all, and further investigations are mandatory to explain the above observations.

rf sputtered Ta_2O_5. Figure 5.20a shows current density J vs applied voltage for the as-deposited (at 293 and 493 K) 25 nm Ta_2O_5 before and after OA. (The characteristics did not show a difference from capacitor to capacitor on one and the same wafer.) For the as-deposited films, leakage current about and below 10^{-8} A/cm at 0.5 MV/cm can be achieved without annealing steps. The films fabricated at 493 K have somewhat better leakage current characteristics at low applied fields. The annealed films show improved characteristics, $J \sim 10^{-8}$ A/cm for applied voltages up to

~6 V. One can see that after OA there is a general shift of the curves toward higher voltages, indicating an increase of breakdown fields and dielectric strength. The effect seems to result from the repairing of oxygen vacancies in Ta_2O_5 and densification of the layers as a whole. The comparison of Fig. 5.20a and b shows that a 10^4 Gy dose has negligible influence on the leakage current up to voltages which are actual from the practical point of view and are close to the breakdown voltages. The effect of irradiation is well pronounced for 10^5 Gy: J increases by 1–3 orders of magnitude when the applied voltage increases up to 5 V. The irradiation does not alter the I–V characteristics up to fields of ~0.5 MV/cm. For simplicity, the effect of dose on the I–V curves is presented in Fig. 5.20c only for one of the layers (annealed at 873 K). In the case of 5×10^5 Gy, the leakage current is nearly equally deteriorated as that for 10^5 Gy dose. So, the results indicate that the layers are stable to γ-irradiation up to a dose of 10^4 Gy, i.e., this dose does not change the quality of the capacitors in terms of leakage current. Relatively severe degradation of the leakage current can be observed after exposure to 10^5–5×10^5 Gy. The reason for worsening of the electrical properties in this case is that the layers are damaged by introduction of radiation defects in the form of broken Ta–O and/or Si–O bonds. The radiation-induced crystallization of these films also cannot be ruled out.

From an analysis of Fig. 5.20 it is clear that the initial quality of starting oxide influences the magnitude of the leakage current after irradiation: the irradiated annealed films have lower current in comparison with the irradiated as-deposited ones. This means that oxygen-annealed layers have higher γ-radiation hardness. It emerges that for higher voltages the relative change of the leakage current after irradiation as compared to the initial current value is nearly the same (Fig. 5.20c), i.e., the relative change depends on the average electric field in the oxide rather than on the absolute current level. As is seen, the curve corresponding to 10^5, 5×10^5 Gy shifts parallel to lower voltages with respect to the curve of the non-irradiated oxide. This implies that most probably the radiation-induced damage is uniformly distributed throughout the Ta_2O_5.

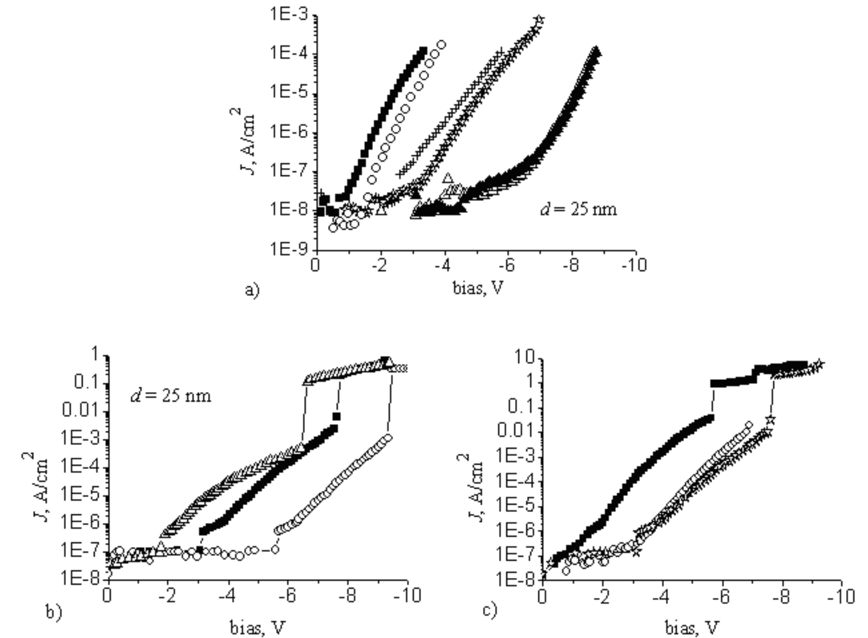

Fig. 5.20. a – current density–voltage curves for rf sputtered Ta_2O_5 MOS capacitors: T_s = 293 K, X as-deposited, ○ OA, 873 K; ● OA, 1173 K; T_s = 493 K, Δ as-deposited; ■ OA, 873 K; * OA, 1123 K, (b) I–V curves of *rf* sputtered Ta_2O_5 MOS capacitors after 10^4 Gy γ-irradiation; T_a = 493 K, Δ as-deposited; ○ OA, 873 K; ● OA, 1173 K, (c) I–V curves of MOS capacitors with rf sputtered oxygen annealed at 873 K Ta_2O_5 layers before (O) and after γ-irradiation (* 10^4, ■ 10^5, 5×10^5 Gy).

In general, three possible explanations [3] exist for the observed increase of the leakage current after γ-irradiation: (i) lowering of the barrier height at the Al–Ta_2O_5 interface because build-up of a charge in Ta_2O_5 near this contact seems possible, (ii) reduction of Ta_2O_5 to tantalum suboxides and hence an increase of the layer conductivity (the oxygen deficiency in Ta_2O_5 is one of the reasons for the leakage current through the films), and (iii) modification of the Si–Ta_2O_5 interface as a result of reduction of Ta_2O_5 and oxidation of Si substrate

during irradiation, leading to enlargement of the mixed transition layer consisting generally of both tantalum and silicon suboxides. The possibility for such modification is supported by the observed changes in Q_s. So, we have obtained that the irradiated films have leakage current larger than the starting ones. We have shown by XRD technique [18] that the sputtered as-deposited as well as annealed at 873 K layers are amorphous, whereas crystalline Ta_2O_5 (orthorhombic β-Ta_2O_5 phase) was obtained after OA at 1123 K. It should be kept in mind, however, that in order to detect crystallinity with XRD techniques, a certain size of crystallites is required. The absence of diffraction peaks provides only an upper limit of the volume fraction of the crystalline phase. For XRD the lower limit of detection is approximately a volume fraction of the crystalline phase of 0.001 [46]. That is why XRD data have to be considered only in terms of the sensitivity of this method. A combination of XRD data and the present leakage current and Q_f data suggests and reveals that the crystalline Ta_2O_5 (obtained after heating at 1123 K) shows better leakage current properties. The *I–V* data for the rf sputtered layers strongly suggest also that the radiation hardness is completely independent of the amorphous status of the layers: the relative increase of the leakage current is practically the same for the amorphous and crystalline Ta_2O_5. The current magnitude after irradiation depends on the initial value before the exposure – the annealed layers have better leakage current characteristics before as well as after irradiation. Having in mind also the dielectric constant data, one can see that for the amorphous (as-deposited and annealed at 873 K) films the intrinsic dielectric constant of Ta_2O_5 is 23–27 and for the 1123 K annealed (when a crystalline phase appeared) it is significantly higher (32–37), i.e., the crystalline Ta_2O_5 shows bigger values of dielectric constant. The deviation of the measured dielectric constant ε_{eff} from the values of the relative dielectric constant of the bulk Ta_2O_5 is due to the presence of the ultrathin SiO_2 at the interface with Si. Usually, Ta_2O_5 leakage current increases with its crystallization. In contrast, we obtain that for the crystalline 1123 K annealed layers the leakage current is smaller. On the other hand, the leakage

current degradation after irradiation can be correlated with eventual critically high level of radiation-induced crystallization of the films, leading actually to the increase of the current. However, none of the presented possible explanations for the current degradation could be ruled out at this stage of our investigations. The exact clarification of this fact requires further detailed study of an eventual crystallization of the irradiated layers.

Breakdown fields

Breakdown characteristics of the layers before and after irradiation are discussed in this section. The breakdown field E_{bd} is detected when the leakage current is over 10^{-6} A. As is seen in Fig. 5.21, the breakdown characteristics of the annealed rf sputtered Ta_2O_5 layers are better than that of the as-deposited one. Since no obvious dependence of E_{bd} histograms on the substrate temperature is observed, for simplicity only the data for T_s = 493 K are given in the Figure. The oxide equivalent breakdown field E_{eq} of the annealed layer is as high as 20 MV/cm. E_{eq} is the breakdown field obtained using the “equivalent SiO_2 film thickness”, which is defined by assuming that the films consist of a single layer having a dielectric constant of SiO_2. In general, OA improves the breakdown characteristics of Ta_2O_5 obtained at both deposition temperatures used. The effect is stronger for higher temperature of annealing, Fig. 5.21a. These phenomena indicate that most of the fabrication-induced defects were passivated during the anneal process. We correlate the improvement in E_{bd} with a reduction in oxygen vacancies number and the imperfect Ta–O bonds in the initial layers as well as with the general densification of the layers. The as-deposited layers exhibit a distribution of the measured breakdown fields in the range of 3.5–5.5 MV/cm with a main peak at ~4.2 MV/cm. These parameters for the 1123 K annealed samples are 5–7 MV/cm and ~6.6 MV/cm, respectively. The results are consistent with the leakage current reduction after

OA, and the higher annealing temperature is more effective in reducing the leakage. In general, all the irradiated samples with if sputtered Ta_2O_5 exhibit not very strong deterioration of the breakdown

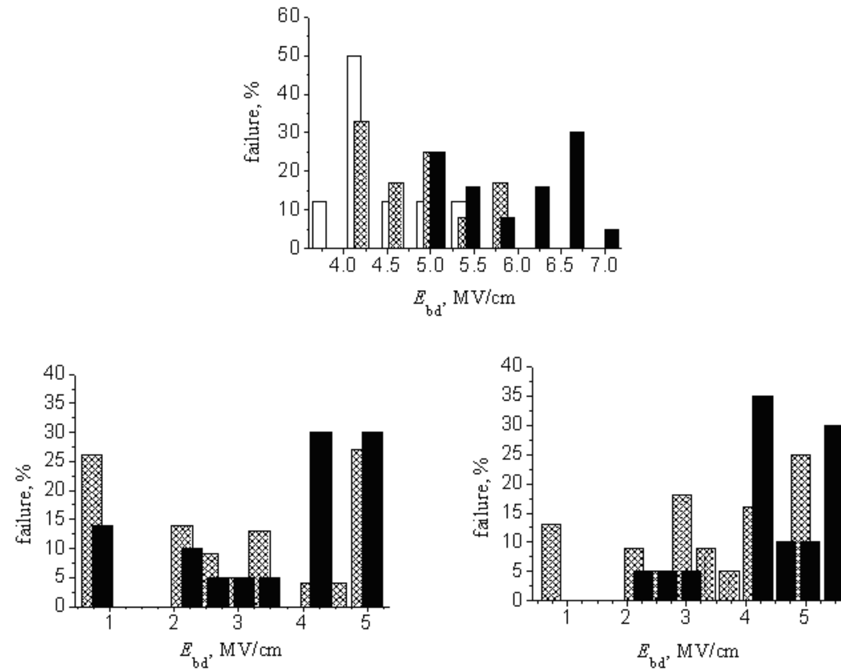

Fig. 5.21. a – breakdown histograms of 25 nm rf sputtered Ta_2O_5 before (□) and after oxygen annealing at 873 K -##, 1123 K ■ ; b – breakdown histograms of 5 nm. 493 K as-deposited Ta_2O_5 after γ-irradiation, ■ 10^4; ## 10^5 Gy, c – breakdown histograms of 25 nm, 493 K, oxygen annealed at 1123 K Ta_2O_5 after γ-irradiation, ■ 10^4; ## 10^5 Gy.

field distribution. The influence of the irradiation on the gate oxide breakdown frequency depends on both the irradiation dose and the initial quality of the layers. The as-deposited films are damaged more severely by irradiation: after 10^4 Gy treatment, a low breakdown appears in the range of 0.2–2 MV/cm with a peak intensity of ~15%; the high breakdown field peak shifts to the left at 4–5 MV/cm without intensity reduction. The higher dose irradiation (Fig. 5.21b) produces additional degradation – a main fraction of capacitors (~27%) break at 0.1–2.2 MV/cm; the high field breakdown localizes at about 5 MV/cm

with an intensity of ~ 30%. The irradiation slightly affects the annealed samples – the degradation after the higher dose is more pronounced. The distribution for 10^4 Gy dose is characterized with two main peaks at ~4 and 5.5 MV/cm with 30% intensity, and peaks with low intensity (<10%) in the ranges of 2–3 and 4.5–5 MV/cm (Fig. 5.21c). The higher dose leads to more random distribution of the breakdown fields: low and medium breakdowns appear in the ranges of 0.2–2 and 2.2–4 MV/cm, respectively; the maximum E_{bd} is at 5 MV/cm, with a slight reduction of the intensity.

The breakdown field of the thermal Ta_2O_5 slightly increases with increasing the growth temperature implying that the higher oxidation temperature is beneficial in terms of breakdown characteristics. The breakdown fields are practically the same for the two thicknesses used (Fig. 5.22) suggesting that the composition and the microscopic structure of thermal oxides do not change significantly when varying the thickness from 40 to 90 nm. There is a weak tendency for slight increase of high field breakdowns for thinner oxides: a peak with a small intensity (<10%) at 3–4 MV/cm appears. The intensity of high field breakdowns, however, remains low for all samples. After irradiation the breakdown field characteristics worsen (the low and medium field breakdowns increase and the effect is stronger for the higher dose) with slight dependence on d and T_{ox}. Figure 5.22 shows the radiation-induced breakdown histogram changes. All irradiated thermal Ta_2O_5 films break down at an electric field of about 0.5–1 MV/cm for 823 K and 0.5–2 MV/cm for 873 K formed layers respectively, indicating that the higher oxidation temperature is more beneficial for radiation hardness of Ta_2O_5 in terms of breakdown. (For non-irradiated samples the breakdown frequencies have also a more random distribution.) The damage of devices exposed to 5×10^5 Gy is not heavier than that of devices with 10^5 Gy and it is higher than in 10^4 Gy irradiated oxide. The breakdown of 90 nm Ta_2O_5 does not critically depend on dose in the range used. For thinner (40 nm) films, however, the radiation damage is a severe problem: the main fraction of capacitors breaks down in the field range of 0.2–1 MV/cm after exposure to 10^4 as well as to

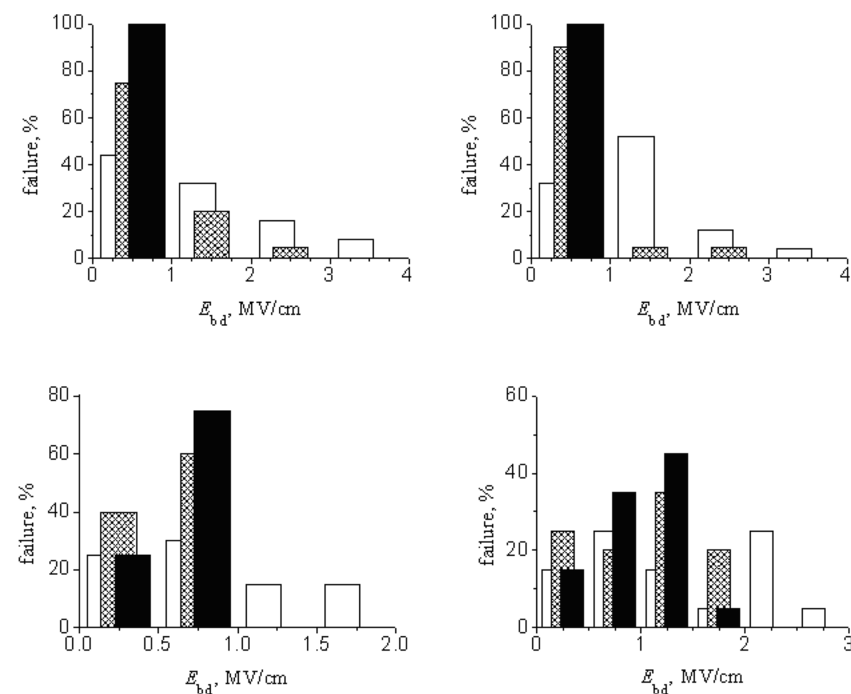

Fig. 5.22. Breakdown histograms of thermal Ta_2O_5 with two thicknesses obtained at two oxidation temperatures, before □ and after ## 10^4, ■ 10^5 Gy γ-irradiation.

10^5 Gy. Based on these results, one would tend to conclude that the radiation-induced breakdown depends on the oxide thickness rather than on the irradiation dose. It means also that the radiation-induced damage (in the form of interface states and bulk traps) is relatively heavy and affects the breakdown characteristics. It can be concluded also that the tantalum oxides with a thickness above ~40 nm prepared at relatively high oxidation temperatures (like those used here) have good radiation hardness. The breakdown data for Ta_2O_5 of both types (rf sputtered and thermal) are consistent with the results deduced from the *I–V* and *C–V* measurements. To understand and control the

degradation of the electrical characteristics of the irradiated layers it is desirable to relate them to the composition and microscopic structure of the film and its interface. Usually the breakdown is manifested by the formation of a conductive path through the oxide, initiated by the presence of weak spots. It is related in this way to the microscopic properties of the layers and interface with Si and is basically associated with defects induced by the technological process (intrinsic defects like oxygen vacancies) as well as defects generated by the radiation. Although the true mechanism of the radiation-induced breakdown in Ta_2O_5 is unclear, it is probably associated with broken bonds (Ta–O and/or Si–O). The exact answer of this question is related to the more general question concerning the mechanism of breakdown in Ta_2O_5 and particularly to the presence of ultrathin SiO_2 at the interface with Si. At present these questions remain open. We cannot eliminate a priori the possibility for the radiation-induced crystallization effects in Ta_2O_5 (the issue that is not studied at all).

The results presented allow one to draw the following conclusions about the γ-irradiation effect on the dielectric and electrical parameters of Ta_2O_5 layers on Si.

rf Sputtered Ta_2O_5

The radiation causes higher leakage current and lower dielectric constant, which decreases to values of 5–6 independently of its initial value as well as of the dose. The lower dielectric constant value confirms that the film structure is modified by irradiation. The as-deposited films are not radiation-hard enough and the exposure generates significant defects in the form of positive oxide charge ($5{\times}10^{11}$–$3{\times}10^{12}$ cm^{-2}) and slow states with a concentration of about $2{\times}10^{11}$ cm^{-2}. The effect seems to result from some kind of oxygen vacancies-generation-related reaction. The formation of oxygen vacancies in the as-fabricated oxides results mainly from imperfect oxidation. The results provide evidence, however, of *a negligible amount of oxygen vacancies in the annealed layers*. Even the highest dose used does not cause generation of oxide charge in the annealed samples.

The leakage current of the as-fabricated layers is bigger after irradiation, with different values of increase depending on the dose. A relatively severe degradation is detected after 10^5–5×10^5 Gy. The increase in the leakage current density most likely is attributed to broken Ta–O and/or Si–O bonds. The radiation-induced crystallization of the as-deposited films also cannot be ruled out, and the leakage current degradation can be related to an eventual critically high level of radiation-induced crystallization of the films leading actually to current increase. The irradiated annealed films have lower current in comparison with the irradiated as-deposited ones, i.e., *the oxygen annealed layers have higher radiation hardness*. In this context, it can be concluded that the initial quality of starting oxide influences the magnitude of the leakage current after irradiation and OA *is beneficial for radiation hardness*. These phenomena indicate that most of the irradiation-induced defects are oxygen vacancies and/or some kind of degradation in the stoichiometry of the layers. They also support the argument that the latent defects, which are activated during irradiation, are in the form of oxide traps and are responsible also for deterioration of breakdown characteristics. Since the radiation-induced decrease of breakdown field is relatively weak, it can be concluded that the irradiation does not worsen the interface and the bulk to an extent at which the radiation-induced catastrophic breakdown occurs and in fact the oxide is only slightly weakened.

Thermal Ta_2O_5

The radiation does not degrade the dielectric properties of the layers significantly: the dielectric constant decreases slightly for thinner layers and does not change for thicker ones at all; the density of oxide charge increases 2–4 times for 10^4 Gy and saturates above a dose of 10^5 Gy; no generation of slow states is observed – the presence of extremely thin SiO_2 layer between Ta_2O_5 and Si may be responsible for the formation of high-quality interface transition region. The results show, however, that γ-*irradiation will be a problem in terms of leakage current* – the extent of the current increase after irradiation depends

on the layer thickness and the applied voltage; the effect of radiation is stronger for thinner layers and higher doses – the current increase is 4–6 orders of magnitude at low (≤0.7 MV/cm) applied fields. This result is attributed to the generation of electrically active defects in Ta_2O_5 and at the interface as well as to the radiation-induced increase of interfacial SiO_2 layer as indicated by the decrease of the global dielectric constant after γ-radiation for thinner oxides.

The higher oxidation temperature is more beneficial for the radiation hardness of Ta_2O_5 in terms of breakdown, which is consistent with the data on the dielectric and electrical parameters of the layers. The results give evidence that *a suitable choice of the oxidation temperature can improve the radiation hardness*. The radiation-induced breakdown depends on the oxide thickness rather than the irradiation dose: the data clearly show that Ta_2O_5 with a thickness above ~40 nm prepared at a relatively high oxidation temperature has good radiation hardness.

In summary, we have shown that γ-irradiation can increase leakage current and oxide charges significantly. In fact, the presence of radiation-induced traps in the Ta_2O_5–Si system is expected. The results prove the introduction of damage by radiation and the high level of leakage current is attributed to the presence of these traps. Although the true mechanism of radiation-induced breakdown in Ta_2O_5 is unclear yet, it is most likely associated with broken and imperfect Ta–O and Si–O bonds with a key influence of the interface transition region where SiO_2 and the intermediate oxidation states of Si coexist. Additional support of this suggestion is the good correspondence between the breakdown data and the results deduced from the *I–V* and *C–V* measurements. In the context of advanced MOS technologies it is clear that *irradiation will give rise to reliability problems*, which may be related to oxide failures, i.e., *radiation-induced damage remains a major concern for Ta_2O_5 reliability*. Based on the results, however, one would tend to conclude that γ irradiation-induced damage will have less impact on devices with thicker Ta_2O_5 and obtained or annealed at relatively high temperatures.

The microwave exposure for extremely short times (several seconds) has a potential to replace undesired high-temperature annealing

processes for high-*k* dielectrics in nanoscale Si devices (DRAMs and MOSFETs), to meet the future road map requirements.

Insufficient experimental data about the behavior of high-*k* dielectrics in radiation-rich conditions will motivate future intensive work in this field. Our first experiments (γ-irradiation, 10^4–10^6 Gy) show that the irradiation will be, especially for Ta_2O_5 as a typical high-*k* insulator, a problem in terms of leakage current – the extent of the current increase depends on the layer thickness, and the effect is stronger for thinner films and higher doses. There is, however, a potential to improve and control additionally the current by using appropriate annealing steps.

CONCLUSION

In this book we made an attempt to consider and explain some processes of interaction of microwave radiation with semiconductors and device structures (among them the submicron and nanostructured materials) that are of importance for electronics. The effects of structural relaxation (resulted from microwave treatment, as well as rapid thermal annealing and ^{60}Co γ-irradiation) and their influence on the parameters of single crystals and barrier contacts are considered.

It was found that, despite some general features of the effect of active actions on the electrical and structural properties of different semiconductor objects (single crystals, hetero- and *p-n* junctions, metal–semiconductor, dielectric–semiconductor and metal–dielectric–semiconductor contacts), the mechanism of the effect of microwave radiation is more complex than had been suspected. Both the heating effects (leading to degradation of the parameters of semiconductor materials and device structures) and non-thermal effects (accompanied with defect gettering) are observed in this case. One should take these factors into account when developing the mm-wave devices with heterojunction and Schottky barrier, as well as MIS structures with nanometer thick dielectric.

It should be noted that the theoretical and experimental investigations made to date did not give final solution to the problem of interaction between microwave radiation and semiconductors. However, the model approaches and experimental technique which are progressing rapidly give grounds to expect further widening of the scope of our knowledge in the area and application of the results obtained in practice by the technologists and those engaged in development of electronic devices.

REFERENCES

Preface

1. S. Luryi, J. Xu, A. Zaslavsky. *Future Trends in Microelectronics. The Road Ahead.* John Willey & Sons, Inc., 1999.

2. *Nanotechnologies in Semiconductor Electronics.* Ed. A.L. Aseev. Nauka SO RAN, Novosibirsk, 2004.[1]*

3. E.V. Buzaneva. Microstructures of Integrated Electronics. Radio i Svyaz', Moscow, 1990.*

4. V.P. Dragunov, I.G. Neizvestnyi, V.A. Gridchin. *Foundations of Nanoelectronics.* NGTU, Novosibirsk, 2004.*

5. V.G. Verbitskii. *Ionic Nanotechnologies in Electronics.* Lesya, Kiev, 2002.*

6. V.F. Oleinik, V.L. Bulgach, V.V. Valyaev, A.V. Zorenko, D.V. Mironov, V.E. Chaika. *Mm- and Submm-wave Electronic Devices on the Basis of Nanotechnologies.* GUIKT, Kiev, 2004.*

7. A.V. Bobyl, S.F. Karmanenko. *Physico-chemical Foundations of Semiconductor Technology. Beam and Plasma Processes in the Planar Technology.* Polytechnic Institute Publishers, Sankt-Peterburg, 2005.*

8. V.A. Pilipenko. *Rapid Thermal Treatments in VLSI Technology.* BGU, Minsk, 2004.*

9. C. Claeys, E. Simoen. *Radiation Effects in Advanced Semiconductor Materials and Devices.* Springer, Berlin, 2002.

10. V.A. Pilipenko, V.A. Gorushko, N.I. Sterzhanov, V.A. Yakovtsova. Laser gettering of defects when manufacturing semiconductor devices and ICs. *ET Ser. 3* no 1, 107-112, 1984.*

11. T.W. Sigmon, L. Cberegi, L.M. Mayer. Ion-implantation gettering of gold in silicon. *J. Electrochem. Soc.* 123(7), 1116-1121, 1976.

12. K. Prasad. Scanned electron beam irradiation of Ti Schottky contacts to *n*-GaAs. *J. Materials Sci.: Materials in Electronics* 3, 16-19, 1992.

13. S.M. Khanna, C. Rejeb, A. Jorio, M. Perentean, C, Carlonc, J.W. Gerdes. Electron and neutron radiation-induced order effect in galliumarsenide. *IEEE Trans. Nucl. Sci.* 40(6), pt. 1-2, 1350-1359, 1993.

1 *In Russian (throughout the list of references).

14. T.R. Weatherford, W.T. Anderson. Historical perspective of radiation effects in III–V devices. *IEEE Trans. Nucl. Sci.* **50**(3), 704-710, 2003.

15. R. Zuleeg. Radiation effects in GaAs FET devices. *Proc. IEEE* **77**(3), 389-407, 1989.

16. J.R. Srour, J.M. McGarrity. Radiation effects on microelectronics in space. *Proc. IEEE* **76**(11), 1443-1469, 1988.

17. *Thin Films. Interdiffusion and Reactions.* Eds. J.M. Poate, K.N. Tu, W. Mayer. Wiley, 1978.

18. F. Bechstedt, R. Enderlein. *Semiconductor Surfaces and Interfaces. Their Atomic and Electronic Structures.* Akademie-Verlag, Berlin, 1988.

19. I.B. Ermolovich, I.Yu. Ilyin, R.V. Konakova, V.V. Milenin. The properties of Al(AuGe)–GaAs contacts made by combining ionic treatment and metallization. *ZhTF* **67**(2), 123-124, 1997.*

20. V.F. Dorfman. *Micrometallurgy in Microelectronics. Technological Principles in Semiconductor Device Production.* Metallurgiya, Moscow, 1978.*

21. *Mm- and Submm-wave Electronics and Radio Physics.* Ed. A.Ya. Usikov. Naukova Dumka, Kiev, 1986.*

22. O.A. Agueev. *The Technological Problems of Contacts to Silicon Carbide.* TRTU Publishers, Taganrog, 2005.*

23. S.P. Murarka, *Silicides for VLSI Application.* Academic Press, New York–London, 1983.

24. V.M. Anischik, V.A. Gorushko, V.A. Pilipenko, V.N. Ponomar, V.V. Ponaryadov, I.V. Pilipenko. *Physical Foundations of Rapid Thermal Treatment. Making of Multilevel Metallization.* BGU Publishers, Minsk, 2000.*

25. *Nanotechnology. Physics, Processes, Diagnostics, Devices.* Ed. V.V. Luchinin, Yu.M. Tairov. Fizmatlit, Moscow, 2006.*

26. O.G. Vendik, Yu.N. Gorin, V.F. Popov. *Particle-photon Technology.* Vysshaya Shkola, Moscow, 1984.*

27. E.R. Astvatsaturian, D.V. Gromov, V.M. Lomako. *Radiation Effects in Gallium Arsenide Devices and Integrated Circuits.* Universitetskoe, Minsk, 1992.*

28. L.R. Shaginyan. The mechanisms of formation of thin films obtained using various ion-plasma deposition techniques. *Author's Synopsis of the Doctor of Phys.-Math. Sci. Thesis.* IPM, Kiev, 2001.*

29. *The Problems of Radiation Technology of Semiconductors.* Ed. L.S. Smirnov. Nauka, Novosibirsk, 1980.*

30. V.N. Brudnyi, S.N. Grinayev, N.G. Kolin. A model for Fermi-level pinning in semiconductors: radiation effects, interface boundaries. *Physica B: Cond. Mater.* **348**(1-4), 213-225, 2004.

31. V.N. Brudnyi. Radiation effects in semiconductors. *Vestnik Tomskogo Gosudarstvennogo Universiteta, Ser. Fizika* no 285, 95-102, 2005.*

32. V.N. Brudnyi, V.V. Peshev, A.P. Surzhikov. *Radiation Defect Production in Electric Fields. Gallium Arsenide, Indium Phosphide.* Nauka, Novosibirsk, 2001.*

33. P.H. Sigel. Terahertz technology. *IEEE Trans. MTT* **50**(3), 910-928, 2002.

34. D.L. Woolard, E.R. Brown, M. Pepper, M. Kemp. Terahertz frequency sensing and imaging: A time of reckoning future applications. *Proc. IEEE* **93**(10), 1722-1743, 2005.

35. B.V. Kozeikin, V.V. Perinsky, A.I. Frolov, B.A. Marenko, Yu.N. Yurasov. Ion-implantation processing of metal layers in the HIC technology. *OET, Ser. 7* no 2(1427), 1989.*

36. Yu.D. Chistyakov, V.V. Kaminsky, V.M. Grishin, V.V. Shvedova. Use of electromagnetic radiation in the gas-discharge processes of semiconductor technology. *OET, Ser. 2* no 5, 1976.*

37. B.S. Danilin, V.K. Syrchin. *Magnetron and Spraying Systems.* Radio i Svyaz, Moscow, 1982.*

38. Z.Yu. Gotra. *Technology of Microelectronic Facilities: A handbook.* Radio i Svyaz, Moscow, 1991.*

39. Author's Certificate USSR # 989754 H05 B6/46. Method for heating of a dielectric or semiconductor material. N.I. Solin, A.A. Samokhvalov, V.V. Belolugov, A.Ya. Afanasiev, G.I. Gladkov. Institute for Metal Physics of the Ural Scientific Center of the Academy of Sciences of USSR. 1980.*

40. Patent Hungary # 194444 H01L 21/263. Method for microwave annealing of semiconductor. B. Kovacs, I. Mojzes, M. Nemeth-Salay, R. Veresegyhazy, N.N. Gerasimenko, S.V. Vasiliev. 1985.

41. Author's Certificate USSR # 880174 H01L 21/268. A method for annealing of semiconductor wafers with pulses of incoherent electromagnetic radiation. 1980.*

42. Patent USA # 4303455 H01L 21/263. Low-temperature microwave annealing of semiconductor devices. M.R. Splinter, R.F. Palys, M.M. Begrawaia. Rockwell Int. Corp. 1980.

43. Patent Japan # 1-38368 4H01L 21/268; 21/324; 29/80. A method for local annealing of semiconductor wafers. 1989.

44. Patent France # 8118656 H01L 21/324. Procédé de recuit superficiel par énergie micro-onde pulsé de matériaux semi-conducteurs. J. Cohen, G. Kamarinos, P. Chenevier. Centre National de la Recherche Scientifique (CNRS). 1983.

45. Patent USA # 4314128 H068 6/80, 6/72. Silicon growth technique and apparatus using controlled microwave heating. R. Sanjeev, Photowatt Int. Inc. 1982.

46. Patent USA # 4517026 H01L 21/263. Method of backside heating a semiconductor substrate in an evacuated chamber by directed microwaves for vacuum treating and heating a semiconductor substrate. Minirn Inone, Yokohama, Fujitsu Ltd. (Japan). 1985.

47. Patent Ukraine # 13397 C1 H01L 21/268. A technique for processing of semiconductor materials. V.E. Sklyarevich, M.V. Shevelev, V.I. Guroshev, A.I. Bunenko, E.O. Paton. Institute of Electric Welding of the National Academy of Sciences of Ukraine. 1997.[2**]

48. Patent USA # 4565913 H05 B 6/80. Method for the disintegration of silicon for semiconductor. Yatsurugi, Yoshifumi; Katayama, Meiseki. Komatsu Electronic Metals Co., Ltd. (Tokyo, Japan). 1986.

49. Yu.V. Bykov, A.G. Eremeev, V.I. Pashkov, V.A. Perevoschikov, V.D. Skupov. Gettering of impurities and defects in silicon at treatment in microwave field. NGU Publishers, Nizhniy Novgorod, 1991. – Deposit copy VINITI # 2322-B91.*

50. A.V. Skripal. Investigation of the features of interaction between electromagnetic fields and semiconductor devices in microwave circuits. *Author's Synopsis of the Doctor of Phys.-Math. Sci. Thesis*. SGU, Saratov, 1998.

51. A.A. Kletsov. Investigation of the effect of high-power microwave radiation on IMPATT diodes and microwave Schottky-barrier transistors. *Author's Synopsis of the Candidate of Phys.-Math. Sci. Thesis*. SGU, Saratov, 2003.*

52. A.V. Abramov. The features of the effect of microwave and optical radiations in microwave semiconductor devices. *Author's Synopsis of the Candidate of Phys.-Math. Sci. Thesis*. SGU, Saratov, 2005.*

---

2 **In Ukrainian (throughout the list of references).

53. V.A. Statov. Study of the interphase interactions in refractory metals–GaAs contacts. *Author's Synopsis of the Candidate of Phys.-Math. Sci. Thesis.* ISP NASU, Kiev, 1996.

54. P.M. Lytvyn. Structural defects transformation in single crystals and epitaxial structures on the base of GaAs under external excitation detected by x-ray diffraction methods. *Author's Synopsis of the Candidate of Phys.-Math. Sci. Thesis.* ISP NASU, Kiev, 1997.**

55. O.S. Lytvyn. Morphological and structural changes in III–V and II–VI semiconductors and related systems caused by post-growth treatments. *Author's Synopsis of the Candidate of Phys.-Math. Sci. Thesis.* ISP NASU, Kiev, 2001.**

56. O.E. Rengevych. Effect of γ–radiation and microwave radiation on the GaAs SB FET parameters. *Author's Synopsis of the Candidate of Tech. Sci. Thesis.* ISP NASU, Kiev, 2001.*

57. Ya.Ya. Kudryk. Effect of active actions on the formation processes and properties of ohmic and barrier contacts to silicon carbide. *Author's Synopsis of the Candidate of Tech. Sci. Thesis.* ISP NASU, Kiev, 2004.**

58. G. Doshchenko. Modification of structure and properties of copper phosphate glass in the field of electromagnetic radiation. *Author's Synopsis of the Candidate of Tech. Sci. Thesis.* ISP NASU, Kiev, 1999.**

59. A.B. Kamalov. Investigation of radiation in GaAs device structures with Schottky barrier stimulated by γ-, β- and microwave irradiations. *Author's Synopsis of the Candidate of Phys.-Math. Sci. Thesis.* PTI AS RUz, Tashkent, 2003.

60. V.V. Starostenko, E.P. Taran, E.V. Grigor'ev, A.A. Borisov. Effect of electromagnetic fields on the integrated microcircuits. *Izmeritel'naya Tekhnika* no 4, 65-67, 1998.*

61. E.P. Taran, V.V. Starostenko, M.V. Glumova, A.V. Rukavishnikov. Dynamics of development of irreversible degradation processes in conducting IC microstructures under action of pulsed electromagnetic fields. *Vestnik Kharkovskogo Natsional'nogo Universiteta. Radiofizika i Elektronika* 544(1), 167–172, 2002.*

62. E.P. Taran, V.V. Starostenko, E.V. Grigor'ev. Local degradation of metallization in ICs under action of electromagnetic fields. *Radiofizika i Elektronika* 3(1), 123-126, 1998.*

63. S.B. Bludov, N.P. Gadetsky, K.A. Kravtsov, Yu.F. Lonin, I.I. Magda, S.I. Naisteter, E.A. Prasol, Yu.V. Prokopenko, S.S. Pushkarev, Yu.V. Tkach, I.F. Kharchenko, V.I. Chumakov. Generation of high-power ultra-short microwave pulses and their action on the electronic facilities. *Fizika Plazmy* 20(7-8), 712-717, 1994.*

64. V.I. Chumakov. A model for action of electromagnetic radiation on the element base of radio electronic installation. In: *All-Ukrainian Interdepartmental Scientific & Technical Collection. Radio Engineering*, no 106, 120-123, 1998.*

65. A.E. Belyaev, E.F. Venger, I.B. Ermolovich, R.V. Konakova, P.M. Lytvyn, V.V. Milenin, I.V. Prokopenko, G.S. Svechnikov, E.A. Soloviev, L.L. Fedorenko. *Effect of Microwave and Laser Radiations on the Parameters of Semiconductor Structures*. Kiev: Intas. 2002.

Chapter 1

1. A.V. Dvurechensky, A.G. Kachurin, E.V. Nidaev, L.S. Smirnov. *Pulsed Annealing of Semiconductor Materials*. Nauka, Moscow, 1982.*

2. O.G. Vendik, Yu.N. Gorin, V.F. Popov. *Particle-photon Technology*. Vysshaya Shkola, Moscow, 1984.*

3. V.A. Pilipenko. *Rapid Thermal Treatments in VLSI Technology*. BGU, Minsk, 2004.*

4. V.M. Anischik, V.A. Gorushko, V.A. Pilipenko, V.N. Ponomar, V.V. Ponaryadov, I.V. Pilipenko. *Physical Foundations of Rapid Thermal Treatment. Temperature Fields and Installation Design Features*. BGU Publishers, Minsk, 2000.*

5. V.M. Anischik, V.A. Gorushko, V.A. Pilipenko, V.N. Ponomar, V.V. Ponaryadov. *Physical Foundations of Rapid Thermal Treatment. Gettering, Annealing of Ion-implanted Layers, RTA in VLSI Technology*. BGU Publishers, Minsk, 2001.*

6. I.A. Kolyabina, G.A. Krysov. Application of pulsed annealing modes in the semiconductor structure technology. *OET, Ser. 7* no 12, 1981.*

7. M.S. Yunusov, S.I. Abdurakhmanova, M.A. Zamkovskaya. *Subthreshold Radiation Effects in Semiconductors*. Fan, Tashkent, 1989.*

8. V.S. Vavilov, B.M. Gorin, N.S. Danilin, A.E. Kiv, Yu.L. Nurov, V.I. Shakhovtsov. *Radiation Techniques in Solid-state Electronics*. Radio i Svyaz', Moscow, 1990.*

9. E.F. Venger, M. Grendel, V. Daniska, R.V. Konakova, I.V. Prokopenko, Yu.A. Tkhorik, L.S. Khazan. *Structural Relaxation in Semiconductor Crystals and Device Structures*, Phoenix, Kiev, 1994.*

10. A.V. Rzhanov, N.N. Gerasimenko, A.V. Vasiliev, V.I. Obodnikov. Microwave heating as a technique for thermal treatment of semiconductors. *PZhTF* 7(20), 1221-1223, 1981.*

11. A.M. Brigidin, N.A. Titovich, V.M. Kirillov, Yu.P. Yusupov, N.I. Listopad, G.I. Yasyulya. Effect of electromagnetic disturbances on working capacity of semiconductor devices and ICs. *ET, Ser. 8* no 1, 3-13, 1992.*

12. A.E. Belyaev, A.A. Belyaev, E.F. Venger, I.B. Ermolovich, S.M. Komirenko, R.V. Konakova, V.G. Lyapin, I.I. Magda, V.V. Milenin, I.V. Prokopenko, S.V. Svechnikov, E.A. Soloviev, Yu.A. Tkhorik, M.V. Shevelev. Effect of microwave radiation on structural, physico-chemical and electrophysical properties of a number of semiconductor materials and device structures. In: *6th Int. Crimean Conf. "Microwave & Telecommunication Technology", Conf. Proc., Sevastopol, Weber Co., 1996*, 71-89.*

13. A.E. Belyaev, E.F. Venger, I.B. Ermolovich, R.V. Konakova, P.M. Lytvyn, V.V. Milenin, I.V. Prokopenko, G.S. Svechnikov, E.A. Soloviev, L.L. Fedorenko. *Effect of Microwave and Laser Radiations on the Parameters of Semiconductor Structures*. Kiev, Intas, 2002.

14. S. Bhunia, D.N. Bose, Microwave synthesis, single crystal growth and characterization of ZnTe. *J. Cryst. Growth* **186**, 535-542, 1998.

15. E. Vigil, L. Saadoun, J.A. Ayllón, X. Domènech, I, Zumeta, R. Rodriguez-Clemente. TiO_2 thin film deposition from solution using microwave heating. *Thin Sol. Films* **365**(1), 12-18, 2000.

16. R. Winter, D. Korzec, J. Engemann, Large area plasma clearing with 26″microwave slot antenna plasma source SLAN II. *Surf. and Coating Technology* **93**, 134-141, 1997.

17. H. Zohm, E. Kasper, P. Mehringer, G.A. Muller, Thermal processing of silicon wafers with microwave co-heating. *Microelectron. Eng.* **54**, 247-253, 2000.

18. A.A. Belyaev, A.E. Belyaev, I.B. Ermolovich, S.M. Komirenko, R.V. Konakova, V.G. Lyapin, V.V. Milenin, E.A. Soloviev, M.V. Shevelev. Effect of microwave processing on electrophysical characteristics of semiconductors and surface-barrier structures of industrial importance. *ZhTF* 68(2), 49-53, 1998.*

19. T.G. Kryshtab, G.N. Semenova, P.M. Lytvyn, R.V. Konakova, I.V. Prokopenko, M.A. Mazin. *Non-monotony of structural relaxation processes at* microwave treatment of gallium arsenide. *OPT* no 81, 140-145, 1996.*

20. *Thermally Activated Processes in Crystals*. Ed. A.N. Orlov. Nauka, Moscow, 1973.*

21. R.M. Cohen. Point defects and diffusion in thin films of GaAs. *Materials Sci. & Eng.* **R20**, 167-280, 1999.

22. T.A. Briantseva, Z.M. Lebedeva, I.A. Markov, T.J. Bullough, D.V. Lioubtchenko. Process-induced modification to the surface of crystalline GaAs measured by photometry. *Appl. Surf. Sci.* **143**(1), 223-228, 1999.

23. T.A. Briantseva, V.Yu. Vinnichenko, G.G. Dvoriankina, E.B. Sokolova, E.O. Iunevich. Variation of GaAs {100} surface structure in the course of gold deposition. *Neorgan. Mater.* 25(9), 1422, 1989.

24. A. Bosacchi, S. Franchi, Y.O. Kanter, S.I. Chikichev. Study of GaAs MBE growth under Ga-rich conditions by RHEED intensity oscillations. *J. Cryst. Growth* **96**(4), 899-905, 1989.

25. L.I. Gursky, N.V. Rumak, V.V. Kukso. *Charge Properties of MOS-structures*. Nauka, Minsk, 1980.*

26. H.F. Matare. *Defect Electronics in Semiconductors*. Wiley-Interscience, New York, 1971.

27. T.A. Briantseva, D.V. Lioubtchenko, V.V. Lopatin. Ga migration process in Au film on (100) GaAs under temperature treatment in vacuum. *Appl. Surf. Sci.* **100/101**, 169-173, 1996.

28. L.A. Shuvalov, A.A. Urusovskaia, I.S. Joludev, A.V. Zalesskii, S.A. Semiletov, B.N. Grechushnikov, I.G. Chistiakov, S.A. Pikin. *Modern Crystallography, vol. 4. Physical Properties of Crystals*. Nauka, Moscow, 1981.*

29. B.S. Bokshtein. *Diffusion in Metals*. Metallurgiya, Moscow. 1978.*

30. N.S. Boltovets, V.N. Ivanov, R.V. Konakova, Ya.Ya. Kudryk, O.S. Lytvyn, P.M. Lytvyn, V.V. Milenin. Interactions between phases and the features of structural relaxation in the TiB_x–n-GaAs (InP, GaP, 6H–SiC) contacts exposed to active treatments. *FTP* 38(7), 769-774, 2004*

31. R.V. Konakova, A.B. Kamalov, P.M. Lytvyn, O.Ya. Olikh, V.A. Statov. Effect of microwave irradiation on the residual level of intrinsic stresses and parameters of deep levels in the GaAs epitaxial structures. In: *Proc. 3rd Int. Conf. "Radiation-thermal Effects and Processes in Inorganic Materials", Gornyi Altai, 29 July–3 Aug. 2002*, 21-22.*

32. N.S. Boltovets, A.B. Kamalov, E.Yu. Kolyadina, R.V. Konakova, P.M. Lytvyn, O.S. Lytvyn, L.A. Matveeva, V.V. Milenin, A.E. Rengevich. Relaxation of intrinsic stresses in gallium arsenide device structures induced by microwave treatment. *PZhTF* 28(4), 57-64, 2002*

33. V.V. Milenin, R.V. Konakova, Ya.Ya. Kudryk, O.S. Lytvyn, P.M. Lytvyn, S.I. Vlaskina, V.E. Rodionov. Interactions between phases and effects of intrinsic stress relaxation in the TiB_2–GaAs (InP, GaP, SiC) structures. In: *Proc. Int. Scientific-Practical Conf. "Structural Relaxation in Solids", Vinnitsa, 13–15 May 2003*, 124-125.*

34. N.S. Boltovets, A.B. Kamalov, E.Yu. Kolyadina, R.V. Konakova, L.A. Matveeva, V.V. Milenin, A.E. Rengevich, E.A. Soloviev. Relaxation of intrinsic stresses in semiconductor structures induced by electronic subsystem excitation. In: *Proc. XI Int. Conf. "Radiation Physics of Solid", Sevastopol, 25–30 June 2001.* Ed. G.G. Bondarenko. NII PMT, Moscow, 2001, 170–175.*

35. N.S. Boltovets, A.B. Kamalov, R.V. Konakova, E.Yu. Kolyadina, L.A. Matveeva, V.V. Milenin, E. Atanassova. Effects in semiconductor structures induced by high-power electromagnetic radiation. In: *Proc. 4th Int. Conf. "Interaction of Radiation with Solid", Minsk, 3–4 Oct. 2001*, 114-116.*

36. N.S. Boltovets, A.B. Kamalov, E.Yu. Kolyadina, R.V. Konakova, L.A. Matveeva, V.V. Milenin, A.E. Rengevich, E.A. Soloviev. Relaxation of intrinsic stresses in thin-film gallium arsenide device structures induced by microwave radiation. In: *Diamond and Related-Materials Films. Collection of reports made at the 12th Int. Sympos. "Thin Films in Electronics", Kharkov, 23–Apr. 2001*, 313-316.*

37. M.L. Dmytruk, I.B. Ermolovich, R.V. Konakova, O.S. Lytvyn, P.M. Lytvyn, V.V. Milenin, I.V. Prokopenko, E.F. Venger, D.I. Voitsikhovskiy, N.S. Boltovets, V.N. Ivanov. On the nature of transition layer and heat tolerance of TiB_2/GaAs-based contacts. *Appl. Surf. Sci.* **166**(1-4), 520-525, 2000.

38. B.E. Paton, V.E. Sklyarevich, V.G. Slusarchuk. Gyrotron processing of materials. *MRS Bulletin* **18**(11), 58-63, 1993.

39. E.V. Vinnik, V.I. Guroshev, A.V. Prokhorovich, M.V. Shevelev. Application of high-power microwave radiation for annealing of gallium arsenide. *OPT* no 15, 48-50, 1989.*

40. M. Covač, H.C. Gay. Recuit termique rapide de semiconducteur par energie. *J. Phys. France* **3**(5), 973-983, 1993.

41. H. Zohm, E. Kasper, P. Mehringer, G.A. Muller. Thermal processing of silicon wafers with microwave co-heating. *Microelectron. Eng.* **54**(3), 247-253, 2000.

42. S. Bhunia, D.N. Bose. Microwave synthesis, single crystal growth and characterization of ZnTe. *J. Crystal Growth* **186**(2), 535-542, 1998.

43. V.I. Pashkov, V.A. Perevoschikov, V.D. Skupov. Effect of annealing in microwave radiation field on residual strain and impurity composition of silicon near-surface layers. *PZhTF* **20**(8), 14-17, 1994.*

44. Yu.Yu. Bacherikov, R.V. Konakova, A.N. Kocherov, A.M. Svetlichnyi, O.B. Okhrimenko. Effect of microwave annealing on the silicon dioxide–silicon carbide structures. *ZhTF* **73**(5), 75-78, 2003.*

45. T.G. Kryshtab, P.M. Lytvyn, M.A. Mazin, I.V. Prokopenko. The structural relaxation in single crystals stimulated by microwave radiation. *Metal Phys. Adv. Technol.* **19**(5), 21-26, 1977.

46. V.V. Milenin, R.V. Konakova, V.A. Statov, V.E. Sklyarevich, Yu.A. Tkhorik, M.Yu. Filatov, M.V. Shevelev. Physico-chemical processes at the Au/Pt/Cr/Pt/GaAs interfaces enhanced by microwave treatment. *PZhTF* **20**(4), 32-34, 1994.*

47. B.M. Ashkinadze, E. Cohen, Arza Ron, E. Linger, L.N. Pfeiffer. The effect of photogenerated free carriers and microwave electron heating on exciton dynamics in GaAs/AlGaAs quantum wells. *Solid State Electron.* **40**(3), 561-565, 1996.

48. I.B. Ermolovich, E.F. Venger, R.V. Konakova, V.V. Milenin, S.V. Svechnikov, M.V. Sheveljev. Photoluminescent investigations of SHF irradiation effect on defect states in GaAs:Sn(Te). *Proc. SPIE* **3359**, 265-272, 1998.

49. E.F. Venger, I.B. Ermolovich, V.V. Milenin, R.V. Konakova, G.E. Chaika. Effect of external radiation, microwave and mechanical excitations on defect formation in non-metal crystals. *Voprosy Atomnoi Nauki i Tekhniki. Ser. Fizika Radiatsionnykh Povrezhdenii i Radiatsionnoe Materialovedenie* no 2, 60-72, 1999.*

50. E.F. Venger, I.B. Ermolovich, R.V. Konakova, V.V. Milenin, S.V. Svechnikov. Effect of high-power electromagnetic radiation on defect structure of III–V semiconductor materials. In: *7th Int. Crimean Conf. "Microwave & Telecommunication Technology", Conf. Proc., Sevastopol, Weber Co., 1997*, 1, 278-281.*

51. A.A. Belyaev, A.E. Belyaev, I.B. Ermolovich, R.V. Konakova, V.G. Lyapin, V.V. Milenin, E.A. Soloviev, V.A. Statov, S.V. Svechnikov, E.F. Venger. Effect of microwave radiation on the physico-chemical properties of some semiconductor materials (GaAs, GaP, InP) and heterostructures, as well as on the parameters of surface-barrier diode structures. In: *CAS'99 Proc. (1999 Int. Semicond. Conf., Oct. 5–9, 1999, Sinaia, Romania*) 1, 385-388.

52. O.Ya. Olikh. Acoustoelectric transient spectroscopy of microwave treated GaAs-based structures. *SPQEO* **6**(4), 450-453, 2003.

53. R.V. Konakova, P.M. Lytvyn, O.Ya. Olikh. Effect of microwave treatment on deep levels in the GaAs and SiC single crystals. *PZhE* no 1, 20-23, 2004.*

54. R.V. Konakova, P.M. Lytvyn, O.Ya. Olikh. Effect of microwave treatment on the residual strain level and parameters of deep levels in silicon carbide single crystals. *Fizika i Khimiya Obrabotki Materialov* no 2, 19-22, 2005.*

55. K. Godwod, A.T. Nagy, Z. Rek.. The application of the X-ray triple crystal spectrometer for measuring the radius curvature of bent single crystals. *phys. stat. sol.(a)* 34(2), 705-710, 1976.

56. E.F. Venger, M.L. Dmytruk, V.M. Komashchenko. Promising photovoltaic materials and structures on the basis of II–VI semiconductors (physico-technological aspects). *OPT* no 37, 220-235, 2002.**

57. S.Yu. Pavelets, Yu.N. Bobrenko, A.V. Komashchenko, T.E. Shengeliya. A novel structure of CdS-based surface-barrier sensor of ultraviolet radiation. *FTP* 35(5), 626-628, 2001.*

58. A.M. Kamuz, P.F. Oleksenko, V.G. Kamuz, O.A. Kamuz. A novel method for production of quantum-sized structures in III–V and II–VI semiconductors. *OPT* no 37, 47-54, 2002.*

59. L.V. Borkovska, B.M. Bulakh, L.Yu. Khomenkova, N.O. Korsunska, I.V. Markevich. Metastable interstitials in CdSe and CdS crystals. *SPQEO* **6**(4), 437-440, 2003.

60. V.K. Komar', V.M. Puzikov. *II–VI Group Single Crystals. Growth, Properties, Application*. Institute of Single Crystals, Kharkov, 2002.*

61. V.Yu. Rud', Yu.V. Rud', H.W. Schock. Polarization photosensitivity of ZnO/CdS/Cu(In, Ga)Se_2 solar cells.*FTP* 33(4), 484-487, 1999.*

62. V.E. Lashkaryov, A.V. Lyubchenko, M.K. Sheinkman. *Nonequilibrium Processes in Photoconductors*. Naukova Dumka, Kiev, 1981.*

63. V.E. Lashkaryov, G.A. Fedorus. Some features of CdS single-crystal photoconductivity. *Izvestiya AN SSSR. Ser. Phys.* **16**(1), 84-85, 1952.*

64. N.I. Vitrikhovsky, I.B. Mizetskaya. Obtaining of specific CdS-CdSe single crystals from vapor phase and some their characteristics. *FTT* **1**(3), 397-402, 1959.*

65. I.B. Mizetskaya, G.S. Oleinik, L.D. Budennaya. *Physico-chemical Basics of Semiconductor Single-crystal Synthesis.* Naukova Dumka, Kiev, 1976.*

66. V.V. Zavertanny, L.S. Zavertannaya, V.D. Eremka. The features of long-term process kinetics in nonuniform cadmium sulfide single crystals in a microwave field. In: *8th Intern. Crimean Conf. "Microwave & Telecommunication Technology", Conf. Proc., Sevastopol, Weber Co. 1998.* **1**, 162-164.*

67. L.S. Zavertannaya, V.V. Zavertanny, V.D. Eremka. Effect of microwave energy on nonequilibrium charged states in cadmium-sulfide detectors of radiation. In: *8th Intern. Crimean Conf. "Microwave & Telecommunication Technology", Conf. Proc., Sevastopol, Weber Co. 1998.* **1**, 165-167.*

68. I.B. Ermolovich, R.A. Red'ko. Effect of short-term irradiation of CdS crystals on the spectrum of radiation recombination centers in them. In: *Proc. 6th Int. Conf. "Interaction of Radiation with Solid", Minsk, 28–30 Sept. 2005*, 36-38.*

69. G.L. Belen'ky, I.B. Ermolovich, M.K. Sheinkman. Mechanism of orange, red and infrared photoluminescence in CdS single crystals and parameters of the corresponding luminescent centers. *FTT* **10**(9), 2628-2635, 1968.*

70. I.B. Ermolovich, G.I. Matvievskaya, M.K. Sheinkman. On the nature of orange luminescence centers in cadmium sulfide. *FTP* 9(8), 1620-1623, 1975.*

71. I.B. Ermolovich, G.I. Matvievskaya, M.K. Sheinkman. Electron-phonon interactions at radiative carrier capture on deep centers in cadmium sulfide single crystals. *J. of Luminescence* **10**(1), 58-68, 1975.

72. I.B. Ermolovich, V.V. Gorbunov, I.D. Konozenko. Inherent defects in CdS irradiated with thermal neutrons. *FTP* 11(9), 1812-1817, 1977.*

73. I.B. Ermolovich, V.V. Gorbunov. Properties of R_n and IR-1 bands in cadmium sulfide irradiated with thermal neutrons. *phys. stat. sol.(b)* **106**(1), 45-53, 1981.

74. I.B. Ermolovich, G.I. Matvievskaya. Electron-phonon interactions at charge carrier capture on the deep emission K_H-centers in CdS irradiated with thermal neutrons. *UFZh* **26**(9), 1510-1514, 1981.*

Chapter 2

1. Yu.P. Dokuchaev, V.F. Sinkevich, P.V. Taran. Development and production of radar microwave modules. *PZhE* no 3-4, 135-146, 2004.*

2. I.G. Akopyan, A.N. Korolev. Element base and production of highly reliable radio-locating homing heads. *PZhE* no 3-4, 96-100, 2004.*.

3. A.N. Getmanets. Element base quality assurance with an allowance for the atomics requirements. *PZhE* no 3-4, 34-37, 2004.*.

4. S.B. Pisarev, P.M. Bigijanov, O.D. Osipov, M.A. Konovalov. Development and large-scale production of highly reliable satellite navigation equipment. *PZhE* no 3-4, 71-77, 2004.*.

5. M.E. Il'chenko, A.A. Lipatov, N.A. Mogil'chenko, T.N. Narytnik, A.V. Savel'ev, Yu.I. Yakimenko. *Integrated Facilities of Microwave Telecommunication Systems*. Tekhnika, Kiev, 1998.*

6. T.N. Narytnik, V.P. Babak, M.E. Il'chenko, S.A. Kravchuk. *Microwave Technologies in Telecommunication Systems*. Tekhnika, Kiev, 2000.*

7. Ch.P. Poole, Jr., F.J. Owens. *Introduction to Nanotechnology*. Wiley, Hoboken, 2003.

8. A.V. Rzhanov. *Electronic Processes at Semiconductor Surface*. Nauka, Moscow, 1971.*

9. Zh.I. Alferov. History and future of semiconductor heterostructures. *FTP* 32(1), 3-18, 1998.*

10. S.I. Stenin, B.Z. Olshanetsky. Progress of semiconductor surface physics and new capabilities of thin-film technology. In: *Proc. IV All-Union School-Workshop on Semiconductor Surface Physics*. Ed. P.P. Konorov. LGU Publishers, Leningrad, 1979, 120-139.*

11. V.B. Aleskovsky. Theoretical and experimental basics of chemical assembling – purposeful synthesis of solids. In: *Proc. IV All-Union School-Workshop on Semiconductor Surface Physics*. Ed. P.P. Konorov. LGU Publishers, Leningrad, 1979, 94-120.*

12. V.F. Kiselev. *Surface Effects in Semiconductors and Dielectrics*. Nauka, Moscow, 1970.*

13. S.F. Timashev. Role of electrostatic fields in kinetics of physico-chemical processes at boundaries between phases. In: *Proc. IV All-Union School-Workshop on Semiconductor Surface Physics*. Ed. P.P. Konorov. LGU Publishers, Leningrad, 1979, 139-155.*

14. V.I. Strikha. *Theoretical Foundations of the Metal–semiconductor Contact Operation*. Naukova Dumka, Kiev, 1974.*

15. B. Nesterenko, O. Snitko. *Physical Properties of Atomically Clean Semiconductor Surface*. Nauka Publishers, Moscow, 1988.

16. *Nanotechnologies in Semiconductor Electronics*. Ed. A.L. Aseev. SO RAN Publishers, Novosibirsk, 2004.*

17. V.P. Dragunov, I.G. Neizvestny, V.A. Gridchin. *The Basics of Nanoelectronics*. NGTU Publishers, Novosibirsk, 2004.*

18. L.E. Vorob'ev, E.L. Ivchenko, D.A. Firsov, V.A. Shalygin. *Optical Properties of Nanostructures*. Nauka, Sankt-Peterburg, 2001.*

19. A.Ya. Shik, L.G. Bakueva, S.F. Musikhin, S.A. Rykov. *Physics of Low-dimensional Systems*. Nauka, Sankt-Peterburg, 2001.*

20. Zh.I. Alferov, V.M. Andreev, V.D. Rumyantsev. The trends and prospects for development of solar energetics. *FTP* 38(8), 933-948, 2004.*

21. Yu.S. Tikhodeev, O.T. Markov. Two-dimensional electron gas in heterostructures: properties and microelectronic applications. *OET, Ser. 2* no 8(1129), 1985.*

22. A.S. Tager. Dimensional quantum effects in submicron semiconductor structures and prospects for their application in microwave electronics. *ET. Ser. 1* no 9(403), 21-34, 1989.*

23. A.S. Tager. Promising lines in semiconductor microwave electronics. *Litovskii Fizicheskii Sbornik* no 4, 23-44, 1971.*

24. D.A. Usanov, A.V. Skripal. *Physics of Semiconductor Devices Operation in the Microwave Circuits*. SGU Publishers, Saratov, 1999.*

25. D.A. Usanov, A.V. Skripal. *Semiconductor Physics. Transfer Effects in the Structures with Tunnel-thin Semiconductor Layers*. SGU Publishers, Saratov, 1996.*

26. E. V. Buzaneva. *Microstructures of Integrated Electronics*. Radio i Svyaz', Moscow, 1990.*

27. Z.S. Gribnikov, K. Hess, G.A. Kosinovsky. Nonlocal and nonlinear transport in semiconductors: Real-space transfer effects. *J. Appl. Phys.* 77(4), 1337-1373, 1995.

28. A.S. Tager. Resonant tunneling diodes and transistors. *ET. Ser. 1* no 2, 17-33, 1988.*

29. V.N. Danilin, Yu.P. Dokuchaev, T.A. Zhukova, M.A. Komarov. High-power high-temperature capable and radiation-tolerant new-generation microwave devices with wide-gap AlGaN/GaN heterojunction structures. *OET. Ser. 1* no 1, 2001.

30. D.V. Lang. Review of radiation-induced defects in III–V compounds. In: *Radiation Defects in Semiconductors, 1976*, 70-94. Eds. N.B. Urli, J.W. Corbett. IOP, Bristol and London, 1977.

31. E.P. Astvatsaturian, D.V. Gromov, V.M. Lomako. *Radiation Effects in Gallium Arsenide Devices and ICs*. Universitetskoe, Minsk, 1992.*

32. C. Claeys, E. Simoen. *Radiation Effects in Advanced Semiconductor Materials and Devices*. Springer, Berlin, 2002.

33. A.A. Belyaev, A.E. Belyaev, R.V. Konakova, S.A. Vitusevich, V.V. Milenin, E.A. Soloviev, L.N. Kravchenko, T. Figielski, T. Wosniski, A. Makosa. Radiation hardness of AlAs/GaAs based resonant tunneling diodes. *SPQEO* **2**(1), 98-101, 1999.

34. A.E. Belyaev, S.A. Vitusevich, R.V. Konakova, I.Yu. Il'in, L.N. Kravchenko, E.A. Soloviev. Degradation of parameters of multilayered quantum heterostructures under gamma-irradiation. In: *Proc. 5th Int. Sympos. on Recent Advances in Microwave Technology. Kiev, Ukraine, 1995*, **1**, 63-66.

35. E. Badaljan, L. Dozsa, B. Pödör, Vo Van Tuyen, A.E. Belyaev, R.V. Konakova, S.A. Vitusevich, L.N. Kravchenko, I. Mojzes. Effect of microwave heat treatment on the current-voltage characteristics of GaAlAs/GaAs resonant tunneling diodes. In: *Proc. XXVIII Int. School on Physics of Semiconducting Compounds. Jaszowiec, 1999*, 174-176.

36. E.G. Badaljan, N.N. Gerasimenko, B. Kovác, I. Mojzes, M. Nemeth-Sallay, S.V. Vasilev, R. Veresegyhazy. Microwave heat treatment of metallized compound semiconductor wafers. In: *Proc. 17th Int. Spring Seminar on Electron Technology. Dresden, 31 May–3 June 1994*. 321-326.

37. J. Pfeifer, E.G. Badaljan, P. Tekula-Buxbaum, K. Vadasdi. Microwave Decomposition of Solid Crystalline Ammonium Paratungstate and Ammonium Metatungstate. *J. Solid State Chem.* **105**, 588-594, 1993.

38. L. Dózsa, F. Riesz, J. Karányi, Vo Van Tuyen, B. Szentpáli, A. Müller. A transient method for measuring current–voltage characteristics with negative differential resistance regions. *phys. stat. sol.(a)* **163**(1), R1-R2, 1997.

39. B. Pödör, S.A. Vitusevich, E. Badaljan, L. Dozsa, A.E. Belyaev, R.V. Konakova, Vo Van Tuyen, L.N. Kravchenko, I. Mojzes. Effect of microwave heat treatment of the properties of GaAlAs/GaAs double barrier resonant tunneling diodes. In: *Proc. 10th Microcoll. Budapest, Hungary, 1999.* 445-448.

40. M.J. Kelly. *Low-Dimension Semiconductors: Materials, Physics, Technology, Devices.* Clarendon Press, Oxford, 1995.

41. P. Roblin, R.C. Potter, A. Fathimulla. Interface roughness scattering in AlAs/InGaAs resonant tunneling diodes with an InAs subwell. *J. Appl. Phys.* 79(5), 2502-2508, 1996.

42. F.P. Korshunov, G.V. Gatalsky, G.M. Ivanov. *Radiation Effects in Semiconductor Devices.* Nauka i Tekhnika, Minsk, 1978.*

43. F.P. Korshunov, Yu.V. Bogatyrev, V.A. Vavilov. *Radiation Action on Integrated Microcircuits.* Nauka i Tekhnika, Minsk, 1986.*

44. V.A. Litvinov, N.A. Ukhin. *Effect of Nuclear Radiation on Parameters of Devices Based on* GaAs. I.V. Kurchatov Institute of Atomic Energy, Moscow, 1979.*

45. O.A. Mezrin, A.Y. Shik, V.O. Mezrin. Gated δ-layer structures. *Semicond. Sci. Technol.* 7, 664-670, 1992.

46. D.V. Gromov, G.V. Petrov, V.G. Elenskii. Radiation defects in microwave semiconductor devices based on GaAs. *Zarubezhnaya Radioelektronika* no 11, 64-87, 1980.*

47. A.E. Belyaev, E.F. Venger, I.B. Ermolovich, R.V. Konakova, P.M. Lytvyn, V.V. Milenin, I.V. Prokopenko, G.S. Svechnikov, E.A. Soloviev, L.L. Fedorenko. *Effect of Microwave and Laser Radiations on the Parameters of Semiconductor Structures.* Kiev, Intas, 2002.

48. A.E. Belyaev, R.V. Konakova, E.A. Soloviev, D.I. Sheka, B. Pödör, E. Badaljan. Effect of high-power microwave radiation on characteristics of combined resonant tunneling structures. In: *5th Int. Workshop on Expert Evaluation and Control of Compound Semiconductor Materials and Technologies. Crete, Greece, 2000*, 74.

49. A.E. Belyaev, N.S. Boltovets, R.V. Konakova, E.A. Soloviev, D.I. Sheka, B. Pödör, E. Badaljan, S.A. Vitusevich. Degradation effects in microwave resonant tunneling diodes enhanced by low-temperature heating and microwave radiation. In: *Extended Abstracts of the 2nd Workshop on Micromachined Circuits for Microwave and Millimeter Wave Applications "Memswave-II", Budapest, Hungary, 2000*, 7-8.

50. S.A. Vitusevich, L. Dózsa, R.V. Konakova, B. Pödör, E. Badaljan, A.E. Belyaev. Effect of microwave processes in a two-barrier AlGaAs/GaAs heterostructure. In: *Proc. VI Int. Conf. on Physics and Technology of Thin Films. Ivano-Frankivsk. Ukraine, 1997*, Pt. 1, 118.

51. A.E. Belyaev, N.S. Boltovets, R.V. Konakova, E.A. Soloviev, D.I. Sheka, B. Pödör, E. Badaljan, S.A. Vitusevich. Effect of thermal annealing and high-power microwave radiation on characteristics of combined resonant tunneling structures. In: *Proc. The Third Int. EuroConf. on Advanced Semiconductor Devices and Microsystems. Smolenice Castle, Slovakia, 2000*, 457-460.

52. A.E. Belyaev, N.S. Boltovets, R.V. Konakova, E.A. Soloviev, D.I. Sheka. Degradation effects in microwave resonant tunneling diodes. In: *Abstracts of the Second Russian-Ukrainian Workshop "Nanophysics and Nanoelectronics", Kiev, 22–24 Nov. 2002*, 123.*

53. E.F. Schubert. Delta doping of III–V compound semiconductors: Fundamentals and device applications. *J. Vac. Sci. Technol.* **8**(3), 2980-2996, 1990.

54. *Physico-chemical Properties of Semiconductor Substances. A handbook.* Ed. A.V. Novoselova. Nauka, Moscow, **1978**.*

Chapter 3

1. *VLSI Electronics: Microstructure Science*. Eds. N.G. Einspruch, W.R. Wisseman. Vol.11 (*GaAs Microelectronics*). Academic Press, Orlando–San Diego–New York–London–Toronto–Montreal–Sydney–Tokyo, 1985.

2. M. Shur. GaAs *Devices and Circuits*. Plenum Press, New York and London, 1987.

3. C.W. Wilmsen. *Chemical composition and formation of thermal and anodic oxide/III–IV compound semiconductor interfaces. J. Vac. Sci. Technol.* **19**(3), 279-288, 1981.

4. G.P. Schwartz. *Analysis of native oxide films and oxide-substrate reactions on III–V semiconductors using thermochemical phase diagrams. Thin Solid Films* **103**, 3-16, 1983.

5. W. Eitel. *Physikalische Chemie der Silikate*. J.A. Barth Verlag, Leipzig, 1941.

6. K.S. Evstropiev, N.A. Toropov. *Chemistry of Silicon and Physical Chemistry of Silicates*. Gosstroyizdat, Moscow, 1956*.

7. A.S. Berezhnoi. *Silicon and Its Binary Compounds*. Izd. AN UkrSSR, Kiev, 1958*.

8. O.K. Botvinkin. *Physical Chemistry of Silicates*. GILSM Publishers, Moscow, 1955*.

9. A.I. Rabukhin, V.G. Saveliev. *Physical Chemistry of Refractory Nonmetal and Silicate Compounds*. Infra-M, Moscow, 2004*.

10. G.Ya. Krasnikov, N.A. Zaitsev. *Silicon–Silicon Dioxide System in Submicron VLSI*. Tekhnosfera, Moscow, 2003*.

11. M.I. Gorlov, V.A. Emel'yanov, A.V. Strogonov. *Gerontology of Silicon ICs*. Nauka, Moscow, 2004*.

12. T.A. Bryantseva, A.I. Volkov, Z.M. Lebedeva, I.N. Svetnikova. Investigation of oxidized layers on the gallium arsenide surface. *Izvestiya AN SSSR. Neorganicheskie Materialy* 16(4), 753-754, 1980.*

13. T.I. Kovalevskaya, V.V. Limberova, V.M. Astakhov, V.A. Usova. Structure and composition of some compounds on the gallium arsenide surface. *Mikroelektronika* 6(3), 280-284, 1977.*

14. V.I. Belyi, T.P. Smirnova. Experimental investigation and the ways to stabilize phase composition of oxide films on the *III–V semiconductors. In: Materials of Electronic Engineering, Pt. 2. SO Nauka,* Novosibirsk, 1983, 15-28.*

15. T.P. Smirnova, N.F. Zakharchuk, A.N. Golubenko, V.I. Belyi. Phase composition and structure of intrinsic oxide layers on the *III–V semiconductors*. In: *New Materials of Electronic Engineering*. SO Nauka, Novosibirsk, 1990, 62-83.*

16. E.M. Semashko. Interaction of metal and dielectric layers with the gallium arsenide surface. *Author's Synopsis of the Candidate of Phys.-Math. Sci. Thesis*. IMP AN USSR, Kiev, 1985.*

17. V.G. Aleshin, V.V. Nemoshkalenko, E.M. Semashko, A.I. Senkevich. Investigation of the processes of gallium arsenide surface oxidation. *Poverkhnost'* no 2, 111-114, 1983.*

18. V.G. Aleshin, V.V. Nemoshkalenko, E.M. Semashko, A.I. Senkevich. Effect of conditions of dielectric layers deposition on the gallium arsenide surface composition. *Doklady AN USSR. Ser. Phys.-Math. & Tech. Sci.* no 11, 54-56, 1983.*

19. B.I. Seleznev, V.A. Tkal, L.A. Lishnev. Investigation of electric strength of gallium arsenide anodic oxide films. *ET Ser. 2* no 7(166), 3-6, 1983.*

20. N.L. Dmitruk. MIS structures on the basis of III–V compositions with intrinsic oxide. *OPT* no 4, 11-20, 1982.*

21. V.A. Skorikov, Yu.I. Pashintsev. Gallium arsenide–dielectric system. *ET Ser. 2* no 7(79), 47-55, 1973.*

22. S.A. Vasilkovsky, I. Ivancho. Raman scattering investigation of the effect of SiO_2 and Si_3N_4 dielectric films deposition and low doses of γ-irradiation on GaAs near-surface region. *ZhTF* 63(6), 80-86, 1993.*

23. J. Breza, A.M. Evstigneev, R.V. Konakova, V.G. Lyapin, V.V. Milenin, V.A. Statov, S.A. Vasilkovsky, E.F. Venger, Yu.A. Tkhorik. Structure disruptions in SiO_2–GaAs transition layers and effect of small γ-radiation doses on those layers. *Functional Materials* 4(3), 370-374, 1997.

24. A.M. Evstigneev, R.V. Konakova, V.G. Lyapin, V.V. Milenin, V.A. Statov, S.A. Vasilkovsky, E.F. Venger, J. Breza, J. Liday, P. Vogrinčič. Gamma-radiation induced changes in SiO_2–GaAs structures. *J. Electrical Eng.* 48(7-8), 219-220, 1997.

25. S.A. Vasilkovskii. Raman scattering study of influence of γ-irradiation on a near-surface region GaAs in the structure SiO_2–GaAs. In: *Proc. Int. Conf. on Microelectronics and Computer Science, Kishinev, 1992*, **1**, 141-143.

26. S.A. Vasilkovsky. Investigation of the features of plasmon-phonon interaction and optical diagnostics of the GaAs-based structures. *Author's Synopsis of the Candidate of Phys.-Math. Sci. Thesis.* ISP AS USSR, Kiev, 1994.*

27. J. Breza, P.I. Didenko, R.V. Konakova, V.V. Milenin, G.F. Romanova. Effect of *γ-irradiation on the properties of* SiO_2–GaAs *structures. ZhTF* 65(5), *122-131, 1995.**

28. J. Breza, A.M. Evstigneev, R.V. Konakova, V.G. Lyapin, V.V. Milenin, V.A. Statov, S.A. Vasilkovsky, E.F. Venger, P. Vogrinčič. *Radiation-enhanced effect in* SiO_2–GaAs *structures.* In: *Proc. ASDAM'96, Bratislava, 1996*, 221-224.

29. R.V. Konakova, V.G. Lyapin, V.V. Milenin, V.A. Statov. Radiation-stimulated effects at the SiO_2–GaAs *structure interface. PZhE* no 2, 27-31, 2000.*

30. N. Bottka, D.K. Gaskill, R.J.M. Griffiths, R.R. Bradley, T.B. Joyce. Photoreflectance characterization of OMVPE GaAs on Si. *J. Cryst. Growth* 93(1-4), 481-486, 1988.

31. A.G. Kotov, V.V. Gromov. *Radiation Physics and Chemistry of Heterogeneous Systems.* Energoatomizdat, Moscow, 1988.*

32. G.V. Kukolev. *Chemistry of Silicon and Physical Chemistry of Silicates.* Vysshaya Shkola, Moscow, 1966.*

33. S.V. Vavilov, B.M. Gorin, N.S. Danilin, A.E. Kiv, Yu.L. Nurov, V.I. Shakhovtsov. *Radiation Methods in Solid-state Electronics.* Radio i Svyaz', Moscow, 1990.*

34. V.N. Brudnyi, V.V. Peshev, A.P. Surzhikov. *Radiation Defect Production in Electric Fields. Gallium Arsenide, Indium Phosphide.* Nauka, Novosibirsk, 2001.*

35. A.P. Mamontov, I.P. Chernov. *Effect of Small Doses of Ionizing Radiation.* Energoatomizdat, Moscow, 2001.*

36. A.V. Dvurechensky, A.G. Kachurin, E.V. Nidaev, L.S. Smirnov. *Pulsed Annealing of Semiconductor Materials.* Nauka, Moscow, 1982.*

37. F.P. Korshunov, G.V. Gatalsky, G.M. Ivanov. *Radiation Effects in Semiconductor Devices.* Nauka i Tekhnika, Minsk, 1978.*

38. *Problems of Radiation Technology of Semiconductors.* Ed. L.S. Smirnov. Nauka, Novosibirsk, 1980.*

39. A.E. Belyaev, J. Breza, E.F. Venger, M. Vesely, I.Yu. Il'in, R.V. Konakova, J. Liday, V.G. Lyapin, V.V. Milenin, I.V. Prokopenko, Yu.A. Tkhorik. *Radiation Resistance of GaAs-based Microwave Schottky-barrier Devices. Some Physico-technological Aspects.* Kiev. Interpress Ltd. 1998.

40. A.E. Belyaev, E.F. Venger, I.B. Ermolovich, R.V. Konakova, P.M. Lytvyn, V.V. Milenin, I.V. Prokopenko, G.S. Svechnikov, E.A. Soloviev, L.L. Fedorenko. *Effect of Microwave and Laser Radiations on the Parameters of Semiconductor Structures.* Kiev, Intas, 2002.

41. R.V. Konakova, Yu.A. Tkhorik, L.S. Khazan. The features of radiation technology when making GaAs diodes for microwave electronics. In: *Gallium Arsenide.* Ed. V.I. Gaman. TGU, Tomsk, 1982, 183-185.*

42. R.V. Konakova, Yu.A. Tkhorik, L.S. Khazan. The capabilities of radiation technology when making diodes. *ET Ser. 2* no 2, 47-56, 1988.*

43. N.S. Boltovets, G.N. Kashin, R.V. Konakova, V.G. Lyapin, V.V. Milenin, E.A. Soloviev. Properties of SiO_2–GaAs and Au–Ti–SiO_2–GaAs structures used in production of transmission lines. *SPQEO* 5(2), 183-187, 2002.

44. Zh.I. Alferov, D.Z. Garbuzov, Yu.V. Zhilyaev, E.P. Morozov, E.L. Portnoi. Photoluminescence of epitaxial layers of *n*-type gallium arsenide. *FTP* 2(10), 1441-1447, 1968.*

45. K.D. Glinchuk, A.V. Prokhorovich. Luminescence of gallium arsenide. *Poluprovodnikovaya Tekhnika i Mikroelektronika* no 13, 16-33, 1973.*

46. E.V. Vinnik, V.I. Guroshev, A.V. Prokhorovich. The features of luminescence of gallium arsenide exposed to short-time thermal treatment. *OPT* no 16, 64-69, 1989.*

47. V.I. Gavrilenko, A.M. Grekhov, D.V. Korbutyak, V.G. Litovchenko, *Optical Properties of Semiconductors (A Handbook)*. Naukova Dumka, Kiev, 1987*.

48. G.P. Peka, V.F. Kovalenko, V.N. Kutsenko. *The Luminescence Techniques to Control Parameters of Semiconductor Materials and Devices*. Tekhnika, Kiev, 1986*.

49. *Physics and Materials Science of Semiconductors with Deep Levels*. Ed. V.I. Fistul'. Metallurgiya, Moscow, 1987*.

50. V.F. Masterov, B.E. Samorukov. Deep centers in the III–V compounds. *FTP* 12(4), 625-652, 1978*.

51. E.F. Venger, V.V. Milenin, I.B. Ermolovich, R.V. Konakova, V.N. Ivanov, D.I. Voitsikhovskiy. The formation features and thermal stability of contacts formed by titanium borides and nitrides with gallium arsenide. *FTP* 33(8), 948-952, 1999.*

52. I.B. Ermolovich, R.V. Konakova, V.V. Milenin, A.I. Senkevich. The nature of a junction region when depositing titanium boride and nitride films onto gallium arsenide. *PZhTF* 25(19), 71-76, 1999.*

53. E.F. Venger, A.A. Belyaev, N.S. Boltovets, I.B. Ermolovich, V.N. Ivanov, R.V. Konakova, V.V. Milenin, D.I. Voitsikhovskiy, T. Figielski, A. Makosa. Effect of rapid thermal annealing on properties of contact Au–Mo–TiB_x–GaAs. *SPQEO* 2(3), 57-61, 1999.

54. V.V. Milenin, I.B. Ermolovich, R.V. Konakova, V.G. Lyapin, A.A. Belyaev, D.I. Voitsikhovskiy, O.D. Smijan, V.N. Ivanov, N.S. Boltovets. Reactions between phases and electronic processes at the TiB_x(TiN_x)–GaAs heterostructure interfaces. *J. Korean Phys. Soc.* 34, S447-S450, 1999.

55. Ye.F. Venger, V.V. Milenin, I.B. Ermolovich, R.V. Konakova, D.I. Voitsikhovskiy, I. Hotovy, V.N. Ivanov. Heat tolerance of titanium boride and titanium nitride contacts to gallium arsenide. *SPQEO* 2(1), 124-132, 1999.

56. A.A. Belyaev, A.E. Belyaev, I.B. Ermolovich, S.M. Komirenko, R.V. Konakova, V.G. Lyapin, V.V. Milenin, E.A. Soloviev, M.V. Shevelev. Effect of microwave treatment on the electrophysical characteristics of semiconductors and surface-barrier structures which are of importance in engineering. *ZhTF* 68(2), 49-53, 1998.*

57. I.B. Ermolovich, R.V. Konakova, V.V. Milenin, L.P. Primenko, I.V. Prokopenko, V.L. Gromashevsky. Effect of ultrasonic treatment on the strain effects and structure of local centers in substrate and near-contact regions of the M/n-n^+-GaAs (M = Pt, Cr, W) structures. *FTP* 31(4), 503-507, 1997.*

58. C. Feldman, J.W. Mayer. *Fundamentals of Surface and Thin Film Analysis*. North-Holland, New York–Amsterdam–London, 1986.

59. Yu.P. Pshenichnikov. *Revelation of Fine Crystal Structure. A Handbook*. Metallurgiya, Moscow, 1974.*

60. S.M. Sze. *Physics of Semiconductor Devices*, 2nd Ed. John Wiley & Sons, Inc., New York–Chichester–Brisbane–Toronto–Singapore, 1981.

61. V.I. Belyi. Chemistry of III–V semiconductor surfaces. In: *Problems of Elemental Materials Science*. Nauka, Novosibirsk, 1986, 24-40.*

62. V.V. Nemoshkalenko, V.G. Aleshin, L.G. Gassanov, E.M. Semashko, A.I. Senkevich, V.M. Prokopenko, N.N. Varchenko. Effect of physico-chemical actions on gallium arsenide surface. *Poverkhnost'* no 2, 88-94, 1983.*

63. P.H. Holloway, C.H. Mueller. Chemical reactions at metal/compound semiconductor interfaces: Au and GaAs. *Thin Solid Films* 221(1-2), 254-261, 1992.

64. V.I. Pashkov, V.A. Perevoschikov, V.D. Skupov. Effect of annealing in microwave radiation field on residual strain and impurity composition of silicon near-surface layers. *PZhTF* 20(8), 14-18, 1994.*

65. A.A. Belyaev, A.E. Belyaev, E.F. Venger, I.B. Ermolovich, S.M. Komirenko, R.V. Konakova, V.G. Lyapin, I.I. Magda, V.V. Milenin, I.V. Prokopenko, S.V. Svechnikov, E.A. Soloviev, Yu.A. Tkhorik, M.V. Shevelev. Effect of microwave radiation on structural, physico-chemical and electrophysical properties of a number of semiconductor materials and device structures. In: *6th Int. Crimean Conf. "Microwave & Telecommunication Technology", Conf. Proc.*, Sevastopol, Weber Co., 1996, 71-89.

66. A.V. Klyuchnik. Effect of intense microwave radiation on sea ice structure. *ZhTF* 62(7), 99-107, 1992.*

67. P. Grosse. *Free Electrons in Solids*. Springer-Verlag, Berlin, 1979.

68. A.G. Milnes. *Deep Impurities in Semiconductors*. Wiley, New York, 1973.

69. V.L. Indenbom. A hypothesis on the mechanism of radiation-stimulated processes. *PZhTF* 5(8), 489-492, 1979.*

70. Yu.V. Bykov, A.G. Eremeev, N.A. Zharova, I.V. Plotnikov, K.I. Rybakov, M.N. Drozdov, Yu.N. Drozdov, V.D. Skupov. Diffusion processes in semiconductor structures at microwave annealing. *Izvestiya Vuzov. Radiofizika* no 8-9, 836-843, 2003.*

71. V.D. Skupov, D.I. Tetel'baum. On the effect of elastic stresses on transformation of defect aggregates in semiconductors. *FTP* 21(8), 1495-1497, 1987.*

72. O.A. Agueev. Physico-technological basics of formation of contacts to silicon carbide with pulsed thermal treatment techniques. *Author's Synopsis of the Doctor of Tech. Sci. Thesis.* TGRU, Taganrog, 2005.*

73. O.A. Agueev. *Problems of Technology of Contacts to Silicon Carbide.* TGRU, Taganrog, 2005.*

74. O.A. Agueev. *Rapid Thermal Treatment of Contacts to Silicon Carbide Using Incoherent IR Radiation.* TGRU, Taganrog, 2003.*

75. D.A. Sechenov, O.A. Agueev, A.M. Svetlichnyi, F.D. Kasimov, G.G. Kadymov. *Gas Sensors on the Basis of Silicon Carbide.* Mutarjim Publishers, Baku, 2004.*

76. Ya.Ya. Kudryk. Effect of active actions on the formation processes and properties of ohmic and barrier contacts to silicon carbide. *Author's Synopsis of the Candidate of Tech. Sci. Thesis.* ISP NASU, Kiev, 2004.**

77. C. Claeys, E. Simoen. *Radiation Effects in Advanced Semiconductor Materials and Devices.* Springer, Berlin, 2002.

78. V.V. Luchinin, Yu.M. Tairov. Silicon carbide - a promising material for electronic engineering. *Izvestiya Vuzov. Elektronika* no 1, 10-37, 1997.*

79. V.V. Luchinin, P.P. Maltsev, E.P. Malyakov. Silicon carbide - a strategic material of future electronics. *Elektronika. Nauka, Tekhnologiya, Bizness* no 3-4, 61, 1997.*

80. V.V. Kozlovsky. *Modification of Semiconductors with Proton Beams.* Nauka, Sankt-Peterburg, 2003.*

81. A.A. Lebedev, V.V. Kozlovsky, N.B. Strokan, D.V. Davydov, A.M. Ivanov, A.M. Strel'chuk, R. Yakimova. Radiation strength of wide-gap semiconductors (illustrated by silicon carbide). *FTP* 36(11), 1354-1359, 2002.*

82. *Properties of Silicon Carbide.* Ed. G.L. Harris. Howard University, Washington DC., USA, 1995.

83. A.A. Lebedev, A.M. Ivanov, N.B. Strokan. Radiation tolerance of SiC and hard radiation detectors on its basis: A review. *FTP* 38(2), 129-150, 2004.*

84. A.V. Afanas'ev, V.A. Il'in, I.G. Kazarin, A.A. Petrov. Investigation of thermal stability and radiation strength of Schottky diodes made on the basis of silicon carbide. *ZhTF* 71(5), 78-81, 2001.*

85. J.M. McGarrity, F.B. McLean, W.M. DeLancey, J. Palmour, C. Carter, J. Edmond, R.E. Oakley. Silicon carbide JFET radiation response. *IEEE Trans. Nucl. Sci.* **39**, 1974-1981, 1992.

86. F.B. McLean, J.M. McGarrity, C.J. Scozzie, C.W. Tipton, W.M. DeLancey. Analysis of neutron damage in high-temperature silicon carbide JFETs. *IEEE Trans. Nucl. Sci.* **41**, 1884-1894, 1994.

87. M. Yoshikawa, K. Saitoh, T. Ohshima, H. Itoh, I. Nashiyama, S. Yoshida, H. Okumura, Y. Takahashi, K. Ohnishi. Depth profile of trapped charges in oxide layer of 6H-SiC metal–oxide-semiconductor structures. *J. Appl. Phys.* **80**, 282-287, 1996.

88. M. Yoshikawa, K. Saitoh, T. Ohshima, H. Itoh, I. Nashiyama, Y. Takahashi, K. Ohnishi, H. Okumura, S. Yoshida. Generation mechanisms of trapped charges in oxide layers of 6H-SiC MOS structures irradiated with gamma-rays. *Mat. Sci. Forum* **264-268**, 1017-1020, 1998.

89. T. Ohshima, H. Itoh, H. Yoshikawa. Effect of gamma-ray irradiation on the characteristics of 6H silicon carbide metal–oxide-semiconductor field effect transistor with hydrogen-annealed gate oxide. *J. Appl. Phys.* **90**, 3038-3041, 2001.

90. T. Ouisse, N. Becourt, C. Jaussaud, F. Templier. Low-frequency, high-temperature conductance and capacitance measurements on metal–oxide-silicon carbide capacitors. *J. Appl. Phys.* **75**, 604-607, 1994.

91. M. Di Ventra. Can we make the $SiC–SiO_2$ interface as good as the $Si–SiO_2$ interface? *Appl. Phys. Lett.* **79**, 2402-2404, 2001.

92. M. Yoshikawa, H. Itoh, Y. Morita, I. Nashiyama, S. Misawa, H. Okamura, S. Yoshida. Effects of gamma-ray irradiation on cubic silicon carbide metal–oxide-semiconductor structure. *J. Appl. Phys.* **70**, 1309-1312, 1991.

93. N.V. Rumak. *Silicon–silicon dioxide System in MOS Structures*. Nauka i Tekhnika, Minsk, 1986.*

94. N.V. Rumak, V.V. Khat'ko. *Dielectric Films in Solid-state Microelectronics*. Nauka i Tekhnika, Minsk, 1990.*

95. V.N. Vertoprakhov, B.M. Kuchumov, E.G. Sal'man. *The Structure and Properties of the $Si–SiO_2$ Structures*. SO Nauka, Novosibirsk, 1981.*

96. F.D. Kasimov, Ya.Yu. Guseinov, A.M. Svetlichnyi, V.V. Polyakov, A.N. Kocherov. *Light-stimulated Processes of Silicon Carbide Oxidation.* Mutarjim Publishers, Baku, 2005.*

97. A.N. Kocherov. Development and investigation of light-stimulated technological processes of obtaining oxide silicon films on SiC. *Author's Synopsis of the Candidate of Tech. Sci. Thesis.* TGRU, Taganrog, 2004.*

98. Yu.Yu. Bacherikov, R.V. Konakova, A.N. Kocherov, O.B. Okhrimenko, A.M. Svetlichnyi. Effect of microwave radiation on impurity absorption spectra in the SiO_2/SiC structures. In: *Proc. III Int. Conf. "Radiation-thermal Effects and Processes in Inorganic Materials", Tomsk, TPU, 2002,* 188-190.*

99. Yu.Yu. Bacherikov, R.V. Konakova, A.N. Kocherov, P.M. Lytvyn, O.S. Lytvyn, O.B. Okhrimenko, A.M. Svetlichnyi. Effect of microwave annealing on *the silicon dioxide–silicon carbide structures. ZhTF* **73**(5), 75-78, 2003.*

100. Yu.Yu. Bacherikov, R.V. Konakova, E.Yu. Kolyadina, A.N. Kocherov, O.B. Okhrimenko, A.M. Svetlichnyi. Effect of microwave radiation on optical transmission spectra in SiO_2/SiC structures. *SPQEO* **5**(4), 391-394, 2002.

101. Yu.Yu. Bacherikov, E.Yu. Kolyadina, R.V. Konakova, A.N. Kocherov, O.S. Lytvyn, P.M. Lytvyn, O.B. Okhrimenko, A.M. Svetlichnyi. Relaxation processes caused by microwave action in the SiO_2/SiC structures. In: *Proc. Eights Int. Sci.-Tech. Conf. "Topical Problems of Solid-state Electronics and Microelectronics" PEM-2002, Divnomorskoe, Russia, 14–19 Sept. 2002, Pt. 1.* Taganrog, 2002, 135-137.*

102. A.M. Svetlichnyi, O.A. Agueev, D.A. Shlyakhovoi. The peculiarities of obtaining thin SiO_2 films with rapid thermal treatment. *Tekhnologiya i Konstruirovanie v Elektronnoi Apparature* no 4-5, 38-43, 2001.*

103. A.M. Svetlichnyi, V.V. Polyakov, A.N. Kocherov. Silicon carbide oxidation using rapid thermal annealing. *Izvestiya TRTU* (*Taganrog*) no 1(36), 104-105, 2004.*

104. G.B. Dubrosky, E.I. Radovanova. Optical absorption in the 0.6 μm region and the α(6H)-SiC conduction band structure. *FTT* 11(3), 680-684, 1969.*

105. I.S. Gorban, V.P. Zavada, A.S. Skirda. Photoluminescence spectra of impurity centers in α-SiC(6H) at high temperatures. *FTT* 14, 3095-3097, 1972.*

106. I.S. Gorban, A.S. Skirda. Absorption spectra of nitrogen impurities in different polytypes of α-SiC. *UFZh* 26(2), 228-232, 1981.*

107. I.S. Gorban, A.P. Krokhmal. Impurity optical absorption and 6H-SiC conduction band structure. *FTP* 35(11), 1299-1305, 2001.*

Chapter 4

1. V.S. Vavilov. *Radiation Action on Semiconductors*. Fizmatgiz, Moscow, 1963.*

2. V.S. Vavilov, M.A. Ukhin. *Radiation Effects in Semiconductors and Semiconductor Devices*. Nauka, Moscow, 1969.*

3. R.F. Konopleva, V.L. Litvinov, N.A. Ukhin. *The Features of Radiation Damaging of Semiconductors by High-energy Particles*. Atomizdat, Moscow, 1971.*

4. J.P. Mitchell, D.K. Wilson. Surface effects of radiation on semiconductor devices. *Bell. Syst. Tech. J.* **46**, 1–4 (1967).

5. *Effect of Radiation on Materials and Components*. Eds. J.F. Kircher, R.E. Bowman. Reinhold, New York, 1964.

6. F.P. Korshunov, G.V. Gatalsky, G.M. Ivanov. *Radiation Effects in Semiconductor Devices*. Nauka i Tekhnika, Minsk, 1978.*

7. F.P. Korshunov, Yu.V. Bagatyrev, V.A. Vavilov. *Action of Radiation on Integrated Microcircuits*. Nauka i Tekhnika, Minsk, 1986.*

8. *Physical Basics of Radiation Technology of Solid-state Electronic Devices*. Ed. A.F. Lubchenko. Naukova Dumka, Kiev, 1978.*

9. V.M. Kulakov, E.A. Ladygin, V.I. Shakhovtsov, E.N. Volodygin, Yu.N. Andreev. *Effect of Penetrating Radiation on the Products of Electronic Engineering*. Sov. Radio, Moscow, 1980.*

10. *Radiation Effects in Semiconductors*. Ed. L.S. Smirnov. SO Nauka, Novosibirsk, 1979.*

11. *Physical Processes in Irradiated Semiconductors*. Ed. L.S. Smirnov. SO Nauka, Novosibirsk, 1977.*

12. R.F. Konopleva, V.N. Ostroumov. *Interaction of High-energy Charged Particles with Germanium and Silicon*. Atomizdat, Moscow, 1975.*

13. A.V. Dvurechensky, A.G. Kachurin, E.V. Nidaev, L.S. Smirnov. *Pulsed Annealing of Semiconductor Materials*. Nauka, Moscow, 1982.*

14. V.S. Vavilov, B.M. Gorin, N.S. Danilin, A.E. Kiv, Yu.L. Nurov, V.I. Shakhovtsov. *Radiation Techniques in Solid-state Electronics*. Radio i Svyaz', Moscow, 1990.*

15. A.P. Mamontov, I.P. Chernov. *Effect of Small Doses of Ionizing Radiation*. Energoatomizdat, Moscow, 2001.*

16. V.N. Brudnyi, V.V. Peshev, A.P. Surzhikov. *Radiation Defect Production in Electric Fields. Gallium Arsenide, Indium Phosphide*. Nauka, Novosibirsk, 2001.*

17. V.I. Shakhovtsov. Investigation of radiation effects in nonuniform structures of solid-state electronics. *Author's Synopsis of the Doctor of Phys.-Math. Sci. Thesis*. ISP NASU, Kiev, 1993.*

18. *Problems of Radiation Technology of Semiconductors*. Ed. L.S. Smirnov. Nauka, Novosibirsk, 1980.*

19. V.G. Verbitskii. *Ionic Nanotechnologies in Electronics*. Lesya, Kiev, 2002.*

20. P.V. Serba. Migration of atoms in surface layers at ion-beam processing of solids. *Author's Synopsis of the Doctor of Phys.-Math. Sci.* UGTU, Ekaterinburg, 2003.*

21. O.G. Vendik, Yu.N. Gorin, V.F. Popov. *Particle-photon Technology*. Vysshaya Shkola, Moscow, 1984.*

22. V.A. Popenko. *Rapid Thermal Treatments in VLSI Technology*. BGU, Minsk, 2004.*

23. E.I. Zorin, P.V. Pavlov, D.I. Tetel'baum. *Ion Implantation of Semiconductors*. Nauka, Moscow, 1970.*

24. J.W. Mayer, L. Eriksson, J.A. Davis. *Ion Implantation in Semiconductors. Silicon and Germanium*. Academic Press, New York and London, 1970.

25. L.I. Mirkin. *Physical Basics of Material Processing with Laser Beams*. MGU, Moscow, 1975.*

26. Yu.V. Bykov, A.G. Eremeev, V.I. Pashkov, V.A. Perevoschikov, V.D. Skupov. Gettering of impurities and defects in silicon at treatment in microwave field. NGU Publishers, Nizhniy Novgorod, 1991. – Deposit copy VINITI # 2322-B91.*

27. A.A. Belyaev, A.E. Belyaev, I.B. Ermolovich, S.M. Komirenko, R.V. Konakova, V.G. Lyapin, V.V. Milenin, E.A. Soloviev, M.V. Shevelev. Effect of microwave treatment on the electrophysical characteristics of semiconductors and surface-barrier structures which are of importance for technology. *ZhTF* 68(12), 49-53, 1998.*

28. A.E. Belyaev, E.F. Venger, I.B. Ermolovich, R.V. Konakova, P.M. Lytvyn, V.V. Milenin, I.V. Prokopenko, G.S. Svechnikov, E.A. Soloviev, L.L. Fedorenko. *Effect of Microwave and Laser Radiations on the Parameters of Semiconductor Structures*. Kiev: Intas. 2002.

29. Yu.V. Bykov, A.G. Eremeev, N.A. Zharova, I.V. Plotnikov, K.I. Rybakov, M.N. Drozdov, Yu.N. Drozdov, V.D. Skupov. Diffusion processes in semiconductor structures at microwave annealing. *Izvestiya Vuzov. Radiofizika* no 8-9, 836-843, 2003.*

30. T. Brozhek, V.Ya. Kiblik, V.G. Litovchenko, R.O. Litvinov, L.G. Plotnikova. Radiation-induced effects in layered MIS-structures. *Preprint # 4-88. IS AS USSR*, Kiev, 1988.*

31. O.Yu. Borkovskaya, N.L. Dmitruk, R.V. Konakova, V.G. Litovchenko, Yu.A. Tkhorik, V.I. Shakhovtsov. Effects of radiation-induced ordering in layered structures on the basis of III–V compounds. *Preprint # 6. IS AS USSR*, Kiev, 1986.*

32. I.D. Konozenko, A.K. Semenyuk, V.I. Khivrich. *Radiation Effects in Silicon*. Naukova Dumka, Kiev, 1974.*

33. N.L. Dmitruk, V.G. Litovchenko. Effects of radiation-induced gettering at the III–V semiconductor interfaces. *OPT* no 3, 13-22, 1983.*

34. V.A. Litvinov, N.A. Ukhin. *Effect of Nuclear Radiation on Parameters of Devices Based on* GaAs. I.V. Kurchatov Institute of Atomic Energy, Moscow, 1979.*

35. R.V. Konakova, Yu.A. Tkhorik, L.S. Khazan. The features of radiation technology when making GaAs diodes for microwave electronics. In: *Gallium Arsenide*. Ed. V.I. Gaman. TGU, Tomsk, 1982, 183-185.*

36. E.F. Uvarov. Radiation effects in wide-gap III–V semiconductors. *OET, Ser. 2* no 13(584), 1978.*

37. L.S. Smirnov. Physical basics of radiation technology. In: *Proc. VII Winter School on Semiconductor Physics*. LIYaF, Leningrad, 1975, 232-244.*

38. V.L. Litvinov, N.A. Ukhin, B.A. Tsitovich. *Radiation-induced changes of LED and laser diode parameters*. I.V. Kurchatov Institute of Atomic Energy, Moscow, 1979.*

39. *Radiation Effects on Organic Materials*. Eds. R.O. Bolt, J.G. Carroll. Academic Press, New York and London, 1963.

40. T.M. Agakhanyan, E.P. Astvatsaturian, I.K. Skorobagatov. *Radiation Effects in Integrated Microcircuits*. Energoatomizdat, Moscow, 1989.*

41. V.S. Pershenkov, V.D. Popov, A.V. Shalnov. *Surface Radiation Effects in IMCs*. Energoatomizdat, Moscow, 1988.*

42. V.N. Ustyuzhaninov, A.Z. Chepizhenko. *Radiation Effects in Bipolar Integrated Microcircuits*. Radio i Svyaz', Moscow, 1989.*

43. L.G. Shirshev. *Ionizing Radiations and Electronics*. Sov. Radio, Moscow, 1969.*

44. Yu.A. Bykovsky, V.A. Karavansky, G.E. Kotovsky, M.B. Kuznetsov, A.A. Chistyakov, A.A. Lomov, S.A. Gavrilov. Photophysical processes induced in nanoporous silicon by high-power laser radiation. *ZhETF* 117(1), 136-144, 2000.*

45. E.V. Astrova, R.F. Vitman, V.V. Emtsev, A.A. Lebedev, D.S. Poloskin, A.D. Romenyuk, Yu.V. Rud'. Effect of γ-irradiation on the properties of porous silicon. *FTP* 30(3), 507-515, 1996.*

46. E.B. Kaganovich, S.I. Kirillova, E.G. Manoilov, V.E. Prymachenko, S.V. Svechnikov, R.V. Konakova, E.F. Venger, I.P. Bazylyuk, I.M. Kizyak. Effect of microwave electromagnetic radiation on the photoluminescence and electronic properties of the nanocrystalline silicon–silicon systems. *UFZh* 47(12), 1139-1145, 2002.**

47. E.F. Venger, V.E. Primachenko, E.B. Kaganovich, S.V. Svechnikov, R.V. Konakova, S.I. Kirillova, E.G. Manoilov, I.P. Bazylyuk, I.M. Kizyak. Effect of microwave electromagnetic radiation on the photoelectron properties of the nanocrystalline silicon/silicon systems. In: Collection of the Works of Int. Sci.-Tech. Conf. "*Simulation of Electronic Devices and Technical Processes, Provision of Quality, Reliability and Radiation Strength of Devices and Equipment*", *Sevastopol, 7–15 Sept. 2002*. Ed. I.V. Ryzhikov. MGAPI, Moscow, 2003, 27-40.*

48. E.B. Kaganovich, I.M. Kizyak, S.I. Kirillova, R.V. Konakova, O.S. Lytvyn, P.M. Lytvyn, E.G. Manoilov, V.E. Primachenko, I.V. Prokopenko. Effect of microwave electromagnetic radiation on the structure, photoluminescent and electronic properties of nanocrystalline silicon films on silicon substrate. *SPQEO* 6(4), 471-478, 2003.

49. E.B. Kaganovich, A.A. Kudryavtsev, E.G. Manoilov, S.V. Svechnikov, I.Z. Indutnyi. Optical properties of Si nanocomposite films prepared by laser ablation. *Thin Solid Films* 349, 298-302, 1999.

50. E.B. Kaganovich, E.G. Manoilov, I.R. Bazylyuk, S.V. Svechnikov. Spectra of photoluminescence from silicon nanocrystals. *Semiconductors* 37(3), 336-339, 2003.

51. E.B. Kaganovich, E.G. Manoilov, S.V. Svechnikov. The role of oxygen in radiative recombination of nanocrystalline silicon. *UFZh* 46(11), 1196-1201, 2001.

52. P.M. Lytvyn, O.S. Lytvyn, I.V. Prokopenko, E.B. Kaganovich, I.M. Kizyak, E.G. Manoilov. Structure of photoluminescent nanocrystalline silicon films obtained with pulsed laser deposition technique. *Nanosystemy, Nanomaterialy, Nanotekhnologii* **1**(2), 601-610, 2003.**

53. http://www.di.com.

54. http://www. ntmdt.com.

55. V. Bykov, A. Gologanov, V. Shevyakov. Test structure for SPM tip shape deconvolution. *Appl. Phys. A: Mater. Sci. & Processing* **66**(5), 499-502, 1998.

56. J.S. Villarrubia. Algorithms for scanned probe microscope image simulation, surface reconstruction, and tip estimation. *J. Res. Natl. Inst. Stand. Technol.* **102**(4), 425-454, 1997.

57. P.M. Williams, K.M. Shakesheff, M.C. Davies, D.E. Jackson, C.J. Roberts, S.J.B. Tendler. Blind reconstruction of scanning probe image data. *J. Vac. Sci. Technol. B* 14(2), 1557-1563, 1996.

58. K. Godwod, A.T. Nagy, Z. Rek. The application of the X-ray triple-crystal spectrometer for measuring the radius of curvature of bent single crystals. *phys. stat. sol.(a)* 34(2), 705-710, 1976.

Chapter 5

1. *International Technology Roadmap for Semiconductors (ITRS)*. SIA, San Jose, CA; 1999; http://public.itrs.net

2. S. Kamiyama, H. Suzuki, H. Watanabe, A. Sakai, H. Kimura, J. Mizuki, Ultrathin tantalum oxide capacitor process using oxygen-plasma annealing. *J. Electrochem. Soc.* **141**, 1246-1251, 1994.

3. C. Chaneliere, J.L. Autran, R.A.B. Devine, B. Balland, Y.J. Chabal, D.A. Muller, R.L. Opila, J.R. Kwo. Materials characterization of alternative gate dielectrics. *Mater. Sci. Eng.* **R22**, 269-319, 1998.

4. B.K. Moon, C. Isole, J. Aoyama. Insulating properties of tantalum pentoxide capacitor films obtained by annealing in dry ozone. *J. Appl. Phys.* **85**, 1731-1738, 1999.

5. E. Atanassova. Thin RF sputtered and thermal Ta_2O_5 on Si for high density DRAM application. *Microel. Reliab.* **39**, 1185-1217, 1999.

6. K. Forsgren, A. Harsta. Halide chemical vapour deposition of Ta_2O_5. *Thin Solid Films* **343/344**, 111-114, 1999.

7. G.D. Wilk, R.M. Wallace, J.M. Anthony. High-*k* gate dielectrics: current status and materials properties considerations. *J. Appl. Phys.* **89**, 5243-5275, 2001.

8. E. Atanassova, T. Dimitrova. Thin Ta_2O_5 layers on Si as an alternative to SiO_2 for high-density DRAM applications. In: *Handbook of Surfaces and Interfaces of Materials*. Ed. H.S. Nalva. Academic Press, San Diego, CA, USA, 2001. Vol. 4, 439-479.

9. R.W. Busch, O.P. Pluchery. Tantalum pentoxide (Ta_2O_5) thin films for advanced dielectric applications. *MRS Bull.* 27(3), 206-211, 2002.

10. T.V. Petlickaia. *MOS Capacitors Based on* Ta_2O_5. Ph.D. Thesis, Minsk, University of Informatics & Radioelectronics, Belarus, 2003.*.

11. E. Atanassova, A. Paskaleva, N. Novkovski, M. Georgieva. Conduction mechanisms and reliability of thermal Ta_2O_5–Si structures and the effect of the gate electrode. *J. Appl. Phys.* **97**, 094104, 2005.

12. D. Spassov, E. Atanassova, G. Beshkov. Effects of rapid thermal annealing in vacuum on electrical properties of thin Ta_2O_5–Si structures. *Microelectron. J.* **31**, 653-661, 2000.

13. E. Atanassova, M. Kalitzova, G. Zollo, A. Paskaleva, A. Peeva, M. Georgieva, G. Vitali. High temperature-induced crystallization in tantalum pentoxide layers and its influence on the electrical properties. *Thin Solid Films* **426**, 191-199, 2003.

14. E. Atanassova, D. Spassov, A. Paskaleva, J. Koprinarova, M. Georgieva. Influence of oxidation temperature on the microstructure and electrical properties of Ta_2O_5 on Si. *Microelectron. J.* **33**, 907-920, 2002.

15. S. Ezhilvalan, T.Y. Tseng. Conduction mechanisms in amorphous and crystalline Ta_2O_5 thin films. *J. Appl. Phys.* **83**, 4797-4801, 1998.

16. J.L. Autran, R.A.B. Devine, C. Chaneliere, B. Balland. Fabrication and characterization of Si MOSFETs with PECVD amorphous Ta_2O_5 gate insulator. *IEEE El. Dev. Lett.* **18**, 447-449, 1997.

17. K. Kishiro, N. Inone, S.C. Chen, M. Yoshimani. Structure and electrical properties of Ta_2O_5 deposited on metal electrodes. *Jpn. J. Appl. Phys.* **37**, 1336-1339, 1998.

18. T. Dimitrova, K. Arshak, E. Atanassova. Crystallization effects in oxygen-annealed Ta_2O_5 thin films on Si. *Thin Solid Films* **381**, 31-38, 2001.

19. E. Atanassova, N. Novkovski, A. Paskaleva, M. Pecovska-Gjorgievich. Oxygen annealing modification of conduction mechanism in thin rf sputtered Ta_2O_5 on Si. *Solid St. Electron.* **46**, 1887-1898, 2001.

20. W.S. Lau, P.W. Qian, N.P. Sandler, K.A. McKinley, P.U. Chu. Evidence that N_2O is stronger oxidation agent than O_2 for post-deposition annealing of Ta_2O_5 on Si capacitors. *Jpn. J. Appl. Phys.* **36**, 661-666, 1997.

21. A.I. Kingon, J.P. Maria, S.K. Streiffer. Alternative dielectrics to silicone dioxide for memory and logic devices. *Nature* **406**, 1032-1038, 2000.

22. R. Beyers. Thermodynamic considerations in refractory metal–silicon–oxygen systems. *J. Appl. Phys.* **56**, 147-152, 1984.

23. E. Atanassova, D. Spassov. Hydrogen annealing effects on the properties of thermal Ta_2O_5 on Si. *Microelectron. J.* **30**, 265-274, 1999.

24. W.S. Lau, T.S. Tan, N.P. Sandler, B.S. Page. Characterization of defect states responsible for leakage current in tantalum pentoxide films for very high density Dynamic Random Access Memory (DRAM) applications. *Jpn. J. Appl. Phys.* **34**, 757-761, 1995.

25. E. Atanassova, G. Tyuliev, A. Paskaleva, D. Spassov, K. Kostov. XPS study of N_2 annealing effect on thermal Ta_2O_5 layers on Si. *Appl. Surf. Sci.* **225**, 86-99, 2004.

26. T. Dimitrova, E. Atanassova. Electrical and transport properties of rf sputtered Ta_2O_5 on Si. *Solid. St. Electron.* **42**, 307-315, 1998.

27. E. Atanassova, T. Dimitrova, J. Koprinarova. XPS study of thin rf sputtered Ta_2O_5. *Appl. Surf. Sci.* **84**, 193-202, 1995.

28. E. Atanassova, R. V. Konakova, V.F. Mitin, J. Koprinarova, O.S. Lytvyn, O.B. Okhrimenko, V.V. Shynkarenko, D. Virovska. Effect of microwave radiation on the properties of Ta_2O_5–Si microstructures. *Microel. Reliab.* **45**, 123-135, 2005.

29. E. Atanassova, N.S. Boltovets, E.Yu. Kolyadina, R.V. Konakova, J. Koprinarova, L.A. Matveeva, V.V. Milenin, V.F. Mitin, V.V. Shynkarenko, D.I. Voitsikhovskyi. Structural-phase ordering in Ta_2O_5–*p*–Si heterosystem enhanced by microwave processing. In: *Proc. 23rd Int. Conf. Microel. 2002, Nish, Yugoslavia, IEEE El. Dev. Soc.* **2**, 531-534, 2002.

30. E. Atanassova, E.Yu. Kolyadina, R.V. Konakova, J. Koprinarova, O.S. Lytvyn, P.M. Lytvyn, L.A. Matveeva, V.V. Milenin, V.F. Mitin, V.V. Shynkarenko, D.I. Voitsikhovskyi. The effects in Ta_2O_5–*p*–Si heterostructures induced by microwave treatment. In: *Proc. 14th Int. Sympos. "Thin Films in Optics and Electronics", Kharkov Sci. Assembly, 22–27 Apr. 2002, Kharkov, Ukraine*, Pt. 1, 84-87.

31. E. Atanassova, A. Paskaleva, R.V. Konakova, D. Spassov, V.F. Mitin. Influence of γ-radiation on thin Ta_2O_5–Si structures. *Microel. J.* **32**, 553-562, 2001.

32. C. Wyon. Future technology for advanced MOS devices. *Nucl. Instr. Methods Phys. Res. B* **186**(1), 380-391, 2002.

33. W.L. Warren, D.M. Fleetwood, M.R. Shaneyfelt, J.R. Schwank, P.S. Winokur, R.A.B. Devine. Links between oxide interface and border traps in high-temperature annealed Si–SiO_2 systems. *Appl. Phys. Lett.* **64**, 3452-3454, 1994.

34. J.S. Johannesen, W.E. Spicer, Y. Strausser. An Auger analysis of the Si–SiO_2. *J. Appl. Phys.* **47**, 3028-3037, 1976.

35. H.H. Holloway, G.S. Nelson. Preferential sputtering of Ta_2O_5 by argon ions. *J. Vac. Sci. Technol.* **16**, 793-797, 1979.

36. G.S. Oehrlein. Oxidation temperature dependence of the electrical conduction characteristics and dielectric strength of thin Ta_2O_5 films on Si. *J. Appl. Phys.* **59**, 1587-1595, 1986.

37. T. Dimitrova, E. Atanassova, J. Koprinarova. Dielectric characteristics of MOS capacitors with rf sputtered Ta_2O_5. In: *Proc. 22nd Int. Conf. Microel. 2000, Nish, Yugoslavia, IEEE El. Dev. Soc.* **1**, 373-376, 2000.

38. A. Dargis, J. Kundrotas. *Handbook on Physical Properties of* Ge, Si, GaAs *and* InP. Sci. and Encycl. Publishers, Vilnius, 1994.

39. J.J. Wortman, R.A. Evans. Young's modulus, shear modulus and Poisson's ratio in Si and Ge. *J. Appl. Phys.* **36**, 153-156, 1965.

40. R. Yu, L.A. Holiney, L.A. Matveeva, E.F. Venger. Investigation on the undersurface damaged layers in Si wafers. *SPQEO* **2**, 10-13, 1999.

41. N.S. Boltovets, A.B. Kamalov, R.V. Konakova, E.Yu. Kolyadina, L.A. Matveeva, V.V. Milenin, E. Atanassova. The effects in metal-semiconductor-structures stimulated by high-power electromagnetic radiation. In: *Proc. 4th Int. Conf. "Interaction of Radiation with Solids", 3-5 Oct. 2001, Minsk, Belarus, 2001*, 114-116.

42. D. Spassov, E. Atanassova. Thermal Ta_2O_5 films as a gate insulator for thin film capacitor. *Int. J. Electr.* 84(5), 453-466, 1998.

43. E. Atanassova, D. Spassov. X-ray photoelectron spectroscopy of thermal thin Ta_2O_5 films on Si. *Appl. Surf. Sci.* **135**, 71-82, 1998.

44. P.A. Murawala, M. Sawai, T. Tatsuta, O. Tsuji, S. Fujita, S. Fujita. Structural and electrical properties of Ta_2O_5 grown by the plasma-enhanced liquid source CVD using penta ethoxy tantalum source. *Jpn. J. Appl. Phys.* Part 1 **32**(1B), 368-375, 1993.

45. T. Aoyama, Sh. Saida, Y. Okayama, M. Fujisaki, K. Iwai, Ts. Arikado. Leakage current mechanism of amorphous and polycrystalline Ta_2O_5 films grown by chemical vapor deposition. *J. Electrochem. Soc.* **143**(3), 977-983, 1996.

46. J.J. Hammel. Nucleation in glass-forming materials. In: *Nucleation*. Ed. A.C. Zettlemoyer. Marcel Dekker, New York, 1969, 489-525.

Some abbreviated journal titles:

ET - Elektronnaya Tekhnika

FTP - Fizika I Tekhnika Poluprovodnikov

FTT - Fizika Tverdogo Tela

OET - Obzory po Elektronnoi Tekhnike

OPT - Optoelektronika i Poluprovodnikovaya Tekhnika

PZhE - Peterburgskii Zhurnal Elektroniki

PZhTF – Pis'ma v Zhurnal Tekhnicheskoi Fiziki

SPQEO - Semiconductor Physics, Quantum Electronics & Optoelectronics

UFZh – Ukrainskii Fizicheskii Zhurnal

ZhETF – Zhurnal Eksperimental'noi i Teoreticheskoi Fiziki

ZhTF – Zhurnal Tekhnicheskoi Fiziki

CONTENTS

PRINCIPAL ACRONYMS AND SYMBOLS 5

PREFACE 9

Chapter I. INVESTIGATION OF THE ROLE OF THERMAL AND NON-THERMAL FACTORS IN TRANSFORMATION OF STRUCTURAL PARAMETERS OF III–V SEMICONDUCTOR COMPOUNDS, SiC AND CdS EXPOSED TO HIGH-POWER MICROWAVE IRRADIATION 15

1.1. PROCESSES OF STRUCTURAL ORDERING INDUCED BY MICROWAVE TREATMENT AT THE SURFACES OF GaAs SINGLE CRYSTALS AND CONTACT SYSTEMS ON THEIR BASIS 16

1.1.1. Structural ordering at the surface of GaAs single crystals 18

1.1.2. Structural ordering in the TiB_2–GaAs barrier contacts 27

1.2. DEFORMATION EFFECTS IN THE TiB_2–GaAs (InP, GaP) STRUCTURES INDUCED BY EXTERNAL ACTIONS (RAPID THERMAL ANNEALING, MICROWAVE AND ^{60}Co γ-IRRADIATION) 35

1.3. STRUCTURAL RELAXATION IN THE n-GaAs AND n-SiC 6H INDUCED BY MICROWAVE IRRADIATION 41

1.4. EFFECT OF MICROWAVE TREATMENT ON THE IMPURITY-DEFECT STATE OF CdS CRYSTALS 47

Chapter 2. EFFECT OF γ-RADIATION AND MICROWAVE RADIATION ON THE ELECTRICAL CHARACTERISTICS OF RESONANT TUNNELING AND TUNNEL DIODES MADE ON THE BASIS OF GaAlAs–GaAs HETEROJUNCTIONS AND GaAs 52

2.1. RADIATION EFFECTS IN RESONANT TUNNELING DIODES EXPOSED TO ^{60}Co γ-RADIATION AND MICROWAVE RADIATION 56

2.2. ENHANCED RADIATION TOLERANCE OF TUNNEL DIODES WITH δ-DOPING 64

2.3. EFFECT OF MICROWAVE IRRADIATION ON I–V CURVES OF GaAs TUNNEL DIODES WITH δ-LAYERS 68

2.3.1. Total heating model 70

2.3.2. Local heating model 70

Chapter 3. EFFECT OF ^{60}Co γ-RADIATION AND MICROWAVE RADIATION ON THE PROPERTIES OF SiO_2–GaAs (SiC) STRUCTURES 74

3.1. RADIATION-INDUCED EFFECTS AT THE SiO_2–GaAs INTERFACE 74

3.2. EFFECTS INDUCED BY MICROWAVE IRRADIATION IN THE SiO_2-GaAs STRUCTURE 81

3.3. MECHANISMS OF MODIFICATION OF SiO_2–GaAs DEFECT STRUCTURE BY MICROWAVE IRRADIATION 87

3.4. EFFECT OF MICROWAVE RADIATION ON THE SiO_2–SiC STRUCTURES 95

Chapter 4. EFFECT OF MICROWAVE IRRADIATION ON THE MORPHOLOGICAL AND STRUCTURAL PROPERTIES OF NANOCRYSTALLINE SILICON–SILICON SYSTEMS 105

4.1. EXPERIMENTAL PROCEDURES 106

4.2. EFFECT OF THE CONDITIONS OF FORMATION OF NANOCRYSTALLINE SILICON FILMS ON THEIR STRUCTURE . 108

4.3. EFFECT OF MICROWAVE TREATMENT ON THE STRUCTURAL PROPERTIES OF NANOCRYSTALLINE SILICON–SILICON SYSTEMS 115

Chapter 5. MICROWAVE AND γ-RADIATION IMPACT ON Ta_2O_5–Si STACK CAPACITORS **118**

5.1. *EFFECT OF MICROWAVE RADIATION ON* Ta_2O_5–Si MICROSTRUCTURES: RF SPUTTERED Ta_2O_5 122

5.1.1. Experimental procedure 122

5.1.2. Results and discussion 124

Dielectric parameters and C–V curves 124
Auger analysis 127
I–V curves and conduction mechanisms 131
Breakdown fields 140
Surface roughness parameters andtransmittance spectra 142

5.2. EFFECT OF MICROWAVE RADIATION ON Ta_2O_5–Si MICROSTRUCTURES: THERMAL Ta_2O_5 ON Si 148

5.2.1. Experimental procedure 148

5.2.2. Results and discussion 149

5.3. EFFECT OF γ-RADIATION ON THIN Ta_2O_5–Si MICROSTRUCTURES 159

5.3.1. Experimental procedure 159

5.3.2. Results and discussion 160

Dielectric parameters 160
Leakage current characteristics 164
Breakdown fields 170
rf Sputtered Ta_2O_5 174
Thermal Ta_2O_5 175

CONCLUSION **178**

REFERENCES **179**

Національна академія наук України
НТК «Інститут монокристалів»
Стан та перспективи розвитку функціональних матеріалів
для науки та техніки

ВПЛИВ АКТИВНИХ ДІЙ НА ВЛАСТИВОСТІ НАПІВПРОВІДНИКОВИХ МАТЕРІАЛІВ І СТРУКТУР

Атанасова Єлена Дімова, докт. наук, проф.;
Беляєв Олександр Євгенович, член-кор. **НАН України**,
докт. фіз.-мат. наук, проф.;
Конакова Раїса Василівна, докт. техн. наук, проф.;
Литвин Петро Мар'янович, канд. фіз.-мат. наук;
Міленін Віктор Володимирович, канд. фіз.-мат. наук;
Мітін Вадим Федорович, канд. фіз.-мат. наук;
Шинкаренко Володимир Вікторович, м.н.с.

Відпов. секретар Є.В. Щербина
Компьютерна верстка Д.В. Ткачов

Здано в набір 25.02.2007. Підписано до друку 10.04.2007.
Формат 60×84 1/16. Папір офс. Гарнітура Century Schoolbook
Друк високий с ФПФ. Обл. вид. л. 13,5
Наклад 300 экз.

Харків
НТК «Інститут монокристалів»
2007